Vol. 51 · No. 1 · February 2026

RDE
Restorative Dentistry & Endodontics

Editorials

Research Articles

Case Report

The Korean Academy of Conservative Dentistry

www.rde.ac

RDE Restorative Dentistry & Endodontics
Vol. 51 · No. 1 · February 2026
The Korean Academy of Conservative Dentistry

eISSN 2234-7666

Vol. 51 · No. 1 · February 2026

RDE
Restorative Dentistry & Endodontics

The Korean Academy of Conservative Dentistry

www.rde.ac

RDE Restorative Dentistry & Endodontics

Vol. 51 · No. 1 · February 2026

eISSN 2234-7666

Aims and Scope

The *Restorative Dentistry and Endodontics* (officially abbreviated as Restor Dent Endod; RDE) is a peer-reviewed and open access journal providing up-to-date information regarding the research and developments on new knowledge and innovations pertinent to the field of contemporary clinical operative dentistry, restorative dentistry, and endodontics. In the field of operative and restorative dentistry, the journal deals with diagnosis, treatment planning, treatment concepts and techniques, adhesive dentistry, esthetic dentistry, tooth whitening, dental materials and implant restoration. In the field of endodontics, the journal deals with a variety of topics such as etiology of periapical lesions, outcome of endodontic treatment, surgical endodontics including replantation, transplantation and implantation, dental trauma, intracanal microbiology, endodontic materials (MTA, nickel-titanium instruments, etc), molecular biology techniques, and stem cell biology. RDE publishes original articles, review articles and case reports dealing with aforementioned topics from all over the world.

RDE is indexed/tracked/covered by Web of Science-Emerging Sources Citation Index (ESCI), Scoups, PubMed, PubMed Central, EBSCO, KoreaMed, Synapse, KCI, Crossref, DOAJ, and Google Scholar.

This Journal was supported by the Korean Federation of Science and Technology Societies Grant funded by the Korean Government (MEST).

History

RDE (eISSN 2234-7666) is the official journal of the Korean Academy of Conservative Dentistry and was renamed from the *Journal of Korean Academy of Conservative Dentistry* (pISSN 1225-0864; eISSN 2093-8179), which was first published in 1975. It was initially published once a year but became a biannual journal in 1986, a quarterly journal in 1999, and then a bimonthly journal in 2001. From 2012, the journal name was renamed, the official language of the journal was changed to English, and it is currently published quarterly. This journal is supported in part by a Grant from the Korean Federation of Science and Technology Societies funded by the Korean Government (MEST).

Distribution

Restor Dent Endod is not for sale, but is distributed to members of Korean Academy of Conservative Dentistry and relevant researchers and institutions world-widely on the last day of February, May, August, and November of each year. Full text PDF files are also available at the official website (https://www.rde.ac; http://www.kacd.or.kr), KoreaMed Synapse (https://synapse.koreamed.org), and PubMed Central. To report a change of mailing address or for further information contact the academy office through the editorial office listed below.

Open Access

Official Publication of Korean Academy of Conservative Dentistry

Published on February 28, 2026

Publisher

The Korean Academy of Conservative Dentistry

B163, Seoul National University Dental Hospital, 101 Daehak-ro, Jongno-gu, Seoul, Korea

Tel: +82-2-763-3818

Fax: +82-2-763-3819

Email: kacd@kacd.or.kr

Editorial Office

The Korean Academy of Conservative Dentistry

B163 Seoul National University Dental Hospital, 101 Daehak-ro, Jongno-gu, Seoul 03080, Korea

Tel: +82-2-763-3818

Fax: +82-2-763-3819

Email: editor@rde.ac

Publishing Office

M2PI

#805, 26 Sangwon 1-gil, Seongdong-gu, Seoul 04779, Korea

Tel: +82-2-6966-4930

Fax: +82-2-6966-4945

Email: support@m2-pi.com

RDE Restorative Dentistry & Endodontics

Editorial Board

RDE Restorative Dentistry & Endodontics

Contents

Vol. 51 · No. 1 · February 2026

Editorials

Research Articles

Case Report

RDE Restorative Dentistry & Endodontics

Editorial

eISSN 2234-7666
Restor Dent Endod. 2026 February;51(1):e13
https://doi.org/10.5395/rde.2026.51.e13

Restorative Dentistry and Endodontics news: celebrating the 50th anniversary of the journal

Yeon-Jee Yoo, Editorial Executive Director, *Restorative Dentistry and Endodontics*

On October 25, 2025, a ceremony commemorating the 50th anniversary of *Restorative Dentistry and Endodontics* (RDE) was held during the Fall Scientific Meeting of the Korean Academy of Conservative Dentistry (KACD) at the Sotaesan Memorial Hall in Seoul. At the event, Prof. Kyung-San Min, Editor-in-Chief of RDE, delivered a commemorative address and received a Meritorious Service Award in recognition of his contributions to the advancement of society (Figures 1 and 2).

In his address, Prof. Min reflected on the history and academic achievements of the KACD, while also highlighting the future vision of conservative dentistry and endodontics and the evolving role of the society. He particularly emphasized the importance of expanding international academic collaboration, upholding research ethics, and nurturing young researchers, calling for a shared sense of responsibility within the academic community.

The award was presented in recognition of Prof. Min's long-standing dedication to academic development through his service as Editor-in-Chief of RDE and his significant contributions to enhancing the standing of the society. He has been widely credited with advancing the journal and promoting both domestic and international academic exchange.

In his acceptance remarks, Prof. Min stated, "It is a great honor to receive such a prestigious award on this meaningful occasion," adding, "I will continue to devote

Figure 1. Prof. Kyung-San Min, Editor-in-Chief of *Restorative Dentistry and Endodontics*, is delivering a speech commemorating the 50th anniversary of the founding of the journal.

Figure 2. Prof. Jin-Woo Kim, President of the Korean Academy of Conservative Dentistry, is presenting the award to Prof. Kyung-San Min, Editor-in-Chief of *Restorative Dentistry and Endodontics*.

my utmost efforts to the further development of RDE." A representative of the KACD commented, "Prof. Min's dedication and leadership have served as a vital foundation for the society's growth. This award reflects the collective appreciation of all our members."

Below is the English version of Prof. Min's commemorative address. The Korean version is available in the Supplementary Material.

50TH ANNIVERSARY ADDRESS

Distinguished members of our society, and esteemed researchers, clinicians, and readers joining us today, it is with great honor and profound significance that we gather here to celebrate the 50th anniversary of *Restorative Dentistry and Endodontics* (RDE).

In 1975, at a time when the concept of conservative dentistry was still unfamiliar in Korea, our journal took its first steps under the name *Korean Journal of Operative Dentistry*. It was founded through the academic passion and dedication of our pioneering scholars, who sought to share research achievements spanning both the foundations and clinical practice of conservative dentistry, thereby laying an essential cornerstone for the advancement of dental science in Korea. Half a century later, RDE has grown into a truly international journal, bringing together researchers from around the world. As you are well aware, RDE is now indexed in major international databases, including PubMed, Scopus, and Web of Science. This year, we reached another import-

https://doi.org/10.5395/rde.2026.51.e13

ant milestone by receiving our first Impact Factor from Clarivate. This achievement represents not only recognition of academic quality but also the collective efforts of our entire community.

On this meaningful occasion, I would like to express my deepest gratitude to all those who have made RDE what it is today. Over the past 50 years, countless individuals have devoted themselves to the journal as editors, authors, and reviewers, shaping its history with unwavering commitment. I also extend sincere appreciation to the authors who have consistently submitted high-quality research, to the reviewers who have evaluated manuscripts with integrity and rigor, and to the readers who have placed their trust in and shown enduring support for RDE. You are, without question, the true protagonists of this journal. I offer my highest respect for your dedication and passion.

Looking back, the past 50 years have been a period of profound transformation in dentistry. Restorative materials have evolved from simple filling substances into bioactive and intelligent materials, while endodontic treatment has expanded beyond infection control toward tissue regeneration. Digital technologies and artificial intelligence have become deeply integrated into both research and clinical practice, and conservative dentistry has emerged as a truly interdisciplinary science. Throughout these changes, RDE has served as an open platform for sharing new knowledge and as an academic bridge connecting generations of scholars.

Today's 50th anniversary is not merely a commemoration of time passed. It is also a moment of reflection—one that asks not only how we began, but also where we are headed. I firmly believe that RDE will continue to build upon its strong traditions while embracing new innovations, moving confidently toward a broader global horizon. We will actively welcome research in fields that shape the future of dentistry, including biomaterials science, regenerative dentistry, digital dentistry, and artificial intelligence-based diagnosis and treatment, while steadfastly pursuing both scientific rigor and clinical relevance.

Furthermore, RDE will continue to place the highest priority on academic integrity and research ethics. We will strengthen transparency in the editorial and peer-review processes, expand international collaboration and networks, and provide researchers with a fair, dignified, and trustworthy scholarly forum. We are also committed to creating opportunities for young researchers to grow, fostering a community in which we learn and advance together. This 50th anniversary marks not only a celebration of our achievements, but also the starting point of a new and more mature half-century for RDE.

Finally, I would like once again to extend my heartfelt thanks to everyone who has accompanied RDE on its 50-year journey. Today's gathering honors the accomplishments of the past while also serving as a promise for the future. Just as RDE has walked hand in hand with the progress of dentistry over the past five decades, I sincerely hope that it will continue to shine as a guiding light for the future of our field.

With your continued interest and support, I pledge to you, as Editor-in-Chief, that RDE will move forward with an even greater sense of vision and responsibility—serving as a bridge between basic science and clinical practice, and between tradition and innovation.

Thank you very much.

Kyung-San Min
Editor-in-Chief, *Restorative Dentistry and Endodontics*

SUPPLEMENTARY MATERIALS

The Korean version of the 50th anniversary address

https://doi.org/10.5395/rde.2026.51.e13

RDE Restorative Dentistry & Endodontics

Editorial

eISSN 2234-7666
Restor Dent Endod. 2026 February;51(1):e14
https://doi.org/10.5395/rde.2026.51.e14

Restorative Dentistry and Endodontics 2025 annual highlights: gratitude to our reviewers and achievement of the first journal impact factor

Kyung-San Min

In 2025, *Restorative Dentistry and Endodontics* (RDE) published a total of 40 articles, including review articles, original research papers, and case reports. Each manuscript underwent rigorous peer review by 155 dedicated reviewers whose unwavering commitment to excellence ensured the scientific quality of our journal.

Thanks to the reviewers' diligent and constructive efforts, RDE has continued to publish high-quality research in a timely manner. In particular, Dr. Andrea Whitehurst Ary Leitão and Dr. Abayomi O. Baruwa were recognized with Certificates of Appreciation in acknowledgment of their outstanding contributions to the peer-review process. We sincerely extend our gratitude to all reviewers for their invaluable service and kindly ask for your continued support in the coming year.

We are also delighted to share that in 2025, RDE achieved a significant milestone by receiving its first-ever Journal Impact Factor of 1.5 from Clarivate's Journal Citation Reports. This accomplishment brings great pride to our journal and reflects the growing international recognition of the impactful and high-quality research we publish in the field of dentistry.

We express our heartfelt appreciation to our dedicated editorial board members, conscientious reviewers, and passionate authors. Your unwavering support and commitment to excellence have been the driving force behind the continued growth and success of RDE. Although our current ranking may not yet be among the highest, we are confident that through sustained effort and collective dedication, RDE will continue to evolve into an even more influential journal in the years ahead.

Kyung-San Min
Editor-in-Chief, *Restorative Dentistry and Endodontics*

2025, REVIEWER THANK YOU LIST

ABDELRAHMAN, Tariq
ABUSTEIT, Omar
ABUZAR, Ma Sathar
AGGARWAL, Shalini
AGRAWAL, Deep
AGRAWAL, Vineet
AGRAWAL, Pratik
AHMAD, Lubna
ALGARNI, Amnah
ALI, Islam
ANASTASIADIS, Konstantinos
ARHAKIS, Aristidis
ARILI ÖZTÜRK, Esra
ARZANI, Sarah
B J, Prathima
BACHESK, Andressa
BALACHANDRAN, Janani
BALASUBRAMANIAN, Saravana Karthikeyan
BALKANLIOĞLU, Esra
BARBOSA, Carolina
BARUWA, O. Abayomi
BELLADONNA, Felipe
BHARATBHAI, Aakanxa
BOHORA, Aarti
BRAIDO, Arian
ÇAĞLAR, Kemal
CATELAN, Anderson
CAVALLI, Vanessa
CAVIEDES-BUCHELI, Javier
CHANDWANI, Neelam
CHANG, Hoon-Sang
CHO, Sin-Yeon
CHOI, Yoorina

CHOMPU-INWAI, Papimon
CORRER, Gisele
COSTA, Joatan
DA SILVA-FILHO, José Evando
DAVIDOPOULOU, Sotiria
DUARTE, Marco Antonio Hungaro
DUTTA, Arindam
ERTURK-AVUNDUK, Ayse
ESTRELA, Carlos
FARIA-E-SILVA, Andre
FERNÁNDEZ, Eduardo
FERREIRA, Claudio
FOUAD, Eman
GOKUL R, Naveen
GOMEZ-SOSA, Jose
GUIMARÃES, Bruno
GÜNDOĞAR, Mustafa
GUPTA, Alpa
GUTIÉRREZ ALVAREZ, Oscar
H. HAMOY KATAOKA, Simony
HA, Jung-Hong
HOSEINZADEH, Melika
IANDOLO, Alfredo
İSLAMOĞLU, Ayşe
JANG, Ji-Hyun
JANTARAT, Jeeraphat
JEON, Mi-jeong
JO, Hyoung Hoon
K, Madhuram
KALYONCUOGLU, Elif
KARIMPOUR, Sahar
KESKIN, Cangül
KIELBASSA, Andrej
KIM, Hee-Jin
KIM, Hyun-Jung
KIM, Duck-su
KIM, Sinyoung
KIM, JaeHoon
KIM, Sooyoun
KIM, Ukseong
KIM, Jeffrey
KIM, Hee-Sun
KIM, Hae-Young
KLAISIRI, Awiruth
KODONAS, Konstantinos
KOKOTI, Maria
KUL, Abdurrahman
KURY, Matheus
KWAK, Sangwon
LAI, Gordon
LAZIC, Ema
LEE, Myung Jin
LEE, Yuna
LEE, Chang-Ha
LIMOEIRO, Ana Grasiela
LINS-FILHO, Paulo
MARTINS, Jorge
MEENA, N
MELO, Ana
MILOSEVIC, Alexander
MISHRA, Lora
MOUROUZIS, Petros
MUÑOZ-ALVEAR, Hernan
NABESHIMA, Cleber
NAM, Daniel
NIK ABDUL GHANI, Nik Rozainah
OH, Soram
PALMA, Paulo J.
PANDA, Bandana
PANDEY, Sanket Hans
PANPISUT, Piyaphong
PAPADOPOULOS, Constantinos
PARK, Jeong-Kil
PARK, Sujung
PARK, Jinyoung
PATEL, Biraj
PATIL, DAMINI
PAUWELS, Ruben
PEDROSA, Marlus
PEREIRA MALTA, Cristiana
PLASCENCIA, Hugo
PORTIGLIATTI, Ricardo
RASHMI, K
REIS, Isabella
SAMUEL, Linda Christabel
SANZ, Carolina
SAVIOLI, Ricardo
SAYGILI, Selin
SHAH, Vyoma
SHEHAB, Njwan
SHERWOOD, Anand
SHIN, Bo-Kyung
SILVA, Emmanuel João
SIMÕES DE CARVALHO, Marco
ŞIŞMANOĞLU, Soner
SOBHY, Sabah
SOLETE, Pradeep
SOMAY, Efsun
SON, SungAe
SONG, Minju
SOUSA-LIMA, Rodolfo
SOUSA-NETO, Manoel
SOVIERO, Vera
THAMRONGANANSKUL, Niyom
TOLIBAH, Yasser
TOPBAŞ, Celalettin
TULGAR, Mustafa Mert
TUPPADMATH, Kanchan
UJARIYA, Urvashi
ÜRÜN, Zübeyde Gökçe
USTA, Sıla
VALERI, Cristina
VALVERDE HARO, Henry
VELMURUGAN, Natanasabapathy
VERMA, Devansh
VERSIANI, Marco
VIEIRA JUNIOR, Waldemir
WHITEHURST ARY LEITÃO, Andrea
YENIÇERI ÖZATA, Merve
YOO, Yeon-Jee
YOON, Ji Young
YOUCHAROEN, Kwanchanok

RDE Restorative Dentistry & Endodontics

Research Article

eISSN 2234-7666
Restor Dent Endod. 2026 February;51(1):e2
https://doi.org/10.5395/rde.2026.51.e2

Enhancing antimicrobial properties of a resin-based material via incorporation of a powdered phytotherapeutic extract: an *in vitro* experimental study

Rodolfo Xavier de Sousa-Lima[1,*], Maria Eduarda Lima do Nascimento Marinho[2], Janielly Cristina Costa da Silva[3], Moan Jéfter Fernandes Costa[4], Pedro Henrique Sette-de-Souza[4], Giana da Silveira Lima[2], Boniek Castillo Dutra Borges[3]

[1]Department of Restorative Dentistry, Universidade Federal da Paraíba (UFPB), João Pessoa, PB, Brazil
[2]Graduate Program in Dentistry, Universidade Federal de Pelotas (UFPel),Pelotas, RS, Brazil
[3]Department of Dentistry, Universidade Federal do Rio Grande do Norte (UFRN), Natal, RN, Brazil
[4]Department of Dentistry, Universidade de Pernambuco (UPE), Arcoverde, PE, Brazil

ABSTRACT

Objectives: This study aimed to evaluate the degree of conversion (DC), immediate enamel bond strength (IEBS), antimicrobial activity, and release of the active principle of a resin-based material (RBM) enriched with the powdered *Schinopsis brasiliensis* (Braúna) stem antibacterial extract.

Methods: The RBM was enriched with 0, 1.25, 2.5, 5, 10, and 20 wt% powdered Braúna extract. The DC (n = 7) was assessed using micro-Raman spectroscopy. The IEBS (n = 7) was determined through the microshear test until failure, and failure modes were examined under a stereomicroscope. The antimicrobial activity (n = 15) was assessed by quantifying colony-forming units, and the release of the active principle was determined using ultra-high-performance liquid chromatography. One-way analysis of variance/Tukey and Kruskal-Wallis/Dunn tests were utilized to analyze the data (p < 0.05).

Results: Materials with 10 wt% and 20 wt% extract showed the lowest DC statistically. However, for IEBS, there were no statistically significant differences among the different groups. All materials released the active principle, but only those with 20 wt% and 10 wt% extract could inhibit biofilm formation similarly to 0.12% chlorhexidine.

Conclusions: Adding powdered Braúna extract between 10 wt% and 20 wt% is a promising alternative to provide an antimicrobial function to RBMs.

Keywords: Composite resins; Dental caries; Phytotherapy

Received: March 25, 2025 **Revised:** August 15, 2025 **Accepted:** September 11, 2025

Citation
Sousa-Lima RX, Marinho MELN, Silva JCC, Costa MJF, Sette-de-Souza PH, Lima GS, Borges BCD. Enhancing antimicrobial properties of a resin-based material via incorporation of a powdered phytotherapeutic extract: an *in vitro* experimental study. Restor Dent Endod 2026;51(1):e2.

***Correspondence to**
Rodolfo Xavier de Sousa-Lima, DDS, PhD
Department of Restorative Dentistry, Universidade Federal da Paraíba (UFPB), Conj. Pres. Castelo Branco III, João Pessoa – PB 58050-585, Brazil
Email: rodolfo.xavier@academico.ufpb.br

INTRODUCTION

Resin-based dental restorative materials (RBDMs) are a category of composites designed for direct or indirect tooth restorations, featuring a polymerizable resin matrix reinforced with inorganic fillers or fibers [1]. These materials are typically formulated using methacrylate monomers, polymerization initiators, and reinforcing fillers and undergo curing through radical polymerization, producing durable and rigid final structures [2]. RBDMs are commonly used in dentistry for a range of applications, owing to their advantageous properties. These include light-controlled curing time, a more conservative preparation technique, the ability to mimic natural tooth appearance closely, and adequate mechanical strength to withstand the forces of mastication [3]. The use of such composites has increasingly supplanted metal-based restorative materials in recent years [2].

However, RBDMs do not offer any advantages in terms of modulating caries risk factors, which tend to promote greater biofilm accumulation compared to other restorative materials like amalgam and glass ionomer [4]. Caries lesions around restorations remain one of the most frequent causes of failure and replacement of RBDMs, representing a major challenge to the longevity of restorations [5]. A systematic review reported that, among studies evaluating posterior restorations, 78.6% identified caries around restorations and/or fractures as the primary reasons for failure [6]. Notably, while the global prevalence of primary caries has decreased over the past decades, the incidence of caries lesions around restorations has remained relatively stable, raising concerns about potential overdiagnosis or misinterpretation of marginal defects and staining as active lesions [5]. This clinical ambiguity may result in unnecessary restoration replacements. As bacterial colonization of RBDMs plays a key role in lesion development, improving the antimicrobial properties of these materials has become a focus of research [5]. The development of RBDMs capable of inhibiting microbial activity could enhance the prevention of caries lesions around restorations and extend restoration longevity.

Efforts to develop antimicrobial resin composites have shown promising results, with a review identifying 34 active ingredients. Dimethylaminododecyl methacrylate (DMAHDM) is a well-studied example, consistently demonstrating positive antibacterial effects and mechanical properties, making it a promising candidate for clinical use. In contrast, some substances, such as graphene oxide decorated with ZnO nanoblasts and titanium dioxide nanoparticles, have been shown to negatively impact the composites' degree of conversion (DC) [7]. This highlights the need to investigate alternative agents, particularly natural ones. An innovative approach involves embedding curcumin, a natural photosensitizer, into methacrylate-based resin systems to enable antimicrobial photodynamic therapy, which has shown promising antibacterial activity against *Streptococcus mutans,* at low concentrations with minimal effect on mechanical properties [8]. The use of herbal medicines with confirmed antimicrobial activity is also a promising research avenue [8].

In this context, *Schinopsis brasiliensis* (Braúna), a native tree from the semi-arid region of northeastern Brazil, has been traditionally used for medicinal purposes and has recently gained scientific attention due to its diverse biological properties. Phytochemical analyses revealed the presence of bioactive compounds such as tannins, flavonoids, phenols, and polyphenols, which are associated with antimicrobial, antioxidant, and anti-inflammatory effects [9]. Recent evidence has indicated that the stem extract of Braúna possesses various biological activities, including *in vitro* activity against oral microorganisms associated with the caries process, such as *S. mutans*, *Streptococcus mitis*, and *Streptococcus salivarius*, with effects comparable to chlorhexidine [10]. Moreover, it was found that the extracts of *S. brasiliensis* have low cytotoxicity and a good selectivity index, suggesting their potential incorporation into dental materials [9].

However, it remains unknown whether the addition of *S. brasiliensis* extract to resin-based materials can confer antimicrobial properties and alter their physical and mechanical behavior. While the DC is often evaluated, a significant gap in this field is the lack of information on immediate bond strength to dental enamel, a property crucial for optimal performance in the oral environment [7]. Therefore, this study aimed to evaluate the DC, immediate enamel bond strength (IEBS), antimicrobial ac-

https://doi.org/10.5395/rde.2026.51.e2

tivity, and release of the active principle of a resin-based material enriched with powdered *S. brasiliensis* (Braúna) stem extract. The null hypothesis posits that incorporating *S. brasiliensis* stem extract in the resin-based material does not alter the tested properties.

METHODS

Ethical considerations

This study followed the CRIS (Checklist for Reporting *In-vitro* Studies) guidelines of the 2014 concept note for *in vitro* studies [11]. This study was approved by the Research Ethics Committee of Universidade Federal do Rio Grande do Norte (certificate of presentation for ethical appreciation No. 59712722.2.0000.5537).

Experimental design, sample size, and randomization

This *in vitro* experimental study investigated the dependent variables: DC, IEBS, failure mode, antimicrobial activity, and release of the active principle. The independent variables consisted of different concentrations of the powdered *S. brasiliensis* stem extract (0 wt%, 1.25 wt%, 2.5 wt%, 5 wt%, 10 wt%, and 20 wt%). The sample size was defined for each test according to previous investigations [12–16], and the specimens underwent testing in a randomized manner through a selection process utilizing numerical identifiers corresponding to the specimens within each group. The materials and instruments used in this investigation are shown in Table 1.

Extract preparation

The extract of *S. brasiliensis* preparation followed a previously described method [10]. Stem barks of *S. brasiliensis* were collected from the herbarium of the Universidade Federal da Paraíba (EAN-14049) in the semi-arid region of Sertão da Paraíba, Brazil. The barks were dried at 40°C ± 1°C (Figure 1) and then subjected to extraction using ethanol (Merck, Darmstadt, Germany) as the solvent. The percolation process was conducted in three cycles at 30°C for 5 days. The ethanolic extract underwent concentration in a rotary vacuum evaporator operating at 40°C and 55 revolutions/min until complete solvent removal.

Modified resin-based material preparation

The modified resin-based materials were prepared by homogenizing the powdered *S. brasiliensis* extract with Fluroshield (Dentsply Sirona, Petrópolis, RJ, Brazil), a commercial light-cured fluoride-releasing resin sealant, in the following proportions: 1.25 wt%, 2.5 wt%, 5 wt%, 10 wt%, and 20 wt%. According to the manufacturer, the Fluroshield composition includes urethane-modified bisphenol A-glycidyl methacrylate (Bis-GMA) dimethacrylate (<40%), Bis-GMA (<20%), other polymerizable dimethacrylate resins (<20%), barium boron alumino silicate glass (<30%), sodium fluoride (<5%), and dipentaerythritol pentaacrylate phosphate (<5%). Initially, a 220-g ATY224 Precision Analytical Balance (Shimadzu, Kyoto, Japan) weighed 1 g of the material. The extract was macerated with a pestle in a grater (Chiarotti, Mauá, SP, Brazil) to ensure complete disintegration of the grains, and the resulting powder was weighed according to the proportion established for each group (Figure 1). Homogenization was performed manually using a

Table 1. Specifications of materials and instruments used in the research

Material	Trade Name	Shade	Lot	Composition/ pecifications
Fissure sealant	FluroShield (Dentsply Sirona, Petrópolis, RJ, Brazil)	Matte	376737N	Urethane modified Bis-GMA dimethacrylate (<40%); barium boron alumino silicate glass (<30%); polymerizable dimethacrylate resins (<20%); Bis-GMA (<20%); sodium fluoride (<5%); dipentaerythritol pentaacrylate phosphate (<5%)
Adhesive system	Adper Single Bond 2 (3M ESPE, Maplewood, MN, USA)	-	2100700761	Ethyl alcohol (25%–35%); Bis-GMA (10%–20%); silane treated silica (10%–20%); HEMA (5%–15%); copolymer of acrylic and itaconic acids (5%–10%); glycerol 1,3 dimethacrylate (5%–10%); UDMA (<5%); water (<5%); diphenyliodonium hexafluorophosphate (<0.5%)
Phosphoric acid	UltraEtch, (Ultradent, Salt Lake City, UT, USA)	-	-	Phosphoric acid (<40%); cobalt aluminate blue spinel (<1%); siloxane (<1%)
Light-curing unit	Valo Grand Cordless, (Ultradent)	-	-	Standard power 1,000 mW/cm^2

Bis-GMA: bisphenol A-glycidyl methacrylate; HEMA: 2-hydroxyethyl methacrylate; UDMA, urethane dimethacrylate.

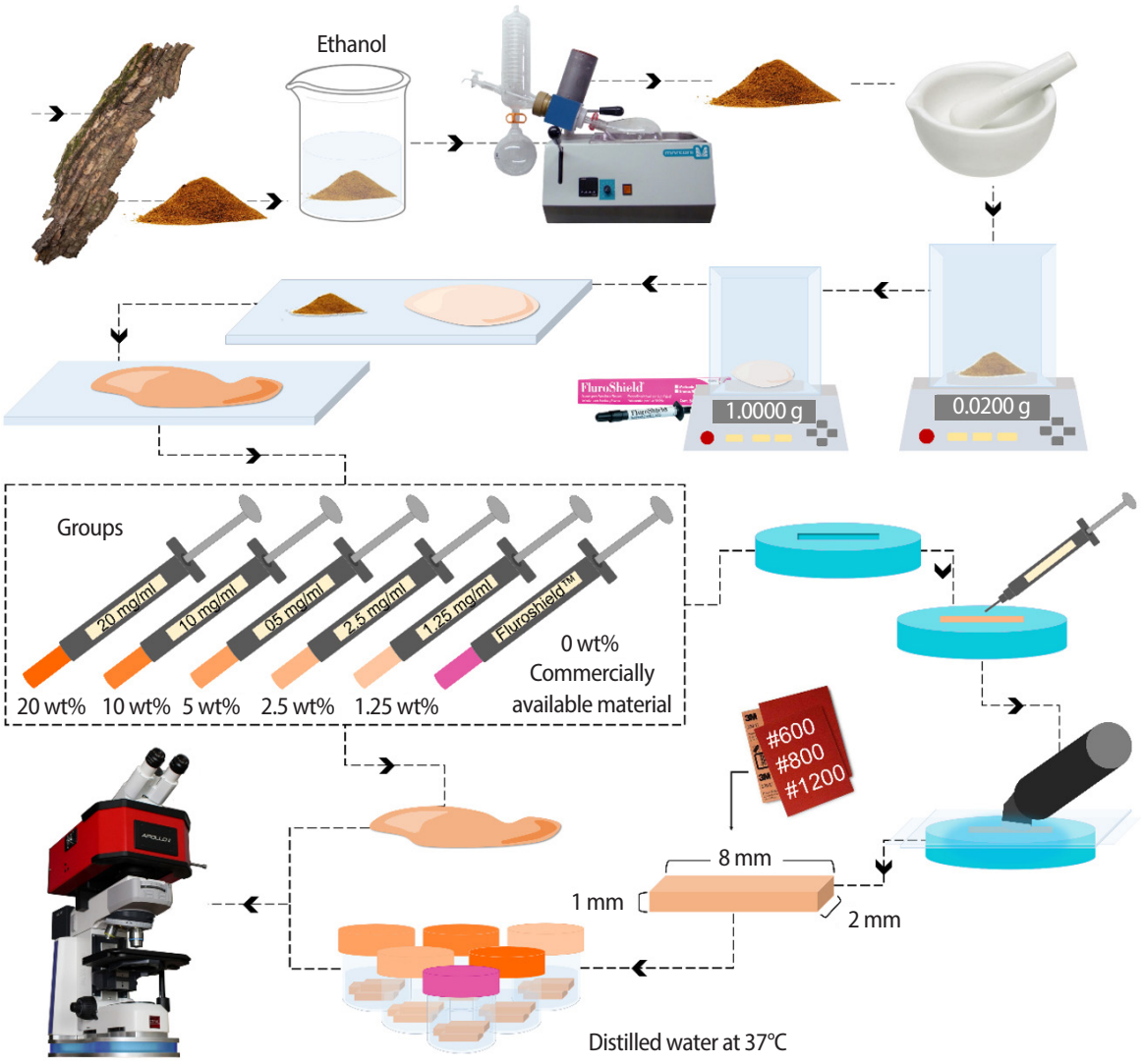

Figure 1. Schematic representation of the extract preparation and fissure sealant handling. Stem bark dried and crushed with ethanol, followed by rotary evaporation to obtain pure powder. The powder was macerated and filtered to remove grains, weighed with the sealant, and mixed. The mixture was then placed in syringes for group allocation. For the degree of conversion, specimens were prepared using a silicone matrix, covered with a polyester strip and glass slide, photoactivated for 40 seconds, sanded, and stored for micro-Raman analysis.

spatula on a glass plate and occurred in an environment protected from light exposure to prevent unwanted photoactivation of the product. Subsequently, the mixtures were labeled and stored in disposable syringes, protected from light, until further testing.

Degree of conversion

DC was measured using micro-Raman spectroscopy. Specimens were prepared by forming bars (n = 7 per group) using a silicone matrix (Express XT, Soft Dense Paste; 3M ESPE, Maplewood, MN, USA) with dimensions of 8 mm (length)× 2 mm (width)× 1 mm (height). The material application was carried out with syringe applicator tips. A polyester strip and a glass slide were placed over the material to standardize the photoactivation distance, which was photoactivated for 40 seconds using a third-generation light-emitting diode (LED) device (Valo Grand Cordless, 1,000 mW/cm^2; Ultradent, Salt Lake City, UT, USA). Subsequently, all specimens were manually finished and polished using #600, #800,

https://doi.org/10.5395/rde.2026.51.e2

and #1200 water sandpaper (3M ESPE). Figure 1 presents a schematic illustration of the extract preparation and specimen fabrication procedures.

The bars were immersed in distilled water at 37°C for 24 hours and analyzed using micro-Raman spectroscopy (FORAM, CRAIC Technologies, San Dimas, CA, USA) with 785 nm laser excitation, 50× lens, and 50% power (90 mW) for 60 seconds. For unpolymerized materials, three readings were taken, and the average was used to calculate the DC. For polymerized materials, readings were taken on each bar. Measurements were performed at least 1 mm away from the edges of the specimens. The DC was calculated by comparing the relative change in the peak height of the vinyl C=C band (1,640 cm^{-1}) before (unpolymerized) and after polymerization (polymerized) using the following equation:

$$DC\ (\%) = 100 \times [1 - R_{polymerized}/R_{unpolymerized}]$$

where R is the ratio of aliphatic (1,640 cm^{-1}) and aromatic (1,610 cm^{-1}) peak intensities.

Immediate enamel bond strength

The IEBS was assessed through the shear bond strength test. Proximal surfaces of human third molars were sectioned with standardized dimensions of 3 mm × 3 mm × 2 mm thickness, yielding 42 enamel specimens (n = 7 per group). These specimens were obtained using diamond discs under refrigeration (KG Sorensen, Cotia, SP, Brazil), following a method previously described [17]. The specimens were affixed in circular holders for adaptation in the universal testing machine, using epoxy-based resin (Redelease, Vila Arcadia, SP, Brazil), ensuring only the flat surface of the dental enamel was exposed (Figure 2).

The enamel surface of each specimen underwent conditioning with phosphoric acid (Ultradent) for 15 seconds, followed by a 30-second rinse and air drying at 15 cm for 10 seconds. Two layers of Adper Single Bond 2 adhesive (3M ESPE) were applied with friction

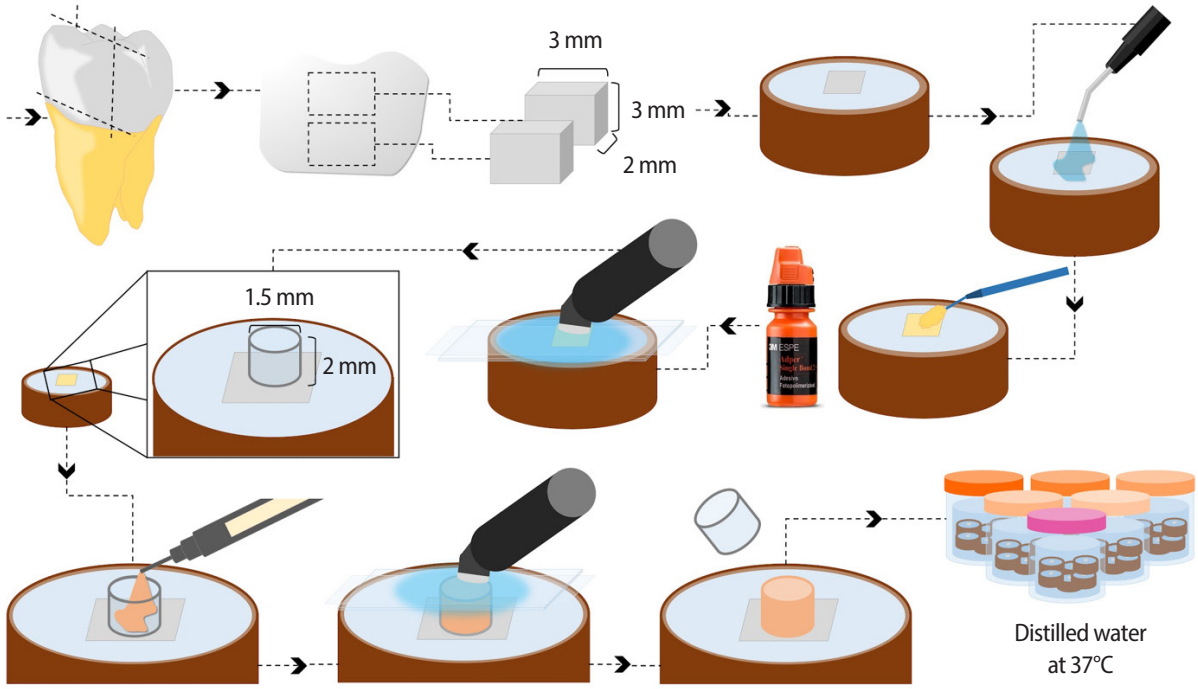

Figure 2. Schematic representation of immediate enamel bond strength specimen preparation. Sectioning of the third molars was followed by proximal cuts that generated sub-fragments with standardized sizes. The sub-fragments were soaked in polystyrene resin, exposing the enamel. A 35% phosphoric acid solution was applied for 15 seconds, followed by washing for 30 seconds and air drying. Two layers of adhesive were then applied. A polyester strip and glass slide were positioned, and photoactivation was performed for 10 seconds. A plastic microtubule was then placed on the enamel and filled with the experimental sealants. The strip and slide were repositioned, followed by photoactivation for 40 seconds. Finally, the plastic tubule was removed, leaving a cylindrical sample of sealant on the enamel, which was stored in distilled water.

on the etched surface, followed by photoactivation for 10 seconds using a third-generation LED device (Valo Grand Cordless, 1,000 mW/cm^2) [18,19]. Subsequently, a cylindrical plastic tubule with a diameter of 1.5 mm (Labor Import, Osasco, SP, Brazil) was cut into standardized pieces of 2 mm height and positioned over the tooth. The modified resin-based material was deposited carefully inside the tubule to avoid bubble formation. A polyester strip and a glass slide were used to ensure a standardized light-curing distance, and photoactivation was performed for 40 seconds. Following photoactivation, the plastic tubule was removed, resulting in cylindrical specimens composed only of the materials of the studied groups on the dental enamel (1.5 mm in diameter, 2 mm in height), which were stored in distilled water for 24 hours in an incubator at 37°C. Figure 2 presents a schematic illustration of the IEBS specimen preparation.

To assess the IEBS, the specimens were positioned in the Universal Testing Machine OM100 (Odeme, Luzerna, SC, Brazil), and a hard steel orthodontic wire (Morelli, Sorocaba, SP, Brazil) was aligned parallel to the dental surface, encircling the cylindrical specimen. This arrangement subjected the specimen to a shear force using a load cell with a capacity of up to 50 Kgf at a speed of 0.5 mm/min. The recorded data included the load required to rupture the specimen. The maximum value of micro-shear strength was determined by dividing the force needed to rupture the specimen (N) by the adhesive surface area (mm^2).

Failure mode

The failure mode was analyzed using a stereomicroscope (Infinity 1, SMZ800; Nikon, Melville, NY, USA) with a 50× magnification lens. Failures were classified into adhesive, cohesive (in enamel or the material), and mixed categories. Adhesive failure occurs at the interface between the material and the tooth. Cohesive enamel failure happens within dental enamel without affecting the bond with the material. Cohesive material failure involves a fracture within the material itself. Mixed failure combines two or more patterns [17].

Antimicrobial assay

1. Saliva collection

Stimulated saliva was collected in a sterile 2-mL Eppendorf tube from a randomly selected donor registered in the research laboratory after signing the informed consent form regarding the donation of the material. Before collection, the donor refrained from oral hygiene for 12 hours. The collected saliva was centrifuged at 2,000 ×*g* for 10 minutes. Subsequently, 50 μL of the supernatant was diluted in 35 mL of brain heart infusion (BHI) broth, following a predefined proportion [20].

2. Antimicrobial activity

Antimicrobial activity was assessed through the colony-forming unit (CFU) count test. Circular specimens (n = 15 per group) measuring 5 mm × 1 mm were created using a silicone matrix (Express XT, Soft Dense Paste). The material for each experimental group was applied to the circular matrix with a syringe applicator tip. A polyester strip and a glass slide were then placed over the material to standardize the photoactivation distance, and photoactivation was performed for 40 seconds (Valo Grand Cordless, 1,000 mW/cm^2). All specimens underwent manual finishing and polishing with #600, #800, and #1200 water sandpaper (3M ESPE).

The specimens were positioned at the bottom of wells in 48-well plates and covered with culture medium containing the inoculum (BHI broth and saliva). The positive control included 0.12% chlorhexidine digluconate (Sigma-Aldrich, Jurubatuba, SP, Brazil). In addition to the groups with specimens made from materials with different concentrations of the extract, the same mass concentrations used to create the materials' groups were diluted in distilled water, resulting in five other control groups: E1, E2, E3, E4, and E5. The plates were then incubated at 37°C ± 1°C for 24 hours. After this period, 10-μL aliquots from each well were taken, seeded onto a Petri dish containing BHI agar (in triplicate), and incubated for 24 hours at 37°C to assess microbial growth. The CFUs were counted to verify microbial viability. Figure 3 presents a schematic illustration of the antimicrobial assay.

Release of the active principle

The release of the active principle was evaluated through ultra-high-performance liquid chromatography (UHPLC), following previously established standards [21,22]. Gallic acid was a marker substance [23]. The proximal

https://doi.org/10.5395/rde.2026.51.e2

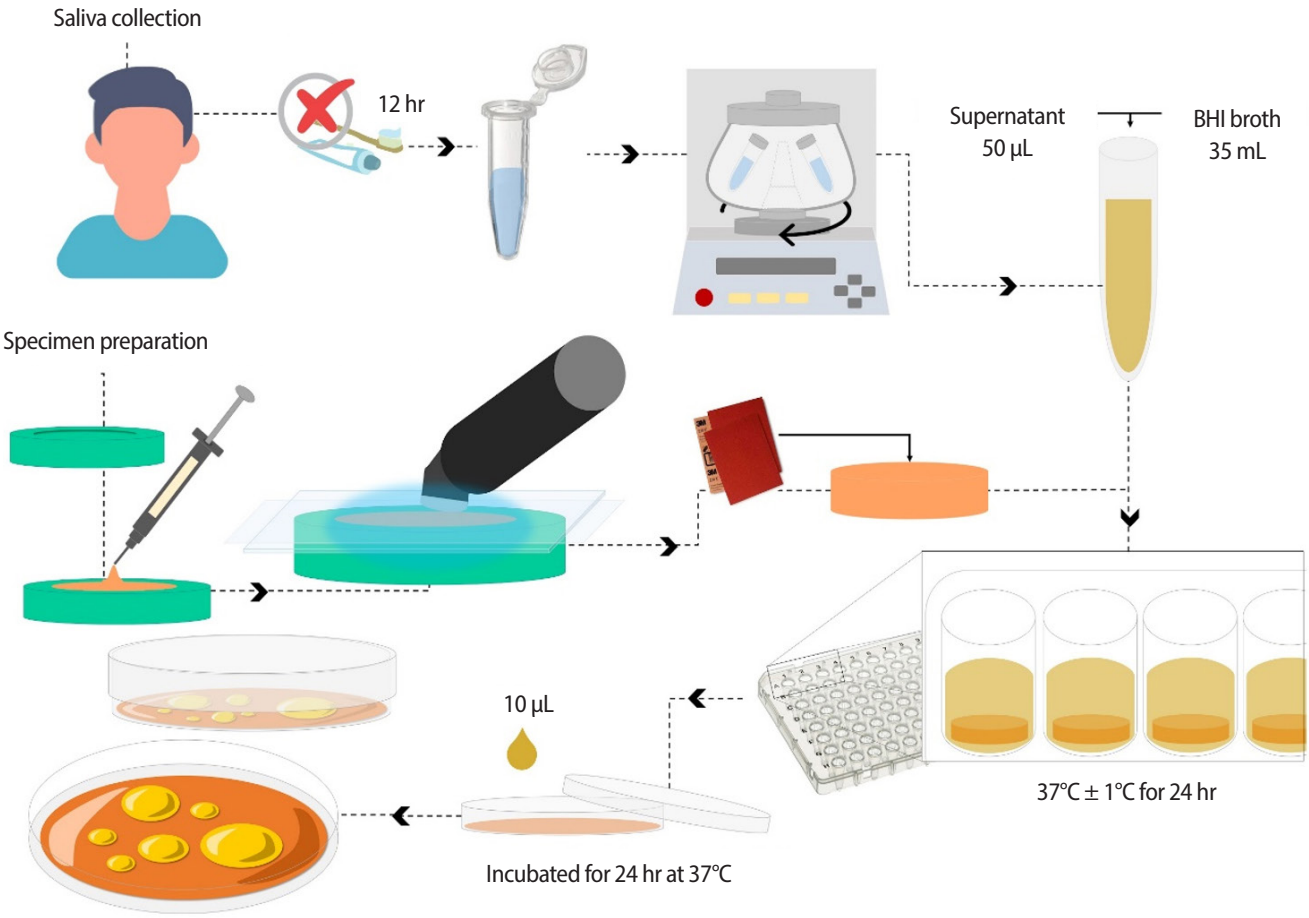

Figure 3. Schematic representation of the antimicrobial assay. Saliva was collected from the donor after 12 hours without oral hygiene and placed in an Eppendorf tube containing 2 mL of saliva. The sample was centrifuged at 2,000 ×g for 10 minutes, and 50 µL of the supernatant was mixed with 35 mL of brain heart infusion (BHI) broth to prepare the inoculum. Sealant specimens were made using a circular matrix, covered with a polyester strip and glass plate, and photoactivated for 40 seconds. The specimens were finished and inserted into wells containing the inoculum, where they remained in contact for 24 hours. Then, 10-µL aliquots were transferred in triplicate to Petri dishes, and colony-forming unit counting was performed after 24 hours.

surfaces of nine human third molars donated after signing a consent statement were utilized to produce rectangular specimens with dimensions of 5 mm × 2 mm with a thickness of 3 mm ($n = 3$ per group), simulating the size of the main groove of a molar that would be sealed with the resin-based material. Figure 4 presents a schematic representation of the release of the active principle assay.

These specimens were placed in a silicone mold positioned one mm above the specimen surface, standardized with a 150-mm digital caliper rod (MTX, Guarulhos, SP, Brazil), resulting in a volume of 10 mm^3. The material was applied to this space using syringe applicator tips, covered with a polyester strip and a glass slide, and photoactivated for 40 seconds (Valo Grand Cordless, 1,000 mW/cm^2). Following photoactivation, the specimens were manually sanded with #600, #800, and #1200 water sandpaper (3M ESPE) and stored in a solution of methanol (75%)/H_2O (25%) for 48 hours.

The gallic acid release was quantified using a high-performance liquid chromatography (HPLC) with diode array detector (DAD) coupled to a UHPLC (Shimadzu). The equipment included a binary analytical pump (LC-20A3 XR), an automatic injector (SIl-20AD XR), a degasser (DGU-20A3), a column oven (CTO-20AC), and a DAD (SPD-M20A). The analysis utilized a Zorbax

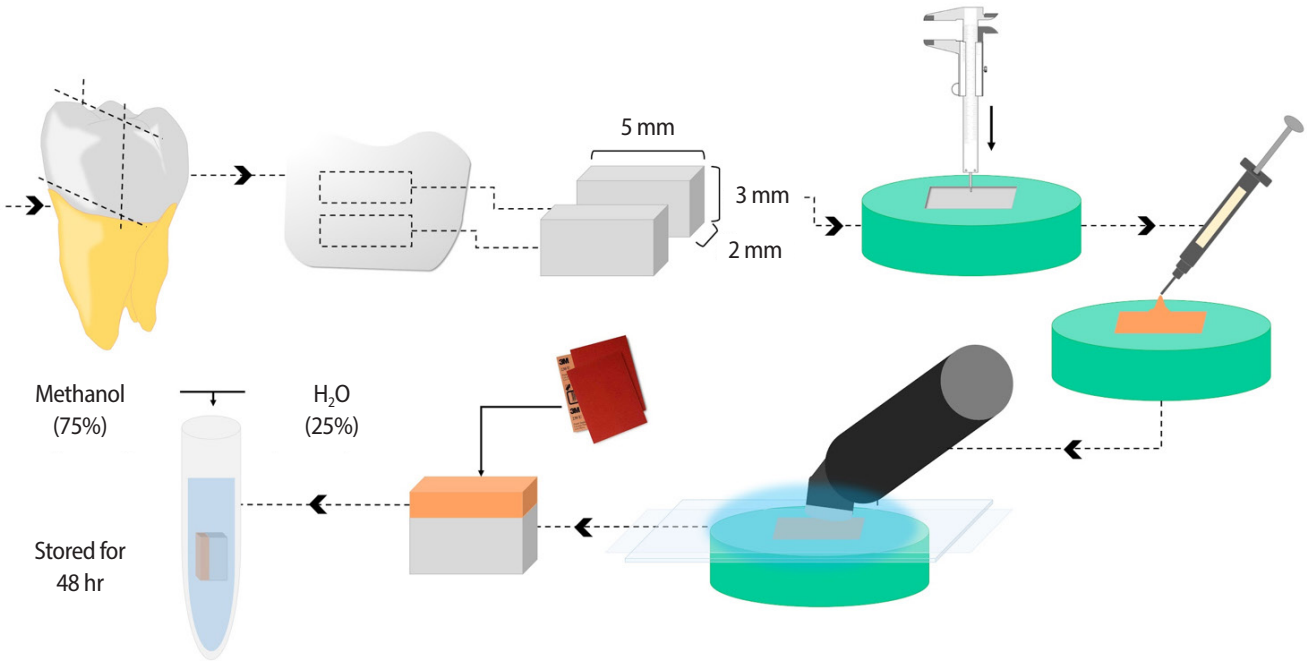

Figure 4. Schematic representation of the release of the active principle assay. Healthy molars were sectioned, and the specimens were cut to standard sizes. Each specimen was immersed in silicone, leaving a 1-mm (10 mm^3) gap that was measured using a caliper. The fissure sealant was then inserted, followed by the positioning of a polyester strip and glass slide. Photoactivation was performed for 40 seconds. The specimens were manually finished with sandpaper, and the final appearance of the tooth and sealant was documented. Finally, the specimens were immersed in a water-methanol solution for 48 hours.

Eclipse Plus C18 column (Phenomenex, Torrance, CA, USA) controlled by the LC Solution software (Shimadzu). The wavelength employed was 272 nm, with a flow rate of 1.0 mL/min and a temperature of 30°C. The mobile phase consisted of formic acid 1%: methanol 90:10 (v/v), and the specimen injection volume was 0.4 µL.

Statistical analysis

The final values of the samples for each test underwent a normality assessment using the Shapiro-Wilk test ($p > 0.05$) and the Levene test. Parametric data underwent analysis of variance, followed by the Tukey test ($p < 0.05$). Nonparametric data underwent the Kruskal-Wallis test ($p < 0.05$), followed by the Dunn test. All analyses were conducted using Prism 8 software (Insight Venture Partners, GraphPad Holdings, LLC, San Diego, CA, USA) and Microsoft Excel 2018 (Microsoft, Redmond, WA, USA). Parametric data are presented as means ± standard deviations. Nonparametric data are presented as median (range). The quantity of the active principle released and failure modes were analyzed descriptively.

RESULTS

Degree of conversion, immediate enamel bond strength, and failure modes

Statistically significant differences were observed among the concentrations of powdered *S. brasiliensis* stem extract, regarding the DC ($p < 0.05$). Table 2 presents the group comparisons. The control group exhibited the highest mean value (68.34 ± 2.5), followed by concentrations of 1.25 wt% (64.09 ± 3.16), 2.5 wt% (61.71 ± 5.2), groups, with no statistically significant differences among them. The 5 wt% group (50.0 ± 7.0) showed a statistically lower value than the control, while the 10 wt% (37.11 ± 5.6) and 20 wt% (33.84 ± 7.7) groups exhibited the lowest mean values, differing significantly from the lower-concentration groups.

Regarding immediate bond strength to dental enamel, no statistically significant differences were observed among the tested concentrations of powdered *S. brasiliensis* stem extract ($p > 0.05$). The mean and standard deviation values for each group, as detailed in Table 2,

https://doi.org/10.5395/rde.2026.51.e2

Table 2. The degree of conversion, IEBS, and failure mode according to the different concentrations of powdered *Schinopsis brasiliensis* stem extract ($p < 0.05$)

Group	Degree of conversion (%)	IEBS (MPa)	Failure mode (%), adhesive/mixed
Control (0 wt%)	68.34 ± 2.5^{A}	4.04 ± 0.92^{A}	85/15
1.25 wt%	64.09 ± 3.16^{AB}	4.30 ± 1.91^{A}	70/30
2.5 wt%	61.71 ± 5.2^{AB}	3.71 ± 1.02^{A}	85/15
5 wt%	50.0 ± 7.0^{B}	3.24 ± 0.64^{A}	70/30
10 wt%	37.11 ± 5.6^{C}	4.31 ± 1.90^{A}	70/30
20 wt%	33.84 ± 7.7^{C}	4.11 ± 2.03^{A}	85/15

Values are presented as mean ± standard deviation.
Different capital letters indicate statistically significant differences between groups in each column ($p < 0.05$).
IEBS, immediate enamel bond strength.

were comparable, indicating that the incorporation of the extract did not have a measurable effect on the bond strength to enamel. A notable finding, observed across all groups, was the predominance of adhesive failure, as also presented in Table 2. This suggests that the bond interface was the weakest point, a characteristic that was consistent regardless of the extract concentration used.

Antimicrobial activity

Statistically significant differences were observed among the tested groups ($p < 0.05$). The materials groups with 20 wt% (0; range, 0–0) and 10 wt% extract (45.5; range, 16–79) demonstrated an ability to inhibit microbial growth statistically similar ($p > 0.05$) to the positive control, 0.12% chlorhexidine digluconate (0; range, 0–0). Other groups exhibited uncountable CFU values (999; range, 999–999), which were statistically similar ($p > 0.05$) to the negative control, distilled water (999; range, 999–999).

Solutions containing water and 20 wt% (0; range, 0–0), 10 wt% (0; range, 0–0), and 5 wt% extract (246.5; range, 115–362) showed a statistically similar ability to inhibit microbial growth ($p > 0.05$) compared with the positive control, 0.12% chlorhexidine digluconate (0; range, 0–0). Other solutions exhibited uncountable CFU values (999; range, 999–999), statistically similar to the negative control, distilled water (999; range, 999–999).

Release of the active principle

Qualitative analysis of the experimental groups revealed that all groups, regardless of the concentration of the powdered *S. brasiliensis* stem extract, were capable of releasing the active principle. The successful release was consistently demonstrated by measuring the presence of the chemical marker, gallic acid, in the aqueous medium (methanol 75%/H_2O 25%). This consistent finding across all tested concentrations highlights that the incorporation of the extract into the material did not hinder the release mechanism. Thus, the extract's ability to be released from the material was maintained, providing a foundation for potential biological activity in subsequent analyses.

DISCUSSION

The null hypothesis, which stated that incorporating powdered *S. brasiliensis* stem extract would not alter the tested properties, was rejected based on statistically significant reductions in the DC at higher concentrations (10 wt% and 20 wt%), and enhanced antimicrobial activity observed at these same concentrations, compared to the control ($p < 0.05$).

In this study, higher concentrations of powdered *S. brasiliensis* stem extract were associated with a lower DC, showing an approximate 30% reduction compared to the control group. Higher concentrations of the extract can act as a physical barrier to the passage of light in the material, potentially reducing the percentage of monomer-to-polymer conversion. However, even the 5 wt% group (50.0 ± 7.0) was inferior to the 10 wt% and 20 wt%, it still demonstrated an acceptable conversion value (50%) for resin-based materials, falling within 50% to 75% [24]. The selection of a pit and fissure sealant as the resin-based composite material to be modified in this study is supported by previous research that highlights

the use of sealants as a foundation for incorporating antimicrobial agents [25].

In addition to monomer conversion, evaluating the impact of extract addition on adhesion potential becomes crucial. While Fluroshield is a resin-based sealant that does not mandate the use of an adhesive system, a systematic review with meta-analysis has shown that applying a conventional two-step adhesive system, such as Adper Single Bond 2, enhances the retention of the material [19]. Consequently, given that the application of adhesive systems is a standard procedure for resin-based restorations, Adper Single Bond 2 was used prior to the sealant to replicate a common clinical protocol designed to improve adhesion. This also ensured standardized and reproducible adhesion conditions across all samples, facilitating reliable comparative analysis. In this study, IEBS results indicate no statistically significant differences between the experimental materials and the highly positive control group. These findings suggest that incorporating the *S. brasiliensis* extract did not impair the adhesive performance of the resin-based sealant. This outcome is particularly relevant given that bond strength is a critical factor in ensuring the success and longevity of sealants [26]. Similar results have been reported in studies evaluating non-self-adhesive sealants, where conventional bonding protocols are employed to enhance retention and minimize microleakage. Pitchika *et al.* [26] demonstrated that a separate bonding step prior to sealant application significantly improved shear bond strength compared to self-etch systems applied alone, highlighting the importance of the adhesive interface in clinical performance. Although immediate bond strength is an important indicator, it does not account for long-term degradation phenomena such as hydrolysis or mechanical fatigue. Therefore, future studies should focus on evaluating bond durability over time, especially in aged specimens, to determine whether the addition of plant-derived components affects adhesive stability under intraoral conditions.

The occurrence of adhesive and mixed failures aligns with the typical observation of debonded fissure sealants [27]. The predominance of adhesive and mixed failures observed in this study is consistent with previous findings for conventional fissure sealants [26], where similar failure modes were identified following shear bond strength testing. Notably, the control group, without the *S. brasiliensis* extract, exhibited failure patterns comparable to the experimental groups, suggesting that the incorporation of the extract did not negatively affect the adhesive interface or compromise the material's cohesive strength. The retention of sealant remnants within the deeper fissures, even after partial failure, may maintain the release of bioactive compounds, potentially prolonging antimicrobial action at the tooth–material interface. Nevertheless, this hypothesis warrants further investigation, particularly through studies evaluating sustained release and long-term antibacterial efficacy.

It is noteworthy that the characteristics of plant-derived secondary metabolites can be influenced by several factors, such as the climatic conditions of the collection period (rainfall index during that period), seasonality, and the presence of natural predators [28,29]. Thus, adding the powdered pure extract diluted in a water-based environment aimed to validate its isolated antimicrobial effect in the same concentrations included in the resin-based material. Considering the wide array of chemical combinations that can occur when adding a plant extract to a resin-based material, it is essential to characterize this extract as isolated chemically. In a previous study using HPLC, gallic acid was obtained as the main active principle of *S. brasiliensis* stem extract [23], so it was utilized in this study as well.

Incorporating powdered functional substances into resin-based materials, such as a fissure sealant, which undergoes a polymerization process resulting in a highly dense polymeric network, raises uncertainty about whether these molecules can detach from these chains and be released into aqueous environments. The release into a water-based environment was evaluated using UHPLC, simulating what would occur in saliva in the oral environment. Upon qualitative analysis of the results, it was observed that all experimental groups could release gallic acid into the aqueous medium where the specimens were immersed for 48 hours.

In the present study, all concentrations of powdered *S. brasiliensis* stem extract added to resin-based material were higher than the previously determined minimum inhibitory concentration of 0.5 mg/mL for *S. mutans*, *Streptococcus oralis*, *S. mitis*, and *S. salivarius* [9,21]. However, only extract concentrations above 10 wt%

https://doi.org/10.5395/rde.2026.51.e2

demonstrated antimicrobial activity in the resin-based materials tested. It can be inferred that concentrations below 10 wt% of extract in the material, although releasing the chemical marker, do not sufficiently impair bacterial growth.

On the other hand, the two highest concentrations of extract into the material (10 wt% and 20 wt%) provided statistically similar values to the positive control (0.12% chlorhexidine digluconate), confirming the release of antimicrobial agents from the polymer chain into the water-based environment in therapeutic quantities. Thus, although all materials released the active principle, they may have been released in different quantities, which should be further evaluated.

This study presents limitations that should be acknowledged. Although a multispecies biofilm model derived from stimulated saliva was employed, the specific microbial taxa affected by the antimicrobial activity of the extract were not identified, despite previous studies demonstrating proven activity against *S. mutans*, *S. oralis*, *S. mitis*, and *S. salivarius* [9,30,31]. Therefore, additional investigations are necessary to deepen the understanding of the interactions between caries-associated microorganisms and the bioactive compounds released from the resin-based material containing powdered *S. brasiliensis* stem extract. Moreover, long-term outcomes, such as the stability of the antimicrobial effect and the sustained release of active components, were not addressed in this study. Future research should include microbial profiling and prolonged evaluation periods to validate and expand the current findings.

The methods and results presented in this study empower researchers to investigate a range of alternative extract concentrations and synthesize a drug delivery system. Also, further investigations might develop a drug delivery system by conjugating gallic acid to a nanocarrier and incorporating it into resin-based dental materials. This proposed approach would be an alternative to formulating antimicrobial materials, including resin-based fissure sealants, resin composites, adhesive systems, luting agents, and resin-modified glass ionomer, which should be further evaluated.

CONCLUSIONS

Incorporating powdered *S. brasiliensis* stem extract at concentrations of 10 wt% and 20 wt% showcased the capability to augment the antimicrobial effect of the tested resin-based material. While higher concentrations led to a reduction in conversion, the immediate bonding potential remained constant, and the primary type of failure observed was adhesive. All experimental groups demonstrated the ability to release the active agent when immersed in a water-based environment.

CONFLICT OF INTEREST

No potential conflict of interest relevant to this article was reported.

FUNDING/SUPPORT

The authors have no financial relationships relevant to this article to disclose.

AUTHOR CONTRIBUTIONS

Conceptualization, Project administration, Supervision, Validation: Borges BCD; Data curation: Borges BCD, Sousa-Lima RX. Formal analysis: Marinho MELN, Sousa-Lima RX; Investigation: Silva JCC, Marinho MELN, Sousa-Lima RX, Costa MJF, Sette-de-Souza PH. Methodology: Borges BCD, Sousa-Lima RX, Sette-de-Souza PH. Writing - original draft: Marinho MELN, Sousa-Lima RX. Writing - review & editing: Lima GS, Borges BCD. All authors read and approved the final manuscript.

DATA SHARING STATEMENT

The datasets are not publicly available but are available from the corresponding author upon reasonable request.

REFERENCES

1. Zhang X, Zhang Q, Meng X, Ye Y, Feng D, Xue J, *et al*. Rheological and mechanical properties of resin-based materials applied in dental restorations. Polymers (Basel) 2021;13:2975.
2. Barot T, Rawtani D, Kulkarni P, Hussain CM, Akkireddy S. Physicochemical and biological assessment of flowable resin composites incorporated with farnesol loaded halloysite nanotubes for dental applications. J Mech Behav Biomed Mater 2020;104:103675.
3. German MJ. Developments in resin-based composites. Br Dent J 2022;232:638-643.

4. Nedeljkovic I, De Munck J, Ungureanu AA, Slomka V, Bartic C, Vananroye A, *et al*. Biofilm-induced changes to the composite surface. J Dent 2017;63:36-43.
5. Demarco FF, Collares K, Correa MB, Cenci MS, Moraes RR, Opdam NJ. Should my composite restorations last forever?: why are they failing? Braz Oral Res 2017;31(suppl 1):e56.
6. Demarco FF, Cenci MS, Montagner AF, de Lima VP, Correa MB, Moraes RR, *et al*. Longevity of composite restorations is definitely not only about materials. Dent Mater 2023;39:1-12.
7. Sales-Junior RA, de Bessa MS, Oliveira FJ, Barbosa BF, Santos KS, Owen M, *et al*. Multifaceted characterization of antibacterial resin composites: a scoping review on efficacy, properties, and in vivo performance. Jpn Dent Sci Rev 2025;61:112-137.
8. Comeau P, Panariello B, Duarte S, Manso A. Impact of curcumin loading on the physicochemical, mechanical and antimicrobial properties of a methacrylate-based experimental dental resin. Sci Rep 2022;12:18691.
9. Barreto Linhares LP, Pereira BV, Dantas MK, Bezerra WM, Viana-Marques DA, de Lima LR, *et al*. Schinopsis brasiliensis Engler-phytochemical properties, biological activities, and ethnomedicinal use: a scoping review. Pharmaceuticals (Basel) 2022;15:1028.
10. Sette-DE-Souza PH, Santana CP, Sousa IM, Foglio MA, Medeiros FD, Medeiros AC. Schinopsis brasiliensis Engl. to combat the biofilm-dependents diseases in vitro. An Acad Bras Cienc 2020;92:e20200408.
11. Krithikadatta J, Gopikrishna V, Datta M. CRIS guidelines (Checklist for Reporting In-vitro Studies): a concept note on the need for standardized guidelines for improving quality and transparency in reporting in-vitro studies in experimental dental research. J Conserv Dent 2014;17:301-304.
12. Hu YT, Yu F, Tang XY, Wu WZ, Zhang P, Hu ZH, *et al*. The antibacterial effect and physical performance of pit and fissure sealants based on an antibacterial core-shell nanocomposite. J Mech Behav Biomed Mater 2021;117:104414.
13. Lai CC, Lin CP, Wang YL. Development of antibacterial composite resin containing chitosan/fluoride microparticles as pit and fissure sealant to prevent caries. J Oral Microbiol 2022;14:2008615.
14. Khan MA, Muhammad N, Liaqat S, Ejaz M, Fayyaz S, Ali H, *et al*. Mechanical and antibacterial properties of conventional pit and fissure sealants with addition of miswak fibers. Biomater Investig Dent 2023;10:2271972.
15. Borges BC, Souza-Júnior EJ, Catelan A, Lovadino JR, Dos Santos PH, Paulillo LA, *et al*. Influence of extended light exposure time on the degree of conversion and plasticization of materials used as pit and fissure sealants. J Investig Clin Dent 2010;1:151-155.
16. Feitosa S, Carreiro AFP, Martins VM, Platt JA, Duarte S. Effect of a chlorhexidine-encapsulated nanotube modified pit-and-fissure sealant on oral biofilm. Dent Mater J 2021;40:758-765.
17. Borges BC, Catelan A, Sasaki RT, Ambrosano GM, Reis AF, Aguiar FH. Effect of the application of a casein phosphopeptide-amorphous calcium phosphate (CPP-ACP) paste and adhesive systems on bond durability of a fissure sealant. Odontology 2013;101:52-59.
18. Bedran-Russo A, Leme-Kraus AA, Vidal CMP, Teixeira EC. An overview of dental adhesive systems and the dynamic tooth-adhesive interface. Dent Clin North Am 2017;61:713-731.
19. Bagherian A, Sarraf Shirazi A, Sadeghi R. Adhesive systems under fissure sealants: yes or no?: a systematic review and meta-analysis. J Am Dent Assoc 2016;147:446-456.
20. An SQ, Hull R, Metris A, Barrett P, Webb JS, Stoodley P. An in vitro biofilm model system to facilitate study of microbial communities of the human oral cavity. Lett Appl Microbiol 2022;74:302-310.
21. Sette-de-Souza PH, de Santana CP, Amaral-Machado L, Duarte MC, de Medeiros FD, Veras G, *et al*. Antimicrobial activity of Schinopsis brasiliensis Engler extract-loaded chitosan microparticles in oral infectious disease. AAPS PharmSciTech 2020;21:246.
22. Sousa-Lima R, Justo-Fernandes A, Kaizer M, Isolan C, Moraes R, Aragão C, *et al*. Monomer conversion, release and cytotoxicity analyses of experimental GDMA-P based adhesives. Int J Adhes Adhes 2021;105:102792.
23. Fernandes FH, de Batista RS, de Medeiros FD, Santos FS, Medeiros AC. Development of a rapid and simple HPLC-UV method for determination of gallic acid in Schinopsis brasiliensis. Rev Bras Farmacogn 2015;25:208-211.
24. Vasudeva G. Monomer systems for dental composites and their future: a review. J Calif Dent Assoc 2009;37:389-398.
25. Ibrahim MS, Garcia IM, Kensara A, Balhaddad AA, Collares FM, Williams MA, *et al*. How we are assessing the developing antibacterial resin-based dental materials?: a scoping review. J Dent 2020;99:103369.
26. Pitchika V, Birlbauer S, Chiang ML, Schuldt C, Crispin A, Hickel R, *et al*. Shear bond strength and microleakage of a new self-etch adhesive pit and fissure sealant. Dent Mater J

https://doi.org/10.5395/rde.2026.51.e2

2018;37:266-271.
27. De Araújo DF, Borges BC, Mendes AM, Souza-Junior EJ, De Assunção IV, Dos Santos AJ. CPP-ACP pretreatment effect on microshear bond strength of simplified etch-and-rinse adhesive systems plus a flowable composite to enamel. J Adhes Sci Technol 2015;29:109-115.
28. Li X, Svedin E, Mo H, Atwell S, Dilkes BP, Chapple C. Exploiting natural variation of secondary metabolism identifies a gene controlling the glycosylation diversity of dihydroxybenzoic acids in Arabidopsis thaliana. Genetics 2014;198:1267-1276.
29. Moore BD, Andrew RL, Külheim C, Foley WJ. Explaining intraspecific diversity in plant secondary metabolites in an ecological context. New Phytol 2014;201:733-750.
30. Formiga Filho AL, Carneiro VS, Souza EA, Santos RL, Catão MH, Medeiros AC. In vitro evaluation of antimicrobial photodynamic therapy associated with hydroalcoholic extracts of Schinopsis brasiliensis Engl.: new therapeutic perspectives. Photomed Laser Surg 2015;33:240-245.
31. de Lima-Saraiva SR, Oliveira FG, Junior RG, Araújo CS, de Oliveira AP, Pacheco AG, *et al*. Chemical analysis and evaluation of antioxidant, antimicrobial, and photoprotective activities of Schinopsis brasiliensis Engl. (Anacardiaceae). ScientificWorldJournal 2017;2017:1713921.

RDE Restorative Dentistry & Endodontics

Research Article

eISSN 2234-7666
Restor Dent Endod. 2026 February;51(1):e3
https://doi.org/10.5395/rde.2026.51.e3

Ex vivo comparative analysis of retrievability among four calcium silicate-based sealers for regaining apical patency

Darian Shomali[1], Timothy Kirkpatrick[2], Sang Won Kwak[3], Hyeon-Cheol Kim[3,*], Ji Wook Jeong[2,*]

[1]Department of Endodontics, School of Dentistry, The University of Texas Health Science Center at San Antonio, San Antonio, TX, USA
[2]Department of Endodontics, School of Dentistry, University of Texas Health Science Center at Houston, Houston, TX, USA
[3]Department of Conservative Dentistry and Dental Research Institute, Pusan National University School of Dentistry, Yangsan, Korea

ABSTRACT

Objectives: Efficient retrievability is a key requirement for endodontic sealers. This study evaluated the retrievability of four different calcium silicate-based sealers (CSS).

Methods: A total of 153 single-rooted human teeth with straight canals were decoronated to a standardized working length of 12 mm. The canals were negotiated to working length using K files up to size 15/.02, followed by rotary instrumentation up to 35/.04, 2 mm short of working length. The teeth were randomly assigned to five groups: NeoSEALER Flo (NEO; Avalon Biomed), Ceraseal (CS; Meta Biomed), Endosequence BC Sealer (BC; Brasseler USA), AH Plus Bioceramic Sealer (AHB; Dentsply Sirona), and a negative control group. Sealer application and obturation with a 35/.04 gutta-percha cone were performed. After incubation at 37°C in 100% humidity for 7 days, retreatment was performed until apical patency was obtained, with retrievability assessed by regaining apical patency. One-way analysis of variance and Tukey contrast test were used to determine whether there was a significant difference among the four different CSS ($p < 0.05$).

Results: Success rates in regaining apical patency were NEO (79.4%), CS (37.0%), BC (50.0%), and AHB (69.7%). NEO demonstrated the highest retrievability, while CS had the lowest ($p < 0.01$).

Conclusions: The type of CSS used has a considerable impact on retreatment difficulty. Among the tested sealers, NeoSEALER Flo showed the highest retrievability, making it the most retrievable CSS in terms of retreatment efficacy.

Keywords: Calcium silicate; Endodontics; Epoxy resin; Retreatment; Root canal sealer

Received: July 2, 2025 **Revised:** July 25, 2025 **Accepted:** August 12, 2025

Citation
Shomlai D, Kirkpatrick T, Kwak SW, Kim HC, Jeong JW. *Ex vivo* comparative analysis of retrievability among four calcium silicate-based sealers for regaining apical patency. Restor Dent Endod 2026;51(1):e3.

***Correspondence to**
Hyeon-Cheol Kim, DDS, MS, PhD
Department of Conservative Dentistry and Dental Research Institute, Pusan National University School of Dentistry, 20 Geumo-ro, Mulgeum-eup, Yangsan 50612, Korea. Email: golddent@pusan.ac.kr

Ji Wook Jeong, DMD, MSD
Department of Endodontics, School of Dentistry, The University of Texas Health Science Center at Houston, 7500 Cambridge Street, Suite 6400, Houston, TX 77054, USA. Email: Ji.wook.jeong@uth.tmc.edu

Hyeon-Cheol Kim and Ji Wook Jeong contributed equally to this work as co-corresponding authors.

INTRODUCTION

Nonsurgical endodontic retreatment is typically the first choice of treatment when an endodontic treatment fails. The goal of retreatment is to remove all the existing obturation materials from the previous root canal treatment, disinfect the entire root canal system through proper cleaning and shaping, and then obturate the canals. The success rate of retreatment shows a similar success rate in comparison to initial nonsurgical endodontic therapy [1]. Root canal obturations with short fills greater than 2 mm have been shown to have a lower success rate compared to fills within 2 mm of the apex [2]. By extending working length, cleaning and obturating to the apical foramen is a major contributing factor in determining the success of retreatment. Instrumenting the root canal mechanically and chemically the root canal to its full length directly increased the success of treatment [3,4].

Calcium silicate-based sealers (CSS) or bioceramic sealers are being used around the world today. Advantages associated with these sealers include biocompatibility with surrounding tissue and osteoconductivity, the presence of calcium phosphate, which results in a chemical composition that is similar to tooth and bone, and an improvement in dentin-to-sealer bonding [5–7]. There are a few outcome studies that show favorable results from the treatment of CSS using both warm vertical and single cone techniques [8–10], while multiple brands of bioceramic sealers have been released in the market around the world.

Retrievability is a desirable property for any root canal sealers and achieving apical patency through the adequate removal of previous root canal contents increases the survivability of the tooth [11]. While bioceramic sealers have many advantages, it is important to note that the literature on the retrievability of bioceramic sealers is not consistent [12]. Some studies have shown that conventional retreatment techniques may not effectively remove CSS [12,13]. Other studies have indicated that there is similar efficacy in retreatment for both bioceramic sealers compared to traditional sealers [14]. Moreover, it was reported that CSS was likely to be extruded through the apical foramen [15,16].

Sodium hypochlorite (NaOCl, 0.5%–6%) is a primary liquid used to clean and irrigate root canals in nonsurgical root canal treatment due to its tissue-dissolving and antibacterial efficacy [17]. In addition, NaOCl can dissolve traditional root canal sealers such as calcium hydroxide-, polyketone-, zinc oxide eugenol-, and epoxy resin-based sealers [18]. Therefore, NaOCl can be used as a solution to simultaneously remove root canal sealers and disinfect root canals in nonsurgical retreatment. However, this conventional retreatment technique using NaOCl did not considerably remove the bioceramic sealer and regain apical patency during retreatment [12]. Moreover, in the case of short obturation with a bioceramic sealer in the study, the regaining patency rate was only 30% [12]. However, only one type of CSS was used in this previous study [12].

Interestingly, a study showed that the retrievability of different brands of CSS significantly varied [19]. Therefore, clinicians need to predict the retrievability of different brands of CSS before they execute the retreatment procedure. However, in this previous study, the sample design was extremely focused on the penetrability of the sealers for regaining apical patency, and a 2 mm length of thick sealer set in the apex was tested. For this reason, the sample design might not be realistic enough to prove the retrievability of the sealers in everyday retreatment cases and the results might not reflect the clinician's decision.

This study aimed to evaluate the retrievability of four different brands of CSS in a straight root canal with a short obturation model.

METHODS

Selection of teeth

This study was exempt from review by the Institutional Review Board of the University of Texas Health Science Center at Houston for the protection of human subjects (HSC-DB-21-0088). One hundred fifty-three fully developed human extracted teeth with straight canals were selected. Exclusion criteria involved the root with curvatures, multiple canals, and calcified canals by radiographic scanning.

Root canal preparation and obturation

All teeth were decoronated to create a standardized

https://doi.org/10.5395/rde.2026.51.e3

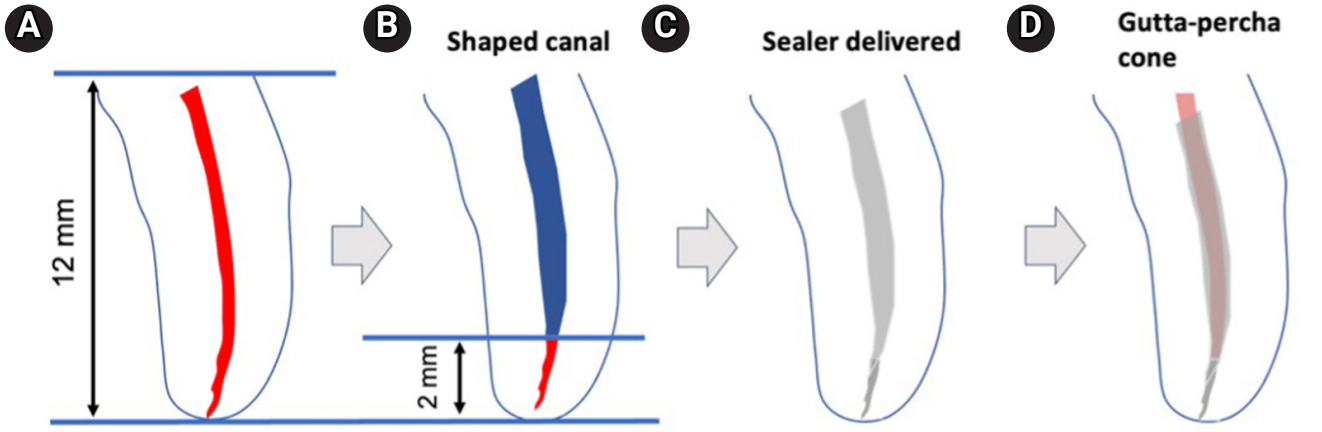

Figure 1. Schematic design of the tooth sample. (A) A decoronated tooth with a single untreated canal (red). (B) Shaped canal (blue) by instrumentation up to 35/.04, 2 mm short of the working length. (C) Injecting BC sealer (grey) into the canal. (D) A 35/.04 gutta-percha cone was placed into the sealer-filled canal.

length of 12 mm (Figure 1A). The teeth were then randomly divided into four experimental groups (n = 34) and one negative control group (n = 17). The sample size (experimental group and negative control) was determined based on our previously published study with similar experimental designs and outcomes assessing apical patency [19].

The experimental groups were based on which calcium silicate sealer was used: NeoSEALER Flo (NEO; Avalon Biomed, Houston, TX, USA), Ceraseal (CS; Meta Biomed, Colmar, PA, USA), Endosequence BC Sealer (BC; Brasseler USA, Savannah, GA, USA), AH Plus Bioceramic (AHB; Dentsply Sirona, Charlotte, NC, USA).

After working length was established with a 10/.02 K file, apical patency was achieved and confirmed by visualizing the file exiting the apical foramen. Each canal was instrumented to a 15/.02 K file at working length. The teeth were then instrumented 2 mm short of the working length using Vortex Blue nickel-titanium rotary instruments (Dentsply Tulsa Dental, Tulsa, OK, USA) to a master apical size 35/.04 taper (Figure 1B). A 35/.04 gutta-percha cone (GP) was placed, and a radiograph was taken to confirm the fit (Figures 2A and 2C). Throughout instrumentation, each canal was irrigated with 6 mL of 6% NaOCl after each file was used, followed by 3 mL of 17% ethylenediaminetetraacetic acid for 1 minute. All root canals were irrigated using 30-gauge irrigation needles (Max-I-Probe or Prorinse, Dentsply Tulsa Dental) and dried with paper points. The minimum waste tip from each sealer in its respective group was then inserted into the coronal third of each canal and ensured the sealer would travel through the apical foramen (Figure 1C). The sealer was placed in the canal until it could be seen extruding from the apical foramen. Using a single cone technique, each canal was obturated with a 35/.04 GP cone and the sealer (Figure 1D). Radiographs were also taken to confirm that the apical 2 mm had sufficient sealer (Figure 2B). If the remaining 2 mm of the canal was poorly obturated with voids, the tooth sample was excluded from its group (Figure 2D). Each sample was placed in an Eppendorf tube containing a wet sponge soaked in Hanks' balanced salt solution (HBSS), ensuring only the root tip was in contact with the sponge. All tubes were positioned in stabilizing stands to maintain sample orientation. The teeth were stored at 37°C in 100% humidity in HBSS for 7 days.

Endodontic retreatment

The teeth were retreated one week later. Retreatment was performed using hand files, with irrigation using 6% NaOCl. GP was removed using a stepwise technique starting with a size 30 H file to engage and extract the bulk of the material, followed by size 25 and/or 20 H files until complete removal of GP. Successful retreatment was measured by regaining apical patency with the 10/.02 or 15/.02 K file. No solvent was used for softening the root canal filling.

Failure was defined as the inability to advance further

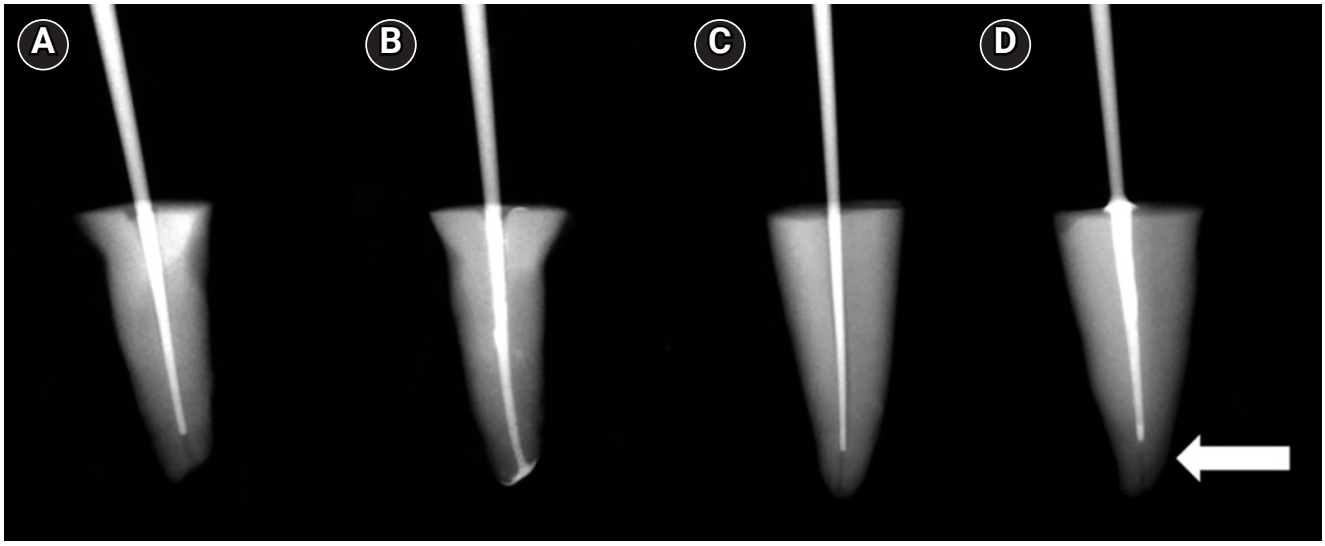

Figure 2. Representative examples of the accepted and rejected fillings. (A, B) Accepted samples: radiographs with a master cone (A) and with the cone and sealer (B). (C, D) Rejected samples: radiographs with a master cone (C) and with the cone and sealer (D), showing a large void in the apical 2 mm (white arrow).

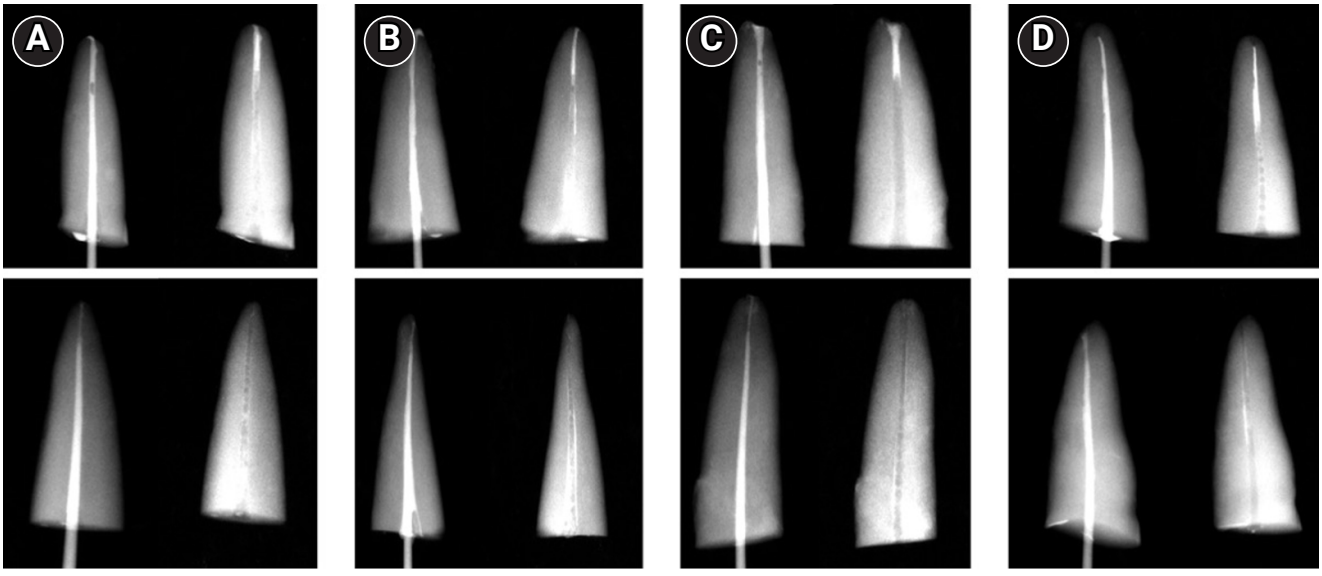

Figure 3. Representative radiographic images of the experimental groups with achieved apical patency (upper row) and with failed apical patency (lower row). Left: after obturation. Right: after retreatment. (A) NeoSEALERFlo (Avalon Biomed, Houston, TX, USA). (B) Ceraseal (Meta Biomed, Colmar, PA, USA). (C) Endosequence BC Sealer (Brasseler USA, Savannah, GA, USA). (D) AH Plus Bioceramic (Dentsply Sirona, Charlotte, NC, USA).

apically and achieve apical patency within a 10-minute period. The timing began immediately after the complete removal of GP and continued until the initiation of attempts to regain patency. Postoperative radiographs were taken regardless of success or failure (Figure 3).

Statistical analysis

One-way analysis of variance and Tukey contrast test were used to determine whether there was a significant difference among four different CSS ($p < 0.05$). Data were analyzed using a generalized linear model spec-

https://doi.org/10.5395/rde.2026.51.e3

ifying a binomial error distribution in R software ver. 4.3.1 (R Foundation for Statistical Computing, Vienna, Austria).

RESULTS

The success rates for regaining apical patency were 79.4% (NEO), 69.7% (AHB), 50.0% (BC), and 37.0% (CS) (Figure 4). NEO showed the highest regaining apical patency rate, while CS showed the lowest patency. The patency rate was significantly different between NEO and CS ($p < 0.01$). According to Tukey contrast test, the difference in patency rates between CS and AHB is marginally significant ($p = 0.056$).

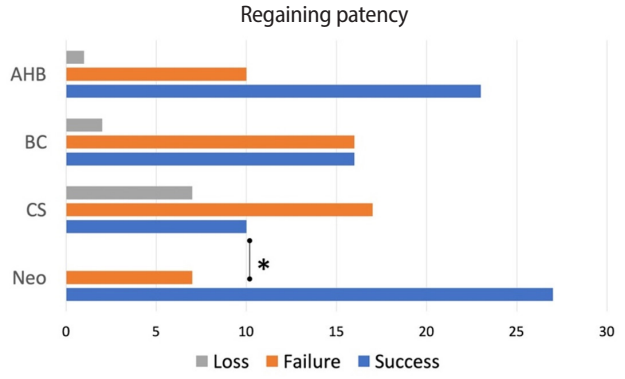

Figure 4. Apical patency success rate (%) among NeoSEALER Flo (NEO; Avalon Biomed, Houston, TX, USA), Ceraseal (CS; Meta Biomed, Colmar, PA, USA), Endosequence BC Sealer (BC; Brasseler USA, Savannah, GA, USA), and AH Plus Bioceramic (AHB; Dentsply Sirona, Charlotte, NC, USA) groups. Tukey contrast test reveals a marginally significant difference in patency rates between CS and AHB ($p = 0.055$). *$p < 0.01$.

DISCUSSION

An *ex vivo* sample design was used in this study to assess the retrievability of four different CSS in the unshaped canal of the apex (Figure 1). Radiographs were taken before and after the obturation to ensure that the apical 2 mm was full of sealer without voids (Figure 2B). Thus, the samples could be standardized with the sealers in the 2 mm of root canals from the apices to strictly assess the retrievability of the CSS without the additional factor of voids in the sealer.

Apical patency was achieved in this study with rates ranging from 37% to 79%. The results of 50% (BC) and 79% (NEO) in this study are similarly patterned to those of the previous study, which showed 64% (BC) and 100% (NEO) [19]. Also, the texture of NEO was soft when it was removed from the root canal with a hand file, while the texture of CS or BC was hard. Based on the results of this study, clinicians should be careful when attempting to regain apical patency into CS or BC during retreatment, trying carefully not to create a ledge or transport the canal. It could be useful to measure the softness of CSS set for predicting retrievability in the future.

The brands of bioceramic sealers have similar but variable chemical compositions and setting properties (Table 1). The chemical compositions of the sealers in our study are as follows. NEO consists of tricalcium silicate (<25%), calcium aluminate (<25%), dicalcium silicate (<10%), grossite (<6%), tricalcium aluminate (5%), and radiopacifiers [20]. AH Plus consists of zirconium dioxide (50%–75%), tricalcium silicate (5%–15%), dimethyl sulfoxide (10%–30%), lithium carbonate (<0.5%), and a thickening agent [20,21]. CS consists of tricalcium silicate (20%–30%), dicalcium silicate (1%–10%), and

Table 1. Chemical composition of root canal calcium silicate sealers

Sealer	Composition
NeoSEALER Flo	Tricalcium silicate (<25%), dicalcium silicate (<10%), calcium aluminate (<25%), calcium aluminum oxide (<6%), tricalcium aluminate (<5%), tantalite (50%)
Ceraseal	Tricalcium silicate (20%–30%), dicalcium silicate (1%–10%), tricalcium aluminate (1%–10%), zirconium dioxide (45%–50%)
AH Plus Bioceramic	Zirconium dioxide (50%–75%), tricalcium silicate (5%–15%), dimethyl sulfoxide (10%–30%), lithium carbonate (<0.5%), thickening agent (<6%)
Endosequence BC	Zirconium oxide, tricalcium silicate, dicalcium silicate, calcium hydroxide, calcium phosphate monobasic, filler, thickening agents

NeoSEALER Flo: Avalon Biomed, Houston, TX, USA. Ceraseal: Meta Biomed, Colmar, PA, USA. AH Plus Bioceramic: Dentsply Sirona, Charlotte, NC, USA. Endosequence BC: Brasseler USA, Savannah, GA, USA.

tricalcium aluminate (1%–10%), along with a radiopacifier and thickening agents [20]. BC consists of zirconium oxide, calcium silicates, calcium phosphate monobasic, calcium hydroxide filler, and thickening agents (Table 1) [22]. Furthermore, NEO and AH Plus have shown a higher volume of open pores within the sealer upon setting when compared to CS [20].

The variability in chemical composition among the different brands of CSSs could also play a role in the softness of the sealers. At this point, it is unknown how each type of calcium silicate and its percentage within the sealer has an impact on setting softness. However, it is known that NEO has a higher volume of open pores within the sealer upon setting, which could explain the softer composition of the sealer [20].

The authors suggest five potential causes for the formation of pores in CSS after root canal filling. First, since CSS is set via hydration [23], its setting reaction can release water vapor or trap air as calcium silicates react with water to form calcium silicate hydrate and calcium hydroxide. Second, inconsistent mixing can lead to voids or air entrapment. Third, if the canal is excessively dried, CSS may set incompletely or exhibit delayed setting [23]. Fourth, CSS secondarily generates a hydroxyapatite crystalline structure [24], which may not compact tightly. Fifth, the handling of CSS during placement can also introduce voids. Further research is needed to better understand how the setting mechanism of CSS affects the micro- and macro-structure of each sealer.

Different canal types and sample designs can lead to variations in the success rates of patency. The success rate of patency for BC in straight canals was 50% in this study, while the patency rate for BC in the previous study was 30% in mesiobuccal canals of mandibular molars [12]. In the previous study, the regaining patency rate for BC was 64% in straight root canals [19]. In the present study, the tooth samples with voids of BC were thoroughly evaluated (Figure 2D). Ten samples with voids were discarded: 7, 2, and one sample in CS, BC, and AHB, respectively. Excluding these factors might contribute to the different success rates of regaining patency. The success rates were likely higher if those samples with voids had been included.

There have been suggestions to utilize solvents or solutions for the dissolution of CSS. A promising report was published that the regaining patency for BC in straight canals with short fills was achieved, ranging from 93% to 100% with the solvents of chloroform, formic acid, or hydrochloric acid [25]. This is not consistent with the results of the present study, indicating a 50% patency rate for BC in straight canals with short fills. Because NaOCl irrigation is generally used to disinfect root canals, 6% NaOCl was, in this present study, used to irrigate and remove the canal fillings until apical patency was regained. However, the authors in the present study did not use acids while standardizing the samples (Figure 1) and screening the teeth samples by radiographs (Figure 2B and 2D). Ten-minute time frame of this study design could affect the results. In addition, the short fills by 2 mm in this study could reduce the patency rate compared to the short fills by 1.5 mm in the previous study [25]. For those reasons, we suggest that the retrievability of CSS with different methods by *ex vivo* needs to be tested and compared using standardized teeth samples.

The period of storage after obturation can affect the rate of regaining apical patency. The samples in this study were obturated with CSS and stored in an incubator for 7 days. Clinically, it is not common to retreat a case that has been obturated recently. Theoretically, CSS may be more difficult to regain apical patency after many years due to the additional calcification that may occur in the canal. An *ex vivo* study reported that retreating the teeth containing CSS a year after obturation was more challenging than the case after a month [26]. For this reason, the patency rate of the present study might be overestimated compared to the retreatment cases on the chair side.

To reduce the bias of the tooth samples, only straight roots were selected in this study. Therefore, GP was removed with fewer morphological changes in the canal walls. However, it is common for clinicians to touch and modify the canal wall with files during the removal of GP, possibly resulting in ledge, zip, or transportation, especially when removing GP in curved canals. Those morphological changes are considerable factors in reducing the success rates of retreatment [27]. Therefore, the patency rates of the present study should be conservatively applied for retreatment cases when clinicians

https://doi.org/10.5395/rde.2026.51.e3

remove GP in short fills with curved canals containing CSS.

Given the significant variation in retrievability among different CSS, it is important for clinicians to document the specific sealer used at the time of root canal obturation. In retreatment scenarios, knowing which CSS was previously applied can help practitioners anticipate the difficulty of removal and select appropriate techniques and solvents. This information may be especially valuable when patients are referred or when retreatment is performed by a different provider. Therefore, in addition to the obturation technique, recording the brand and type of CSS in the patient's chart should be considered a standard part of endodontic documentation.

CONCLUSIONS

The tested CSSs showed significantly different retrievability in terms of regaining apical patency. Upon endodontic retreatment, the retrievability of NEO was significantly higher than CS. In retreatment cases, identifying the type of CSS previously used is essential, as it significantly influences the ease and success of retreatment.

CONFLICT OF INTEREST

Hyeon-Cheol Kim is the Editor of *Restorative Dentistry and Endodontics* and was not involved in the review process of this article. The authors declare no other conflicts of interest.

FUNDING/SUPPORT

The authors have no financial relationships relevant to this article to disclose.

ACKNOWLEDGEMENTS

The authors would like to thank Dr. Julian N. Holland for the statistical analysis.

AUTHOR CONTRIBUTIONS

Conceptualization, Methodology: Jeong JW. Data curation: Shomali D. Formal analysis: Jeong JW, Shomali D. Visualization: Shomali D, Jeong JW, Kim HC. Writing - original draft: Shomali D, Jeong JW. Writing - review & editing: Kirkpatrick T, Kim HC, Kwak SW. All authors read and approved the final manuscript.

DATA SHARING STATEMENT

The datasets are not publicly available but are available from the corresponding author upon reasonable request.

REFERENCES

1. Ng YL, Mann V, Gulabivala K. A prospective study of the factors affecting outcomes of nonsurgical root canal treatment: part 1: periapical health. Int Endod J 2011;44:583-609.
2. Smith CS, Setchell DJ, Harty FJ. Factors influencing the success of conventional root canal therapy: a five-year retrospective study. Int Endod J 1993;26:321-333.
3. Sjogren U, Hagglund B, Sundqvist G, Wing K. Factors affecting the long-term results of endodontic treatment. J Endod 1990;16:498-504.
4. Souza RA. The importance of apical patency and cleaning of the apical foramen on root canal preparation. Braz Dent J 2006;17:6-9.
5. Al-Haddad A, Che Ab Aziz ZA. Bioceramic-based root canal sealers: a review. Int J Biomater 2016;2016:9753210.
6. Coşar M, Kandemir Demirci G, Çalışkan MK. The effect of two different root canal sealers on treatment outcome and post-obturation pain in single-visit root canal treatment: a prospective randomized clinical trial. Int Endod J 2023;56:318-330.
7. Pontoriero DIK, Ferrari Cagidiaco E, Maccagnola V, Manfredini D, Ferrari M. Outcomes of endodontic-treated teeth obturated with bioceramic sealers in combination with warm Gutta-percha obturation techniques: a prospective clinical study. J Clin Med 2023;12:2867.
8. Zavattini A, Knight A, Foschi F, Mannocci F. Outcome of root canal treatments using a new calcium silicate root canal sealer: a non-randomized clinical trial. J Clin Med 2020;9:782.
9. Chybowski EA, Glickman GN, Patel Y, Fleury A, Solomon E, He J. Clinical outcome of non-surgical root canal treatment using a single-cone technique with endosequence bioceramic sealer: a retrospective analysis. J Endod 2018;44:941-945.
10. Kim JH, Cho SY, Choi Y, Kim DH, Shin SJ, Jung IY. Clinical efficacy of sealer-based obturation using calcium silicate sealers: a randomized clinical trial. J Endod 2022;48:144-151.
11. Komabayashi T, Colmenar D, Cvach N, Bhat A, Primus C, Imai Y. Comprehensive review of current endodontic sealers. Dent Mater J 2020;39:703-720.
12. Hess D, Solomon E, Spears R, He J. Retreatability of a bioceramic root canal sealing material. J Endod 2011;37:1547-1549.

13. Agrafioti A, Koursoumis AD, Kontakiotis EG. Re-establishing apical patency after obturation with Gutta-percha and two novel calcium silicate-based sealers. Eur J Dent 2015;9:457-461.
14. Kim H, Kim E, Lee SJ, Shin SJ. Comparisons of the retreatment efficacy of calcium silicate and epoxy resin-based sealers and residual sealer in dentinal tubules. J Endod 2015;41:2025-2030.
15. Fonseca B, Coelho MS, Bueno CE, Fontana CE, Martin AS, Rocha DG. Assessment of extrusion and postoperative pain of a bioceramic and resin-based root canal sealer. Eur J Dent 2019;13:343-348.
16. Stanley E, Strother KK, Kirkpatrick T, Jeong JW. Calcium silicate-based sealer extrusion into the mandibular canal: 3 different recovery outcomes: a report of 3 cases. J Endod 2023;49:735-741.
17. Zehnder M. Root canal irrigants. J Endod 2006;32:389-398.
18. Keleş A, Köseoğlu M. Dissolution of root canal sealers in EDTA and NaOCl solutions. J Am Dent Assoc 2009;140:74-79.
19. Carrillo CA, Kirkpatrick T, Freeman K, Makins SR, Aldabbagh M, Jeong JW. Retrievability of calcium silicate-based root canal sealers during retreatment: an ex vivo study. J Endod 2022;48:781-786.
20. Zamparini F, Prati C, Taddei P, Spinelli A, Di Foggia M, Gandolfi MG. Chemical-physical properties and bioactivity of new premixed calcium silicate-bioceramic root canal sealers. Int J Mol Sci 2022;23:13914.
21. Hamdy TM, Galal MM, Ismail AG, Saber S. Physicochemical properties of AH plus bioceramic sealer, Bio-C Sealer, and ADseal root canal sealer. Head Face Med 2024;20:2.
22. Takahara S, Edanami N, Ibn Belal RS, Yoshiba K, Takenaka S, Ohkura N, *et al*. An evaluation of the biocompatibility and chemical properties of two bioceramic root canal sealers in a sealer extrusion model of rat molars. J Funct Biomater 2025;16:14.
23. Koo J, Kwak SW, Kim HC. Differences in setting time of calcium silicate-based sealers under different test conditions. J Dent Sci 2023;18:1042-1046.
24. Sfeir G, Zogheib C, Patel S, Giraud T, Nagendrababu V, Bukiet F. Calcium silicate-based root canal sealers: a narrative review and clinical perspectives. Materials (Basel) 2021;14:3965.
25. Rezaei G, Liu X, Jalali P. Efficacy of different solvents for achieving patency in teeth obturated using bioceramic sealer. J Endod 2023;49:219-223.
26. Bardini G, Cotti E, Congiu T, Caria C, Aru D, Mercadè M. Medium- and long-term re-treatment of root canals filled with a calcium silicate-based sealer: an experimental ex vivo study. Materials (Basel) 2022;15:3501.
27. Gorni FG, Gagliani MM. The outcome of endodontic retreatment: a 2-yr follow-up. J Endod 2004;30:1-4.

https://doi.org/10.5395/rde.2026.51.e3

RDE Restorative Dentistry & Endodontics

Research Article

eISSN 2234-7666
Restor Dent Endod. 2026 February;51(1):e4
https://doi.org/10.5395/rde.2026.51.e4

Effect of combined application of premixed bioceramic paste and diode laser in vital pulp therapy: an immunohistochemical randomized controlled split-mouth *in vivo* animal experiment

Mo'men A. Salama[1,*], **Dalia M. Fayyad**[1], **Mohamed I. Rabie**[1], **Manar A. A. Selim**[2], **Mahmoud F. Ahmed**[3,4]

[1]Department of Endodontics, Faculty of Dentistry, Suez Canal University, Ismailia, Egypt
[2]Department of Oral Biology, Faculty of Dentistry, Suez Canal University, Ismailia, Egypt
[3]Department of Surgery, Anesthesiology and Radiology, Faculty of Veterinary Medicine, Suez Canal University, Ismailia, Egypt
[4]Department of Surgery and Theriogenology, Faculty of Veterinary Medicine, King Salman International University, Ras Sudr, Egypt

ABSTRACT

Objectives: This study aimed to evaluate the effect of premixed bioceramic paste (Well-Root PT; Vericom) compared to mineral trioxide aggregate (MTA) on the expression of the mineralization-related marker dentin sialoprotein (DSP) in dental pulp following direct pulp capping, with or without prior diode laser application.

Methods: Direct pulp exposures were performed in the upper and lower incisors of eight dogs (n = 96 teeth). Cavities (Class V) were created and received pulp capping with either Well-Root PT (n = 32), MTA (n = 32), or no capping material (polytetrafluoroethylene disc only) (n = 32), with or without the application of a diode laser. Immunohistochemical analysis of DSP expression was conducted and quantified as the mean area percentage using ImageJ software at 2 and 8 weeks posttreatment.

Results: Both the Well-Root PT and MTA groups showed significantly increased DSP expression compared to the control group at both 2 and 8 weeks ($p < 0.05$). No significant difference in the mean area percentage of DSP expression was found between the Well-Root PT and MTA groups. The diode laser application did not produce a significant effect on DSP expression. Within-group comparison revealed a significant increase in DSP expression between the 2- and 8-week follow-up periods ($p < 0.05$).

Conclusions: Well-Root PT demonstrated comparable efficacy to MTA in promoting DSP expression, supporting its use as an effective direct pulp capping material. Diode laser application prior to capping had no effect on DSP expression in this experimental model.

Keywords: Dental pulp capping; Dogs; Laser therapy; Mineral trioxide aggregate; Phosphoproteins; Pulp capping and pulpectomy agents

Received: August 17, 2025 **Revised:** October 11, 2025 **Accepted:** October 14, 2025

Citation
Salama MA, Fayyad DM, Rabie MI, Selim MAA, Ahmed MF. Effect of combined application of premixed bioceramic paste and diode laser in vital pulp therapy: an immunohistochemical randomized controlled split-mouth *in vivo* animal experiment. Restor Dent Endod 2026;51(1):e4.

***Correspondence to**
Mo'men A. Salama, PhD
Department of Endodontics, Faculty of Dentistry, Suez Canal University, 4.5 Km Ring Road, Ismailia 41522, Egypt
Email: momen_salama@dent.suez.edu.eg

INTRODUCTION

Preserving pulp vitality is a core component of modern minimally invasive dentistry, boosted by advancements in biomaterials and an enhanced comprehension of pulp biology [1,2]. These advancements have instigated a paradigm change from traditional root canal treatment to more conservative approaches aimed at conserving pulp tissue where clinically feasible [3,4]. Direct pulp capping (DPC) is a crucial procedure of vital pulp therapies for addressing pulp exposures resulting from trauma or caries, especially when the pulp is healthy or shows only reversible inflammation [5]. The principal objective of DPC is to preserve the vitality and functionality of the dental pulp by efficiently sealing the exposure site and facilitating reparative dentinogenesis, particularly through the development of a protective dentin bridge [6,7].

Emerging evidence from comparative investigations highlights the advantages of premixed bioceramic materials, such as Well-Root PT (Vericom, Chuncheon, Korea), over traditional calcium hydroxide formulations for DPC [8]. The premixed bioceramic material, Well-Root PT, is composed of calcium aluminosilicate, zirconium oxide, tantalum oxide, calcium phosphate monobasic, and various fillers [9]. This material's unique composition enhances biocompatibility, minimizes cytotoxicity, and provides superior sealing properties upon application [9]. The inherent high alkalinity of Well-Root PT creates a favorable microenvironment conducive to pulp healing while simultaneously inhibiting bacterial ingress. Furthermore, Well-Root PT provides clinical performance analogous to mineral trioxide aggregate (MTA) but improved handling characteristics, positioning it as a dependable alternative for both pulp capping procedures and broader regenerative endodontic applications [8,10].

The incorporation of low-level laser therapy (LLLT) alongside DPC represents a notable progression in minimally invasive endodontics, utilizing photobiomodulation to improve dental pulp tissue regeneration [11]. LLLT, with a typical power range of 10–500 mW [12], primarily acts through the absorption of light by mitochondrial photoreceptors, particularly cytochrome C oxidase in the electron transport chain [13]. This absorption leads to a short-term activation of the respiratory chain, enhancing oxidative phosphorylation and increasing adenosine triphosphate production. This process alters the redox state of mitochondria and the cytoplasm, affecting cellular redox mechanisms. The generation of reactive oxygen species at controlled levels acts as signaling molecules to activate various molecular pathways and transcription factors, which promote cellular proliferation, differentiation, and reduced inflammation [13,14]. It has demonstrated efficacy in pain reduction, enhancement of wound healing, the promotion of bone repair and remodeling, assistance in pulp regeneration, and stimulation of angiogenesis [5,14,15]. It improves reparative dentinogenesis by stimulating odontoblast activity and promoting dental pulp stem cell differentiation [16]. Furthermore, LLLT improves dentin matrix structure and mineralization by upregulating the production of structural proteins, such as dentin sialo phosphoprotein (DSPP) [14]. This process promotes the formation of a thicker, more uniform dentin bridge, which enhances long-term sealing efficiency and reduces the possibility of microleakage [17].

The most prevalent non-collagenous protein present in the dentin matrix is dentin sialoprotein (DSP). It regulates dentinogenesis and biomineralization [18]. Furthermore, DSP regulates transcriptional activity and intracellular signaling cascades. These regulatory roles regulate the differentiation of dental pulp stem/progenitor cells, which support both physiological homeostasis and the reparative/regenerative ability of dental tissues [19].

Although both LLLT and advanced bioceramics such as Well-Root PT have individually demonstrated significant therapeutic potential, their combined effects in DPC remain insufficiently explored. Moreover, the available evidence is limited regarding their comparative influence on dentinogenesis-related markers, particularly DSP.

Therefore, this study hypothesized that Well-Root PT would promote pulpal healing and upregulate dentinogenesis-related markers compared to the gold-standard material, White MTA Angelus, and that adjunctive use of LLLT would further enhance this effect. Accordingly, the study aimed to evaluate the pulpal response to DPC using Well-Root PT, with and without adjunctive LLLT,

https://doi.org/10.5395/rde.2026.51.e4

and to compare its efficacy with Angelus MTA through immunohistochemical analysis of DSP expression as a key marker of odontoblastic activity and dentin matrix formation.

METHODS

Experimental design

The study was performed at the Department of Surgery, Anesthesiology and Radiology, Faculty of Veterinary Medicine, Suez Canal University. The protocol was approved by the Research Ethics Committee of the Faculty of Dentistry, Suez Canal University (approval No. 529/2022), in accordance with ethical standards and regulations for animal research, and in compliance with the ARRIVE (Animal Research: Reporting of *In Vivo* Experiments) guidelines. The study was carried out as a randomized, controlled, experimental trial. Eight mature Mongrel dogs were used in this study with intact dentition. The dogs aged between 19 ± 3 months and weighed (15.4 ± 3.2 kg). Dogs were kept for 2 weeks at the animal house before the study for close observation and acclimatization. Sample size was calculated based on prior research [17,20]. Sample size estimation was performed using G*Power version 3.1.9.2 (Heinrich Heine University Düsseldorf, Düsseldorf, Germany) [21], with a significance level (α) of 0.05 and a power (1–β) of 0.80. Adjustments were made to account for potential specimen loss and the clustered (split-mouth) design, resulting in a final allocation of 96 teeth (32 teeth per material group; 16 per subgroup), thereby ensuring adequate statistical power.

The incisor teeth were randomly evaluated by three independent observers who were blinded to the material and technique used. Only the allocator (M.A.S) was aware of the group assignments, which corresponded to the different capping materials. Using a split-mouth design, the teeth were randomly allocated to one of three groups according to a computer-generated random sequence (Microsoft Excel RAND function) prepared by an investigator independent of the surgical procedures. For each dog, the 12 incisors were allocated so that each group (Well-Root PT, MTA, and control) was represented by four teeth per dog. Within each group, two teeth were assigned to the LLLT subgroup and two to the non-LLLT subgroup. The dogs were randomly assigned to be euthanized at either 2 weeks (dogs 1–4) or 8 weeks (dogs 5–8), ensuring equal numbers for each period (Table 1).

Pulp exposure and direct pulp capping

The dogs received premedication consisting of an intramuscular injection of 0.5 mg/kg body weight Xylazine (Xyla-Ject; Adwia Pharmaceuticals, 10th of Ramadan City, Egypt), 1 mg/kg nalbuphine HCl (Nalufin; Amoun Pharmaceutical Company, Al Qalyubia, Egypt), and 0.04 mg/kg atropine sulfate (Memphis Pharmaceutical, Cairo, Egypt). The dogs then received an intravenous injection of propofol (Diprivan; AstraZeneca, Macclesfield, UK) at a dosage of 2 mg/kg; general anesthesia was maintained with a combination of 2% isoflurane (IsoFlo; Zoetis Inc., Parsippany, NJ, USA) and oxygen [22]. Standard Class V cavities were induced in each incisor as previously described [23].

Briefly, rubber dam isolation was applied to each jaw separately to allow endotracheal intubation. A high-speed air turbine handpiece with copious water coolant and a sterile round diamond bur was used to prepare a standardized cavity. A sterile round carbide bur (No. 1) in a high-speed handpiece was then used to create a standardized mechanical pulp exposure approximately 1.0 mm in diameter. Hemostasis was achieved using sterile saline irrigation and gentle pressure with sterile cotton pellets; only sites where bleeding was controlled within 5 minutes were included for capping. In the control group, the exposed pulp sites were capped with Teflon discs made from sterilized polytetrafluoroethylene sheets (Chemours, Wilmington, DE, USA), without the use of any capping material. The pulp exposure sites in the MTA group were sealed with White MTA (Angelus,

Table 1. Number of teeth assigned to each experimental subgroup at 2 and 8 weeks

Group	Subgroup	2 weeks	8 weeks
Control ($n = 32$)	Non-LLLT	8	8
	LLLT	8	8
MTA ($n = 32$)	Non-LLLT	8	8
	LLLT	8	8
Well-Root PT ($n = 32$)	Non-LLLT	8	8
	LLLT	8	8

LLLT, low-level laser therapy; MTA, mineral trioxide aggregate; Well-Root PT: Vericom, Chuncheon, Korea.

Londrina, Brazil), prepared according to the manufacturer's instructions to a creamy consistency and applied using an MTA applicator. In the Well-Root PT group, the exposed pulps were capped with premixed bioceramic putty (Well-Root PT; Vericom Co., Ltd., Chuncheon, Korea), applied directly from the syringe/putty carrier according to the manufacturer's instructions.

For the LLLT subgroups, a diode laser (Liposuction Smart, 810 nm wavelength; Lasotronix, Piaseczno, Poland) was used in continuous wave mode at a low power setting of 20 mW. The laser was hand-held and positioned approximately 2 mm from the exposed pulp by the operator. Laser irradiation was applied for 150 seconds, with a spot size of approximately 0.2 cm^2, delivering an energy dose of 15 J/cm^2. Following laser application and placement of the respective capping material or Teflon disc, all cavities were restored using a light-cured glass ionomer cement (GC Fuji II; GC Corp., Tokyo, Japan). Dogs received a daily injection of meloxicam (Mobitil; MUP, Cairo, Egypt) at a dose of 0.2 mg/kg for 3 consecutive days.

Immunohistochemical analysis

After 2 weeks, four dogs were euthanized, and the remaining four were euthanized after 8 weeks, following the previously described protocol [24]. The teeth along with the surrounding tissues were block-sectioned and fixed in 10% buffered formalin. Subsequently, the specimens were decalcified in 17% ethylenediaminetetraacetic acid (EDTA) over a period of 6 months and embedded in paraffin. Using a microtome, paraffin-embedded tissues were sectioned in the buccolingual direction into slices 4–6 μm thick.

To assess the expression of the mineralization-related marker DSP, the tissue sections were deparaffinized in xylene, rehydrated through a graded alcohol series, and incubated with an endogenous peroxidase blocker for 10 minutes. After washing with Tris-buffered saline, sections were incubated with a primary anti-DSP antibody (polyclonal anti-osteopontin; Biospes, Chongqing, China) at 4°C for 1 hour. This was followed by the application of the biotin-streptavidin peroxidase complex. Hematoxylin was used for counterstaining. Negative controls consisted of untreated pulp samples, while positive controls involved replacing the primary DSP antibody with 1% bovine serum albumin. Histological evaluation was performed using Leica Qwin 500 image analysis software (Leica Microsystems, Wetzlar, Germany). The extent of DSP staining in the newly formed hard tissue was quantified as the stained area per 10 fields at 100× magnification, using a standardized measuring frame and visualized under light microscopy on a monitor [17]. All immunohistochemical evaluations were performed by three independent, blinded evaluators. The slides were coded to ensure that the evaluators were unaware of the material and laser subgroup allocations. Immunostaining-positive areas were quantified using Fiji (ImageJ version 1) [25]. The mean area percentages of the positively stained regions were calculated within a defined region of interest. Threshold adjustment was applied to distinguish positive staining from the background, and the obtained mean area percentage values were used for statistical comparison among groups to ensure consistency and accuracy.

Statistical analysis

The collected data were analyzed using the statistical software package IBM SPSS ver. 26.0 (IBM Corp., Armonk, NY, USA). The data were assessed for normality using the Shapiro-Wilk test. Descriptive statistics were then calculated, including the mean and standard deviation. To compare outcomes among the different study groups, a one-way analysis of variance (ANOVA) was performed. When the ANOVA revealed statistically significant differences, Bonferroni *post hoc* tests were conducted. For comparisons of results at different time points within the same group, the unpaired sample *t*-test was used. Statistical significance was defined as $p < 0.05$.

RESULTS

Quantitative analysis was performed using the mean area percentage of DSP expression. The DSP expression was evaluated in the pulp tissue at two time points: 2 weeks and 8 weeks. In both the control and MTA groups without LLLT, relatively low mean area percentages for DSP were observed in different parts of the pulp, such as odontoblasts, fibroblasts, collagen fibers, ground substance, and blood vessel walls after 2 weeks. In contrast,

https://doi.org/10.5395/rde.2026.51.e4

the Well-Root PT subgroup exhibited a higher mean area percentage of DSP at the same time point (Figure 1A, C, and E). After 8 weeks, the control subgroup without LLLT maintained low area percentage values, while the MTA subgroup displayed a moderate increase. The Well-Root PT subgroup demonstrated a more pronounced response, with the highest mean area percentage observed in staining (Figure 2A, C, and E).

In the LLLT control subgroup, a slight increase in the mean area percentage was observed at 2 weeks (Figure 1B), with a more pronounced increase by the 8-week time point (Figure 2B). However, both the MTA and Well-Root PT subgroups with LLLT showed higher mean percentages (Figure 1D and F), with a further increase at 8 weeks (Figure 2D and F).

Statistical analysis of the mean area percentage between the study groups and between the indicated time

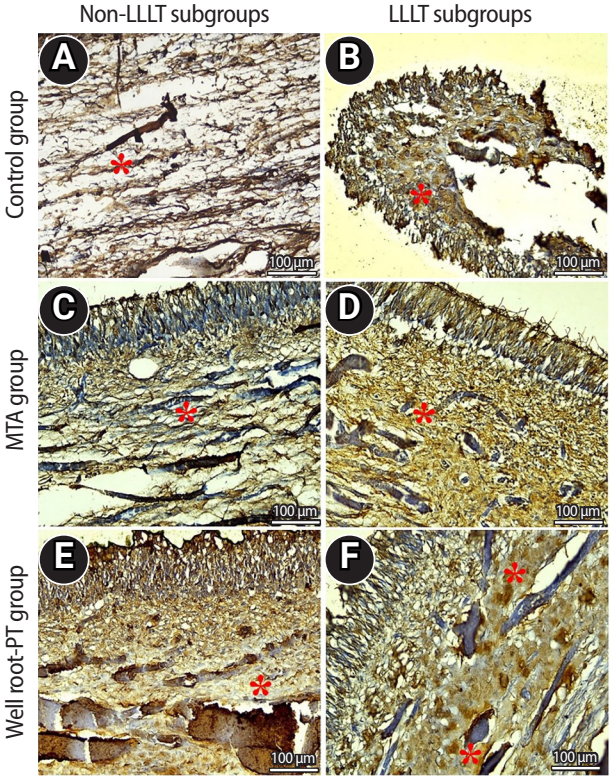

Figure 1. Representative microscopic images showing immunohistochemical staining of dentin sialoprotein in pulp tissue (*) after 2 weeks. (A, B) Showing diffuse expression in the control group, with (A) non-LLLT subgroup demonstrating staining of collagen fibers, and (B) LLLT subgroup showing staining of both collagen fibers and the cytoplasm of odontoblasts. (C, D) Showing expression in the MTA group, with (C) non-LLLT subgroup demonstrating patchy staining in collagen fibers and diffuse cytoplasmic staining in odontoblasts, and (D) LLLT subgroup showing extensive staining in both collagen fibers and odontoblasts. (E, F) Showing expression in the Well-Root PT group, with (E) non-LLLT subgroup demonstrating patchy staining in collagen fibers and diffuse staining in odontoblasts, and (F) LLLT subgroup showing similar expression patterns. LLLT, low-level laser therapy; MTA, mineral trioxide aggregate; Well-Root PT: Vericom, Chuncheon, Korea.

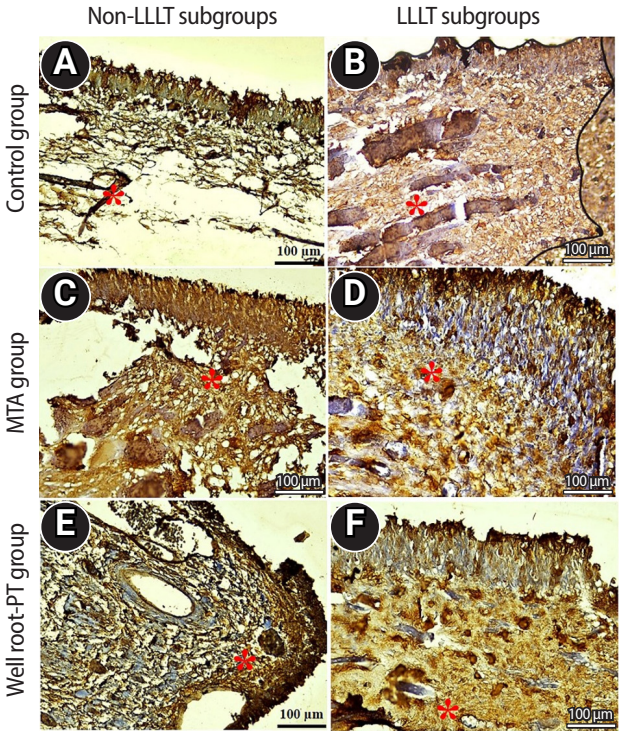

Figure 2. Representative microscopic images showing immunohistochemical staining of dentin sialoprotein in pulp tissue (*) after 8 weeks. (A, B) Showing expression in the control group, with (A) non-LLLT subgroup demonstrating patchy expression in collagen fibers and patchy expression in odontoblasts, and (B) LLLT subgroup demonstrating diffuse expression in collagen fibers and in the cytoplasm of odontoblasts. (C, D) Showing expression in the MTA group, with (C) non-LLLT subgroup demonstrating patchy expression in both collagen fibers and odontoblasts, and (D) LLLT subgroup showing patchy expression in collagen fibers, diffuse cytoplasmic expression, and some nuclear expression in odontoblasts. (E, F) Showing expression in the Well-Root PT group, with (E) non-LLLT subgroup demonstrating patchy expression in collagen fibers and diffuse cytoplasmic expression in odontoblasts, and (F) LLLT subgroup demonstrating patchy expression in collagen fibers and diffuse cytoplasmic and nuclear expression in odontoblasts. LLLT, low-level laser therapy; MTA, mineral trioxide aggregate; Well-Root PT: Vericom, Chuncheon, Korea.

points within the same group was performed. There were significant variations in DSP expression between the non-LLLT and LLLT subgroups within the three groups ($p < 0.001$). However, *post hoc* testing did not reveal any significant differences between the non-LLLT MTA and Well-Root PT subgroups, nor between the MTA and Well-Root PT subgroups after the LLLT, at either the 2-week or 8-week time points (Table 2).

At the 2-week evaluation, the highest mean area percentage of DSP expression was observed in the LLLT Well-Root PT subgroup, followed by the non-LLLT Well-Root PT, the LLLT MTA, and the non-LLLT MTA subgroups. The control group exhibited the lowest levels. By the 8-week time point, a similar trend persisted; however, the LLLT MTA subgroup showed a slightly higher mean value than the non-LLLT Well-Root PT subgroup. In intragroup comparisons, all subgroups showed a statistically significant increase in DSP mean area percentage from 2 to 8 weeks ($p < 0.001$), indicating a general time-dependent increase regardless of treatment. However, despite differences in mean values, no significant differences were observed between the LLLT and non-LLLT subgroups at either time point in the same group (Table 3). These findings supported the conclusion that the various capping materials significantly influenced the DSP expression signals.

DISCUSSION

In this study, the quality of the dentin bridge formed following DPC was evaluated using immunohistochemical analysis to assess the expression of DSP, a reliable marker of odontoblastic activity within the pulp tissue. The efficacy of Well-Root PT and MTA was compared to determine their respective performance. Additionally, the potential role of LLLT in enhancing DSP expression and promoting pulp tissue regeneration was also investigated.

Dogs were selected as the animal model for this study due to their close anatomical and physiological resemblance to human teeth [26]. Their similar pulp-to-dentin ratio and overall tooth structure make them well-suited for investigating pulp responses and dentin bridge formation [27]. Moreover, the healing patterns and tissue reactions in dogs closely mirror those in humans, enhancing the clinical relevance and translational value of the study's findings [28]. However, it should be noted that healing in dogs occurs more rapidly than in humans. This limitation should be taken into account

Table 3. Descriptive statistics of the intergroup comparison of DSP immunoexpression area percentage

Group	Subgroup	DSP immunoexpression area (%)	F-test	*p*-value
Control	Non-LLLT	$2.12^{b} \pm 1.68$	11.76	0.0003**
	LLLT	$1.38^{b} \pm 0.73$		
MTA	Non-LLLT	$11.22^{a} \pm 2.91$		
	LLLT	$11.12^{a} \pm 2.22$		
Well-Root PT	Non-LLLT	$9.27^{a} \pm 1.18$		
	LLLT	$11.44^{a} \pm 4.00$		

Values are presented as mean ± standard deviation.
DSP, dentin sialoprotein; LLLT, low-level laser therapy; MTA, mineral trioxide aggregate; Well-Root PT: Vericom, Chuncheon, Korea.
Within the subgroups, different letters indicate a significant difference ($p < 0.05$). **$p < 0.001$, significant difference.

Table 2. Descriptive statistics of the intragroup comparison of DSP immunoexpression area percentage between 2 and 8 weeks

Group	Subgroup	DSP immunoexpression area (%)		Unpaired *t*-test	*p*-value
		2 weeks	8 weeks		
Control	Non-LLLT	$17.00^{b} \pm 0.68$	$19.12^{b} \pm 1.95$	−10.88	<0.001***
	LLLT	$18.84^{b} \pm 1.90$	$20.22^{b} \pm 2.48$	−17.41	<0.001***
MTA	Non-LLLT	$27.15^{a} \pm 1.51$	$38.38^{a} \pm 2.25$	−36.16	<0.001***
	LLLT	$28.96^{a} \pm 1.21$	$40.08^{a} \pm 1.32$	−45.15	<0.001***
Well-Root PT	Non-LLLT	$29.85^{a} \pm 2.30$	$39.12^{a} \pm 3.24$	−71.08	<0.001***
	LLLT	$29.96^{a} \pm 2.26$	$41.40^{a} \pm 1.96$	−25.76	<0.001***
F-test		33.46	62.90		
p-value		<0.001***	<0.001***		

Values are presented as mean ± standard deviation.
DSP, dentin sialoprotein; LLLT, low-level laser therapy; MTA, mineral trioxide aggregate; Well-Root PT: Vericom, Chuncheon, Korea.
Within the subgroups, different letters indicate a significant difference ($p < 0.05$). ***$p < 0.001$, significant difference at the same subgroup point.

https://doi.org/10.5395/rde.2026.51.e4

when extrapolating the findings to clinical scenarios.

In this study, Well-Root PT was compared with MTA as a contemporary bioactive material for DPC. Well-Root PT offers a shorter setting time, which may help reduce operator variability and improve clinical efficiency. However, despite its favorable handling and physical properties, research on its biocompatibility and bioactivity remains limited [8,29], highlighting the importance of evaluating its performance against the well-established MTA. Meanwhile, LLLT was used for its ability to promote rapid hemostasis, sterilize the pulp surface, and reduce inflammation [30,31]. In addition, it supports tissue regeneration and aids in dentin bridge formation. It is also compatible with common pulp capping materials, potentially enhancing their effectiveness [20].

In this study, DSP expression was evaluated at two time points: 2 weeks, to assess the early healing response, including odontoblast differentiation and initial dentin formation [32]. Furthermore, the 8-week period was used to examine long-term outcomes such as reparative dentin bridge formation, reduced inflammation, and maintained pulp vitality. These time points are appropriate for evaluating the effectiveness of pulp capping materials [17,33]. However, the present study cannot fully confirm the long-term formation of a reparative dentin bridge.

Immunohistochemical analysis conducted at both 2 weeks and 8 weeks revealed that the highest mean values of DSP expression were observed in the subgroups treated with MTA and Well-Root PT, with or without adjunctive LLLT. In contrast, the control subgroups, which received only a Teflon barrier without any bioactive material, exhibited the lowest levels of DSP expression. The increased DSP expression observed with MTA and Well-Root PT is attributed to their bioactive properties, which promote odontoblast differentiation and reparative dentin formation. These materials release calcium ions that form hydroxyapatite-like crystals, fostering a favorable environment for pulp healing [1,34]. They also upregulate growth factors like bone morphogenetic protein-2 and transforming growth factor-beta and create an alkaline pH that reduces inflammation, further enhancing odontoblastic activity and DSP synthesis [35,36]. The findings of this study are in agreement with the results reported by Chae *et al.* [8], who demonstrated that despite releasing fewer calcium ions compared to MTA, Well-Root PT exhibited comparable bioactivity, as evidenced by hard tissue formation and DSP expression.

The study found no significant difference in DSP expression between the LLLT and non-LLLT groups, suggesting that the diode laser, under the applied parameters, did not enhance DSP expression beyond the effect of the capping materials alone. Similarly, Martín *et al.* [37] reported that diode laser activation during dentin conditioning resulted in lower expression levels of odontoblast-related markers such as DSPP and DMP-1 compared with EDTA alone, supporting the notion that diode laser irradiation may not significantly enhance DSP expression or odontoblastic differentiation. Additionally, the laser settings used may not have been optimal for influencing odontoblastic activity. On the other hand, Alharbi *et al.* [17] reported that the application of LLLT prior to DPC enhanced the expression of other markers, such as RUNX2 and osteocalcin. This discrepancy may be attributed to differences in the biomarkers assessed, as DSP is specifically associated with odontoblastic differentiation, whereas RUNX2 and osteocalcin are more broadly related to early osteogenic activity. Additionally, variations in LLLT parameters—such as energy settings, number of applications, and exposure duration—could contribute to the inconsistent outcomes across studies. In contrast, Deng *et al.* [38] attributed this effect to the coagulative and hemostatic properties of the LLLT, which may reduce tissue moisture and potentially interfere with the optimal setting reaction, as it relies on a moist environment for proper hardening.

A notable observation was that at 8 weeks, the LLLT MTA subgroup showed a slightly higher mean DSP expression than the non-LLLT Well-Root PT subgroup. Although not statistically significant, this finding may indicate that the stimulatory effects of LLLT on odontoblastic activity and dentin matrix protein expression were not transient but persisted over time. Future research with extended follow-up periods and varied laser protocols could help clarify the potential synergistic role of LLLT.

Statistically significant differences in DSP expression

were also observed between the two evaluation time points within each subgroup. These findings align with Alharbi *et al.* [17], who reported significant changes in marker expression between early and late follow-up periods in pulp tissues treated with different capping materials, indicating progressive healing and maturation. This temporal variation likely reflects the dynamic nature of the pulp healing process, which begins with an initial inflammatory response followed by progressive reparative events [39]. The increased DSP expression observed at later stages may indicate ongoing odontoblast differentiation and dentin matrix deposition [40]. Additionally, biological variability among the animals, including differences in immune responses and healing capacities, may have contributed to the observed differences between the time points. Finally, the findings of this study support the bioactive potential of both MTA and Well-Root PT in promoting odontoblastic activity and DSP expression.

The limitations of this study include the indirect evaluation of reparative dentin bridges due to insufficient histological clarity; and the use of only a single LLLT wavelength and protocol, which may not capture its full therapeutic potential. Future studies should employ varied laser parameters, longer follow-up periods, and additional odontoblast-specific markers to better elucidate LLLT's role in vital pulp therapy.

CONCLUSIONS

Well-Root PT may serve as a viable alternative to MTA for DPC procedures, demonstrating comparable biological performance in promoting DSP expression and pulp healing. LLLT did not significantly influence the outcomes observed in this study. Therefore, the choice of suitable biocompatible capping material appears to play a more critical role in the success of DPC than the use of LLLT. Further studies are required to explore the optimization of LLLT parameters and their potential synergistic effects with various capping materials.

CONFLICT OF INTEREST

No potential conflict of interest relevant to this article was reported.

FUNDING/SUPPORT

The authors have no financial relationships relevant to this article to disclose.

ACKNOWLEDGEMENTS

The authors acknowledge Dr. Saad L. Saad, Faculty of Veterinary Medicine, Suez Canal University, for being technically supportive during the *in vivo* studies.

AUTHOR CONTRIBUTIONS

Conceptualization, Formal analysis, Investigation, Project administration, Supervision, Validation: all authors. Data curation: Salama MA, Fayyad DM, Ahmed MF. Methodology, Software: Salama MA, Ahmed MF. Resources: Salama MA, Fayyad DM, Rabie MI, Ahmed MF. Visualization: Salama MA. Writing - original draft: all authors. Writing - review & editing: all authors. All authors read and approved the final manuscript.

DATA SHARING STATEMENT

The datasets are not publicly available but are available from the corresponding author upon reasonable request.

REFERENCES

1. Desai PK, Hiwalkar SM, Kim HJ, Shin J, Lee HS, Jun HW, *et al.* Innovations in bioactive materials for dental pulp vitality preservation in children and adolescents. Appl Sci 2025;15:4699.
2. Rajasekar V, Abdalla MM, Huang M, Neelakantan P, Yiu CK. Next-generation biomaterials for vital pulp therapy: exploring biological properties and dentin regeneration mechanisms. Bioengineering (Basel) 2025;12:248.
3. Hanna SN, Perez Alfayate R, Prichard J. Vital pulp therapy an insight over the available literature and future expectations. Eur Endod J 2020;5:46-53.
4. Silva EJ, De-Deus G, Souza EM, Belladonna FG, Cavalcante DM, Simões-Carvalho M, *et al.* Present status and future directions: minimal endodontic access cavities. Int Endod J 2022;55 Suppl 3:531-587.
5. Prasertsuksom N, Osiri S, Jaruchotiratanasakul N, Ongchavalit L. Treatment outcomes and prognostic factors of direct pulp capping in permanent teeth: a systematic review and meta-analysis. Eur Endod J 2024;9:295-307.
6. Galler KM, Weber M, Korkmaz Y, Widbiller M, Feuerer M. Inflammatory response mechanisms of the dentine-pulp complex and the periapical tissues. Int J Mol Sci 2021;22:1480.
7. Islam R, Islam MR, Tanaka T, Alam MK, Ahmed HM, Sano H. Direct pulp capping procedures: evidence and practice. Jpn

https://doi.org/10.5395/rde.2026.51.e4

Dent Sci Rev 2023;59:48-61.
8. Chae YK, Ye JR, Nam OH. Evaluation of biocompatibility and bioactive potential of Well-Root PT by comparison with ProRoot MTA and Biodentine. J Dent Sci 2024;19:2218-2225.
9. Ghaly MS, Abozena NI, Ghouraba RF, Kabbash IA, El-Desouky SS. Clinical and radiographic evaluation of premixed bioceramic putty as an apical plug in nonvital immature anterior permanent teeth. Sci Rep 2025;15:26487.
10. Ashi T, Mancino D, Hardan L, Bourgi R, Zghal J, Macaluso V, *et al*. Physicochemical and antibacterial properties of bioactive retrograde filling materials. Bioengineering (Basel) 2022;9:624.
11. Yong J, Gröger S, Wu Z, Ruf S, Ye Y, Chen X. Photobiomodulation therapy and pulp-regenerative endodontics: a narrative review. Bioengineering (Basel) 2023;10:371.
12. Cotler HB, Chow RT, Hamblin MR, Carroll J. The use of Low Level Laser Therapy (LLLT) for musculoskeletal pain. MOJ Orthop Rheumatol 2015;2:00068.
13. Karoussis IK, Kyriakidou K, Psarros C, Koutsilieris M, Vrotsos JA. Effects and action mechanism of low level laser therapy (LLLT): applications in periodontology. Dentistry 2018;8:1000514.
14. Rezaei F, Shakoori S, Fazlyab M, Esnaashari E, Savadkouhi ST. Effect of low-level laser on proliferation, angiogenic and dentinogenic differentiation of human dental pulp stem cells. BMC Oral Health 2025;25:441.
15. Fazlyab M, Esmaeili Shahmirzadi S, Esnaashari E, Azizi A, Moshari AA. Effect of low-level laser therapy on postoperative pain after single-visit root canal retreatment of mandibular molars: a randomized controlled clinical trial. Int Endod J 2021;54:2006-2015.
16. Borzabadi-Farahani A. Effect of low-level laser irradiation on proliferation of human dental mesenchymal stem cells: a systemic review. J Photochem Photobiol B 2016;162:577-582.
17. Alharbi H, Khalil W, Alsofi L, Binmadi N, Elnahas A. The effect of low-level laser on the quality of dentin barrier after capping with bioceramic material: a histomorphometric analysis. Aust Endod J 2023;49:27-37.
18. Goldberg M, Kulkarni AB, Young M, Boskey A. Dentin: structure, composition and mineralization. Front Biosci (Elite Ed) 2011;3:711-735.
19. Suzuki S, Haruyama N, Nishimura F, Kulkarni AB. Dentin sialophosphoprotein and dentin matrix protein-1: two highly phosphorylated proteins in mineralized tissues. Arch Oral Biol 2012;57:1165-1175.
20. Bidar M, Moushekhian S, Gharechahi M, Talati A, Ahrari F, Bojarpour M. The effect of low level laser therapy on direct pulp capping in dogs. J Lasers Med Sci 2016;7:177-183.
21. Faul F, Erdfelder E, Lang AG, Buchner A. G*Power 3: a flexible statistical power analysis program for the social, behavioral, and biomedical sciences. Behav Res Methods 2007;39:175-191.
22. Clarke KW, Trim CM, Hall LW. Anaesthesia of the dog. In: Clarke KW, Trim CM, Hall LW, editors. Veterinary anaesthesia. 11th ed. Saunders; 2014. p. 405-498.
23. Emara RA, Abu-Seida AM, El Ashry SH. Histological evaluation of the synergistic effect of chitosan and mineral trioxide aggregate on mechanically exposed dental pulp following pulp capping in dogs' teeth. Saudi Endod J 2022;12:25-30.
24. Close B, Banister K, Baumans V, Bernoth EM, Bromage N, Bunyan J, *et al*. Recommendations for euthanasia of experimental animals: part 2. DGXT of the European Commission. Lab Anim 1997;31:1-32.
25. Schindelin J, Arganda-Carreras I, Frise E, Kaynig V, Longair M, Pietzsch T, *et al*. Fiji: an open-source platform for biological-image analysis. Nat Methods 2012;9:676-682.
26. Nokhbatolfoghahaei H, Paknejad Z, Bohlouli M, Rezai Rad M, Khojasteh A. Animal models in dental research. In: Tayebi L, editor. Applications of biomedical engineering in dentistry. Cham: Springer; 2020. p. 377-442.
27. Safy RK, Ragab MH, Abdel-Maksoud HB. Histopathological evaluation of human placental extract as a direct pulp-capping material in dogs' teeth. Eur J Dent 2025;19:144-153.
28. Soliman HA, El-Toukhy RI, Ibrahim MM, Grawish ME, Kader Sobh MA, Mahmoud SH. Impact of corticosteroid administration on the response of exposed dental pulp to capping with bioactive cements: experimental study on mongrel dogs. BMC Oral Health 2023;23:423.
29. Alfahlawy A, Selim MA, Hassan HY. Biocompatibility of three different root canal sealers, experimental study. BMC Oral Health 2023;23:715.
30. Afkhami F, Rostami G, Xu C, Walsh LJ, Peters OA. The application of lasers in vital pulp therapy: a review of histological effects. Lasers Med Sci 2023;38:215.
31. Yazdanfar I, Gutknecht N, Franzen R. Effects of diode laser on direct pulp capping treatment: a pilot study. Lasers Med Sci 2015;30:1237-1243.
32. Pan H, Yang Y, Xu H, Jin A, Huang X, Gao X, *et al*. The odontoblastic differentiation of dental mesenchymal stem cells: molecular regulation mechanism and related genetic syn-

dromes. Front Cell Dev Biol 2023;11:1174579.
33. Hemdan DK, Selim MA, Galhom RA, El Daharawy MH, Hassan HY. Effects of autologous dental pulp stem cells and mineral trioxide aggregate on exposed dogs' dental pulp. J Oral Biol Craniofac Res 2022;12:293-298.
34. Okiji T, Yoshiba K. Reparative dentinogenesis induced by mineral trioxide aggregate: a review from the biological and physicochemical points of view. Int J Dent 2009;2009:464280.
35. Mutar MT, Mahdee AF. Different pulp capping agents and their effect on pulp inflammatory response: a narrative review. Saudi Dent J 2024;36:1295-1306.
36. Okabe T, Sakamoto M, Takeuchi H, Matsushima K. Effects of pH on mineralization ability of human dental pulp cells. J Endod 2006;32:198-201.
37. Martín G, Preve V, Hargreaves K, Diogenes A, Inostroza C, Saint-Jean N, *et al*. Effect of dentin conditioning with EDTA and diode lasers on expression of odontoblast-like cell markers of dental pulp stem cells. Dent J (Basel) 2023;11:210.
38. Deng Y, Zhu X, Zheng D, Yan P, Jiang H. Laser use in direct pulp capping: a meta-analysis. J Am Dent Assoc 2016; 147:935-942.
39. Simon S, Smith AJ, Lumley PJ, Cooper PR, Berdal A. The pulp healing process: from generation to regeneration. Endod Top 2012;26:41-56.
40. Quispe-Salcedo A, Ida-Yonemochi H, Nakatomi M, Ohshima H. Expression patterns of nestin and dentin sialoprotein during dentinogenesis in mice. Biomed Res 2012;33:119-132.

https://doi.org/10.5395/rde.2026.51.e4

RDE Restorative Dentistry & Endodontics

Research Article

eISSN 2234-7666
Restor Dent Endod. 2026 February;51(1):e5
https://doi.org/10.5395/rde.2026.51.e5

Analysis of the reciprocating kinematics of the VDW Silver Reciproc, E-Connect Pro, Ecom, and Endopen endodontic motors: an *in vitro* experimental study

Cristielly França[1], Juliana D. Bronzato[2,*], Dieimes Braambati[1], Adriana de-Jesus-Soares[2], Carla C. R. B. Félix[1], Michelle A. N. S. Ferreira[1], Marcos Frozoni[1]

[1]Department of Endodontics, São Leopoldo Mandic School of Dentistry, Campinas, Brazil
[2]Division of Endodontics, Department of Restorative Dentistry, Piracicaba Dental School, State University of Campinas, Piracicaba, Brazil

ABSTRACT

Objectives: This study aimed to evaluate the actual parameters of four endodontic motors, each adjusted for reciprocating motion, and compare them to the manufacturers' declared values.

Methods: The motors used were the VDW Silver Reciproc (VDW GmbH), E-Connect Pro (MK Life), Ecom (Woodpecker), and Endopen (Schuster Woodpecker). A custom optical target was attached to the motor contra-angle, the movements were recorded with a high-resolution camera, and the images were analyzed. Engagement, disengagement, net angles, and speed for each operation cycle, duration of clockwise (CW) and counter-clockwise (CCW) movement, duration of standstill after CW and CCW movement, and the number of cycles to complete a full rotation were analyzed. The data were statistically analyzed at a significance level of 5%. The replicability of all reciprocal parameters analyzed was statistically different from that reported by the manufacturers.

Results: There was no statistically significant difference between the VDW Silver Reciproc, Ecom, and Endopen for the engagement angle. The E-Connect Pro was the least reliable at the 150°/30° settings for both angle parameters. There was no significant difference between the set and actual cycle net angles for the VDW Silver Reciproc ($p = 0.493$). While the actual values for the Ecom and E-Connect Pro were significantly higher than the set ($p < 0.001$), the actual values for the Endopen were significantly lower than the set ($p < 0.001$).

Conclusions: Experiments on four commercially available reciprocating endodontic motors revealed that the actual motor values differed significantly from the set values.

Keywords: Dental equipment; Dental instruments; Endodontics; Image processing; Root canal preparation; Video recording

Received: August 18, 2025 **Revised:** October 10, 2025 **Accepted:** October 12, 2025

Citation
França C, Bronzato JD, Braambati D, de-Jesus-Soares A, Félix CCRB, Ferreira MANS, Frozoni M. Analysis of the reciprocating kinematics of the VDW Silver Reciproc, E-Connect Pro, Ecom, and Endopen endodontic motors: an *in vitro* experimental study. Restor Dent Endod 2026;51(1):e5.

***Correspondence to**
Juliana D. Bronzato, DDS, PhD
Division of Endodontics, Department of Restorative Dentistry, Piracicaba Dental School, State University of Campinas-UNICAMP, Av. Limeira 901, Bairro Areao, Piracicaba, SP 13414-903, Brazil
E-mail: julianadelatorre_@hotmail.com

INTRODUCTION

Asymmetrical reciprocating kinematics was introduced in endodontics in an attempt to provide safer and more efficient root canal preparation since reciprocating systems permit performing the procedure using only one file [1,2]. Manufacturers claim that this movement reduces the likelihood of instrument twisting due to the periodical change in the direction of rotation, exposing the instrument to lower tension [3–5]. This kinematics has been extensively discussed and studied in recent years and the findings indicate an increase in the files' resistance to cyclic fatigue [5–11].

Endodontic motors have been extensively used as an aid to treatments, particularly to provide different types of reciprocating motion. There are multiple commercially available motors, each priced differently and promising a different performance. However, it is important to note that the reciprocal angles and rotation speeds of these motors can have a significant impact on the endodontic files used. Any deviations from the standard settings can affect the instrument's fatigue resistance, as well as its cutting capacity [8]. A previous study that altered the asymmetrical reciprocating kinematics compared to that recommended by the manufacturer showed that decreasing the reciprocation range of the reciprocating motion increased the time to fracture [8,12]. However, the authors advised against increasing rotation in the counter-clockwise (CCW) direction due to the overload of the instrument [8].

Alternative root canal preparation systems using programs and standards for each file set have been launched, including Reciproc (VDW, Munich, Germany) [12–15] with a 150° CCW and 30° clockwise (CW) rotation [7]. The movements resulted in a net angle of 120º, indicating that each cycle of three movements rotates the file completely [9].

The precision of these angles is critical for the clinical professional because it has a direct impact on instrument performance, on the quality of root canal preparation, and, most importantly, on the risk of file separation. Within this context, previous studies had already questioned the reliability of some endodontic motors regarding the actual reciprocating angle and rotation speed [9,16–19]. However, the present study is the first to assess the reliability of the E-Connect Pro (MK Life, Porto Alegre, Brazil), Ecom (Woodpecker, Guilin, China), and Endopen (Schuster Woodpecker, Guilin, China) endodontic motors. These motors are widely commercialized due to their low investment cost compared to more established models on the market, especially among newly graduated dentists.

Therefore, this study aimed to evaluate the actual parameters of four different endodontic motors, each adjusted for asymmetrical reciprocating motion, and to compare the results with the values provided by the manufacturers. The null hypotheses were that there was no statistically significant difference between the proposed and actual values, nor between the motors tested (VDW Silver Reciproc [VDW], E-Connect Pro, Ecom, and Endopen).

METHODS

Sample size calculation

The sample size was calculated using the results of a previous study [17]. To achieve a 5% level of significance, the calculation indicated that each 10-second recording should be repeated three times per sample. The calculation information was tabulated in a Microsoft Excel 2013 spreadsheet (Microsoft, Redmond, WA, USA).

Selection and adjustment of the endodontic motors

The following endodontic motors were tested: VDW Silver Reciproc, E-Connect Pro, Ecom, and Endopen. They have approximate weights of the handpiece and components of 1,100 g, 800 g, 945 g, and 842 g, respectively. All endodontic motors, new and unused, were utilized in the "Reciproc Reciprocating ALL" mode. For those motors in which this exact mode under this name was not available, but that allowed manual adjustment of the reciprocating angles, the settings were standardized to 150° CCW and 30° CW, following the specifications provided by the manufacturer of the Reciproc system. All motors ran with the battery fully charged but unplugged from the power cord. Furthermore, the motors were calibrated before each use, as recommended by the manufacturers.

https://doi.org/10.5395/rde.2026.51.e5

Kinematic analysis of the endodontic motors

The actual angles were measured in each group using a customized polypropylene target with a diameter of 5 cm and 359 marked lines representing each degree. This method was adopted based on previous research [17,18]. The target was mounted on a disc and then attached to the contra-angle handpieces (Figure 1).

Videos of the optical target operating in asymmetrical reciprocating kinematics were recorded using a super macro lens (Tamron SP AF 90 mm; Canon, Tokyo, Japan), with a focal adjustment of 0.45, connected to a high-speed camera (Phantom VEO 610L; Infinity Photo-Optical Company, Centennial, CO, USA). The lens was positioned 30 cm from the target (Figure 2). The camera was set to record high-quality videos at 3,000 frames per second (FPS) and a resolution of 960 × 960 pixels.

Each cycle of asymmetrical reciprocating motion of the motor with the optical target was recorded three times, with each recording lasting 10 seconds, for a total of 12 shots. In each recording, in MOV file format, 10 complete cycles of sequential reciprocating motions were chosen at random for analysis and evaluation of kinematic data. Each cycle was analyzed to identify the duration of each movement.

Ten sequential cycles within each footage were analyzed using the Vision Research software (Vision Research Inc., Wayne, NJ, USA) installed on a personal computer (Intel i3 8th Gen, 8GB RAM, 1TB HD; Dell, Round Rock, TX, USA). The rotation angle between two consecutive frames was based on the difference in the orientation of the graduated lines (Figure 1) and the values automatically provided by the software (Figure 3). The following data were obtained and used to calculate the kinematic parameters, as defined in previous studies [3,9,17,18]:

(1) Engagement angle ((CCW, °): θe
(2) Disengagement angle (CW, °): θd
(3) CW movement duration (ms): *Dcw*
(4) Duration of standstill after CW movement (ms): *Scw*
(5) CCW movement duration (ms): *Dccw*
(6) Duration of standstill after CCW movement (ms): *Sccw*

After collecting these data, the following parameters were calculated:

(1) Net angle of the cycle (°): $\theta e - \theta d$
(2) Engagement speed (revolutions/min [rpm]): (θe / *Dccw*) × (60,000 ms / 360°)

Figure 1. A 5-cm-diameter polypropylene disc marked in degree intervals from 0° to 360° was used in the experiment.

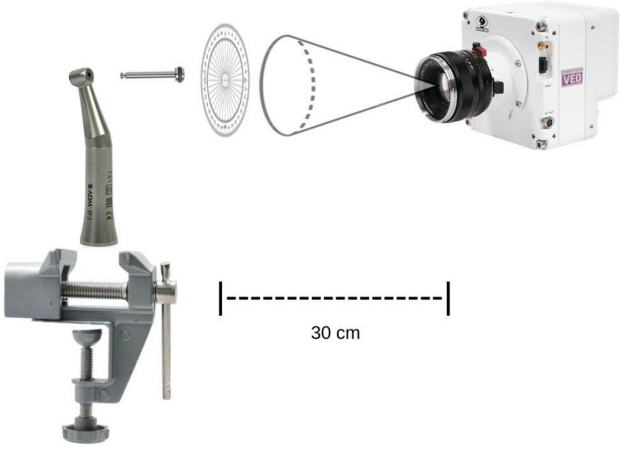

Figure 2. Schematic representation of the camera assembly, lens, target, motor, and water-aligned contra-angle used for image capture.

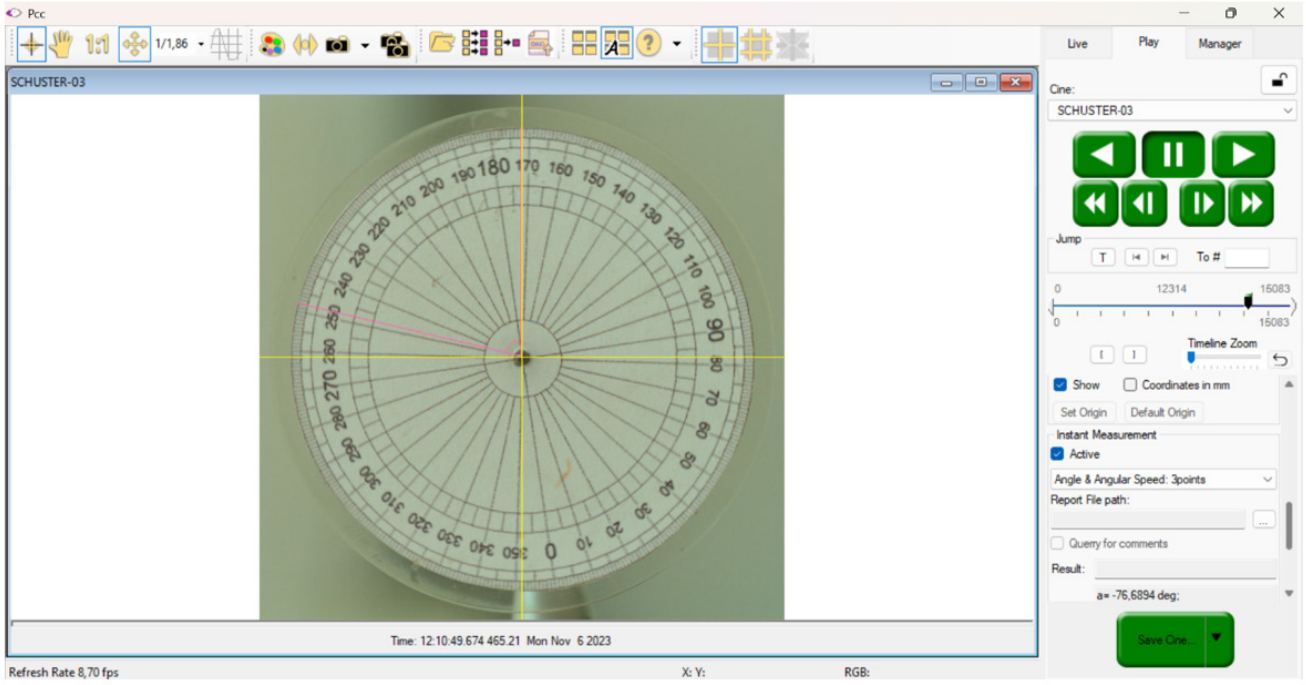

Figure 3. Print screen Vision Research software (Vision Research Inc., Wayne, NJ, USA).

(3) Disengagement speed (rpm): (θd / Dcw) × (60,000 ms / 360°)
(4) Speed of the total reciprocating cycle (rpm): (θe + θd) / ($Dccw$ + $Sccw$ + Dcw + Scw) × (60,000 ms / 360°)
(5) Number of cycles to complete a full rotation: 360° / (net angle)

Statistical analysis

For comparison of the endodontic motors, normally distributed data were analyzed by one-way analysis of variance, followed by the Tukey test for multiple comparisons when the data were homoscedastic and the Games-Howell test when the data were heteroscedastic. The Kruskal-Wallis test was applied when the data did not fit a normal distribution, followed by the Student-Newman-Keuls test. It was observed that most variables showed a normal distribution across the groups. However, some variables, such as the duration of standstill after CW movement, the net angle of the cycle, and the number of cycles to complete a full rotation, exhibited a non-normal distribution in certain groups.

The actual and set values of engagement angle, disengagement angle, and net angle were compared using the Student t-test and one-sample Wilcoxon test. Statistical calculations were performed using IBM SPSS version 23 (IBM Corp, Armonk, NY, USA) and BioEstat 5.0 (Fundação Mamirauá, Belém, PA, Brazil), adopting a level of significance of 5%.

RESULTS

The endodontic motors VDW Silver Reciproc, Ecom, and Endopen, which did not differ statistically from each other regarding the engagement angle, showed significantly lower values than the E-Connect Pro motor. Regardless of the motor, the actual engagement angles were significantly greater than the set values ($p < 0.001$). This finding was also observed for the disengagement angles ($p < 0.001$), where the Ecom motor presented a significantly lower disengagement angle than the VDW Silver Reciproc. In turn, the VDW Silver Reciproc showed a lower value than the Endopen, whose disengagement angle was significantly smaller than that measured for the E-Connect Pro motor (Table 1).

The VDW Silver Reciproc motor had a significantly shorter CCW movement duration compared to the Ecom, which in turn had a shorter duration than

https://doi.org/10.5395/rde.2026.51.e5

Table 1. Mean and standard deviation of the kinematic variables of the different endodontic motors studied

Variable	Motor				*p*-value
	VDW Silver	E-Connect Pro	Ecom	Endopen	
Engagement angle, CCW (º)	193.37 ± 10.80$^{A,a)}$	346.58 ± 0.73$^{B,a)}$	213.85 ± 1.07$^{A,a)}$	227.63 ± 0.72$^{A,a)}$	<0.001
Disengagement angle, CW (º)	78.38 ± 0.50$^{B,c)}$	172.44 ± 1.66$^{D,c)}$	63.52 ± 0.97$^{A,c)}$	117.72 ± 0.90$^{C,c)}$	<0.001
CCW movement duration (ms)	70.53 ± 0.26^{A}	108.63 ± 1.59^{C}	74.75 ± 0.61^{B}	113.12 ± 1.18^{D}	<0.001
Duration of standstill after CCW movement (ms)	1.00 ± 0.14^{C}	0.37 ± 0.05^{A}	0.81 ± 0.20^{BC}	0.38 ± 0.05^{AB}	0.034
CW movement duration (ms)	42.39 ± 0.73^{A}	42.36 ± 1.15^{A}	64.25 ± 0.37^{C}	47.67 ± 0.77^{B}	<0.001
Duration of standstill after CW movement (ms)	0.35 ± 0.02^{A}	0.69 ± 0.05^{AB}	0.34 ± 0.02^{A}	0.95 ± 0.33^{B}	0.006
Net angle of the cycle (º)	114.99 ± 10.43$^{A,c)}$	174.14 ± 2.23$^{B,d)}$	150.33 ± 1.83$^{AB,d)}$	109.92 ± 0.21$^{A,d)}$	0.024
Engagement speed (rpm)	456.97 ± 10.80^{B}	531.83 ± 6.92^{C}	476.85 ± 5.79^{B}	335.43 ± 4.47^{A}	<0.001
Disengagement speed (rpm)	308.17 ± 3.38^{B}	678.70 ± 12.14^{D}	164.79 ± 3.40^{A}	411.58 ± 3.55^{C}	<0.001
Speed of the total reciprocating cycle (rpm)	396.34 ± 15.68^{C}	568.94 ± 3.03^{D}	329.86 ± 1.06^{A}	355.02 ± 1.68^{B}	<0.001
Number of cycles to complete full rotation	3.15 ± 0.30^{B}	2.07 ± 0.03^{A}	2.39 ± 0.03^{AB}	3.28 ± 0.01^{B}	0.023

Values are presented as mean ± standard deviation.
CW, clockwise; CCW, counter-clockwise; rpm, revolutions/min.
For each variable, means in the same row followed by different capital letters differ significantly between the endodontic motors.
[a)]Actual angle differs significantly from the set value (150º); [b)]Actual angle differs significantly from the set value (30º); [c)]Actual angle does not differ significantly from the set value (120º); [d)]Actual angle differs significantly from the set value (120º).
VDW Silver Reciproc: VDW GmbH, Munich, Germany; E-Connect Pro: MK Life, Porto Alegre, Brazil; Ecom: Guilin Woodpecker Medical Instrument, Guilin, China; Endopen: Schuster Woodpecker, Guilin, China.

that observed for the E-Connect Pro motor. The latter showed a significantly shorter duration than the Endopen motor (Table 1). Regarding the duration of the standstill after CCW movement, the E-Connect Pro demonstrated the shortest time, which was significantly shorter than that observed for the Ecom and VDW Silver Reciproc motors, with no significant difference between these two. Meanwhile, the duration of standstill after CCW movement for the Endopen motor did not differ significantly from the values measured for the E-Connect Pro and Ecom motors (Table 1).

The CW movement duration was significantly shorter in the VDW Silver Reciproc and E-Connect Pro motors, which did not differ significantly from each other. For the Endopen motor, the CW movement duration was significantly shorter than that of the Ecom motor (Table 1).

Considering the duration of the standstill after CW movement, the VDW Silver Reciproc and Ecom motors, which did not differ significantly from each other, showed significantly shorter times than that observed for the Endopen motor. As for the E-Connect Pro, the standstill duration after CW movement did not differ from the other three motors (Table 1).

There was no significant difference between the set and actual net cycle angles for the VDW Silver Reciproc motor ($p = 0.493$). While the Ecom and E-Connect Pro motors exhibited actual values significantly greater than the set ones ($p < 0.001$), the Endopen motor ($p < 0.001$) showed actual values significantly lower than the set. When comparing the four motors, the VDW Silver Reciproc and Endopen were associated with significantly smaller net cycle angles than those measured for the E-Connect Pro motor. Additionally, the Ecom motor had a net cycle angle that did not differ significantly from the other three motors (Table 1).

Regarding the engagement speed, the Endopen motor showed a significantly lower value compared to the VDW Silver Reciproc and Ecom motors, which did not differ statistically from each other and had lower values than those found for the E-Connect Pro (Table 1). The E-Connect Pro motor also exhibited the highest values among all motors for both disengagement speed and total reciprocating cycle speed. For these two variables, the Ecom motor had the lowest values compared to the remaining motors. However, while the VDW Silver Reciproc motor had a lower disengagement speed than the Endopen, the result was reversed for the total reciprocating cycle speed between these two motors (Table 1).

The number of cycles required to complete a full rotation was significantly lower for the E-Connect Pro motor compared to the VDW Silver Reciproc and Endopen motors, which did not differ significantly from each other. For the Ecom motor, the number of cycles to complete a full rotation did not differ significantly from any of the other three motors (Table 1).

DISCUSSION

Automated mechanical preparation of root canals is predominantly performed using nickel-titanium instruments. These instruments can operate in either rotary or reciprocating kinematics. However, accurate reproduction of the reciprocating kinematics appears to be more complex [19]. The reliability of these angles is critical because of their effects on instrument performance (such as cutting efficiency and debris removal) and, consequently, on the quality of root canal preparation [8–11].

In addition, file separation within the root canal system is one of the most frequently reported iatrogenic incidents by dentists, caused by several factors. Among these factors, reciprocation angles stand out, as larger angles in asymmetrical reciprocating motion increase the risk of instrument fracture. This highlights the importance of ensuring that the intended angles are properly achieved for each programming setting, thereby providing greater safety during the procedure [7–9]. However, the null hypothesis was rejected, indicating a significant difference between the actual and set values.

Saber *et al.* [8] found that reducing the difference between the engaging and disengaging angles, with lower values in the CCW angle, increases the instrument's resistance to fracture by subjecting it to less stress. However, this comes at the cost of less canal transportation and longer preparation time. Reducing the number of cycles by increasing the CCW angle values was discouraged since it would put more stress on the instrument. Other studies [5,7,16] have indicated that instruments operating at higher speeds, similar to the findings of this research, are more susceptible to fracture compared to when used at lower rotational speeds.

Kinematic values are not fully disclosed by some manufacturers, and there is limited information available regarding the asymmetrical reciprocating motion generated by the motors [19]. Angular kinematic data are neither publicly available nor officially provided by the manufacturer VDW. Therefore, the values assumed in the present study for the Reciproc system, 150° CCW and 30° CW at a speed of 300 RPM, were based on the literature [3,8,9,17–19].

The evaluation of asymmetrical reciprocating kinematics requires a detailed methodology. Previous studies have used different cameras to record this kinematics, including a 1,000 FPS camera with a resolution of 224 × 64 pixels [18], a 1,200 FPS camera with 336 × 96 pixels [17], a 960 FPS camera with 1,136 × 384 pixels [20], a 600 FPS camera with 432 × 192 pixels [19] and a 2,400 FPS camera with 800 × 800 pixels [9]. To achieve optimum precision, this study used a high-resolution camera with 3,000 FPS and a resolution of 960 × 960 pixels, a significant improvement compared to previous investigations.

The low reliability observed in the present study for the reciprocating angles of the VDW Silver Reciproc motor is consistent with the literature [9,17–19]. However, this is the first study that assessed the reliability of the Ecom, Endopen, and E-Connect Pro endodontic motors. These three motors were recently launched on the market. Our findings indicate low reliability of the E-Connect Pro motor at reciprocating angles. Regarding the Ecom and Endopen, both exhibited characteristics and variations similar to the VDW Silver Reciproc motor, which showed values closer to those recommended by the manufacturers.

The VDW Silver Reciproc motor showed actual CCW and CW angles in Reciproc mode that were greater than those reported in the literature [9,19]. On the other hand, our values were consistent with those observed in another study [20]. Variations in FPS and in the number of pixels in the images between studies may explain the divergence in the results compared to the studies by Braambati *et al.* [9] and Fidler *et al.* [19]. Fidler [18] highlighted that the use of high-speed cameras allows for accurate analysis of the kinematics of endodontic motors and that accurate values of alternative angles influence the cyclic fatigue resistance of instruments. Similarly, Irmak and Orhan [17] emphasize that additional studies conducted with high-speed cameras and higher

https://doi.org/10.5395/rde.2026.51.e5

resolutions are necessary and should be carried out to evaluate more accurate real kinematics. Braambati *et al*. [9] demonstrated that higher FPS rates provide greater accuracy in kinematic assessment. An in-depth examination of the reported data reveals that variations in the engagement angles of the VDW motor correspond to the disengagement angles in degrees. This suggests that discrepancies in the set values for the cutting angles are proportionally reflected during the disengagement phase, aligning with the findings of another study [19,20].

When the actual CCW and CW angles exceed the set values, the preparation and shaping capacity are compromised, the instrument's resistance to cyclic fatigue is reduced, and root microcracks may form; however, the preparation time is reduced [8,9,11,16]. Despite their low reliability, the VDW Silver Reciproc, Ecom, and Endopen motors had similar variations, with none of them showing an adjusted engagement angle discrepancy greater than 52%. The highest engagement angle inaccuracy was observed for the E-Connect Pro motor, which was 131%. Furthermore, the VDW Silver Reciproc motor showed a discrepancy of 28% in engagement angle in the reciprocating mode.

The E-Connect Pro motor, on the other hand, produced discrepant values that were twice or more than those set for the engagement and disengagement angles, indicating lower precision when compared to the other motors. These angle errors resulted in a net cycle angle greater than 120° of the stipulated movement, allowing the system to operate much faster and with fewer cycles per rotation. More research is needed to identify possible mechanical and electromagnetic differences in the composition and manufacturing of the E-Connect Pro motor versus other motors.

Recent studies investigated the effect of rotary motor power on kinematic accuracy [9,18,19,21]. While the VDW Silver Reciproc motor requires a battery case and a handpiece connection cable, the Ecom, Endopen, and E-connect Pro motors are wireless, a fact that may improve ergonomics but potentially introduce differences in power stability and control. Although all tested motors have predefined angles for use in the reciprocating mode, only the VDW Silver Reciproc motor has the designation "Reciproc mode" with fixed angular settings, while angle adjustment is possible in the other motors. The flexibility of the other motors, although advantageous in customizing performance, may contribute to inconsistencies between programmed and actual motion parameters. Additionally, discrepancies observed in actual versus set values, especially for engagement and disengagement angles, may reflect limitations in internal motor control mechanisms, such as torque management, sensor feedback, or mechanical inertia.

Each time the motor transitions from CCW to CW and vice versa, it briefly interrupts its displacement. These interruptions are necessary for the motor to stop and change the direction of rotation, and this process is controlled by the endodontic motor unit. Fidler [18] demonstrated that, in order to reach the declared cycle speed, the standstill time was compensated by increasing the speed during the rotation phases, as speculated by Gambarini *et al*. [16]. Fidler [18] found a stopping time of 6.4 ± 0.8 ms for the VDW Silver Reciproc motor, while another study [9] reported a variation of 0.83 ms in the Reciproc mode, which is consistent with the data obtained here. This fraction of a second is caused by the stop required to change direction and, according to some studies [18,21], can be influenced by loose mechanical components. However, Braambati *et al*. [9] used less sensitive cameras, which resulted in longer image frames than those used in the present study. It is worth stating that the present study focused on the angular parameters obtained, with the standstill time information being collected solely to clarify the data presented.

During the CCW movement, there was a progressive reduction in speed after a certain rotation point, especially for the Endopen and E-Connect Pro motors, with the minimum time of stoppage to subsequently initiate the change of direction, resulting in values significantly lower than those observed for the other motors. This is because the speed reduction made the need to immediately stop the engagement angle toward the reverse action less abrupt.

The duration of the standstill after CW movement did not differ significantly between the VDW Silver Reciproc and Ecom motors, whereas the E-Connect Pro and Endopen motors exhibited a significantly shorter duration. The results are consistent with the literature [21] and

can be explained by the lack of clearance between the mechanical parts of the motor, which are new and unused instruments, as well as the absence of a torsional load during the reciprocating movement observed in clinical practice [18,21].

Although most of the analyzed variables showed a normal distribution, some specific variables, such as the duration of standstill after CW movement, the net angle of the cycle, and the number of cycles to complete a full rotation, exhibited a non-normal distribution in certain groups. The limited number of observations per group may hinder the approximation to a normal distribution, especially for variables highly sensitive to small variations. This may contribute to the observed heterogeneity and justifies the use of nonparametric tests in some statistical comparisons.

The engagement and disengagement speed results appear to be associated with the other parameters analyzed (Table 1). The fact that the speed was greater than 300 rpm, as stated by the manufacturer VDW [3,20], may have caused the angles to exceed the adjustment values. Some authors suggest a close relationship between rotational speed and file separation, in which higher engagement and disengagement speeds lead to a reduction in resistance to cyclic fatigue [4,16,18,22–24].

According to a previous study [21], a possible explanation for the asymmetrical kinematic differences between actual and set speed and angulation values is the movement's mechanical inertia, which can compromise reliability [21]. In other words, even after the control unit of the device determined the stop action, inertia may have allowed the movements to continue. As a result, the greater the speed, the more effective this property is.

Another study [19] revealed that asymmetrical reciprocating motion exhibits more complex kinematics when analyzed frame by frame on a computer, showing variations in rotational speed at each phase, similar to the present study. In comparison, both studies showed no statistically significant difference in net cycle values and presented similar results regarding cycle duration and standstill duration for the VDW motor [19].

As previously mentioned, all tests were conducted with the motors operating without any resistance, an uncommon condition during canal preparation in clinical settings. This might have led to the higher actual values compared to the predetermined ones. Previous studies [9,17,25] have also identified this limitation in their methodologies. Further research, whether ex vivo or clinical, using conditions that simulate root canal shaping, is necessary to confirm the clinical efficacy of these motors and to develop strategies aimed at reducing the risk of file separation [3,19]. Furthermore, this study evaluated only one motor from each manufacturer. Although only new motors were used, the specific models tested may differ from other commercially available motors of the same brand. Therefore, future studies should include a larger number of motors to ensure a more comprehensive and representative analysis.

The inherent differences in the manufacturing process and in the mechanical performance of endodontic motors may influence the results obtained. However, manufacturers generally do not provide detailed information regarding the internal architecture of these devices. Although the present study was based solely on experimental performance data, it is important to highlight that factors such as the precision of the electronic control unit and the type of drive system (brushed or brushless) may theoretically influence torque and rotation stability and, consequently, the effective engagement and disengagement angles. A more in-depth analysis of these engineering differences and manufacturing parameters, therefore, represents a relevant aspect that warrants further investigation.

All four motors did not follow the expected 150º/30º engagement/disengagement pattern. However, the VDW Silver and Endopen motors have net angular values near 120º, reaching 360º shortly after three engagement/disengagement cycles.

CONCLUSIONS

Analysis of four different commercially available reciprocating endodontic motors revealed that the actual motor values differed significantly from the set values. Notably, greater discrepancy was observed for the E-Connect Pro endodontic motor compared to the VDW Silver Reciproc, Ecom, and Endopen motors.

https://doi.org/10.5395/rde.2026.51.e5

CONFLICT OF INTEREST

No potential conflict of interest relevant to this article was reported.

FUNDING/SUPPORT

The authors have no financial relationships relevant to this article to disclose.

AUTHOR CONTRIBUTIONS

Conceptualization, Data curation, Investigation, Methodology: França C, Braambati D, Félix CCRB, Ferreira MANS, Frozoni M. Formal analysis: França C, Bronzato JD, Braambati D, Félix CCRB, Ferreira MANS, Frozoni M. Validation: França C, Bronzato JD, Braambati D, de-Jesus-Soares A, Frozoni M. Writing - original draft: França C. Writing - review & editing: França C, Bronzato JD, Braambati D, de-Jesus-Soares A, Frozoni M. All authors read and approved the final manuscript.

DATA SHARING STATEMENT

The datasets are not publicly available but are available from the corresponding author upon reasonable request.

REFERENCES

1. Yared G. Canal preparation using only one Ni-Ti rotary instrument: preliminary observations. Int Endod J 2008;41:339-344.
2. Tinoco JM, De-Deus G, Tinoco EM, Saavedra F, Fidel RA, Sassone LM. Apical extrusion of bacteria when using reciprocating single-file and rotary multifile instrumentation systems. Int Endod J 2014;47:560-566.
3. Kim HC, Kwak SW, Cheung GS, Ko DH, Chung SM, Lee W. Cyclic fatigue and torsional resistance of two new nickel-titanium instruments used in reciprocation motion: Reciproc versus WaveOne. J Endod 2012;38:541-544.
4. Pedullà E, Grande NM, Plotino G, Palermo F, Gambarini G, Rapisarda E. Cyclic fatigue resistance of two reciprocating nickel-titanium instruments after immersion in sodium hypochlorite. Int Endod J 2013;46:155-159.
5. De-Deus G, Moreira EJ, Lopes HP, Elias CN. Extended cyclic fatigue life of F2 ProTaper instruments used in reciprocating movement. Int Endod J 2010;43:1063-1068.
6. Paqué F, Zehnder M, De-Deus G. Microtomography-based comparison of reciprocating single-file F2 ProTaper technique versus rotary full sequence. J Endod 2011;37:1394-1397.
7. Karataş E, Arslan H, Büker M, Seçkin F, Çapar ID. Effect of movement kinematics on the cyclic fatigue resistance of nickel-titanium instruments. Int Endod J 2016;49:361-364.
8. Saber Sel D, Abu El Sadat SM. Effect of altering the reciprocation range on the fatigue life and the shaping ability of WaveOne nickel-titanium instruments. J Endod 2013;39:685-688.
9. Braambati D, Monteiro Netto RC, Coelho MS, Soares AJ, Frozoni M. Reciprocating kinematics of X-smart plus, VDW silver and, iroot endodontic motors: a comparison between real and set values. Braz Dent J 2022;33:28-35.
10. Yared G. Canal preparation with nickel-titanium or stainless steel instruments without the risk of instrument fracture: preliminary observations. Restor Dent Endod 2015;40:85-90.
11. Al-Sudani D, Kaabi H, Al Gamdi A, Al Dakheel A. The influence of different angles and reciprocation on the shaping ability of two nickel-titanium rotary root canal instruments. J Contemp Dent Pract 2014;15:451-455.
12. Kim HC, Hwang YJ, Jung DW, You SY, Kim HC, Lee W. Micro-computed tomography and scanning electron microscopy comparisons of two nickel-titanium rotary root canal instruments used with reciprocating motion. Scanning 2013;35:112-118.
13. Gergi R, Osta N, Bourbouze G, Zgheib C, Arbab-Chirani R, Naaman A. Effects of three nickel titanium instrument systems on root canal geometry assessed by micro-computed tomography. Int Endod J 2015;48:162-170.
14. Plotino G, Ahmed HM, Grande NM, Cohen S, Bukiet F. Current assessment of reciprocation in endodontic preparation: a comprehensive review: part II: properties and effectiveness. J Endod 2015;41:1939-1950.
15. Plotino G, Grande NM, Testarelli L, Gambarini G. Cyclic fatigue of Reciproc and WaveOne reciprocating instruments. Int Endod J 2012;45:614-618.
16. Gambarini G, Rubini AG, Al Sudani D, Gergi R, Culla A, De Angelis F, *et al.* Influence of different angles of reciprocation on the cyclic fatigue of nickel-titanium endodontic instruments. J Endod 2012;38:1408-1411.
17. Irmak Ö, Orhan EO. Kinematic analysis of new and used reciprocating endodontic motors in 2 different modes. Int J Artif Organs 2017;41:17-22.
18. Fidler A. Kinematics of 2 reciprocating endodontic motors: the difference between actual and set values. J Endod 2014;40:990-994.
19. Fidler A, Orhan EO, Irmak Ö. Computer-aided phase identification and frame-to-frame analysis of endodontic asymmetric reciprocation rotation: a preliminary study. Image Anal Stereol 2020;39:91-99.

20. Rodrigues EA, Costa DG, Junior F, Dantas LT, De-Deus G; Simões-Carvalho M, *et al*. A computer-assisted approach to assess the precision of the reciprocating angles and the rotation speeds of endodontic motors. Appl Syst Innov 2022;5:68.
21. Orhan EO, Irmak O, Ertuğrul IF. Kinematics of a novel reciprocating endodontic handpiece. Int Endod J 2019;52:1235-1243.
22. Martín B, Zelada G, Varela P, Bahillo JG, Magán F, Ahn S, *et al*. Factors influencing the fracture of nickel-titanium rotary instruments. Int Endod J 2003;36:262-266.
23. Herold KS, Johnson BR, Wenckus CS. A scanning electron microscopy evaluation of microfractures, deformation and separation in EndoSequence and Profile nickel-titanium rotary files using an extracted molar tooth model. J Endod 2007;33:712-714.
24. Ferreira F, Adeodato C, Barbosa I, Aboud L, Scelza P, Zaccaro Scelza M. Movement kinematics and cyclic fatigue of NiTi rotary instruments: a systematic review. Int Endod J 2017;50:143-152.
25. Orhan EO, Bahadır D, Irmak O. Kinematics of "adaptive motion" under constant torque values. J Endod 2022;48:355-361.

https://doi.org/10.5395/rde.2026.51.e5

RDE Restorative Dentistry & Endodontics

Research Article

eISSN 2234-7666
Restor Dent Endod. 2026 February;51(1):e6
https://doi.org/10.5395/rde.2026.51.e6

Influence of adjacent restorative material and distance on the accuracy of inlay cavity impressions with intraoral scanner: an *in vitro* study

So-Yeon Lee[1,2,3], Sung-Ae Son[1,2,3], Jae-Hoon Kim[2,3,4], Deog-Gyu Seo[5], Jeong-Kil Park[1,2,3,*]

[1]Department of Conservative Dentistry, School of Dentistry, Pusan National University, Yangsan, Korea
[2]Dental and Life Science Institute, School of Dentistry, Pusan National University, Yangsan, Korea
[3]Dental Research Institute, Pusan National University Dental Hospital, Yangsan, Korea
[4]Department of Dental Education, School of Dentistry, Pusan National University, Yangsan, Korea
[5]Department of Conservative Dentistry, Dental Research Institute, School of Dentistry, Seoul National University, Seoul, Korea

ABSTRACT

Objectives: This study aimed to evaluate the influence of adjacent restorative material and interproximal distance on the accuracy of digital impressions of inlay cavities obtained using an intraoral scanner.

Methods: A disto-occlusal inlay cavity was prepared on a mandibular right first molar model, and digital scans were performed using a CEREC Primescan (Dentsply Sirona). The adjacent restorative materials used were Lava (3M ESPE), ENAMIC (VITA Zahnfabrik), Celtra Duo (Dentsply Sirona), and DMAX (DMAX), and the interproximal distances were set to 0.6 mm, 0.8 mm, and 1.0 mm. The obtained scan data were analyzed using GOM Inspect software (GOM GmbH).

Results: Trueness, maximum positive and negative deviations, and precision were significantly influenced by both the adjacent restorative material and the interproximal distance, while their interaction showed a significant effect only on precision. Celtra Duo demonstrated the highest trueness, with mean deviation values decreasing from 7.8 μm at a 0.6 mm interproximal distance to 7.3 μm at 1.0 mm. ENAMIC showed the best precision, presenting mean deviations of 2.6 μm at 0.6 mm, 2.9 μm at 0.8 mm, and 2.4 μm at 1.0 mm. A narrow interproximal distance of 0.6 mm resulted in lower trueness, measured at 8.3 μm, and the highest precision deviation of 3.4 μm. In contrast, an interproximal distance of 1.0 mm yielded improved scan accuracy, with increased trueness and reduced precision variation.

Conclusions: Digital impression accuracy of inlay cavities was influenced by adjacent restorative material and interproximal distance, suggesting clinical consideration is needed in CAD/CAM workflows to optimize restoration fit.

Keywords: Digital impression accuracy; Interproximal distance; Inlay cavity; Intraoral scanner; Restorative materials

Received: June 12, 2025 **Revised:** July 22, 2025 **Accepted:** August 19, 2025

Citation
Lee SY, Son SA, Kim JH, Seo DG, Park JK. Influence of adjacent restorative material and distance on the accuracy of inlay cavity impressions with intraoral scanner: an *in vitro* study. Restor Dent Endod 2026;51(1):e6.

***Correspondence to**
Jeong-Kil Park, DDS, MS, PhD
Department of Conservative Dentistry, School of Dentistry, Pusan National University, 20 Geumo-ro, Mulgeum-eup, Yangsan 50612, Korea
Email: jeongkil@pusan.ac.kr

INTRODUCTION

Digital scanning technology using intraoral scanners has become an essential process in fabricating dental restorations alongside advances in computer-aided design/computer-aided manufacturing (CAD/CAM) systems [1,2]. This technology enables minimal removal, accurate impression acquisition, and efficient workflow while significantly reducing potential distortion or deformation associated with conventional impression materials. These advantages make digital scanning a critical factor in enhancing clinical success and patient satisfaction [3–5].

The accuracy of intraoral scanners is essential when determining the fit and clinical success of final restorations [6,7]. Accuracy consists of two fundamental concepts: trueness and precision. Trueness refers to how closely the measured result matches the actual value, with a lower deviation from the true form indicating higher trueness. Precision refers to the consistency of repeated measurements under the same conditions, where higher consistency among values indicates higher precision [8]. Therefore, accuracy encompasses trueness and precision, and a balance of these two factors is essential to produce high-quality restorations.

The intraoral environment, with factors such as saliva, varying refractive indices of the teeth and gingiva, and limited oral opening, can reduce the scanning accuracy [9]. In particular, the restorative material of the adjacent teeth may alter the reflection and absorption properties of the scanner's light, affecting the quality of scan data [10]. Various restorative materials commonly used in CAD/CAM systems, including resin, hybrid ceramic, lithium silicate, and zirconia, may reduce the clarity of boundary delineation in digital impressions because of differences in refractive indices. In addition, the scanner's field of view becomes restricted as the interproximal distance to adjacent teeth decreases, potentially lowering the scan quality and adversely affecting the fit of the final restoration [11].

When scanning an inlay cavity with an intraoral scanner, the distance to the adjacent restorations is critical in determining the scanning accuracy [12]. Typically, when forming an inlay cavity, maintaining an approximately 0.5 mm gap, including the proximal box with the adjacent tooth, is essential for establishing proper proximal contact [13]. If the distance to the adjacent tooth is too narrow, the scanning beam may fail to reach the deeper areas of the cavity, or excessive light reflection may occur at the interproximal contact point, making accurate impression acquisition challenging [14]. Therefore, the type of restorative material and the distance to the adjacent tooth can directly affect the accuracy of cavity scanning, which, in turn, can affect the fit of the final restoration.

Nevertheless, research on the effects of external factors, such as the type of adjacent restorative material and interproximal distance, on the scanning accuracy of the CEREC Primescan (Dentsply Sirona, Charlotte, NC, USA) remains limited. Therefore, this study examined the effects of adjacent restorative materials and interproximal distances to optimize the digital scan accuracy of inlay cavities and provide foundational data for minimizing clinical errors in digital impression acquisition using CAD/CAM systems. This study examined how adjacent restorative materials and interproximal distance affect the digital scan accuracy of inlay cavities.

Based on this, the following null hypotheses were tested: (1) adjacent restorative materials do not have a significant effect on the accuracy of digital scans; (2) the interproximal distance does not have a significant effect on the accuracy of digital scans; (3) the interaction between adjacent restorative materials and the interproximal distance does not have a significant effect on the accuracy of digital scans.

METHODS

Inlay cavity preparation

A disto-occlusal inlay cavity on an artificial mandibular right first molar was formed. A 3Shape scanner (3Shape E3; 3Shape A/S, Copenhagen, Denmark) was used to scan an artificial tooth, and a cavity design was then formed using Meshmixer software (Autodesk Meshmixer, ver. 3.5; Autodesk Inc., San Rafael, CA, USA). The cavity was designed with an occlusal depth of 2 mm and a proximal box width of 1.5 mm, extending in the disto-occlusal direction with the margins aligned horizontally to the gingiva and adapted to the transitional angles on the lingual and buccal surfaces. The mandib-

https://doi.org/10.5395/rde.2026.51.e6

ular right first molar model with the designed cavity was printed using a three-dimensional (3D) printer (3Shape E3).

Reference scan

The reference scan data for the disto-occlusal inlay cavity were obtained using the same 3Shape scanner. The scanned data were converted into a Standard Tessellation Language (STL) file.

Preparation process for adjacent teeth

The restorative materials for the adjacent tooth included Lava Ultimate CAD/CAM Restorative (3M ESPE, St. Paul, MN, USA), VITA ENAMIC (VITA Zahnfabrik, Bad Säckingen, Germany), Celtra Duo (Dentsply Sirona, Hanau, Germany), and DMAX CAD/CAM Blocks (DMAX, Daegu, Korea). The artificial mandibular right second molar (A5AN-500; Nissin Dental, Kyoto, Japan), used as the adjacent tooth, underwent preparation and was then scanned with an intraoral scanner (IOS; CEREC Primescan AC ver. 5.1.0, Dentsply Sirona). Based on the scanned image, a crown was fabricated using CAD/CAM (CEREC Primescan). All four materials used in this study used A2 shaded blocks. The adjacent restorations were fabricated by a single skilled technician, following the manufacturer's instructions for each block. The surface polishing of the milled restorations was performed under the same conditions. The fabricated crown was cemented onto the adjacent artificial tooth with TempBond NE (Kerr Corporation, Orange, CA, USA).

Adjustment of interproximal distance and scanning procedure

Each adjacent restoration and inlay cavity was positioned as closely as possible using electronic calipers and secured with silicone impression material and a glue gun. After applying a rubber dam, the interproximal distance was adjusted to 0.6 mm, 0.8 mm, and 1.0 mm using electronic calipers. Digital scans were performed using the CEREC Prime AC (Figure 1). The typodont assembly was attached to a Thomas magnet for stability

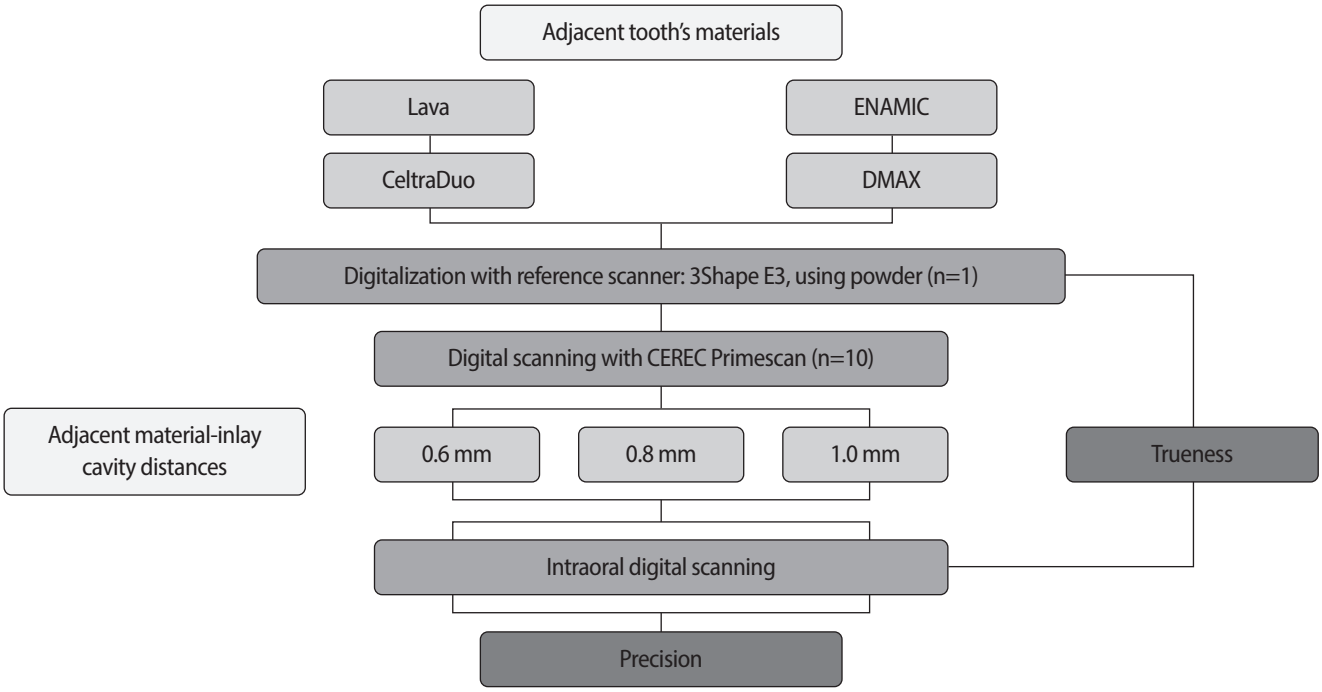

Figure 1. Experimental workflow showing the scanning procedure and variables. Four types of adjacent restorative materials (Lava, ENAMIC, Celtra Duo, DMAX) were tested with three interproximal distances (0.6 mm, 0.8 mm, 1.0 mm). Digital scanning was performed using a reference scanner (3Shape E3; 3Shape A/S, Copenhagen, Denmark) and intraoral scanner (CEREC Primescan; Dentsply Sirona, Charlotte, NC, USA). Trueness and precision were evaluated as outcome measures. Lava: 3M ESPE, St. Paul, MN, USA; ENAMIC: VITA Zahnfabrik, Bad Säckingen, Germany; Celtra Duo: Dentsply Sirona, Hanau, Germany; DMAX: DMAX, Daegu, Korea.

during scanning. Each experimental group was scanned 10 times according to the manufacturer's instructions. The scanned data were saved in STL file format.

Data analysis process

The accuracy of the scanned data from the experimental models was evaluated using 3D inspection software (GOM Inspect 2018; GOM GmbH). The trueness was analyzed by superimposing the reference and STL data using the initial and local best-fit alignment (n = 10). The scan data were quantified using mean deviation, and the mean maximum positive (+) and negative (–) deviations were calculated to assess the magnitude of the local trueness deviation. The precision was determined by superimposing the STL files of each experimental group with other data, consistently using initial alignment and local best-fit alignment for analysis (n = 45).

Statistical analysis

The experimental data were analyzed using statistical software (IBM SPSS Statistics, ver. 20.0; IBM Corp, Armonk, NY, USA). A two-way analysis of variance (ANOVA) was conducted to evaluate the effects of interproximal distance and adjacent tooth restorative material on trueness, mean maximum positive deviation, mean maximum negative deviation, and precision. In addition, a one-way ANOVA and Duncan's multiple comparison tests were used for *post hoc* analysis to assess the effects of each distance on each material and compare the effects of each material at each distance. The significance level (α) was set to 0.05, and p-values ≤0.05 were considered significant.

RESULTS

Effect of the trueness, maximum deviation, minimum deviation, and precision according to distance and material

The restorative materials of adjacent teeth and the interproximal distance had significant effects on the trueness, mean maximum positive deviation, and mean maximum negative deviation, but there was no significant interaction effect between the two variables. In contrast, the materials and interproximal distance significantly affected the precision, and the interaction effect between the two variables was also significant (Table 1).

Comparisons between 0.6, 0.8, and 1.0 mm interproximal distances on the average deviation for trueness, precision, mean maximum positive deviation, and mean maximum negative deviation

1. Trueness

The range of the average trueness value ranged from 7.8 ± 0.8 μm to 8.3 ± 0.9 μm. In addition, the 1.0 mm group showed significantly higher trueness than the 0.6 mm group (p < 0.05) (Table 2).

Table 1. Results of two-way ANOVA of parameters

Parameter	Source	df	SS	MS	F	p-value
Average deviation for trueness	Distance	2	4.0	2.0	4.0	0.02
	Material	3	18.7	6.2	12.5	<0.001
	Distance × Material	6	0.9	0.1	0.3	0.938
Maximum positive deviation	Distance	2	549.6	274.8	6.1	0.003
	Material	3	653.5	217.8	4.8	0.004
	Distance × Material	6	251.6	41.9	0.9	0.48
Maximum negative deviation	Distance	2	4,381.2	2,190.6	17.0	<0.001
	Material	3	1,322.9	441.0	3.4	0.02
	Distance × Material	6	1,523.2	253.9	2.0	0.077
Average deviation for precision	Distance	2	19.7	9.8	23.7	<0.001
	Material	3	72.9	24.3	58.5	<0.001
	Distance × Material	6	35.1	5.9	14.1	<0.001

ANOVA, analysis of variance; df, degree of freedom; SS, sum of squares; MS, mean squares.

https://doi.org/10.5395/rde.2026.51.e6

Table 2. Comparisons between 0.6-mm, 0.8-mm, 1.0-mm interproximal distances for average deviation for trueness, mean maximum deviations, and precision (μm)

Distance (mm)	Average deviation for trueness	Maximum positive deviation	Maximum negative deviation	Average deviation for precision
0.6	8.3 ± 0.9^{A}	45.6 ± 8.8^{A}	32.0 ± 12.6^{A}	3.4 ± 1.0^{A}
0.8	8.2 ± 0.7^{AB}	43.5 ± 7.2^{A}	24.8 ± 12.7^{B}	2.9 ± 0.5^{B}
1.0	7.8 ± 0.8^{B}	40.4 ± 4.4^{B}	17.2 ± 10.5^{C}	3.1 ± 0.7^{C}

Values are presented as mean ± standard deviation.
Different superscript letters within same column indicate statistical difference between interproximal distances by Duncan multiple comparison test ($p < 0.05$).

2. Mean maximum positive deviation

The maximum positive deviation ranged from 45.6 ± 8.8 μm to 40.4 ± 4.4 μm. The 0.6 mm group showed a significantly higher deviation than the 1.0 mm group ($p < 0.05$).

3. Mean maximum negative deviation

The maximum negative deviation was 32.0 ± 12.6 μm, 24.8 ± 12.7 μm, and 17.2 ± 10.5 μm at 0.6 mm, 0.8 mm, and 1.0 mm, respectively, with a significant decrease as the distance increased ($p < 0.05$).

4. Precision

The mean deviation of precision at 0.6 mm, 0.8 mm, and 1.0 mm was 3.4 ± 1.0 μm, 2.9 ± 0.5 μm, and 3.1 ± 0.7 μm, respectively, showing significant differences between each distance ($p < 0.05$). The lowest mean deviation was observed at 0.8 mm.

Comparisons between the adjacent materials for the average deviation for trueness, precision, mean maximum positive deviation, and mean maximum negative deviation

1. Trueness

The average deviation of trueness for each material ranged from 7.9 ± 0.5 μm to 8.6 ± 0.7 μm. Celtra Duo showed the lowest trueness deviation, indicating the highest trueness, followed in order by increasing trueness deviation by Lava, DMAX, and ENAMIC. A significant difference was observed between Celtra Duo, Lava, and DMAX, ENAMIC ($p < 0.05$) (Table 3).

2. Mean maximum positive deviation

Celtra Duo showed the lowest maximum positive deviation, followed in ascending order by Lava, ENAMIC, and DMAX. No significant difference was noted between Celtra Duo and Lava ($p > 0.05$). On the other hand, Celtra Duo showed a significant difference compared to ENAMIC and DMAX ($p < 0.05$). A significant difference was observed between Lava and DMAX ($p < 0.05$).

3. Mean maximum negative deviation

DMAX showed the lowest maximum negative deviation, followed in ascending order by ENAMIC, Celtra Duo, and Lava. No significant difference was observed between DMAX and ENAMIC ($p > 0.05$). Nevertheless, DMAX showed a significant difference compared to Lava and Celtra Duo ($p < 0.05$).

4. Precision

ENAMIC showed the lowest precision value, indicating the highest precision, followed by Lava, Celtra Duo, and DMAX in the ascending order of precision deviation. ENAMIC showed a significant difference from the other materials (Lava, Celtra Duo, and DMAX) ($p < 0.05$). Lava also showed a statistically significant difference from Celtra Duo and DMAX ($p < 0.05$). No significant difference was observed between Celtra Duo and DMAX ($p > 0.05$).

Comparisons of trueness, mean maximum deviations, and precision across different materials and interproximal distances

1. Trueness

Lava and Celtra Duo showed relatively high trueness at all distances. Lava showed a mean deviation of trueness of 8.0 ± 0.3 μm at 0.6 mm and 0.8 mm, with a slight decrease to 7.5 ± 0.6 μm at 1.0 mm. Celtra Duo showed a consistent mean deviation of trueness of 7.8 ± 0.7 μm and 7.8 ± 0.4 μm at 0.6 mm and 0.8 mm, respectively, with a further reduction to 7.3 ± 0.4 μm at 1.0 mm, which was lower than that of Lava. Both materials

Table 3. Comparisons between materials for average deviation for trueness, mean maximum deviations, and precision (μm)

Material	Average deviation for trueness	Maximum positive deviation	Maximum negative deviation	Average deviation for precision
Lava	7.9 ± 0.5^{A}	42.3 ± 4.5^{AB}	28.7 ± 14.1^{A}	2.9 ± 0.5^{A}
ENAMIC	8.6 ± 0.7^{B}	44.1 ± 3.8^{BC}	22.7 ± 8.0^{AB}	2.6 ± 0.4^{B}
Celtra Duo	7.6 ± 0.5^{A}	39.9 ± 3.9^{A}	27.0 ± 18.9^{A}	3.5 ± 0.8^{C}
DMAX	8.4 ± 1.0^{B}	46.3 ± 12.1^{C}	20.3 ± 8.0^{B}	3.5 ± 1.0^{C}

Values are presented as mean ± standard deviation.
Different superscript letters within the same column indicate statistical difference between materials by Duncan multiple comparison test ($p < 0.05$).
Lava: 3M ESPE, St. Paul, MN, USA; ENAMIC: VITA Zahnfabrik, Bad Säckingen, Germany; Celtra Duo: Dentsply Sirona, Hanau, Germany; DMAX: DMAX, Daegu, Korea.

Table 4. Comparisons of trueness, mean maximum deviations, and precision across different materials and interproximal distances (μm)

Parameter	Distance (mm)	Lava	ENAMIC	Celtra Duo	DMAX
Average deviation for trueness	0.6	8.0 ± 0.3^{Aa}	8.9 ± 0.5^{Ba}	7.8 ± 0.7^{Aa}	8.6 ± 1.3^{ABa}
	0.8	8.0 ± 0.3^{ABa}	8.6 ± 0.9^{Ba}	7.8 ± 0.4^{Aa}	8.4 ± 0.9^{ABa}
	1.0	7.5 ± 0.6^{Ab}	8.3 ± 0.6^{Ba}	7.3 ± 0.4^{Ab}	8.3 ± 0.8^{Ba}
Maximum positive deviation	0.6	44.9 ± 4.3^{ABa}	45.7 ± 3.6^{ABa}	41.0 ± 4.0^{Aa}	50.6 ± 15.4^{Ba}
	0.8	42.1 ± 3.0^{ABab}	44.2 ± 4.8^{ABa}	39.7 ± 3.0^{Aa}	48.1 ± 12.0^{Ba}
	1.0	40.0 ± 5.1^{Ab}	42.3 ± 2.1^{Aa}	39.0 ± 4.7^{Aa}	40.1 ± 4.9^{Aa}
Maximum negative deviation	0.6	38.4 ± 13.5^{Aa}	27.2 ± 8.5^{Aa}	34.4 ± 17.9^{Aa}	28.1 ± 4.3^{Aa}
	0.8	23.8 ± 1.9^{ABb}	25.3 ± 1.5^{ABa}	33.2 ± 21.8^{Aa}	16.7 ± 7.7^{Bb}
	1.0	23.8 ± 17.2^{Ab}	15.7 ± 6.9^{ABb}	13.3 ± 6.4^{Bb}	16.1 ± 5.3^{ABa}
Average deviation for precision	0.6	3.1 ± 0.7^{Aa}	2.6 ± 0.3^{Ba}	4.0 ± 1.0^{Ca}	3.8 ± 1.2^{Ca}
	0.8	2.7 ± 0.4^{Ab}	2.9 ± 0.3^{BCb}	2.8 ± 0.4^{ABb}	3.1 ± 0.7^{Cb}
	1.0	2.9 ± 0.3^{Aab}	2.4 ± 0.2^{Bc}	3.7 ± 0.6^{Cc}	3.4 ± 0.8^{Dab}

Values are presented as mean ± standard deviation.
Different capital superscript letters within the same row indicate statistically significant differences between materials ($p < 0.05$) while different lowercase superscript letters within the same column indicate statistically significant differences across distance by Duncan multiple comparison test ($p < 0.05$).
Lava: 3M ESPE, St. Paul, MN, USA; ENAMIC: VITA Zahnfabrik, Bad Säckingen, Germany; Celtra Duo: Dentsply Sirona, Hanau, Germany; DMAX: DMAX, Daegu, Korea.

showed a decrease in the mean deviation of trueness as the distance increased, with a statistically significant difference observed at 1.0 mm ($p < 0.05$). In contrast, ENAMIC and DMAX showed relatively lower trueness. ENAMIC exhibited a mean deviation of trueness of 8.9 ± 0.5 μm, 8.6 ± 0.9 μm, and 8.3 ± 0.6μm at 0.6 mm, 0.8 mm, and 1.0 mm, respectively, showing a gradual decrease with increasing distance. DMAX recorded a similar mean deviation of trueness to ENAMIC, with values of 8.6 ± 1.3 μm, 8.4 ± 0.9 μm, and 8.3 ± 0.8 μm at 0.6 mm, 0.8 mm, and 1.0 mm, respectively. Both materials showed a decreasing trend in the mean deviation of trueness as the distance increased, but the difference was not significant ($p > 0.05$) (Table 4).

2. Mean maximum positive deviation

Celtra Duo recorded consistently low mean maximum positive deviation at all distances, with values of 41.0 ± 4.0 μm, 39.7 ± 3.0 μm, and 39.0 ± 4.7 μm at 0.6 mm, 0.8 mm, and 1.0 mm, respectively, showing a decreasing trend as the distance was increased. Lava showed a mean maximum positive deviation of 44.9 ± 4.3 μm at 0.6 mm, decreasing to 42.1 ± 3.0 μm and 40.0 ± 5.1 μm at 0.8 mm and 1.0 mm, respectively. Both materials exhibited a decrease in the mean maximum positive deviation as the distance increased, with Celtra Duo showing lower values than Lava, but the difference was not significant ($p > 0.05$). ENAMIC recorded a mean maximum positive deviation, with 45.7 ± 3.6 μm at 0.6 mm, decreasing to 44.2 ± 4.8 μm and 42.3 ± 2.1 μm at 0.8 mm and 1.0 mm, respectively. DMAX showed the highest mean maximum positive deviation, with 50.6 ± 15.4 μm at 0.6 mm, decreasing slightly to 48.1 ± 12.0 μm at 0.8 mm and decreasing significantly to 40.1 ± 4.9 μm at 1.0 mm.

https://doi.org/10.5395/rde.2026.51.e6

3. Mean maximum negative deviation

Celtra Duo also showed a decreasing trend in the mean maximum negative deviation as the distance increased. It recorded a mean maximum negative deviation of 34.4 ± 17.9 μm at 0.6 mm, which decreased significantly to 13.3 ± 6.4 μm at 1.0 mm, the lowest value among the materials. Lava exhibited a mean maximum negative deviation of 38.4 ± 13.5 μm at 0.6 mm, decreasing to 23.8 ± 1.9 μm and 23.8 ± 17.2 μm at 0.8 mm and 1.0 mm, respectively, showing a similar decreasing trend to that of Celtra Duo. ENAMIC recorded a mean maximum negative deviation of 27.2 ± 8.5 μm at 0.6 mm, which decreased to 25.3 ± 1.5 μm at 0.8 mm and further to 15.7 ± 6.9 μm at 1.0 mm. DMAX showed a mean maximum negative deviation of 28.1 ± 4.3 μm at 0.6 mm, which decreased sharply to 16.7 ± 7.7 μm at 0.8 mm and remained at a similar level of 16.1 ± 5.3 μm at 1.0 mm.

4. Precision

ENAMIC showed a precision of 2.6 ± 0.3 μm at 0.6 mm, which increased to 2.9 ± 0.3 μm at 0.8 mm and then decreased to 2.4 ± 0.2 μm at 1.0 mm, the lowest precision value observed. Lava recorded a mean deviation of precision of 3.1 ± 0.7 μm at 0.6 mm, which decreased to 2.7 ± 0.4 μm at 0.8 mm, followed by a slight increase to 2.9 ± 0.3 μm at 1.0 mm. Celtra Duo had the highest precision at 0.6mm (4.0 ± 1.0 μm), which decreased to 2.8 ± 0.4 μm at 0.8 mm but increased again to 3.7 ± 0.6 μm at 1.0 mm. DMAX recorded a high deviation of 3.8 ± 1.2 μm at 0.6 mm and showed an increase to 3.1 ± 0.7 μm and 3.4 ± 0.8 μm at 0.8 mm and 1.0 mm, respectively.

DISCUSSION

This study evaluated the effects of adjacent restorative materials (3M Lava Ultimate, VITA ENAMIC, Celtra Duo, DMAX CAD/CAM Blocks) and the distance between the inlay cavity and the adjacent restoration (0.6 mm, 0.8 mm, and 1.0 mm) on the impression accuracy of inlay cavities using an intraoral scanner. Four indicators were measured: mean deviation of trueness, mean maximum positive deviation, mean maximum negative deviation, and mean deviation of precision. The restorative material and the distance had significant effects on each of the four indicators, whereas the interaction between the material and distance had a significant effect only on the mean deviation of precision. These findings suggest that the type of material and the interproximal distance may independently influence trueness and precision. Consequently, the first hypothesis, which posited that adjacent restorative materials would have no significant effect on accuracy, and the second hypothesis, asserting that interproximal distance would not significantly impact accuracy, were rejected. In contrast, the third hypothesis, suggesting that there would be no effect of the interaction between material and distance on accuracy, was partially rejected. Although the interaction between adjacent material type and interproximal distance was not statistically significant in most comparisons, a potential interaction effect was hypothesized based on the optical characteristics of CAD/CAM materials. In clinical situations, the impact of limited interproximal spacing on scan accuracy may not be independent of the adjacent material's surface properties. For instance, highly translucent or reflective materials such as zirconia or lithium disilicate could intensify light scattering or internal reflection when the interproximal space is narrow. These optical disturbances may exacerbate scanning challenges in confined areas, where limited scanner angulation and reduced light penetration already compromise image acquisition. Therefore, the third null hypothesis was included to explore the potential for such compounded effects, even under controlled *in vitro* conditions. While the statistical results did not confirm a significant interaction in most parameters, the rationale for its inclusion was grounded in optical considerations relevant to intraoral scanning in restricted clinical environments.

A dental phantom head model was used to replicate the intraoral environment, providing conditions that closely simulate the clinical setting to enhance the clinical applicability of the results. In addition, the distances between the adjacent restoration and the inlay cavity were set to 0.6 mm, 0.8 mm, and 1.0 mm to assess the effects of interproximal distance on the trueness and precision under various clinical situations. The 0.6-mm-simulated conditions in which the adjacent tooth and restoration are in close proximity allow an evaluation of potential limitations in scanning and possible data omission in narrow spaces. In contrast,

the 1.0 mm distance represented a relatively wider interproximal gap, enabling clear recognition of the cavity margins without interference from adjacent restorations [11]. By setting these various interproximal distance conditions, this study could assess the differences in accuracy at each distance and, more precisely, determine how these changes influence trueness and precision.

These results revealed variations in scanning accuracy based on these distance conditions. The mean deviation of trueness was significantly higher at 0.6 mm (8.3 ± 0.9 μm) compared to that observed at 1.0 mm (7.8 ± 0.8 μm) ($p < 0.05$), indicating a tendency for lower trueness at narrower distances. In addition, the mean deviation of precision was highest at 0.6 mm (3.4 ± 1.0 μm), whereas a lower value of 3.1 ± 0.7 μm was observed at 1.0 mm. Hence, a narrow interproximal distance may adversely affect the trueness and precision.

When scanning an inlay cavity with an intraoral scanner, the restorative material of the adjacent tooth may affect the accuracy of digital impression acquisition. This is because the restorative material of the adjacent tooth can alter the reflection and absorption of the scanner light, making it more difficult to distinguish the cavity margins [14,15]. Consequently, there is a potential for distortion in the shape or depth of the cavity, or even for data omission in certain areas. In addition, the gloss and texture of the restorative surface can also affect the data acquisition of the scanner. According to some reports, highly glossy surfaces may reflect excessive light, potentially reducing the scanner's ability to capture fine details and thus affecting the accurate reproduction of the cavity's form [16,17].

ENAMIC has a hybrid structure, combining a ceramic network with a resin matrix, giving it an opaque quality and high reflectivity [18]. The consistent reflection from the surface of ENAMIC enables the scanner to collect precise, repetitive data, contributing to its superior precision. In the experimental results, ENAMIC showed the best performance in precision, with deviations of 2.6 ± 0.3 μm, 2.9 ± 0.3 μm, and 2.4 ± 0.2 μm at 0.6 mm, 0.8 mm, and 1.0 mm, respectively. In contrast, the mean deviation of trueness for ENAMIC was lowest at 8.9 ± 0.5 μm, 8.6 ± 0.9 μm, and 8.3 ± 0.6 μm at 0.6 mm, 0.8 mm, and 1.0 mm, respectively. This phenomenon may be related to light scattering or multiple reflections within the material due to differences in refractive indices and optical properties of the ceramic and resin components, which can hinder accurate recognition of boundary and depth information, as suggested in previous studies [2,19].

Celtra Duo is composed of lithium silicate ceramic, characterized by high optical translucency and a fine crystalline structure. This structure allows the scanner to reflect some light from the surface while transmitting part of it internally, facilitating accurate recognition of the depth and internal structures [20]. The experimental results showed that the mean deviation of trueness for Celtra Duo was 7.8 ± 0.7 μm, 7.8 ± 0.4 μm, and 7.3 ± 0.4 μm at 0.6 mm, 0.8 mm, and 1.0 mm, respectively. On the other hand, the precision was relatively lower, with deviations of 4.0 ± 1.0 μm, 2.8 ± 0.4 μm, and 3.7 ± 0.6 μm at 0.6 mm, 0.8 mm, and 1.0 mm, respectively. This suggests that although the optical translucency and reflectivity of Celtra Duo are advantageous for achieving high trueness, the multiple scattering pathways and inconsistent boundary recognition contribute to its lower precision.

Lava is a resin-based composite material composed of nano-ceramic particles, enabling uniform reflection and transmission of light and contributing to enhanced trueness performance. In this study, Lava showed consistent trueness deviations of 8.0 ± 0.3 μm at 0.6 mm and 0.8 mm, with a reduction to 7.5 ± 0.6 μm at 1.0 mm. The precision deviations were 3.1 ± 0.7 μm, 2.7 ± 0.4 μm, and 2.9 ± 0.3 μm at 0.6 mm, 0.8 mm, and 1.0 mm, respectively, showing stability, but it was slightly higher than that of ENAMIC. The relatively low optical heterogeneity and consistent light pathways in Lava contributed significantly to its improved trueness performance [21].

DMAX is a zirconia material with high opacity and strong reflectivity that exhibits relatively large deviations in both trueness and precision. The trueness deviations for DMAX were recorded as 8.6 ± 1.3 μm, 8.4 ± 0.9 μm, and 8.3 ± 0.8 μm at 0.6 mm, 0.8 mm, and 1.0 mm, respectively, while precision deviations were 3.8 ± 1.2 μm, 3.1 ± 0.7μm, and 3.4 ± 0.8 μm at 0.6 mm, 0.8 mm, and 1.0 mm, respectively. These results may be explained by the high opacity of zirconia, which limits light penetration and causes most light to be reflected from the surface, as reported in previous studies [15,22]. Consequently, this limits the ability of the scanner to recognize the

https://doi.org/10.5395/rde.2026.51.e6

boundary and depth data, which likely contributed to the observed lower trueness and precision.

Celtra Duo consistently showed superior performance in trueness and maximum positive deviation, maintaining low trueness deviations across all distances and showing minimal impact from the changes in distance. In addition, Celtra Duo exhibited stable and low maximum positive deviation values at all distances, with its best performance in the maximum negative deviation observed at a distance of 1.0 mm. In contrast, ENAMIC showed the best performance in precision, displaying consistently low precision deviations with minimal effect from distance changes. DMAX performed well in the maximum negative deviation at a distance of 0.8 mm but displayed relatively higher deviations at other distances. Lava showed moderate overall performance, but it recorded the highest deviation in maximum negative deviation at 0.6 mm.

The lithium silicate ceramic Celtra Duo showed high trueness, while the hybrid ceramic ENAMIC exhibited high precision, suggesting that these two materials possess distinct advantages. In addition, when the interproximal distance was close (0.6 mm), there was an increased likelihood of data omission or distortion, indicating the need for caution in clinical settings when scanning narrow interproximal spaces for CAD-CAM restoration.

These findings suggest that adjacent restorative material and interproximal distance should be considered carefully during digital impression acquisition using CAD/CAM systems. In particular, a narrow interproximal distance (0.6 mm) increases the likelihood of data omission or distortion, highlighting the need to enlarge the interproximal space or apply supplementary protocols to enhance the scanning accuracy under these conditions. In contrast, most materials provide stable scanning accuracy when the interproximal distance is wider at 1.0 mm, making them clinically suitable [13,14]. This study provides foundational guidance for dental clinicians using CAD/CAM systems in selecting optimal adjacent restorative materials and conditions for digital impressions.

This study was conducted as an *in vitro* experiment in a laboratory setting, which may differ in some respects from clinical conditions. For example, in the oral cavity, factors such as saliva, limited mouth opening, patient movement, and refractive index differences between teeth and gingiva can affect the scanning accuracy. Furthermore, this study did not consider factors such as the gloss and surface roughness (polishing, glazing, and roughness) of each material and used only one type of scanner, limiting the evaluation of how these factors may affect the scanner accuracy. Therefore, future research should incorporate these clinical elements to assess the scanner accuracy and propose methods to improve the accuracy of digital impressions under various clinical conditions.

CONCLUSIONS

Under the conditions of this study, the adjacent restorative material and interproximal distance individually had significant effects on the accuracy variables, trueness, and precision in the digital impression of the inlay cavity. On the other hand, the interaction between the two factors significantly affected only precision. The lithium silicate ceramic Celtra Duo and the hybrid ceramic ENAMIC each showed high trueness and precision, respectively, with trueness and precision being higher at 1.0 mm than at 0.6 mm.

CONFLICT OF INTEREST

Sung-Ae Son is an Editorial Advisory Board member and Deog-Gyu Seo is an Scientific Advisory Board member of *Restorative Dentistry and Endodontics* and these authors were not involved in the peer-review or editorial process of this article. The authors declare no other conflicts of interest.

FUNDING/SUPPORT

This work was supported by a 2-year Research Grant of Pusan National University.

AUTHOR CONTRIBUTIONS

Conceptualization, Funding acquisition, Project administration, Supervision: Park JK. Data curation, Investigation, Software, Visualization: Lee SY. Formal analysis, Resources, Validation: Son SA. Methodology: Kim JH, Seo DG. Writing - original draft: Lee SY. Writing - review & editing: Kim JH, Park JK. All authors read and approved the final manuscript.

DATA SHARING STATEMENT

The datasets are not publicly available but are available from the corresponding author upon reasonable request.

REFERENCES

1. Zimmermann M, Ender A, Mehl A. Local accuracy of actual intraoral scanning systems for single-tooth preparations in vitro. J Am Dent Assoc 2020;151:127-135.
2. Hombesh MN, Sachin B, Prasanna BG, Barmavatu P, Haritha V, Murali S. Intraoral oral scanner - an essential digital device for modern day practice: a review article. Int J Sci Res 2024;13:17-18.
3. Seelbach P, Brueckel C, Wöstmann B. Accuracy of digital and conventional impression techniques and workflow. Clin Oral Investig 2013;17:1759-1764.
4. Diker B, Tak Ö. Comparing the accuracy of six intraoral scanners on prepared teeth and effect of scanning sequence. J Adv Prosthodont 2020;12:299-306.
5. Chauhan K, Koul R, Chauhan K, Kaur J, Mahajan A. From analog to digital: role of intraoral scanners in dentistry—a review article. Int J Res Rev 2025;12:185-189.
6. Coutinho CA, Hegde D, Shetty S, Iyer R, Priya A. Intraoral scanners: a narrative review. J Res Dent 2020;8:1-9.
7. Revilla-León M, Alonso Pérez-Barquero J, Barmak AB, Agustín-Panadero R, Fernández-Estevan L, Gómez-Polo M. Accuracy of intraoral scanner systems for fabricating inlay, onlay, and veneer restorations: a systematic review and meta-analysis. J Esthet Restor Dent 2025;37:727-755.
8. D'haese R, Vrombaut T, Roeykens H, Vandeweghe S. In vitro accuracy of digital and conventional impressions for full-arch implant-supported prostheses. J Clin Med 2022;11:594.
9. Arakida T, Kanazawa M, Iwaki M, Suzuki T, Minakuchi S. Evaluating the influence of ambient light on scanning trueness, precision, and time of intra oral scanner. J Prosthodont Res 2018;62:324-329.
10. Cho JH, Çakmak G, Yilmaz B, Yoon HI. Effect of CAD-CAM restorative materials and scanning aid conditions on the accuracy and time efficiency of intraoral scans. J Prosthodont 2023;32:608-615.
11. Kim SY, Son K, Bihn SK, Lee KB. Effect of the inter-tooth distance and proximal axial wall height of prepared teeth on the scanning accuracy of intraoral scanners. J Funct Biomater 2024;15:115.
12. Huang MY, Son K, Lee KB. Effect of distance between the abutment and the adjacent teeth on intraoral scanning: an in vitro study. J Prosthet Dent 2021;125:911-917.
13. Son SA, Kim JH, Seo DG, Park JK. Influence of different inlay configurations and distance from the adjacent tooth on the accuracy of an intraoral scan. J Prosthet Dent 2022;128:680-687.
14. Kim JH, Son SA, Lee H, Yoo YJ, Hong SJ, Park JK. Influence of adjacent teeth on the accuracy of intraoral scanning systems for class II inlay preparation. J Esthet Restor Dent 2022;34:826-832.
15. Kwon Y, Kim JH, Park JK, Son SA. Evaluating the accuracy of CEREC intraoral scanners for inlay restorations: impact of adjacent tooth materials. BMC Oral Health 2024;24:1033.
16. Revilla-León M, Young K, Sicilia E, Cho SH, Kois JC. Influence of definitive and interim restorative materials and surface finishing on the scanning accuracy of an intraoral scanner. J Dent 2022;120:104114.
17. Agustín-Panadero R, Moreno DM, Pérez-Barquero JA, Fernández-Estevan L, Gómez-Polo M, Revilla-León M. Influence of type of restorative materials and surface wetness conditions on intraoral scanning accuracy. J Dent 2023;134:104521.
18. Coldea A, Swain MV, Thiel N. Mechanical properties of polymer-infiltrated-ceramic-network materials. Dent Mater 2013;29:419-426.
19. Tzimas K, Rahiotis C, Pappa E. Biofilm formation on hybrid, resin-based CAD/CAM materials for indirect restorations: a comprehensive review. Materials (Basel) 2024;17:1474.
20. Pîrvulescu IL, Faur A, Ille C, Jivănescu A. Optical properties of zirconia-reinforced lithium silicate veneers obtained with CAD/CAM milling and hot-pressing techniques: a comparative in vitro study. Med Pharm Rep 2024;97:205-214.
21. Bora PV, Sayed Ahmed A, Alford A, Pitttman K, Thomas V, Lawson NC. Characterization of materials used for 3D printing dental crowns and hybrid prostheses. J Esthet Restor Dent 2024;36:220-230.
22. Silva LH, Lima E, Miranda RB, Favero SS, Lohbauer U, Cesar PF. Dental ceramics: a review of new materials and processing methods. Braz Oral Res 2017;31(Suppl 1):e58.

https://doi.org/10.5395/rde.2026.51.e6

RDE Restorative Dentistry & Endodontics

Research Article

eISSN 2234-7666
Restor Dent Endod. 2026 February;51(1):e7
https://doi.org/10.5395/rde.2026.51.e7

Biological mechanisms underlying the inflammatory radicular cyst formation-focus on epithelial proliferation: a systematic review of experimental cell and tissue models

Néstor Ríos-Osorio[1,2,*], Sandra Briñez-Rodríguez[3], David Betancur-Calle[2], Marggie Grajales[4], Óscar Mauricio Jiménez-Peña[5], Mario Guerrero-Torres[6], Rafael Fernández-Grisales[1]

[1]Postgraduate Endodontics Department, School of Dentistry, CES University, Medellín, Colombia
[2]Faculty of Dentistry, Institución Universitaria Visión de las Américas, Medellín, Colombia
[3]Department of Endodontics, Institución Universitaria Colegios de Colombia UNICOC, Bogotá, Colombia
[4]Laser Dentistry Master Program, European Program, EMDOLA, University of Barcelona, Barcelona, Spain
[5]Department of Endodontics, Universidad Santo Tomas de Aquino, Bogotá, Colombia
[6]Faculty of Dentistry, Universidad Santo Tomas de Aquino, Bucaramanga, Colombia

ABSTRACT

Objectives: This study aimed to assess the molecular and cellular mechanisms involved in the epithelial proliferation that leads to the transformation of periapical granulomas (PGs) into inflammatory radicular cysts (IRCs).

Methods: A comprehensive search was conducted in three databases. Experimental, observational, or descriptive studies using human or animal tissue samples, or epithelial cell cultures that assessed the molecular and/or cellular mechanisms driving the proliferation of epithelial rests of Malassez and their role in the transformation of PGs into IRCs were included. The risk of bias and applicability of the included studies were assessed using the QUADAS-2.

Results: Fourteen studies (including 399 samples) met the inclusion criteria for qualitative synthesis. The studies highlight the role of pro-inflammatory cytokines (IL-1β, IL-6), growth factors (EGF, KGF, TGF-β, and IGF), and signaling pathways (NF-κB, MAPK/ERK, PI3K/AKT, and Smad) in the progression of PG to IRC. Biomarkers of epithelial proliferation, such as Ki-67, PCNA, and CD34, are consistently associated with this process, while MMP-13 emerges as a key regulator of epithelial behavior and matrix remodeling.

Conclusions: IRC development arises from a transition from homeostatic to pathological signaling, in which pro-inflammatory mediator levels inside the periapical chronic inflammation override regulatory checkpoints.

Keywords: Apical periodontitis; Granuloma; Molecular mechanisms; Radicular cyst

Received: August 20, 2025 **Revised:** September 11, 2025 **Accepted:** September 15, 2025

Citation
Ríos-Osorio N, Briñez-Rodríguez S, Betancur-Calle D, Grajales M, Jiménez-Peña ÓM, Guerrero-Torres M, Fernández-Grisales R. Biological mechanisms underlying the inflammatory radicular cyst formation-focus on epithelial proliferation: a systematic review of experimental cell and tissue models. Restor Dent Endod 2026;51(1):e7.

***Correspondence to**
Néstor Ríos-Osorio, DDS, MSc.
Endodontic Research Department, School of Dentistry, CES University, Cl 10A #22-04, El Poblado, Medellín 050021, Antioquia, Colombia
Email: dadopi1981@gmail.com

INTRODUCTION

Inflammatory radicular cysts (IRCs) are the most prevalent cystic lesions in the jaws, accounting for more than two-thirds of all odontogenic cysts [1,2]. IRCs, considered a reactive aftermath to periapical granulomas (PGs), have long been defined as the last stage of a chronic inflammatory continuum, clinically referred to as apical periodontitis (AP) [1,3]. However, this widely accepted model, which assumes a linear, passive progression from PG to IRC, fails to explain a basic paradox: why do only a small proportion of PGs proceed into IRCs, despite sharing similar antigenic triggers and inflammatory microenvironments [1,2]

IRCs arise from epithelial rests of Malassez (ERM), with dormant proliferative capabilities that continue in the periodontal ligament (PDL) following complete radicular development [2,4]. ERMs are arranged in cord-like, net-like, or isolated island structures next to the radicular cementum and consist of pale epithelial-like cells interconnected by desmosomes, with few cytoplasmic organelles, enclosed by a basal lamina, and suspended in the interphase of the cell cycle [2,4,5].

Emerging evidence suggests that ERMs actively contribute to PDL homeostasis by preventing ankylosis and root resorption, thereby preserving PDL space, supporting neural components, and facilitating cementum healing [2,6]. Furthermore, ovine models have identified clonogenic epithelial stem cell populations within ERMs that share phenotypic and functional properties with mesenchymal stem/stromal cells [7,8]. What remains contentious is the exact molecular pathways involved in the reactivation and pathological proliferation of ERMs in the context of chronic AP, which leads to the transition of PG into IRC, and more significantly, why this reactivation occurs selectively [2].

Although epithelial cell rests are detected in approximately 45% of PGs, only about half of these lesions undergo cystic transformation [2,9]. The molecular and cellular mechanisms driving epithelial proliferation and the subsequent formation of IRC remain poorly elucidated and significantly underestimated. This knowledge gap holds significant clinical relevance, as the histopathological nature of AP fundamentally influences clinical decision-making, timely treatment planning, and prognosis [2,3]. Notably, it has been proposed that some cystic lesions may only respond predictably to surgical intervention [2].

Bacterial endotoxins are considered important triggers of the IRC's proliferative stage, as they exhibit high mitogenic activity on epithelial cells and activate cytokine-producing cells, thereby increasing epithelial proliferation [1,2,10]. Both epithelial and endothelial cells in IRC tissues exhibit increased expression of cytokines, including transforming growth factor alpha (TGF-α), keratinocyte growth factor (KGF), epidermal growth factor (EGF), tumor necrosis factor (TNF), interleukin (IL)-1α, IL-1β, IL-6, among others [1,2,10-12]. This suggests that these cytokines may play a key role in the early stages of epithelial proliferation, facilitating the transition from a PG to IRC [1,2,10-12]. Furthermore, it has been proposed that additional molecular mechanisms, such as an increase in intracellular cyclic adenosine monophosphate induced by prostaglandin E2, contribute to the development and proliferation of ERMs [2,10,12]. Notably, whereas the tissues of origin for IRCs are well known, the particular molecular and cellular mechanisms that drive a transition from PG to IRC are poorly understood. Furthermore, the scientific literature on this subject has not been adequately summarized to identify molecular patterns.

The molecular mechanisms and intracellular signaling pathways that drive ERM proliferation likely represent a critical inflexion point in the histopathological transition of AP, notably from PG to IRC. A thorough understanding of these mechanisms would significantly advance our knowledge of AP pathogenesis, facilitate the identification of reliable molecular markers for molecular diagnosis, and aid in the development of targeted therapeutic strategies to halt or reverse cystic transformation, thereby improving endodontic therapy outcomes. To date, these regulatory and pathological mechanisms have not been comprehensively summarized in the literature. To the best of our knowledge, this systematic review is the first to integrate and synthesize the best available experimental evidence on the biological pathways (molecular and cellular) underlying epithelial proliferation and the transition of PGs into IRCs.

https://doi.org/10.5395/rde.2026.51.e7

METHODS

Protocol and registration

A detailed protocol was registered in the PROSPERO database (CRD420251062194). This systematic review follows the recommendations of the Cochrane Handbook of Systematic Reviews of Interventions and the PRISMA (Preferred Reporting Items for Systematic Reviews and Meta-Analyses) statement [13,14].

PICO question

Using the PICO strategy, the focused research question and the inclusion criteria were systematically formulated:

Population (P): Histopathological samples of IRCs, PGs, and ERM obtained from periap-ical tissues.

Intervention (I): Evaluation of biological mechanisms underlying epithelial proliferation, specifically molecular and cellular signaling pathways, assessed through techniques such as histopathology, histochemical stains, immunohistochemistry (IHC), western blotting, *in situ* hybridization, double immunofluorescence assays, and *in vitro* cell culture or proliferation assays.

Comparison (C): Histological or cell samples from periapical lesions or ERMs without evidence of epithelial/cell proliferation or exhibiting low/absent expression of epithelial proliferation markers.

Outcome (O): Qualitative, semiquantitative, or quantitative identification of molecular and cellular pathways involved in epithelial proliferation within endodontic periapical lesions.

Focused question

What molecular and cellular mechanisms are involved in the epithelial proliferation that leads to the transformation of PGs into IRCs?

Inclusion criteria

Experimental (*in vitro*, *in vivo*, or *ex vivo*), observational, or descriptive studies using human or animal tissue samples, or epithelial cell cultures, that assessed the molecular and/or cellular mechanisms driving the proliferation of ERM and their role in the transformation of PGs into IRCs were included in this systematic review. Eligible studies had to report qualitative, semiquantitative, or quantitative data on the expression, regulation, or functional role of cytokines, growth factors, receptors, biomarkers, co-stimulatory molecules, or intracellular signaling path-ways involved in epithelial proliferation within the context of AP. Techniques such as histopathology, IHC, *in situ* hybridization, western blotting, double immunofluorescence, or epithelial cell proliferation assays were considered. Studies were required to compare proliferative versus non-proliferative tissues or cell samples, and to offer mechanistic insights into the biological transition from PG to IRC.

Case reports, editorials, expert opinions, letters to the editor, and studies unrelated to endodontic periapical lesions (PGs or IRCs), lacking molecular or cellular data on epithelial proliferation, or focused primarily on non-inflammatory odontogenic cysts or non-epithelial mechanisms of lesion progression were excluded.

Information sources

The literature search was conducted following the methodological standards outlined by the Cochrane Collaboration. A comprehensive search strategy was developed utilizing Medical Subject Headings (MeSH), Emtree terms, Descriptores en Ciencias de la Salud (DeCS), and relevant text words. The following electronic databases were systematically searched from their inception to August 2025: PubMed, Scopus, ScienceDirect, and Web of Science. To enhance the comprehensiveness of the review and ensure literature saturation, additional sources were explored, including reference lists of pertinent studies, academic conference proceedings, thesis repositories, OpenGrey, Google Scholar, and ClinicalTrials.gov. No language restrictions were applied in the selection of studies (Appendix 1).

Screening and data collection

Initially, two independent reviewers screened the titles and abstracts of all retrieved studies. Full-text articles were then assessed for eligibility based on pre-established inclusion criteria. Any discrepancies were resolved through discussion and consensus; when necessary, a third reviewer was consulted to reach a final decision. Data extraction was performed in duplicate using a standardized data collection form, which captured the following information: Relevant data were in-

dependently extracted in duplicate using a standardized data collection form, which included the following variables: authors, year of publication, title, study design, geographic location, objectives, inclusion and exclusion criteria, sample size, study duration, outcome definitions, reported outcomes, measures of association, funding sources, study limitations, recommendations, and conclusions in correspondence with the main objective, as well as mechanistic insights into the biological processes underlying the transition from PG to IRC.

Synthesis of results

The included studies were evaluated for methodological homogeneity to assess the feasibility of conducting a meta-analysis. However, substantial heterogeneity across studies—particularly regarding the experimental models used and the diverse objectives evaluated in each study—precluded the performance of a quantitative synthesis.

Risk of bias and applicability assessment

Two independent reviewers evaluated the risk of bias and applicability of the included studies using the Quality Assessment of Diagnostic Accuracy Studies-2 (QUADAS-2) tool [15]. This tool involves a four-phase process: (i) formulation of a focused review question; (ii) adaptation of a review-specific guidance document if needed; (iii) examination or reconstruction of the study flow diagram; and (iv) domain-level assessment of risk of bias and applicability concerns. Risk of bias was assessed across four key domains: (i) patient selection, (ii) index test, (iii) reference standard, and (iv) flow and timing. Each domain includes two to four signaling questions with possible responses of "Yes," "No," or "Unclear." A "Yes" indicates low risk of bias, "No" indicates high risk, and "Unclear" reflects insufficient information. Domains where all questions are answered "Yes" are rated as low risk. If any question is answered "No," or if multiple questions are "Unclear," the domain is rated as high risk. A single "Unclear" response results in an overall "unclear" risk for that domain. Applicability concerns were assessed in three domains: (i) patient selection, (ii) index test, and (iii) reference standard. This evaluation measures the degree to which each study aligns with the review's focused question. Applicability is rated as "low," "high," or "unclear," with the latter applied when reporting is insufficient [15].

Although QUADAS-2 was originally designed for diagnostic accuracy studies, its structured domains were suitable for this review because they allowed for a systematic evaluation of key methodological aspects such as sample selection, molecular and histological assay application, reference comparisons, and study flow. Furthermore, the tool's emphasis on risk of bias and application guaranteed that the experimental and observational models included were not only methodologically sound but also relevant to the biological topic at hand [15]. This provides a transparent and reproducible methodology for evaluating the diverse findings on epithelial proliferation and cystic transformation.

RESULTS

Study selection

We initially identified 218 references with the search strategy. Additionally, four records were identified through other sources. After removing 102 duplicates, we screened 120 titles/abstracts. Finally, 14 studies met the inclusion criteria for qualitative synthesis [5,16–28] (Figure 1).

Characteristics of included studies

The general characteristics of the studies included in this systematic review are presented in Table 1. Methods and outcomes are presented in Table 2. The studies were conducted in Germany [5,22], the United States [17,21], Japan [20,25,26], Chile [19], Canada [18], Italy [23,27], India [24], and Romania [16]. All 14 included studies employed case-control designs and were published between 1996 and 2024 [5,16–28]. These studies examined diverse molecular mechanisms related to epithelial proliferation (growth factors, cytokines, intracellular signaling pathways, molecular biomarkers, and co-stimulatory proliferation mediators), either in the context of the physiological regulation of ERM functions or in the pathological progression of PGs into IRCs mediated by epithelial proliferation. All the studies offer a biological explanation for why the investigated mechanisms may be associated with epithelial proliferation linked with the progression of PGs into IRCs. They underscore their

https://doi.org/10.5395/rde.2026.51.e7

decisive contribution to epithelial activation, sustained proliferation, and the pathological reprogramming that drives cystic transformation [5,16-28]. A total of 399 tissue samples were analyzed, comprising 168 PGs, 141 IRCs, 8 dental follicles, 40 dentigerous cysts, 1 lateral cyst, and 1 odontogenic keratocyst [16–18,21–24,26–28]. Furthermore, one study analyzed epithelialized (n = 8) and non-epithelialized (n = 7) apical lesions of endodontic origin but did not provide a differential diagnosis [19]. One study employed 25 deciduous molars, which were processed for immunohistochemical analysis [5]. Three studies were based on experimental cell models [20,25,26]. Multiple methodologies, including histopathology, IHC, *in situ* hybridization, western blotting, double immunofluorescence, and epithelial cell proliferation assays, were employed to investigate the biological mechanisms underlying epithelial proliferation in periapical endodontic lesions. These mechanisms were subsequently assessed through quantitative, semiquantitative, or qualitative approaches according to defined evaluation criteria [5,16–28].

Data synthesis

Of the 14 studies included, three evaluated growth factors—insulin-like growth factor (IGF), fibroblast growth factor-7 (FGF-7)/KGF, and TGF—concerning the regulatory mechanisms of epithelial proliferation [5,25,26]. Three studies investigated growth factors, including EGF and FGF-7/KGF, associated with pathological mechanisms of epithelial proliferation [17,18,21]. Four studies assessed cytokines (IL-6, IL-1β, and interleukins related to macrophage polarization) linked to pathological mechanisms of epithelial proliferation [5,22,25,26]. Two studies examined co-stimulatory molecules, such as matrix metalloproteinase 13 (MMP-13), involved in epithelial proliferation, promoting the transition from

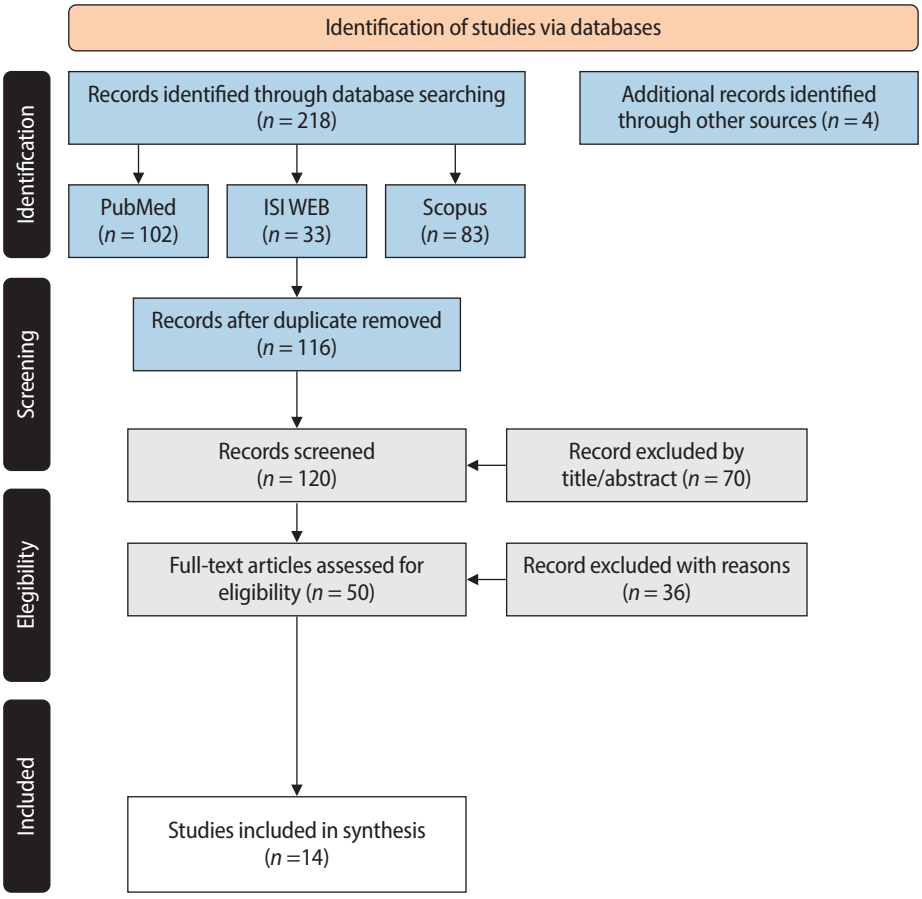

Figure 1. Flow chart of included studies, based on PRISMA (Preferred Reporting Items for Systematic Re-views and Meta-Analyses) guidelines.

Table 1. General characteristics of the studies included

No.	Study (year)	Title	Country	Journal	Quartile (SJR)	Objectives	Conclusions	Limitations	Conclusions consistent with the main objective
1	Lin *et al.* [17] (1996)	Detection of epidermal growth factor receptor in inflammatory apical lesions	USA	*International Endodontic Journal*	Q1	To examine the presence of EGFRs in endodontic periapical lesions.	EGFR promotes epithelial hyperplasia in chronic lesions.	Small sample size, no morphometric quantification.	Yes
2	Gao *et al.* [21] (1996)	Expression of keratinocyte growth factor in periapical lesions	USA	*Journal of Dental Research*	Q1	To investigate the role of KGF in promoting epithelial growth during periapical cyst formation. *In situ* hybridization and RT-PCR were carried out to compare KGF expression patterns in periapical lesions to the normal periodontal ligament.	KGF stimulates epithelial proliferation in cyst development.	Few samples. Lack of quantitative analysis.	Yes
3	Yamanaka *et al.* [25] (2000)	Isolation and serum-free culture of epithelial cells derived from the epithelial rest of Malassez in the human periodontal ligament	Japan	*In Vitro Cell and Developmental Biology - Animal*	Q2	To assess the biological characteristics and function of ERM in PDL isolating and culturing epithelial cells from ERM in a serum-free medium, and evaluating FGF requirements.	FGF-7/KGF regulates ERM preservation in human PDL.	*In vitro* only	Yes
4	Nagano *et al.* [26] (2024)	The IL-1β p65 axis stimulates quiescent odontogenic epithelial cell rests via TGF-b signalling to promote cell proliferation of the lining epithelia in radicular cysts: a laboratory investigation	Japan	*International Endodontic Journal*	Q1	To evaluate the impact of the cytokine pathway link between TGF-β signaling and IL-1β signaling on the control of odontogenic epithelial cell proliferation.	IL-1β-p65 signalling suppresses TGF-β-Smad2 signalling, which would be implicated in the pathophysiology of radicular cysts.	Focus only on cysts	Yes
5	Sako *et al.* [20] (2018)	Response of porcine epithelial rests of Malassez to stimulation by interleukin-6	Japan	*International Endodontic Journal*	Q1	To evaluate the proliferation and migration of Malassez's epithelial cell rests (ERM) in response to IL-6 stimulation.	IL-6 stimulated the proliferation and migration of ERM *in vitro*.	Animal model	Yes
6	Schweitzer *et al.* [19] (2021)	Localization of interleukin-6 signalling complex in epithelialized apical lesions of endodontic origin	Chile	*Clinical Oral Investigations*	Q1	To analyze the immunolocalization of the IL-6 signaling complex in both epithelialized and non-epithelialized ALEOs.	IL-6, IL-6R, and gp-130 support epithelial proliferation during cyst formation.	Small cohort	Yes
7	Nickolaychuk *et al.* [18] (2002)	Evidence for a role of mitogen-activated protein kinases in proliferating and differentiating odontogenic epithelia of inflammatory and developmental cysts.	Canada	*Oral Surgery, Oral Medicine, Oral Pathology, Oral Radiology, and Endodontology*	Q2	To analyze the distribution of ERK1 and its activated form, pERK1/2, in the epithelial components of developmental and inflammatory odontogenic cysts, as well as their correlation with differentiation and proliferation indicators.	ERK1 and pERK1/2 are linked to the differentiation and proliferation of odontogenic cyst epithelia. This suggests that pERK1/2 plays a role in the activation of odontogenic epithelia during inflammation.	No direct statistical test	Yes

(Continued on the next page)

https://doi.org/10.5395/rde.2026.51.e7

Table 1. Continued

No.	Study (year)	Title	Country	Journal	Quartile (SJR)	Objectives	Conclusions	Limitations	Conclusions consistent with the main objective
8	Götz *et al.* [5] (2003)	Immunohistochemical localization of insulin-like growth factor-II and its binding protein-6 in human epithelial cells of Malassez	Germany	*European Journal of Oral Sciences*	Q2	To identify potential IGF system components in human Malassez cells in deciduous teeth by using light and electron IHC.	Autocrine IGF-BP6 may act as an antiproliferative molecule in the normal PDL, reducing IGF-induced mitogenic actions on Malassez cells.	No pathological conditions were presented	Yes
9	Bhalla *et al.* [24] (2014)	Collagenase-3 expression in periapical lesions: an immunohistochemical study	India	*Biotechnic and Histochemistry*	Q2	To assess collagenase-3 location, intensity, and distribution in PGs with and without epithelium, as well as radicular cysts.	Collagenase-3 may help convert a PG with epithelium into a radicular cyst.	No molecular knockdown	Yes
10	Leonardi *et al.* [23] (2005)	Collagenase-3 (MMP-13) is expressed in periapical lesions: an immunohistochemical study	Italy	*International Endodontic Journal*	Q1	To determine MMP-13 presence in PGs with and without epithelium.	MMP-13 is key in the conversion of a granuloma with epithelium into a radicular cyst.	Small sample, lack of quantitative analysis.	Yes
11	Roi *et al.* [16] (2024)	CD34 and Ki-67 immunoexpression in periapical granulomas: implications for angiogenesis and cellular proliferation	Romania	*Diagnostics (Basel)*	Q2	To identify the immunoexpression of CD34 and Ki-67 in PGs and their impact on tissue growth and progression, considering their impact on proliferation and evolution.	Inflammatory environment promotes Ki-67 and CD34 expression, supporting cell proliferation and abnormal angiogenesis.	Small sample, no cyst comparison.	Yes
12	Leonardi *et al.* [27] (2015)	Toll-like receptor 4 expression in the epithelium of the inflammatory periapical lesions. an immunohistochemical study	Italy	*European Journal of Histochemistry*	Q2	To assess TLR4 expression in PGs and radicular cysts, specifically in the epithelial compartment.	TLR4 is pivotal in the inflammatory process related to apical disease.	No functional assays	Yes
13	Weber *et al.* [22] (2018)	Macrophage polarisation differs between apical granulomas, radicular cysts and dentigerous cysts	Germany	*Clinical Oral Investigations*	Q1	To compare macrophage polarization in apical granulomas with radicular cysts, determine if macrophage polarization differs between inflammatory and developmental odontogenic cysts, and evaluate disparities in macrophage density across these three entities.	Macrophage polarisation leads to either apical granulomas or cysts development. Progression of granuloma into tadicular cyst related to increased M1 polarisation. Enhanced M2 polarisation associated with dentigerous cysts.	High degree of variation because the method of TMA to analyse the markers.	Yes
14	Tripi *et al.* [28] (2003)	Proliferative activity in periapical lesions	Italy	*Australian Endodontic Journal*	Q2	IHC evaluation of PCNA. Ki67, CD, and p53 in periapical lesions.	Positive Ki67 and PCNA expression in periapical lesions indicates cell proliferation caused by prolonged irritative stimuli.	No molecular profiling	Yes

ALEO, apical lesions of endodontic origin; CD, cluster of differentiation; EGF, epidermal growth factor; EGFR, epidermal growth factor receptor; ERK, extracellular signal-regulated kinase; ERM, epithelial rests of Malassez; FGF, fibroblast growth factor; gp-130, glycoprotein 130; IHC, immunohistochemistry; IGF, insulin-like growth factor; IGF-BP, insulin-like growth factor binding proteins; IL, interleukin; IL, interleukin; KGF, keratinocyte growth factor; MAPK, mitogen-activated protein kinases; MMP, matrix metalloproteinase; NF-κB, nuclear factor kappa-B; PCNA, proliferating cell nuclear antigen; PDL, periodontal ligament; PG, periapical granuloma; pERK, phosphorylated extracellular signal-regulated kinase; RT-PCR, reverse transcription polymerase chain reaction; SJR, Scimago journal rank; TGF, transforming growth factor; TLR, toll-like receptor; TMA, tissue microarray.

https://doi.org/10.5395/rde.2026.51.e7

Table 2. Methods and outcomes of the studies included

No.	Study (year)	Type of lesions	Sample type/ location	Design/sample size	Main methodology (assays)	Markers/ pathways	Field/magnification	Specific findings	Statistics/ *p*-value	Biological interpretation
1	Lin *et al.* [17] (1996)	Granulomas and cysts	Periapical tissues from human jaws	21 lesions: 14 granulomas, 7 cysts (surgery: extractions) Control: normal human buccal mucosa	IHC staining, ^{125}I-EGF binding	EGFR	Granuloma: 70× Apical cyst: 140×, 280×	EGFR is overexpressed in proliferating epithelial areas; absent in non-proliferative regions	Qualitative only	EGFR likely promotes the proliferation of epithelial rests leading to cysts
2	Gao *et al.* [21] (1996)	Granulomas and cysts	Human mandibular periapical tissues	12 lesions (6 granulomas, 6 cysts) and normal PDL IHC negative control: sense probe IHC positive control: anti-sense probe (retinoic acid detector a)	H&E staining *In situ* hybridization, RT-PCR	KGF	Granuloma: 200 mm Cyst: 0.5 mm, 200 mm	KGF is more expressed by stromal cells of periapical lesions, and it is minimal in normal PDL KGF is associated with epithelial proliferation	Qualitative only	KGF from the stroma may induce ERM proliferation
3	Yamanaka *et al.* [25] (2000)	ERM *in vitro*	Human ERM from PDL (premolar extractions)	# of teeth: NR Serum-free cell culture study IHC negative control	RT-PCR, PCR-Southern hybridization, RPA, WB, IHC	FGF-1, FGF-7, FGFR2-IIIb	ERM: 40×	ERM responded to FGF-1 and FGF-7/KGF via FGFR2-IIIb activation	Functional assays, no *p*-values	FGF-7/KGF supports stromal-epithelial interactions between ERM and PLF for normal structure maintenance and function of PDL
4	Nagano *et al.* [26] (2024)	Radicular cysts	Cellular: SF2, ST-PLF-E, 1-11 Mouse: 8-year female mandible Human: radicular and dentigerous cyst	Experimental group: 52 radicular cysts Control group: 6 dentigerous cysts without inflammation	IF and IHC staining, WB, co-cultures, CyQUANT NF, siRNA, RT-PCR	IL-1β-p65, NF-κB, TGF-β	1 mm, 50 mm, 200 mm	↑p65 and Ki-67, ↓Smad2/3 for radicular cysts TGF-β1–induced Smad2 phosphorylation and suppressed odontogenic epithelial cell proliferation under IL-1β influence	Fisher test, Student t-test, and ANOVA $p < 0.01$ for nuclear p65	IL-1β-65 promotes cystic epithelium by suppressing TGF-β-Smad2
5	Sako *et al.* [20] (2018)	ERM *in vitro*	Porcine PDL ERM	ERM cultures	WST-1 stimulated with IL-6, wound healing, IF	IL-6, integrin α3	Wound healing: 200 mm IF: 50 mm	IL-6–induced ERM proliferation/migration; integrin α3 at leading edges	Kruskal-Wallis, Mann-Whitney U-tests. $p < 0.05$, $p < 0.01$	IL-6 may replicate inflammatory signals driving cysts
6	Schweitzer *et al.* [19] (2021)	Granulomas and cysts	Human ALEOs (dental extractions)	15 lesions: 8 epithelialized, 7 non-epithelialized	H&E, IHC, double IF	IL-6, IL-6R, gp130	100 fields, 40×	IL-6 system is active in epithelial cell proliferation	Qualitative only	Highlights IL-6 involvement in epithelial cells of cyst-like lesions

(Continued on the next page)

https://doi.org/10.5395/rde.2026.51.e7

Table 2. Continued

No.	Study (year)	Type of lesions	Sample type/ location	Design/sample size	Main methodology (assays)	Markers/ pathways	Field/magnification	Specific findings	Statistics/ *p*-value	Biological interpretation
7	Nickolaychuk *et al.* [18] (2002)	Dental follicles, cysts	Dental follicles, dentigerous and radicular cysts	25 lesions: 8 follicles, 4 dentigerous cysts, 8 radicular cysts, 1 radicular cyst, 1 odontogenic keratocyst, 3 developmental odontogenic cysts IHC positive and negative tissue controls	IHC for MAPK markers, anti-PCNA staining	ERK1, pERK1/2, PCNA, cytokeratins	40×	ERK1 and pERK1/2 increased in highly proliferating epithelial component cells	Mean proportion (%), χ^2 test, Fisher test (two-way) $p < 0.05$, $p < 0.01$	MAPK-ERK drives epithelial proliferation MAPK is crucial in cyst lining activation
8	Götz *et al.* [5] (2003)	ERM *in vitro*	Human ERM from PDL of molars extracted	25 deciduous teeth extracted, PDL was adherent IHC positive controls: tissues carrying IGF, receptors or antigens IHC specificity controls: omitting primary antibodies	H&E, IHC, EM, LR-Gold embedding	IGF-II, IGF1R, IGF-BP6	LM: 50 mm, 100 mm, 200 mm EM: 3 mm, 20 mm	IGF-II weak immunoreactivity, and IGF-BP6 is detectable in ERM	Qualitative only	IGF-BP6 inhibits IGF-II, limiting proliferation
9	Bhalla *et al.* [24] (2014)	Granulomas and cysts	Human periapical tissues	39 lesions: 13 PG with epithelium, 16 PG without epithelium, 10 radicular cysts	H&E, IHC	MMP-13	40×	Collagenase-3 is found in the cytoplasm and nucleus (90%) MMP-13 in epithelium and fibroblasts (significant difference)	χ^2 test, Pearson R coefficient ($p \leq 0.05$). $p = 0.00$ for epithelial cells $p = 0.02$ for fibroblasts	MMP-13 facilitates epithelial migration and stromal cell invasion into granulation tissue
10	Leonardi *et al.* [23] (2005)	Granulomas	Human periapical tissues (surgery or dental extraction)	17 Periapical granulomas: 7 without epithelium and 10 with epithelium IHC negative controls: primary antibodies omitted IHC positive controls: breast carcinoma sections	H&E, IHC	MMP-13	200×, 300×, 400×	↑MMP-13 in granulomas with epithelium (small islands and thin strands)	Qualitative only	MMP-13 promotes epithelial cell migration and granulomatous tissue invasion to cyst formation
11	Roi *et al.* [16] (2024)	Granulomas	Human periapical granulomas (dental extraction)	Cross-sectional study 35 lesions	H&E, IHC	Ki-67, CD34	100×, 400×	86.5% lesions were positive for Ki-67 Ki-67 and CD34 overexpression	Shapiro-Wilk test, Welch *t*-test, ANOVA, Mann-Whitney U-test, Kruskal-Wallis test Ki-67 index	Chronic inflammation sustains proliferation and neovascularization

(Continued on the next page)

https://doi.org/10.5395/rde.2026.51.e7

Table 2. Continued

No.	Study (year)	Type of lesions	Sample type/ location	Design/sample size	Main methodology (assays)	Markers/ pathways	Field/magnification	Specific findings	Statistics/ *p*-value	Biological interpretation
12	Leonardi *et al.* [27] (2015)	Granulomas and cysts	Human periapical lesions (surgical samples archived)	Cross-sectional study 31 lesions: 10 granulomas, 21 periapical cysts Control group: 7 dentigerous non-inflamed follicular cysts IHC positive controls: oral squamous cell carcinoma IHC negative controls: primary antibody substitution	H&E, IHC	TLR4	400×, 40×	TLR4 is strongly immunoreactive in epithelial strands of granulomas Basal and suprabasal epithelial layers in cysts were immunostained	Kruskal-Wallis test $p < 0.1$	TLR4 in granulomas may promote ERM, and enhance survival, proliferation, and migration for epithelial strands and islands TLR4 limits apoptosis in cysts
13	Weber *et al.* [22] (2018)	Granulomas, cysts	Human tissues (dental surgery)	Study cohort 87 lesions: 41 granulomas, 23 radicular cysts, 23 dentigerous cysts	TMA: H&E, IHC	CD68, CD11c, CD163, MRC1	7×, 35×	Granulomas: M2 predominant; cysts: M1 predominant	ANOVA $p \leq 0.05$ differences	Macrophage polarisation may influence the granuloma vs cyst pathway
14	Tripi *et al.* [28] (2003)	Granulomas and cysts	Human periapical lesions (biopsy)	Semiquantitative method: Staining scores assigned 24 lesions: 16 granulomas, 8 cysts IHC negative control: omitting primary antibody IHC positive control: skin tissue sections	H&E, IHC	Ki-67, PCNA, CD_3, p53	220×, 380×	All lesions were positive for Ki-67, especially radicular cysts (epithelia); strong PCNA; strong CD_3; p53 negative	Semiquantitative scores	Chronic irritative stimuli lead to cell proliferation

ALEO, apical lesions of endodontic origin; ANOVA, analysis of variance; CD, cluster of differentiation; CyQUANT NF, CyQUANT nuclear fluorescence assay; EGF, epidermal growth factor; EGFR, epidermal growth factor receptor; EM, electron microscopy; ERK1, extracellular signal-regulated kinase 1; ERM, epithelial rests of Malassez; FGF, fibroblast growth factor; FGFR2-IIIb, fibroblast growth factor receptor 2 IIIb isoform; H&E, hematoxylin and eosin; IF, immunofluorescence; IGF, insulin-like growth factor; IGF-II, insulin-like growth factor II; IGF1R, insulin-like growth factor 1 receptor; IGF-BP, insulin-like growth factor binding proteins; IHC, immunohistochemistry; IL, interleukin; KGF, keratinocyte growth factor; LM, light microscopy; MAPK, mitogen-activated protein kinase; MMP, matrix metalloproteinase; MRC1, mannose receptor C-type 1; NF-κB, nuclear factor kappa-light-chain-enhancer of activated B cells; NR, not reported; PCNA, pro-liferating cell nuclear antigen; PDL, periodontal ligament; PG, periapical granuloma; PLF, periodontal ligament-derived fibroblasts; pERK1/2, phosphorylated extracellular signal-regulated kinase 1/2; p53, tumor protein p53; RPA, ribonuclease protection assay; RT-PCR, reverse transcription-polymerase chain reaction; SF2, rat osteogenic epithelial cells; siRNA, small interfering RNA; Smad2/3, mothers against decapentaplegic homolog 2/3; STPLF-E, immortal human heterozygous periodontal ligament cells; TGF, transforming growth factor; TLR, toll-like receptor; TMA, tissue microarray; WB, Western blot; WST-1, water-soluble tetrazolium salt-1 assay; 125I-EGF, iodine-125-labeled epidermal growth factor.

https://doi.org/10.5395/rde.2026.51.e7

PG to IRC [23,24]. Finally, three studies reported biomarkers of epithelial cell proliferation, including toll-like receptors (TLRs), proliferating cell nuclear antigen (PCNA), Ki-67, and cluster of differentiation (CD) 34 [16,27,28].

Regulatory mechanism of epithelial proliferation

Yamanaka *et al*. [25] investigated the KGF/FGF-7 and its receptor (FGFR2-IIIb) in epithelial cells from PGs and IRCs. Both PGs and IRCs were positive for KGF and FGFR2-IIIb, with stronger staining in cystic epithelium. IHC, PCR-Southern blot, RPA, and western blotting confirmed that PDL fibroblasts (PLFs) express FGF-7/KGF messenger RNA (mRNA) and peptide. These results suggest that FGF-7/KGF mediates epithelial–mesenchymal interactions with PLFs, contributing to the maintenance of PDL structure and function [25].

Götz *et al*. [5] assessed the IGF system in human ERMs from 25 deciduous teeth through IHC, light, and electron microscopy. The results showed weak immunoreactivity for IGF-II, minimal or absent expression of IGF-I and its receptors, and consistent cytoplasmic detection of high-affinity IGF-binding protein (IGF-BP) 6. IGF-BP6, due to its high affinity for IGF-II, may function as an autocrine anti-proliferative mechanism that maintains ERMs in a quiescent state. This control could be disrupted under inflammatory conditions [5].

Nagano *et al*. [26] showed that TGF-β1 produced by PLFs suppresses the proliferative activity of odontogenic epithelial cells, as evidenced by reduced Ki-67 expression in co-culture. Inhibition of TGF-β signaling restored proliferation, indicating that PLF-derived TGF-βs, via Smad2/3 signaling, maintain ERMs in a quiescent state under physiological conditions, while this regulation may be disrupted by inflammatory signaling [26].

Pathological mechanisms of epithelial proliferation

1) Growth factors

Lin *et al*. [17] examined the presence of EGF in inflammatory periapical lesions by IHC and ^{125}I-EGF binding assays. Lesions without epithelial proliferation displayed weak or absent ^{125}I-EGF staining, whereas lesions with active epithelial proliferation and cystic transformation exhibited strong immunoreactivity and significantly higher ^{125}I-EGF binding. These findings indicate that EGF expression in odontogenic epithelial cells is upregulated in association with inflammation, suggesting that EGF signaling may drive epithelial proliferation and contribute to cyst transformation [17].

Nickolaychuk *et al*. [18] assessed extracellular signal-regulated kinase 1 (ERK1) and activated ERK1/2 (phosphorylated ERK [pERK] 1/2]) in dentigerous cysts and IRCs compared with dental follicles using IHC. ERK1/pERK1/2 staining was significantly higher in cyst epithelia than in follicles and concentrated in differentiating and highly proliferative epithelial compartments. Stimulation with EGF increased pERK, whereas MEK inhibition (PD98059) reduced it, confirming that epithelial proliferation in odontogenic cysts is mediated through EGF-dependent mitogen-activated protein kinase (MAPK)–ERK signaling, which may contribute to cystic pathogenesis [18].

Gao *et al*. [21] investigated KGF expression in periapical lesions. While KGF mRNA was absent in normal PDL and PGs with minimal inflammation, strong expression was detected in stromal fibroblasts adjacent to inflammatory infiltrates and proliferating epithelium in PGs and IRCs. RT-PCR confirmed elevated KGF in lesion samples. These findings indicate that KGF, upregulated by inflammatory cytokines such as IL-1, TNF-α, and EGF, acts as a paracrine mediator of ERM activation and may drive epithelial proliferation and cyst formation [21].

2) Cytokines

Sako *et al*. [20] examined the effect of IL-6 on porcine ERM cultures. IL-6 significantly enhanced ERM proliferation and migration, effects abolished by IL-6 neutralizing antibody. IL-6 also induced integrin α3 redistribution, indicating activation of migratory pathways. IL-6 directly stimulates ERM activation, linking inflammation to epithelial proliferation in AP [20].

Schweitzer *et al*. [19] demonstrated IL-6 expression in the epithelial lining and stromal cells of radicular cysts. IL-6, through binding to IL-6R and gp130, can activate both classic signaling and trans-signaling pathways, thereby promoting epithelial proliferation and sustaining the inflammatory microenvironment. These findings implicate IL-6 as a central mediator linking chronic

inflammation with histopathologic transformation of AP from PG to IRC [19].

Nagano *et al.* [26] demonstrated that TGF-β1/β2 derived from PLFs suppresses the proliferation of odontogenic epithelial cells through Smad2 signaling, thereby maintaining ERMs in a quiescent state. However, they also showed that IL-1β can activate p65 signaling, which interferes with TGF-β–Smad2 pathways and restores epithelial proliferative activity. While TGF-β exerts a homeostatic inhibitory effect, IL-1β–p65 signaling overrides this control during exacerbated inflammation, driving pathological epithelial proliferation [26].

Weber *et al.* [22] compared macrophage polarization using immunohistochemical markers (CD68, CD11c, CD163, CD206). IRC exhibited the highest degree of M1 macrophage polarization, while PGs showed a predominance of M2 macrophages. M1 polarization in IRCs was associated with pro-inflammatory cytokines such as IL-1 and IL-6, which can stimulate ERM proliferation and perpetuate epithelial activation. Progression from PG to IRC is linked to a shift toward M1 polarization. M1-derived cytokines act as potential drivers of cyst transformation in AP [22].

Biomarkers of epithelial cell proliferation

Roi *et al.* [16] demonstrated high Ki-67 expression (86.5%) and strong CD34 positivity in PGs, with co-expression of CD34 and Ki-67 in endothelial cells and evidence of intussusceptive angiogenesis. The persistent inflammation was shown to promote proliferative activity and abnormal angiogenesis. CD34+/Ki-67+ proliferating vessels in PGs highlight a mechanism by which angiogenesis may support epithelial proliferation and encourage progression towards IRC [16].

Leonardi *et al.* [27] evaluated TLR4 expression in PGs and IRCs. In PGs, TLR4 was strongly expressed in almost all ERM cells, while in IRCs it was weaker and limited to basal/parabasal layers. This suggests that TLR4–nuclear factor kappa-B (NF-κB) signaling supports ERM activation in PGs and maintains epithelial lining in IRCs. It also helps explain why lesions may regress after endodontic therapy when inflammatory stimuli decrease [27].

Tripi *et al.* [28] performed an immunohistochemical evaluation of PCNA, Ki-67, CD_3, and p53 in periapical lesions. Ki-67 was positive in all lesions, primarily in the epithelial cells of the cystic linings. PCNA was positive in 22/24 cases, indicating active DNA synthesis and repair. CD_3 positivity highlighted abundant T-lymphocytes, suggesting their role in sustaining chronic inflammation. No p53 expression was detected. These findings confirm that upregulated levels of pro-inflammatory mediators in chronic inflammation drive epithelial proliferation in periapical lesions, with Ki-67 and PCNA serving as key indicators of proliferative activity [28].

Co-stimulatory molecules

Leonardi *et al.* [23] and Bhalla *et al.* [24] immunohistochemically evaluated the expression of MMP-13 in PGs IRCs. Both studies demonstrated widespread immunopositivity, with stronger expression in the epithelium and fibroblasts of epithelialized PGs and IRCs compared to non-epithelialized PGs. MMP-13 contributes to extracellular matrix degradation and tissue remodeling, facilitating epithelial migration, invasion, and the transition from PG to IRC. Its expression is driven by pro-inflammatory cytokines such as IL-1, IL-6, linking chronic inflammation to epithelial activation and bone resorption [23,24].

Risk of bias assessment

The risk of bias analysis of the included studies reveals that none of the 14 studies received a low risk of bias rating across all four evaluated domains. Two studies [25,26] were rated as low risk of bias in three out of the four domains. In contrast, three studies [5,19,20] were assessed as having an "unclear" or "high" risk of bias across all domains (Table 3).

When analyzing the evaluation by domains, the domain with the most significant issues was "patient selection," as six studies [16–18,20,21,26] were assessed as having a high risk of bias, and seven studies [5,19,22–24,27,28] were rated as "unclear" risk of bias. This was mainly because all studies relied on a case-control design, and in most cases, the method of patient selection—whether consecutive or random—was not clearly reported. The second most problematic domain was "flow and timing," as 12 of the 14 evaluated studies [5,16–25,27,28] did not report or describe a patient selection flowchart. They also failed to describe each of

https://doi.org/10.5395/rde.2026.51.e7

Table 3. Methodological quality graph of included studies (QUADAS-2)

Study (year)	Risk of bias				Applicability concerns		
	Patient selection	Index test	Reference standard	Flow and timing	Patient selection	Index test	Reference standard
Tripi *et al.* [28] (2003)	?	□	?	?	□	□	□
Weber *et al.* [22] (2018)	?	□	□	?	□	□	□
Leonardi *et al.* [27] (2015)	?	□	□	?	□	□	□
Roi *et al.* [16] (2024)	□	□	□	?	□	□	□
Leonardi *et al.* [23] (2005)	?	□	□	?	□	□	□
Bhalla *et al.* [24] (2014)	?	□	□	□	□	□	□
Götz *et al.* [5] (2003)	?	?	?	?	□	□	□
Nickolaychuk *et al.* [18] (2002)	□	□	□	?	□	□	□
Schweitzer *et al.* [19] (2021)	?	?	?	?	□	□	□
Sako *et al.* [20] (2018)	□	?	?	?	□	□	□
Nagano *et al.* [26] (2024)	□	□	□	□	□	□	□
Yamanaka *et al.* [25] (2000)	□	□	□	?	□	□	□
Gao *et al.* [21] (1996)	□	□	□	?	□	□	□
Lin *et al.* [17] (1996)	□	□	□	?	□	□	□

□ Low risk
? Unclear risk
□ High risk

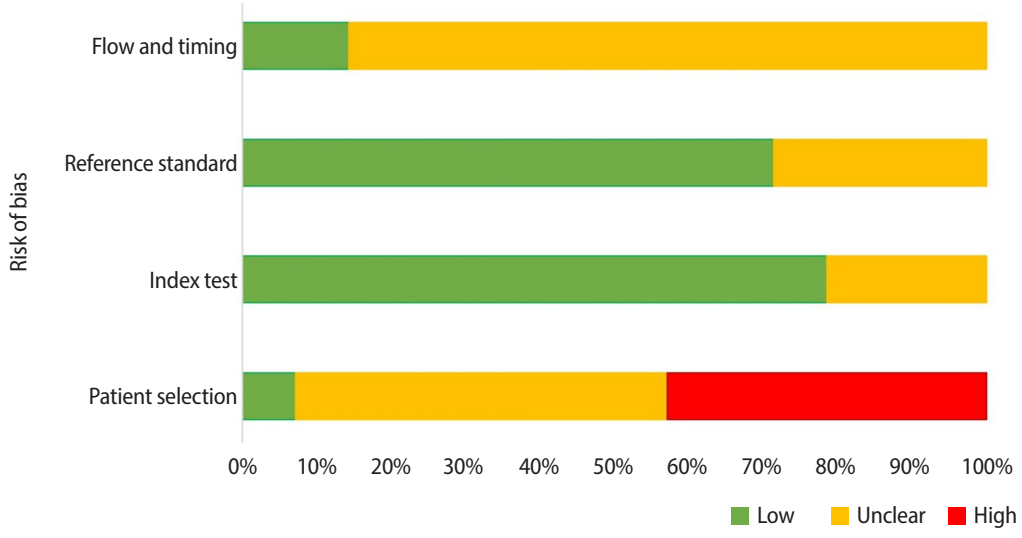

Figure 2. Proportion of studies with low, high, or unclear risk of bias.

the patients included in the study who were evaluated with both the index test and the reference standard test. Additionally, they did not report the time interval between the index test and the reference standard (Table 3 and Figure 2).

In the other two domains, the majority of the studies were rated as having a low risk of bias. In the "Index Test" domain, the few studies [5,19,20] that received an 'unclear" risk rating did so because it was not clear whether the index test results were interpreted without knowledge of the reference standard results. Similarly, in the "reference Standard" domain, only a few studies [5,19,20,28] were rated as "unclear" risk of bias due to a lack of information on who interpreted the tests and whether any blinding was performed (Table 3 and Figure 2).

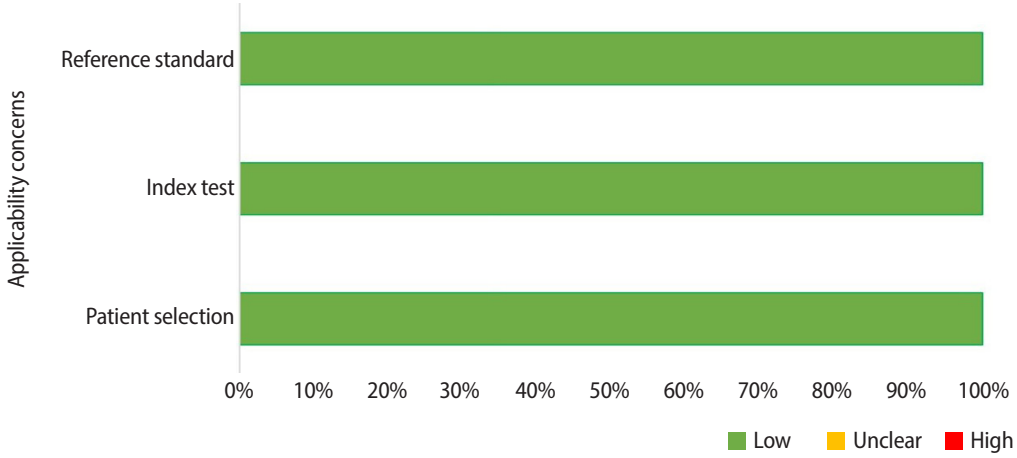

Figure 3. Proportion of studies with low, high, or unclear concerns regarding applicability.

Applicability assessment

In the applicability analysis, all studies were assessed as having a low risk of bias across the three evaluated domains ("patient selection," "index test," and "reference standard"). This was because no issues were identified concerning discrepancies between the included patients and the review question, the conduct or interpretation of the index test, or the condition defined by the reference standard differing from the review question (Table 3 and Figure 3).

DISCUSSION

This systematic review aims to synthesize the best available experimental evidence on the biological pathways underlying epithelial proliferation leading to the transition of PGs into IRCs. Cell and tissue experimental models provide a powerful framework to unravel the intracellular signaling pathways and molecular mediators that govern epithelial activation. These models not only validate the biological relevance of experimental findings but also reveal how molecular alterations translate into structural and functional changes. This dual perspective strengthens the causal link between cellular signaling and lesion development. Findings from this systematic review suggest that biological mechanisms linked to the IGF, FGF-7/KGF, and TGF-β are involved in the regulatory mechanisms of epithelial proliferation within AP under physiological conditions. Under conditions of elevated pro-inflammatory mediators and exacerbated AP, specific growth factors, including EGF and FGF-7/KGF [17,18,21], along with cytokines such as IL-6 and IL-1β, can disrupt homeostatic regulatory pathways, inducing ERM activation and proliferation, thereby facilitating the histopathological progression of PGs into IRC [5,25,26]. Furthermore, macrophage M1 polarization, characterized by Th1-associated cytokines such as IL-1β, IL-6, and TNF-α, drives inflammation, ERM proliferation, and migration, thereby facilitating ERM-driven cyst formation [22]. Additionally, co-stimulatory molecules such as MMP-13 promote epithelial cell migration, proliferation, and stratification within AP, while simultaneously mediating extracellular matrix degradation [23,24]. Finally, several biomarkers of epithelial cell proliferation, including TLRs, PCNA, Ki-67, and CD34, were linked to PG/IRC transition [16,27,28]. The methodological appraisal (QUADAS-2) indicated an overall low-to-moderate risk of bias, with the main concerns arising from patient selection and flow/timing. Several studies lacked clearly defined inclusion criteria or did not provide a flowchart describing patient selection, while others failed to specify whether all patients underwent both the index test and the reference standard. In addition, the time interval between the index test and the reference standard was often not reported, further limiting methodological transparency. In contrast, the validity of index tests (mostly IHC) and reference standards was typically satisfactory, with few questions about application. Thus, the overall strength of evidence of this systematic review can be regarded as

https://doi.org/10.5395/rde.2026.51.e7

moderate, sufficient to support mechanistic hypotheses concerning the transition from PG to IRC, but still insufficient for direct clinical extrapolation due to methodological heterogeneity, small sample sizes, and the predominantly case-control design of the included studies, which limits causal inference and the establishment of temporal relationships.

Regulatory mechanism of epithelial proliferation

FGF-7/KGF is a mesenchyme-derived paracrine mediator with potent mitogenic activity for epithelial cells but not for fibroblasts or endothelial cells [25,29]. FGF-7/KGF exerts its biological effects by binding to specific tyrosine kinase receptors (FGFRs) on the cell surface [25,30]. Immunohistochemical and molecular studies have demonstrated that proliferating human PLFs express and secrete FGF-7/KGF. Expression peaks during the proliferative phase and declines with differentiation, as indicated by increased alkaline phosphatase activity. FGF-7/KGF protein is also detectable in PLF-conditioned medium [25]. When epithelial cells derived from ERMs were cultured in serum-free conditions, their proliferation was selectively stimulated by FGF-7/KGF, following initial PLF outgrowth from the same tissue explants. Notably, ERMs express only the FGFR2-IIIb isoform, a high-affinity receptor for FGF-7/KGF. This isoform-specific expression suggests that ERMs are physiologically responsive to stromal-derived FGF-7/KGF, which regulates their proliferation and differentiation. FGF-7/KGF binding to FGFR2-IIIb induces receptor dimerization and autophosphorylation, activating intracellular signaling pathways such as the MAPK (Ras–Raf–MEK–ERK) cascade, which promotes cyclin D1 expression and G1–S cell cycle progression [31]. Simultaneously, the PI3K–AKT pathway is activated, enhancing epithelial cell survival by phosphorylating pro-apoptotic factors, such as BAD, and suppressing caspase activation [32]. Together, these pathways support epithelial homeostasis by balancing proliferation, differentiation, and survival within the PDL epithelial compartment. However, persistent inflammation, dysregulated FGF-7/KGF expression, or aberrant FGFR2-IIIb activation may disrupt this balance, promoting uncontrolled ERM proliferation and contributing to pathological epithelial proliferation in PGs, leading to transformation into IRCs [21,33].

TGF-β isoforms, particularly TGF-β1 and TGF-β2, are pleiotropic cytokines predominantly released by activated immune cells, platelets, and PLFs [26,34]. TGF-β plays a vital role in maintaining tissue homeostasis by regulating cellular differentiation, inflammation, and proliferation [26,34]. The TGF-β ligand binds to the type II receptor (TGFβ-R2), which then recruits and phosphorylates the type I receptor (TGFβ-R1), thereby activating the intracellular Smad pathway. Specifically, Smad2 and Smad3 become phosphorylated and form a complex with Smad4 that translocates into the nucleus to regulate gene expression [26,35,36]. In epithelial cells, this mechanism has an anti-proliferative effect, partly by upregulating transcription factors like ATF3 and repressing proliferative genes such as Id1. TGF-β signaling helps to keep ERMs in a quiescent state [26,35,36]. Co-culture studies involving human PLFs and odontogenic epithelial cells have demonstrated a reduction in Ki-67 expression, a marker of proliferation, in epithelial cells, indicating growth inhibition [26]. Moreover, blocking TGF-β signaling—through receptor inhibition and small interfering RNA-mediated knockdown of TGF-β1 and TGF-β2—restores proliferative activity in these epithelial cells. These findings suggest that PLF-derived TGF-β, acting via Smad2/3 signaling, serves as a natural control of ERM proliferation. However, under exaggerated inflammatory conditions, this regulatory balance may be disturbed, potentially allowing the abnormal epithelial proliferation that contributes to IRC formation [26].

The IGF system is a pivotal regulator of cell proliferation in diverse cell types, including ERM [5]. IGF ligands, IGF-I and IGF-II, secreted primarily by stromal fibroblasts, exert pleiotropic actions encompassing growth, differentiation, proliferation, and metabolic regulation [5,10]. Signal transduction is mainly mediated by the ubiquitously expressed IGF-1 receptor (IGF-1R) [5,37], whereas the IGF-2 receptor functions predominantly in the sequestration and lysosomal degradation of IGF-II [5].

High-affinity IGF-BPs act as carrier molecules in biological fluids, regulating IGF bioavailability, prolonging their half-life, and modulating receptor interactions [5,38]. IGF-BP6 exhibits the greatest specificity for IGF-

II. Immunohistochemical studies have demonstrated IGF-BP6 localization within the cytoplasm and secretory vesicles of ERMs, suggesting an autocrine regulatory loop. PLFs may constitute an additional source of IGF-BP6 [5]. In ERMs, IGF-BP6 immunoreactivity co-occurs with weak IGF-II and minimal to absent IGF-1R expression, implying negligible sensitivity to IGF-I and the absence of autocrine IGF-I signaling [5]. The preferential binding of IGF-BP6 to IGF-II—up to 100-fold greater than to its receptor—positions IGF-BP6 as a potent inhibitor of IGF-II-mediated mitogenesis [39]. Under physiological conditions, this interaction may restrain ERM proliferation and preserve homeostasis [40].

Inflammatory microenvironments, such as those observed in AP, alter this regulatory balance. A cathepsin D-like protease has been implicated in the proteolytic cleavage of IGF-BP6, liberating bioactive IGF-II within ERMs [5,40]. This IGF-II release may act in an autocrine manner to drive uncontrolled ERM proliferation. Additionally, pro-inflammatory cytokines (IL-1, IL-6) and growth factors such as EGF, TGF-α, and KGF—some of which can be produced by ERMs—may further compromise IGF-BP6-mediated inhibition, thereby facilitating proliferative responses [2,5,25,41].

Pathological mechanisms of epithelial proliferation

Cytokines

IL-1β, a pro-inflammatory cytokine mainly produced by macrophages during the progression of AP, activates NF-κB signaling, with p65 as its key subunit regulating gene transcription and cell proliferation [26,42,43]. In IRCs, elevated IL-1β and p65 expression have been linked to lesion progression. IL-1β also suppresses TGF-β1 expression in PDL cells, disrupting ERM homeostasis [26,44,45]. An immunohistochemical study comparing IRCs and non-inflammatory dentigerous cysts found nuclear and/or cytoplasmic p65 expression in 84.6% of IRCs, significantly higher than in dentigerous cysts ($p < 0.01$). Smad2/3 was consistently expressed in dentigerous cysts but detected in only 25.0% of IRCs. Moreover, Ki-67 positivity was higher in p65-positive IRCs (77.3%) than in p65-negative ones (37.5%), suggesting an inflammation-associated proliferative phenotype [26].

In vitro, SF2 odontogenic epithelial cells stimulated with TGF-β1 showed time-dependent Smad2 phosphorylation and reduced proliferation. Conversely, IL-1β promoted p65 nuclear translocation, induced inducible nitric oxide synthase expression (a direct NF-κB target), and suppressed TGF-β1–induced Smad2 phosphorylation. IL-1β reversed TGF-β1–mediated growth inhibition and proliferation. These findings suggest that IL-1β/p65 signaling promotes epithelial proliferation by antagonizing TGF-β/Smad2 activity, contributing to the histological progression from PG to IRC [26,44,45].

In periapical tissues, IL-6 is secreted by local immune cells—primarily monocytes/macrophages, Th1/Th2 cells, B lymphocytes, and PMNs—in response to endodontic bacterial components like lipopolysaccharides (LPS) [2,19,20,46]. Non-immune cells, such as epithelial, endothelial, and stromal cells, also contribute to IL-6 production under inflammatory stimuli [20]. Elevated IL-6 levels contribute to IRC pathogenesis by enhancing ERM proliferation and migration and sustaining inflammation [2,20].

IL-6 signals via two main pathways: classic signaling, through membrane-bound receptor (mIL-6R), and trans-signaling, through the soluble receptor (sIL-6R) bound to IL-6, which engages gp130 on cells lacking IL-6R [47]. While classic signaling supports tissue homeostasis, trans-signaling mediates pro-inflammatory responses [19,48]. In AP, trans-signaling dominates, as IL-6R is absent in healthy PDL but highly expressed in inflamed lesions. sIL-6R is released by infiltrating mononuclear cells and mediates IL-6 effects on PDL fibroblasts [19,49]. Immature epithelia may respond to IL-6 via trans-signaling from inflammatory or autocrine epithelial sources, while mature lining cells appear responsive to both pathways. Thus, IL-6 may promote proliferation and inflammation via trans-signaling in early lesions (PGs), and migration, regeneration, or apoptosis resistance via classic signaling in IRCs [19,50,51].

Integrins, particularly α3β1, are key regulators of epithelial migration and IL-6 release [20,52]. ERMs express several integrins, including α3, β1, and β3 [20,53,54]. IL-6 stimulation increases ERM proliferation and migration, an effect abolished by IL-6 neutralization. IL-6 also drives spatial redistribution of integrin α3 to filopodia, supporting cytoskeletal reorganization linked to enhanced motility [20]. Cytoskeletal changes during ERM activation involve a shift in cytokeratin expression.

https://doi.org/10.5395/rde.2026.51.e7

Quiescent ERMs express keratins 5 and 19. Upon activation, keratin 14 (a stratifying marker) is upregulated, followed by keratins 13 and 4 (markers of non-keratinizing epithelia). Low levels of keratins 8 and 18 (simple epithelium markers) are also observed, sug-gesting partial epithelial plasticity during cystic transformation [55]. Collectively, IL-6 promotes ERM proliferation and migration through integrin α3 redistribution and cytoskeletal remodeling, contributing to epithelial plasticity and the transition from PG to IRC [19,20,55].

PGs and IRCs are characterized by dense infiltration of macrophages and lymphocytes. In PGs, these immune cells are diffusely distributed throughout the connective tissue, whereas in IRCs they localize primarily within the fibrous cyst wall, contributing to a sustained chronic inflammatory microenvironment [2]. Lymphocytes differentiate into Th1 or Th2 subsets depending on local cytokine cues [56–58], while macrophages polarize into pro-inflammatory M1 or anti-inflammatory M2 phenotypes, typically associated with Th1 and Th2 responses, respectively [56,59].

Immunohistochemical studies reveal that IRCs show a significantly higher prevalence of M1-polarized macrophages, whereas PGs are more enriched in M2 macrophages [22]. M1 polarization, associated with Th1 cytokines such as IL-1β, IL-6, and TNF-α, promotes inflammation, ERM proliferation and migration, and epithelial lining expansion [19,20,26]. In contrast, M2 macrophages, associated with Th2 responses, mediate tissue repair through the clearance of debris, angiogenesis, and the production of anti-inflammatory cytokines such as IL-10 and TGF-β. TGF-β also suppresses ERM proliferation under physiological conditions and contributes to the induction of regulatory T cells (Tregs), reinforcing resolution of inflammation [22,26,56].

Given the stem-like properties of ERMs and their sensitivity to macrophage-derived cytokines [22,60], increased M1 polarization may be a key driver of their activation and the histological transition from PG to IRC. However, the regulation of macrophage polarization in periapical lesions remains incompletely understood. Host factors such as genetic background, the intensity of the inflammatory response, and the composition of the root canal microbiota likely contribute [22,60,61].

In particular, bacterial LPS—abundant in gram-negative organisms—are potent inducers of M1 macrophage activation. IRC fluids often contain gram-negative bacteria, including *Porphyromonas gingivalis*, *Fusobacterium nucleatum*, *Prevotella intermedia*, *Prevotella nigrescens*, *Treponema denticola*, *Tannerella forsythia*, and *Campylobacter rectus*. Notably, *C. rectus* and *T. denticola* induce robust IL-1β production, a hallmark of M1 activation [62]. These data support a model in which the microbial profile of endodontic infections modulates macrophage phenotype and promotes ERM-driven cyst formation via M1-associated inflammatory signaling [22].

Growth factors

EGF is a potent mitogen for epithelial, fibroblastic, and endothelial cells, acting through binding to its high-affinity receptor, EGF-R—a transmembrane protein with intrinsic tyrosine kinase activity [17,63,64]. This interaction triggers intracellular signaling cascades, including MAPK/ERK, leading to gene transcription, cell cycle progression, and epithelial proliferation—key events implicated in IRC pathogenesis [65–67].

EGF-R is abundantly expressed in the epithelial components of the tooth germ, ERMs, and IRC linings, particularly in proliferative epithelial cells [21,63,68]. In contrast, its expression is minimal in PGs [69]. This differential expression suggests that EGF-R upregulation may drive pathological epithelial proliferation in IRCs. EGF produced by stromal fibroblasts is hypothesized to activate ERMs under inflammatory conditions [10].

Inflamed tissues exhibit increased EGF binding and EGF-R expression. IHC and radio-labeled EGF assays have shown strong receptor expression and ligand binding in epithelial cells of IRCs and PGs with epithelial proliferation, but not in lesions lacking such activity [17,70]. Once EGF-R is activated, MAPK/ERK signaling is initiated: ERK1/2 translocates to the nucleus and activates transcription factors like Elk-1, c-Fos, and c-Myc, promoting mitogenic gene ex-pression [18,67]. In ERMs and IRC epithelium, pERK1/2 is associated with proliferation, cytoplasmic vacuolization, and squamous differentiation [18,71]. These findings suggest that ERK phosphorylation functions as a key trigger for reactivating quiescent ERMs, promoting their activation, differentiation, and proliferative response. This observation

is consistent with a mechanistic model in which inflammatory mediators—specifically bacterial endotoxins and pro-inflammatory cytokines such as IL-1 and IL-6—induce MAPK pathway activation, thereby driving ERM proliferation and epithelial differentiation programs [18,72].

KGF/FGF-7 is a stromal-derived paracrine mediator that selectively stimulates epithelial cell proliferation via its high-affinity receptor, FGFR2-IIIb, which is expressed exclusively in epithelial cells [21,33,73]. *In vitro*, fibroblasts constitutively express KGF mRNA and peptide, with expression tightly regulated by epithelial-derived signals [74]. While baseline KGF expression in the PDL is low, AP can upregulate its production in stromal fibroblasts via inflammatory cytokines such as IL-1α/β, TNF-α, and platelet-derived growth factor [10,21].

This cytokine-driven increase in KGF promotes epithelial proliferation indirectly, as shown by elevated KGF expression in PGs and IRCs with active epithelial growth, particularly in stromal cells adjacent to inflammatory infiltrates [21]. *In situ* hybridization and RT-PCR analyses confirm that proliferative periapical lesions express significantly more KGF than normal PDL. KGF expression is notably stronger in early-stage IRCs, suggesting its role in the initial phases of cyst formation [63].

At the signaling level, KGF binding to FGFR2-IIIb activates the Ras–ERK/MAPK pathway, leading to increased cyclin D1 expression and transcriptional activation of c-Fos and c-Myc, driving epithelial cell cycle progression and hyperproliferation [31]. Chronic AP sustains this signaling loop via persistent cytokine stimulation, creating a microenvironment favoring epithelial activation and proliferation, ultimately contributing to IRC pathogenesis [19,26].

Co-stimulatory molecules

MMP-13 exhibits broad substrate specificity [75]. It is produced by fibroblasts, epithelial cells, malignant squamous epithelium, and plasma cells associated with bone-destructive processes [24,75]. In endodontic periapical lesions, MMP-13 has been consistently detected and is considered a major mediator of bone matrix degradation and lesion progression [24,75]. Experimental models of periapical inflammation in rats further demonstrate increased MMP-13 expression during the early stages of lesion development, underscoring a temporally regulated role in extracellular matrix remodeling [76]. Importantly, immunohistochemical studies reveal high levels of MMP-13 immunoreactivity (80%–100%) across PGs and IRCs, with stronger staining in lesions containing epithelial tissue compared with non-epithelial PGs [23,24,77]. Within epithelial compartments, expression is accentuated in PGs with epithelium and IRCs, particularly in thinner epithelial strands indicative of proliferative activity, whereas thicker strands show only scattered positive cells [23,24]. These findings support the concept that ERMs, normally quiescent, can acquire proliferative potential under inflammatory conditions, and that MMP-13 contributes to epithelial migration, proliferation, and invasion. Consequently, MMP-3 is likely involved in the transition from PGs with epithelium to fully developed IRCs [23,24].

Biomarkers of epithelial cell proliferation

Ki-67 is a nuclear protein and an established marker of cellular proliferation [78]. Its upregulation is a hallmark of chronic inflammatory states, including AP. Inflammatory cytokines trigger stress responses that enhance Ki-67 expression in PGs [63,78]. Ki-67 immunoreactivity has been specifically noted in the nuclei of basal epithelial layers in PGs, reflecting epithelial proliferative activity and possible progression toward cyst formation [78].

CD34, a transmembrane sialomucin, is widely expressed in hematopoietic progenitor cells and vascular endothelial cells, as well as in fibrocytes, keratinocytes, and epithelial progenitors [78,79]. Beyond its role in hematopoiesis, CD34 is crucial for angiogenesis, promoting endothelial cell proliferation and migration. In periapical lesions, its expression correlates with areas of intense inflammatory infiltrate, suggesting a dual role in inflammatory modulation and vascular remodeling [78].

Combined immunohistochemical analyses of Ki-67 and CD34 in PGs have demonstrated that Ki-67 marks epithelial cell activation and proliferative potential, while CD34 highlights regions of neovascularization associated with inflammatory cell recruitment. Their co-expression supports a link between inflammation, microvessel density, endothelial proliferation, and epithelial remodeling—key features in the transition from granuloma to cystic pathology [78].

https://doi.org/10.5395/rde.2026.51.e7

PCNA is a key regulatory protein involved in DNA replication and cell cycle control. Under inflammatory conditions, PCNA is upregulated in epithelial cells and serves as a sensitive marker of active proliferation [80]. In periapical lesions, particularly those containing epithelial components such as PGs and IRCs, PCNA immunoreactivity is prominently observed in epithelial linings and the ERMs [28,81]. This pattern reflects a proliferative epithelial response to persistent inflammatory stimuli, consistent with the dynamic interplay between tissue proliferation and degeneration in these lesions.

Proliferative activity in periapical lesions has been consistently demonstrated through immunohistochemical detection of PCNA and Ki-67. All proliferative lesions examined showed concurrent expression of both markers, confirming active cell cycle progression within the epithelial remnants exposed to chronic inflammation [28]. The co-expression of Ki-67 and PCNA provides strong evidence that inflammatory microenvironments stimulate epithelial proliferation, particularly of ERMs, thereby contributing to the pathogenesis of periapical lesions and facilitating their potential transformation into radicular cysts.

TLRs are transmembrane receptors found on immune cells such as macrophages and dendritic cells, but also often or inducibly expressed in epithelial cells, where they serve as primary microbial sensors for pathogen-associated molecular patterns. When ligands bind, TLRs trigger intracellular signaling pathways that lead to the transcription of pro-inflammatory cytokines and other immune mediators [82,83].

In the context of periapical lesions, TLR2 and TLR4 have been strongly implicated in epithelial and immune activation [27]. TLR4 is robustly expressed in epithelial strands and islands derived from ERMs within PGs, while in IRCs, TLR4 expression is predominantly confined to the basal and parabasal epithelial layers, with a patchy immunostaining pattern [27]. This distri-bution reflects TLR4's roles in regulating epithelial survival, proliferation, and migration. In PGs, TLR4 expression may promote ERM activation, whereas in IRCs, it appears to maintain epithelial lining thickness by balancing proliferation and apoptosis.

Functionally, TLR4 activation leads to NF-κB translocation into the nucleus, driving transcription of genes involved in cell survival, proliferation, and inflammatory signaling [27,84]. In PGs, sustained TLR4 signaling in ERMs likely disrupts their quiescent state, inducing pathological epithelial expansion.

Importantly, this inflammation-driven proliferation is reversible. Following non-surgical endodontic therapy, the local decline in inflammatory cytokines and growth factors results in reduced TLR signaling. Consequently, proliferative activity in basal epithelial cells ceases, and differentiated squamous cells undergo apoptosis [10,85]. This regression mirrors the physiological turnover of oral epithelium and underscores the dependence of periapical epithelial structures on chronic inflammatory stimuli [27]. Ultimately, the dynamic balance between proliferation and apoptosis dictates the progression or regression of epithelialized periapical lesions [10,18,86].

Strengths and weaknesses

This systematic review was conducted in full accordance with the Cochrane Handbook for Systematic Reviews of Interventions and the PRISMA statement [13,14], with the protocol prospectively registered in PROSPERO. Only experimental studies (cell and tissue models) using validated assessment methodologies were included. Comprehensive searches were carried out across three major databases and grey literature sources without language restrictions, maximizing coverage and reducing the risk of publication bias. Risk of bias was assessed using QUADAS-2, with two independent reviewers conducting the literature search and data extraction; any disagreements were resolved by consensus. These methodological strengths ensured transparency, reproducibility, and a balanced appraisal of the available evidence, enabling a reliable identification of both strengths and limitations within the included studies.

Methodologically, although this systematic review was rigorously designed, the primary studies included present important limitations: most were small observational or case-control series with heterogeneous and poorly defined inclusion criteria, often lacking patient flowcharts and adequate reporting of the interval between index and reference tests. Sample sizes were generally limited and frequently derived from surgically obtained specimens, introducing potential selection

bias. Considerable variability in immunohistochemical procedures and largely semiquantitative interpretation further restricted cross-study comparability. Furthermore, the lack of longitudinal designs and clinical outcome connections limits the findings' external applicability. Collectively, these flaws limit the total strength of evidence, which should be classified as moderate.

CONCLUSIONS

The transition of PGs into IRCs is governed by a dynamic balance between regulatory and pathological molecular mechanisms acting on ERMs. Under physiological conditions, regulatory mediators such as TGF-β/Smad2/3 and IGF-BP6 maintain ERM quiescence, while stromal-derived KGF/FGF-7 supports controlled epithelial homeostasis. However, exacerbated inflammatory microenvironments disrupt these regulatory circuits: elevated levels of pro-inflammatory cytokines (IL-1β, IL-6, TNF-α), growth factors (EGF, KGF), and bacterial endotoxins activate intracellular pathways such as NF-κB, MAPK/ERK, and PI3K–AKT, reprogramming ERMs towards pathological proliferation, migration, and epithelial plasticity. In parallel, macrophage polarization towards the M1 phenotype amplifies this pathogenic loop through the release of IL-1β, IL-6, and TNF-α, sustaining epithelial activation and cystic expansion.

Co-stimulatory molecules, particularly MMP-13, promote epithelial cell migration, proliferation, and stratification within the lesion while driving extracellular matrix degradation. Its selective upregulation in PGs containing epithelium and in IRCs parallels zones of heightened epithelial activity, indicating that MMP-13 not only remodels the microenvironment but also facilitates invasive epithelial behavior. This dual role positions MMP-13 as a key mediator of the transition from granulomatous to cystic pathology.

Immunohistochemical and molecular biomarkers—including Ki-67, PCNA, CD34, and TLR4—highlight the functional pathways that sustain cystic transformation. Their expression patterns reflect a coordinated interplay of epithelial proliferation, angiogenesis, and immune-driven activation, indicating that epithelial–stromal crosstalk is not a bystander phenomenon but a central driver of lesion progression. Ki-67 and PCNA denote the persistence of epithelial mitotic activity, reinforcing the notion that chronic inflammation maintains ERMs in a proliferative state. CD34 expression underscores the angiogenic support required for epithelial expansion, linking vascular remodeling to proliferative demands. Meanwhile, TLR4 activation integrates microbial sensing with intracellular signaling cascades that potentiate inflammatory amplification, epithelial plasticity, and survival.

Collectively, these biomarkers illustrate that cystic transformation is governed by the convergence of proliferative and inflammatory circuits, sustained by angiogenic reinforcement. Their co-expression delineates a pathogenic signature that not only identifies lesions with higher proliferative potential but also provides a prognostic framework for anticipating cystic behavior. This positions them as candidate tools for molecular stratification of periapical lesions, offering potential clinical value in distinguishing lesions prone to regression from those likely to progress towards irreversible cystic pathology.

Nevertheless, the included studies revealed significant methodological heterogeneity, frequent reliance on case-control designs, limited sample sizes, and incomplete reporting of patient selection and timing, resulting in an overall moderate to high risk of bias. These limitations precluded quantitative synthesis and underscore the urgent need for standardized, longitudinal, and functional studies using advanced molecular tools.

In methodological terms, the predominance of high or unclear risk of bias in patient selection and flow/timing domains weakens the generalizability of current findings. Future investigations should adopt rigorous designs, integrate multiomics approaches, and validate candidate biomarkers in prospective clinical settings.

Collectively, this review emphasizes that IRC development arises from a transition from homeostatic to pathological signaling, in which pro-inflammatory mediator levels inside the periapical chronic inflammation override regulatory checkpoints. To find trustworthy biomarkers and create biologically based diagnostic and treatment approaches, a greater mechanistic knowledge of the biological pathways underlying the transition from PG to IRC is essential. With this information, cystic transformation may be predicted, prevented, or modulated.

https://doi.org/10.5395/rde.2026.51.e7

Future perspectives

While classical pathways such as EGF, KGF, TGF, and IGF and pro-inflammatory cytokines such as IL-1 and IL-6 have been extensively studied, recent evidence indicates that non-canonical mechanisms also influence ERM behavior during chronic inflammation. The Hippo pathway and its effectors YAP and TAZ are particularly relevant, as their dysregulation promotes epithelial proliferation and survival and has been implicated in odontogenic tumors. Although not yet investigated in ERM, the conserved epithelial origin of periapical lesions suggests a similar contribution to abnormal proliferation during cystic transition [87,88]. Epigenetic regulators such as specific microRNAs (e.g., miR-155 targeting SEMA3A) and exosome-mediated miRNA transfer appear to shape the inflammatory milieu, while long non-coding RNAs such as PACER and THRIL are upregulated in IRCs, supporting their role in molecular reprogramming [1,89,90]. Altogether, these insights underscore that integrating transcriptomic, epigenetic, and systems biology approaches is essential to unravel ERM plasticity and to identify early molecular markers of cystic transformation. Such advances may ultimately guide the development of novel therapeutic strategies aimed at preventing or reversing the progression from PG to IRC.

Emerging molecular therapies

Recent advances in the molecular understanding of IRC pathogenesis have unveiled promising therapeutic avenues aimed at restraining ERM proliferation and even reversing early cystic transformation. Among the most compelling targets is IL-6 trans-signaling, mediated by the sIL-6R. Selective blockade with sgp130Fc has been shown to attenuate pathological ERM activation while preserving the beneficial homeostatic effects of classic IL-6 signaling [19]. Equally significant is the MAPK/ERK axis, where pERK1/2 drives epithelial proliferation. Inhibition of this pathway with MEK1/2 inhibitors (e.g., PD98059) could suppress aberrant epithelial growth and halt progression from PG to IRC [18]. Another innovative strategy involves exploiting the TRAIL–DR5 apoptotic axis, which is active in IRC linings; DR5 agonists may selectively eliminate hyperplastic epithelial cells while sparing surrounding tissues [91]. Moreover, the strong upregulation of ΔNp63 and Ki-67 underscores their role in sustaining epithelial stemness and proliferation. Although direct ΔNp63 inhibition remains experimental, epigenetic modulators and inflammatory microenvironment control represent feasible approaches to temper these pro-liferative signals [92]. Finally, the NLR family pyrin domain-containing 3 (NLRP3) inflammasome–IL-1β pathway emerges as a central driver linking inflammation, bone resorption, and epithelial activation. Targeted suppression using NLRP3 inhibitors (mcc950), IL-1 receptor antagonists (Anakinra ((Kineret®, Amgen Inc., Thousand Oaks, CA, USA)), or monoclonal antibodies against IL-1β (Canakinumab (Ilaris®, Novartis Pharma AG, Basel, Switzerland)) holds great translational promise [42]. Together, these molecular strategies herald the prospect of non-surgical modulation of IRC, shifting endodontics toward biologically guided interventions that can actively reprogram epithelial dynamics and redefine the therapeutic landscape of periapical disease.

CONFLICT OF INTEREST

No potential conflict of interest relevant to this article was reported.

FUNDING/SUPPORT

The authors have no financial relationships relevant to this article to disclose.

AUTHOR CONTRIBUTIONS

Conceptualization: Rios-Osorio N. Data curation: Briñez-Rodríguez S; Grajales M, Jiménez-Peña OM. Formal analysis: Grajales M, Jiménez-Peña OM. Investigation: Rios-Osorio N, Briñez-Rodríguez S, Betancur-Calle D, Guerrero-Torres M. Methodology: Rios-Osorio N, Grajales M, Jiménez-Peña OM. Project administration: Rios-Osorio N. Resources: Rios-Osorio N. Software: Jiménez-Peña OM. Supervision: Rios-Osorio N, Fernández-Grisales R. Validation: Rios-Osorio N, Fernández-Grisales R. Writing - original draft: Rios-Osorio N, Fernández-Grisales R. Writing - review & editing: Rios-Osorio N. All authors read and approved the final manuscript.

DATA SHARING STATEMENT

The datasets are not publicly available but are available from the corresponding author upon reasonable request.

REFERENCES

1. Bozgeyik E, Ege B, Erdogmus Z, Bozgeyik I, Koparal M,

Bayazit S, *et al*. Inflammation-associated long non-coding RNA signature in radicular cyst tissues. Pathol Res Pract 2023;245:154456.
2. Rios Osorio N, Caviedes-Bucheli J, Mosquera-Guevara L, Adames-Martinez JS, Gomez-Pinto D, Jimenez-Jimenez K, *et al*. The paradigm of the inflammatory radicular cyst: biological aspects to be considered. Eur Endod J 2023;8:20-36.
3. Rios Osorio N, Jiménez Peña O, Contreras Ibarra M, Grajales M, Fernández Grisales R. Accuracy of ultrasound imaging in the differential diagnosis of inflammatory radicular cyst and periapical granuloma: a systematic review and meta-analysis of operative characteristics. Eur Endod J 2025;10:104-115.
4. Nair PN, Sundqvist G, Sjögren U. Experimental evidence supports the abscess theory of development of radicular cysts. Oral Surg Oral Med Oral Pathol Oral Radiol Endod 2008;106:294-303.
5. Götz W, Lossdörfer S, Krüger U, Braumann B, Jäger A. Immunohistochemical localization of insulin-like growth factor-II and its binding protein-6 in human epithelial cells of Malassez. Eur J Oral Sci 2003;111:26-33.
6. Xiong J, Gronthos S, Bartold PM. Role of the epithelial cell rests of Malassez in the development, maintenance and regeneration of periodontal ligament tissues. Periodontol 2000 2013;63:217-233.
7. Xiong J, Mrozik K, Gronthos S, Bartold PM. Epithelial cell rests of Malassez contain unique stem cell populations capable of undergoing epithelial-mesenchymal transition. Stem Cells Dev 2012;21:2012-2025.
8. Tsunematsu T, Fujiwara N, Yoshida M, Takayama Y, Kujiraoka S, Qi G, *et al*. Human odontogenic epithelial cells derived from epithelial rests of Malassez possess stem cell properties. Lab Invest 2016;96:1063-1075.
9. Nair PN. Pathogenesis of apical periodontitis and the causes of endodontic failures. Crit Rev Oral Biol Med 2004;15:348-381.
10. Lin LM, Huang GT, Rosenberg PA. Proliferation of epithelial cell rests, formation of apical cysts, and regression of apical cysts after periapical wound healing. J Endod 2007;33:908-916.
11. Ohshima M, Nishiyama T, Tokunaga K, Sato S, Maeno M, Otsuka K. Profiles of cytokine expression in radicular cystlining epithelium examined by RT-PCR. J Oral Sci 2000;42:239-246.
12. Brunette DM. Cholera toxin and dibutyryl cyclic-AMP stimulate the growth of epithelial cells derived from epithelial rests from porcine periodontal ligament. Arch Oral Biol 1984;29:303-309.
13. In: Higgins JPT, Thomas J, Chandler J, Cumpston M, Li T, Page MJ, *et a*l, editors. Cochrane handbook for systematic reviews of interventions, version 6.5 (updated August 2024) [Internet]. London, UK: Cochrane; 2024 [cited 2025 Aug 20]. Available from: https://training.cochrane.org/handbook
14. Page MJ, McKenzie JE, Bossuyt PM, Boutron I, Hoffmann TC, Mulrow CD, *et al*. The PRISMA 2020 statement: an updated guideline for reporting systematic reviews. BMJ 2021;372:n71.
15. Whiting PF, Rutjes AW, Westwood ME, Mallett S, Deeks JJ, Reitsma JB, *et al*. QUADAS-2: a revised tool for the quality assessment of diagnostic accuracy studies. Ann Intern Med 2011;155:529-536.
16. Roi C, Riviș M, Roi A, Raica M, Ceaușu RA, Motofelea AC, *et al*. CD34 and Ki-67 Immunoexpression in periapical granulomas: implications for angiogenesis and cellular proliferation. Diagnostics (Basel) 2024;14:2446.
17. Lin LM, Wang SL, Wu-Wang C, Chang KM, Leung C. Detection of epidermal growth factor receptor in inflammatory periapical lesions. Int Endod J 1996;29:179-184.
18. Nickolaychuk B, McNicol A, Gilchrist J, Birek C. Evidence for a role of mitogen-activated protein kinases in proliferating and differentiating odontogenic epithelia of inflammatory and developmental cysts. Oral Surg Oral Med Oral Pathol Oral Radiol Endod 2002;93:720-729.
19. Schweitzer C, Garrido M, Paredes R, Stoore C, Reyes M, Bologna-Molina R, *et al*. Localization of interleukin-6 signaling complex in epithelialized apical lesions of endodontic origin. Clin Oral Investig 2021;25:4075-4083.
20. Sako R, Kobayashi F, Aida N, Furusawa M, Muramatsu T. Response of porcine epithelial rests of Malassez to stimulation by interleukin-6. Int Endod J 2018;51:431-437.
21. Gao Z, Flaitz CM, Mackenzie IC. Expression of keratinocyte growth factor in periapical lesions. J Dent Res 1996;75:1658-1663.
22. Weber M, Schlittenbauer T, Moebius P, Büttner-Herold M, Ries J, Preidl R, *et al*. Macrophage polarization differs between apical granulomas, radicular cysts, and dentigerous cysts. Clin Oral Investig 2018;22:385-394.
23. Leonardi R, Caltabiano R, Loreto C. Collagenase-3 (MMP-13) is expressed in periapical lesions: an immunohistochemical study. Int Endod J 2005;38:297-301.
24. Bhalla G, Astekar MS, Ramesh G, Kaur P, Sowmya GV. Collagenase-3 expression in periapical lesions: an immunohisto-

https://doi.org/10.5395/rde.2026.51.e7

chemical study. Biotech Histochem 2014;89:457-463.
25. Yamanaka T, Sakamoto A, Tanaka Y, Zhang Y, Hayashido Y, Toratani S, *et al*. Isolation and serum-free culture of epithelial cells derived from epithelial rests of Malassez in human periodontal ligament. In Vitro Cell Dev Biol Anim 2000;36:548-553.
26. Nagano R, Nakako Y, Fujii S, Kawano S, Maeda H, Kiyoshima T. The IL-1β-p65 axis stimulates quiescent odontogenic epithelial cell rests via TGF-β signalling to promote cell proliferation of the lining epithelia in radicular cysts: a laboratory investigation. Int Endod J 2024;57:344-354.
27. Leonardi R, Perrotta RE, Loreto C, Musumeci G, Crimi S, Dos Santos JN, *et al*. Toll-like receptor 4 expression in the epithelium of inflammatory periapical lesions: an immunohistochemical study. Eur J Histochem 2015;59:2547.
28. Tripi TR, Bonaccorso A, Rapisarda E, Bartoloni G. Proliferative activity in periapical lesions. Aust Endod J 2003;29:31-33.
29. Finch PW, Rubin JS, Miki T, Ron D, Aaronson SA. Human KGF is FGF-related with properties of a paracrine effector of epithelial cell growth. Science 1989;245:752-755.
30. Beenken A, Mohammadi M. The FGF family: biology, pathophysiology and therapy. Nat Rev Drug Discov 2009;8:235-253.
31. Ornitz DM, Itoh N. The Fibroblast Growth Factor signaling pathway. Wiley Interdiscip Rev Dev Biol 2015;4:215-266.
32. Turner N, Grose R. Fibroblast growth factor signalling: from development to cancer. Nat Rev Cancer 2010;10:116-129.
33. Finch PW, Rubin JS. Keratinocyte growth factor/fibroblast growth factor 7, a homeostatic factor with therapeutic potential for epithelial protection and repair. Adv Cancer Res 2004;91:69-136.
34. Fujii S, Maeda H, Tomokiyo A, Monnouchi S, Hori K, Wada N, *et al*. Effects of TGF-β1 on the proliferation and differentiation of human periodontal ligament cells and a human periodontal ligament stem/progenitor cell line. Cell Tissue Res 2010;342:233-242.
35. David CJ, Massagué J. Contextual determinants of TGFβ action in development, immunity and cancer. Nat Rev Mol Cell Biol 2018;19:419-435.
36. Massagué J. TGFβ signalling in context. Nat Rev Mol Cell Biol 2012;13:616-630.
37. Grothey A, Voigt W, Schöber C, Müller T, Dempke W, Schmoll HJ. The role of insulin-like growth factor I and its receptor in cell growth, transformation, apoptosis, and chemoresistance in solid tumors. J Cancer Res Clin Oncol 1999;125:166-173.
38. Baxter RC. Insulin-like growth factor (IGF)-binding proteins: interactions with IGFs and intrinsic bioactivities. Am J Physiol Endocrinol Metab 2000;278:E967-E976.
39. Bach LA. Insulin-like growth factor binding protein-6: the "forgotten" binding protein? Horm Metab Res 1999;31:226-234.
40. Marinaro JA, Hendrich EC, Leeding KS, Bach LA. HaCaT human keratinocytes express IGF-II, IGFBP-6, and an acid-activated protease with activity against IGFBP-6. Am J Physiol 1999;276:E536-E542.
41. Liu F, Abiko Y, Nishimura M, Kusano K, Shi S, Kaku T. Expression of inflammatory cytokines and beta-defensin 1 mRNAs in porcine epithelial rests of Malassez in vitro. Med Electron Microsc 2001;34:174-178.
42. Cheng R, Wu Z, Li M, Shao M, Hu T. Interleukin-1β is a potential therapeutic target for periodontitis: a narrative review. Int J Oral Sci 2020;12:2.
43. Giridharan S, Srinivasan M. Mechanisms of NF-κB p65 and strategies for therapeutic manipulation. J Inflamm Res 2018;11:407-419.
44. Yang NY, Zhou Y, Zhao HY, Liu XY, Sun Z, Shang JJ. Increased interleukin 1α and interleukin 1β expression is involved in the progression of periapical lesions in primary teeth. BMC Oral Health 2018;18:124.
45. Yu J, Liu M, Zhu L, Zhu S, Lv F, Wang Y, *et al*. The expression of interferon regulatory factor 8 in human periapical lesions. J Endod 2018;44:1276-1282.
46. Bracks IV, Armada L, Gonçalves LS, Pires FR. Distribution of mast cells and macrophages and expression of interleukin-6 in periapical cysts. J Endod 2014;40:63-68.
47. Rose-John S, Winthrop K, Calabrese L. The role of IL-6 in host defence against infections: immunobiology and clinical implications. Nat Rev Rheumatol 2017;13:399-409.
48. Garbers C, Thaiss W, Jones GW, Waetzig GH, Lorenzen I, Guilhot F, *et al*. Inhibition of classic signaling is a novel function of soluble glycoprotein 130 (sgp130), which is controlled by the ratio of interleukin 6 and soluble interleukin 6 receptor. J Biol Chem 2011;286:42959-42970.
49. Hernández-Caldera A, Vernal R, Paredes R, Veloso-Matta P, Astorga J, Hernández M. Human periodontal ligament fibroblasts synthesize C-reactive protein and Threlated cytokines in response to interleukin (IL)-6 trans-signalling. Int Endod J 2018;51:632-640.
50. Rose-John S. IL-6 trans-signaling via the soluble IL-6 recep-

tor: importance for the pro-inflammatory activities of IL-6. Int J Biol Sci 2012;8:1237-1247.
51. Scheller J, Chalaris A, Schmidt-Arras D, Rose-John S. The pro- and anti-inflammatory properties of the cytokine interleukin-6. Biochim Biophys Acta 2011;1813:878-888.
52. Lubin FD, Segal M, McGee DW. Regulation of epithelial cell cytokine responses by the alpha3beta1 integrin. Immunology 2003;108:204-210.
53. Uitto VJ, Larjava H, Peltonen J, Brunette DM. Expression of fibronectin and integrins in cultured periodontal ligament epithelial cells. J Dent Res 1992;71:1203-1211.
54. Talic N, Evans CA, Daniel JC, George A, Zaki AM. Immunohistochemical localization of alphavbeta3 integrin receptor during experimental tooth movement. Am J Orthod Dentofacial Orthop 2004;125:178-184.
55. Gao Z, Mackenzie IC, Williams DM, Cruchley AT, Leigh I, Lane EB. Patterns of keratin-expression in rests of Malassez and periapical lesions. J Oral Pathol 1988;17:178-185.
56. Ribeiro CM, de Carli ML, Nonogaki S, Nogueira DA, Pereira AA, Sperandio FF, *et al*. M2 macrophages coexist with a Th1-driven profile in periapical cysts. Int Endod J 2018;51 Suppl 2:e87-e93.
57. Ihan Hren N, Ihan A. T lymphocyte activation and cytokine expression in periapical granulomas and radicular cysts. Arch Oral Biol 2009;54:156-161.
58. F Cavalla, AC Araujo-Pires, CC Biguetti, GP Garlet. Cytokine networks regulating inflammation and immune defense in the oral cavity. Curr Oral Health Rep 2014;1:104-113.
59. Dey A, Allen J, Hankey-Giblin PA. Ontogeny and polarization of macrophages in inflammation: blood monocytes versus tissue macrophages. Front Immunol 2014;5:683.
60. Mantovani A, Biswas SK, Galdiero MR, Sica A, Locati M. Macrophage plasticity and polarization in tissue repair and remodelling. J Pathol 2013;229:176-185.
61. Li J, Hsu HC, Mountz JD. The dynamic duo-inflammatory M1 macrophages and Th17 cells in rheumatic diseases. J Orthop Rheumatol 2013;1:4.
62. Cinar S, Keskin F, Ciftci S, Cakarer S, Selvi F, Keskin-Yalcin B, *et al*. Species and number of bacterium may alternate IL-1β levels in the odontogenic cyst fluid. Turk Biyokim Derg 2018;43:679-685.
63. Valente WA, Barrocas D, Armada L, Pires FR. Expression of epithelial growth factors and of apoptosis-regulating proteins, and presence of CD57+ cells in the development of inflammatory periapical lesions. J Appl Oral Sci 2022;30:e20210413.
64. Li T, Browne RM, Matthews JB. Immunocytochemical expression of growth factors by odontogenic jaw cysts. Mol Pathol 1997;50:21-27.
65. Gui T, Sun Y, Shimokado A, Muragaki Y. The roles of mitogen-activated protein kinase pathways in TGF-β-induced epithelial-mesenchymal transition. J Signal Transduct 2012;2012:289243.
66. Cargnello M, Roux PP. Activation and function of the MAPKs and their substrates, the MAPK-activated protein kinases. Microbiol Mol Biol Rev 2011;75:50-83.
67. Shaul YD, Seger R. The MEK/ERK cascade: from signaling specificity to diverse functions. Biochim Biophys Acta 2007;1773:1213-1226.
68. Heikinheimo K, Voutilainen R, Happonen RP, Miettinen PJ. EGF receptor and its ligands, EGF and TGF-alpha, in developing and neoplastic human odontogenic tissues. Int J Dev Biol 1993;37:387-396.
69. Tyler LW, Matossian K, Todd R, Gallagher GT, White RR, Wong DT. Eosinophil-derived transforming growth factors (TGF-alpha and TGF-beta 1) in human periradicular lesions. J Endod 1999;25:619-624.
70. Chang KM, Lehrhaupt N, Lin LM, Feng J, Wu-Wang CY, Wang SL. Epidermal growth factor in gingival crevicular fluid and its binding capacity in inflamed and non-inflamed human gingiva. Arch Oral Biol 1996;41:719-724.
71. Bernardi L, Visioli F, Nör C, Rados PV. Radicular cyst: an update of the biological factors related to lining epithelium. J Endod 2015;41:1951-1961.
72. Li M, Wang M, Wen Y, Zhang H, Zhao GN, Gao Q. Signaling pathways in macrophages: molecular mechanisms and therapeutic targets. MedComm (2020) 2023;4:e349.
73. Stadelmann N, Horch RE, Schmid R, Ostendorf D, Peddi A, Promny T, *et al*. Growth factors IGF-1 and KGF and adipose-derived stem cells promote migration and viability of primary human keratinocytes in an in vitro wound model. Front Med (Lausanne) 2025;12:1516116.
74. Niu J, Chang Z, Peng B, Xia Q, Lu W, Huang P, *et al*. Keratinocyte growth factor/fibroblast growth factor-7-regulated cell migration and invasion through activation of NF-kappaB transcription factors. J Biol Chem 2007;282:6001-6011.
75. Khasigov PZ, Podobed OV, Ktzoeva SA, Gatagonova TM, Grachev SV, Shishkin SS, *et al*. Matrix metallo-proteinases of normal human tissues. Biochemistry (Mosc) 2001;66:130-140.

https://doi.org/10.5395/rde.2026.51.e7

76. Matsui H, Yamasaki M, Nakata K, Amano K, Nakamura H. Expression of MMP-8 and MMP-13 in the development of periradicular lesions. Int Endod J 2011;44:739-745.
77. Wahlgren J, Maisi P, Sorsa T, Sutinen M, Tervahartiala T, Pirilä E, *et al*. Expression and induction of collagenases (MMP-8 and -13) in plasma cells associated with bone-destructive lesions. J Pathol 2001;194:217-224.
78. Güler N, Comunoğlu N, Cabbar F. Ki-67 and MCM-2 in dental follicle and odontogenic cysts: the effects of inflammation on proliferative markers. ScientificWorldJournal 2012;2012:946060.
79. Sidney LE, Branch MJ, Dunphy SE, Dua HS, Hopkinson A. Concise review: evidence for CD34 as a common marker for diverse progenitors. Stem Cells 2014;32:1380-1389.
80. Lai MD, Lee LR, Cheng KS, Wing LY. Expression of proliferating cell nuclear antigen in luminal epithelium during the growth and regression of rat uterus. J Endocrinol 2000;166:87-93.
81. Li TJ, Browne RM, Matthews JB. Quantification of PCNA+ cells within odontogenic jaw cyst epithelium. J Oral Pathol Med 1994;23:184-189.
82. Aderem A, Ulevitch RJ. Toll-like receptors in the induction of the innate immune response. Nature 2000;406:782-787.
83. Li D, Wu M. Pattern recognition receptors in health and diseases. Signal Transduct Target Ther 2021;6:291.
84. Kim HJ, Kim H, Lee JH, Hwangbo C. Toll-like receptor 4 (TLR4): new insight immune and aging. Immun Ageing 2023;20:67.
85. Suzuki T, Kumamoto H, Kunimori K, Ooya K. Immunohistochemical analysis of apoptosis-related factors in lining epithelium of radicular cysts. J Oral Pathol Med 2005;34:46-52.
86. Takahashi K, MacDonald D, Murayama Y, Kinane D. Cell synthesis, proliferation and apoptosis in human dental periapical lesions analysed by in situ hybridisation and immunohistochemistry. Oral Dis 1999;5:313-320.
87. Zhao B, Li L, Lei Q, Guan KL. The Hippo-YAP pathway in organ size control and tumorigenesis: an updated version. Genes Dev 2010;24:862-874.
88. Man QW, Ma YQ, Liu JY, Zhao Y, Liu B, Zhao YF. Expression of YAP/TAZ in keratocystic odontogenic tumors and its possible association with proliferative behavior. Biomed Res Int 2017;2017:4624890.
89. Al Gashaamy ZJ, Alomar T, Al-Sinjary L, Wazzan M, Saeed MH, Al-Rawi NH. MicroRNA expression in apical periodontitis and pulpal inflammation: a systematic review. PeerJ 2023;11:e14949.
90. Yue J, Song D, Lu W, Lu Y, Zhou W, Tan X, *et al*. Expression profiles of inflammation-associated microRNAs in periapical lesions and human periodontal ligament fibroblasts inflammation. J Endod 2016;42:1773-1778.
91. Loreto C, Galanti C, Leonardi R, Musumeci G, Pannone G, Palazzo G, *et al*. Possible role of apoptosis in the pathogenesis and clinical evolution of radicular cyst: an immunohistochemical study. Int Endod J 2013;46:642-648.
92. Alsaegh MA, Mahmoud O, Varma SR, Mathew A, Altaie AM, Zhu S. P63 and Ki-67 expression in radicular cyst. J Oral Biol Craniofac Res 2023;13:575-580.

APPENDIX

Appendix 1. Search strategy translated for each database

Database	Search strategy	No. of studies
SCOPUS -KeyWords Plus	TITLE-ABS-KEY (periapical OR "apical periodontitis" OR "periapical granuloma" OR "chronic apical periodontitis") AND TITLE-ABS-KEY ("radicular cyst" OR "periapical cyst" OR "dental cyst" OR "inflammatory cyst") AND TITLE-ABS-KEY (pathogenesis OR progression OR evolution OR transition OR development OR formation) AND TITLE-ABS-KEY (mechanism OR "inflammatory mediator" OR "immune response" OR cytokine OR interleukin OR "growth factor" OR "epithelial cell" OR "epithelial proliferation" OR "cyst expansion" OR "molecular mechanism")	83
PUBMED -Mesh terms	(Periapical OR "apical periodontitis" OR "periapical granuloma" OR "chronic apical periodontitis") AND ("radicular cyst" OR "periapical cyst" OR "dental cyst" OR "inflammatory cyst") AND (pathogenesis OR progression OR evolution OR transition OR development OR formation) AND (mechanism OR "inflammatory mediator" OR "immune response" OR cytokine OR interleukin OR "growth factor" OR "epithelial cell" OR "epithelial proliferation" OR "cyst expansion" OR "molecular mechanism")	102
ISI WEB OF SCIENCE -Key Words	TS=(periapical OR "apical periodontitis" OR "periapical granuloma" OR "chronic apical periodontitis") AND TS=("radicular cyst" OR "periapical cyst" OR "dental cyst" OR "inflammatory cyst") AND TS=(pathogenesis OR progression OR evolution OR transition OR development OR formation) AND TS=(mechanism OR "inflammatory mediator" OR "immune response" OR cytokine OR interleukin OR "growth factor" OR "epithelial cell" OR "epithelial proliferation" OR "cyst expansion" OR "molecular mechanism")	33

https://doi.org/10.5395/rde.2026.51.e7

RDE Restorative Dentistry & Endodontics

Research Article

eISSN 2234-7666
Restor Dent Endod. 2026 February;51(1):e8
https://doi.org/10.5395/rde.2026.51.e8

Comparative evaluation of dentinal tubule occlusion by desensitizing agents after tooth bleaching: an *in vitro* study

Dimitrios Dionysopoulos[1,*], **Petros Mourouzis**[1], **Spyros Papageorgiou**[2], **Kosmas Tolidis**[1]

[1]Department of Operative Dentistry, Faculty of Dentistry, School of Health Sciences, Aristotle University of Thessaloniki, Thessaloniki, Greece
[2]Laboratory of Chemistry-Biochemistry-Cosmetic Science, Department of Biomedical Sciences, University of West Attica, Athens, Greece

ABSTRACT

Objectives: This study aimed to evaluate the efficacy of three commercially available desensitizing agents in occluding dentinal tubules, which may help reduce tooth sensitivity following a bleaching treatment.

Methods: Twenty healthy human third molars were utilized in this investigation. The samples were prepared by transversely sectioning 2.5 mm of the crowns to expose the dentin. They were initially treated with 15% ethylenediaminetetraacetic acid gel for 4 minutes, followed by application of Perfect Bleach (VOCO GmbH) bleaching agent (16% carbamide peroxide) for 2 hours. The samples were randomly allocated into four groups ($n = 5$), each receiving one of the following treatments: group 1: No treatment (control), group 2: treated with UltraEZ (Ultradent Products Inc.,), containing potassium nitrate and sodium fluoride, group 3: treated with Perfect Protect (VOCO GmbH), also containing potassium nitrate and sodium fluoride and group 4: treated with TheraSol Whitening & Sensitive (ABC Kinitron IKE), containing strontium acetate and sodium monofluorophosphate. Subsequently, the specimens were examined using scanning electron microscopy (SEM) and energy-dispersive X-ray spectroscopy to evaluate dentin tubule occlusion.

Results: SEM observations showed no occlusion of dentin tubules in the control group, whereas groups 2 to 4 exhibited significant occlusion. The most effective treatment was Perfect Protect ($p < 0.05$), while UltraEZ and TheraSol Whitening & Sensitive demonstrated similar effectiveness, with no statistically significant difference between them ($p > 0.05$).

Conclusions: The tested desensitizing agents effectively occluded dentin tubules to a considerable extent. Differences in their effectiveness were attributed to variations in their formulations.

Keywords: Protect dentin desensitizer; Scanning electron microscopy; Tooth bleaching; X-ray emission spectrometry

INTRODUCTION

Tooth sensitivity (TS) after tooth bleaching is a common, temporary side effect resulting from the strong bleaching agents typically used during the procedure, including hydrogen peroxide (H_2O_2) or carbamide per-

Received: July 16, 2025 **Revised:** October 6, 2025 **Accepted:** October 27, 2025

Citation
Dionysopoulos D, Mourouzis P, Papageorgiou S, Tolidis K. Comparative evaluation of dentinal tubule occlusion by desensitizing agents after tooth bleaching: an *in vitro* study. Restor Dent Endod 2026;51(1):e8.

***Correspondence to**
Dimitrios Dionysopoulos, PhD
Department of Operative Dentistry, Faculty of Dentistry, School of Health Sciences, Aristotle University of Thessaloniki, 54124 Thessaloniki, Greece
Email: ddionys@dent.auth.gr

oxide ($CH_6N_2O_3$) in various concentrations [1]. These substances penetrate through the enamel and extend into the dentin, irritating the nerve endings inside the teeth. Patients may experience sharp, transient pain or increased sensitivity to hot, cold, or sweet foods and drinks, usually for a few days. Sensitivity usually subsides within 1 to 4 days after treatment, but it can be managed with desensitizing gels, fluoride treatments, and avoiding extreme temperature changes [2].

This sensitivity is thought to arise when H_2O_2 molecules pass through the enamel and dentin, ultimately reaching the pulp and inducing an inflammatory response [2]. It is important to note that this mechanism differs from the typical causes of dentin hypersensitivity (DH). The most common theory proposes that DH results from stimulus-induced fluid movement within the dentin tubules, which subsequently activates nociceptors at the pulp-dentin interface [3]. It is postulated that this fluid shift stimulates intradental myelinated A-fibers, along with some unmyelinated A-fibers, resulting in the characteristic short, sharp pain associated with DH [4]. While bleaching-induced sensitivity is usually temporary, individuals with pre-existing DH may experience more intense and prolonged discomfort following the procedure [5].

TS has been encountered in 49%–100% of patients undergoing tooth bleaching in previous clinical studies [6]. The severity of TS is influenced by various parameters, including the type and composition of the bleaching agent, the duration of the procedure, the precision of the technique, and any pre-existing TS [7]. While the exact mechanism behind bleaching-induced TS remains unclear, it is believed to result from the penetration of H_2O_2 into the dental pulp [8]. Because of its low molecular weight (34.01 g/mol), H_2O_2 and its byproducts, including reactive oxygen species, can pass through the permeable enamel and dentin, and they reach the pulp tissue and initiate the release of inflammatory mediators, like interleukin-1β and receptor activator of nuclear factor kappa B ligand, which initiate an inflammatory response [9]. In this case, pulpal pressure increases, resulting in an increased outflow of fluid. This mechanism amplifies the responsiveness of the pulp nerves, making them more sensitive than they normally are.

To manage TS at home, patients are recommended to use specially formulated toothpastes, gels, and mouthwashes designed to effectively alleviate discomfort [1]. Such products may contain potassium salts [10], sodium fluoride [11], stannous fluoride [12], arginine [13], nano-hydroxyapatite [14], bioactive glass [15], casein phosphopeptide-amorphous calcium phosphate [16], or strontium salts [17]. These active agents work by either blocking dentin tubules or inhibiting nerve impulse transmission [18].

Fluoride-based agents are commonly used for this purpose, acting by promoting remineralization of the tooth hard tissues and by occluding dentinal tubules with calcium fluoride (CaF_2) crystals [11]. Moreover, potassium nitrate-containing agents are often used after tooth bleaching treatments. Potassium nitrate diffuses along dentinal tubules to depolarize nerve endings, reducing nerve excitability [19]. Recently, strontium-based agents have been suggested as a means to alleviate symptoms of TS. Strontium acetate works mainly by occluding dentinal tubules, thereby reducing the transmission of stimuli to the tooth pulp. In particular, strontium ions (Sr^{2+}) precipitate as strontium carbonate or strontium phosphate within open dentinal tubules, creating a physical barrier that blocks fluid movement inside the tubules [20].

Additionally, various techniques have been proposed for managing TS in dental practice, with studies producing divergent results. Dentist-applied treatments that inhibit nerve impulse transmission include gels containing potassium salt [21] and low-level laser therapy [6]. Meanwhile, in-office approaches aimed at occluding dentin tubules involve the application of fluoride-containing varnishes or gels [22], silver diamine fluoride [23,24], oxalate salts [25], air-abrasion with bioactive glasses [26], adhesive agents [27], and high-intensity laser irradiation [28].

This laboratory investigation aimed to assess the efficacy of three contemporary commercially available desensitizing agents in occluding dentin tubules to reduce TS following a bleaching procedure. While various desensitizing agents have been previously studied, there is limited evidence on the performance of recently introduced commercial formulations. Two of the tested products were recently introduced to the market and contained a combination of potassium nitrate (KNO_3)

https://doi.org/10.5395/rde.2026.51.e8

and sodium fluoride (NaF), as well as strontium acetate ($C_4H_6O_4Sr$) and sodium monofluorophosphate (MFP). An older product served as a positive control. Scanning electron microscopy (SEM) and energy-dispersive X-ray spectroscopy (EDS) were used to evaluate the extent of dentin tubule occlusion and analyze the composition of the resulting precipitates. Two null hypotheses were proposed:

H_{01}: The tested desensitizing treatments would not result in the same degree of dentinal tubule occlusion as observed in the untreated control group.

H_{02}: The tested treatments would not exhibit equivalent effectiveness in occluding dentin tubules.

METHODS

Samples preparation

This study was approved by the Ethics and Research Committee of Aristotle University of Thessaloniki (No. 224/21-03-2024) and conducted in accordance with the ethical principles outlined in the 1964 Declaration of Helsinki and its subsequent revisions, as well as the regulations of Aristotle University of Thessaloniki. Informed consent was obtained from all patients for the use of their extracted teeth in research.

A total of twenty healthy human third molars, extracted for periodontal reasons at the Clinic of Oral Surgery, Aristotle University of Thessaloniki, were collected and preserved in a 0.5% chloramine T solution at 6°C for a maximum of 2 months.

To approach the dentin surface, the enamel was carefully sectioned at the midpoint of the crown's occlusal-cervical dimension (approximately 2.5 mm below the occlusal surface) utilizing a low-speed precision cutting device (Isomet 11-1180, Buehler, Lake Bluff, IL, USA) under continuous water rinsing. Additionally, 1 mm-thick sections were also obtained from each tooth to examine the penetration depth of dentin tubule occlusion. The sectioned surfaces were then polished using a grinding device (Jean Wirtz TG 250, Jean Wirtz GmbH, Düsseldorf, Germany) operating at 200 rpm under constant water flow (50 mL/min). Sequential polishing was performed using silicon carbide abrasive papers (Apex S system, Buehler) in grits of 600, 800, 1,000, and 1,200, each applied for 20 seconds.

Next, the dentin surfaces were conditioned with 15% ethylenediaminetetraacetic acid (EDTA; Endo-Prep Cream, CERKAMED, Stalowa Wola, Poland) for 4 minutes to remove the smear layer from the dentinal tubule openings. This was followed by thorough rinsing with distilled water and subsequent air-drying. To ensure complete removal of any residual smear layer, the samples were then immersed in an ultrasonic bath (Euronda Spa, Montecchio Precalcino, Vicenza, Italy) for 5 minutes. After treatment, all specimens were stored in artificial saliva at 37°C. The artificial saliva was composed of 0.103 g/L $CaCl_2$, 0.019 g/L $MgCl_2 \bullet 6H_2O$, 0.544 g/L KH_2PO_4, 2.24 g/L KCl, and buffer (TCP-KOH) was added to adjust the pH to 7 [29].

Bleaching procedure

The cut surfaces of the tooth specimens were subjected to a whitening procedure using a 16% carbamide peroxide bleaching agent (Perfect Bleach, VOCO GmbH, Cuxhaven, Germany). The gel was applied according to the manufacturer's instructions, forming a consistent 1 mm layer evenly distributed over the entire surface of each specimen. The bleaching agent was applied to the dentin surfaces for 2 hours, simulating the first day of a 7–14 day at-home bleaching protocol. The gel remained in place for 2 hours before the samples were carefully rinsed with distilled water and gently brushed with a toothbrush to remove any residual gel. Eventually, all samples were placed in artificial saliva and maintained at 37°C.

Experimental groups

After the bleaching process, the tooth specimens were randomly assigned to four groups (n = 5) and subjected to different desensitizing protocols as follows:

Group 1 (negative control): No desensitizing treatment was applied.

Group 2: UltraEZ (Ultradent Products Inc., South Jordan, UT, USA) desensitizing gel, which contains 3% KNO_3 and 0.25% NaF, was applied evenly and left on the dentin for 60 minutes. The samples were then rinsed with distilled water, brushed with a toothbrush, and stored in artificial saliva at 37°C. This product served as the positive control in the study, as it has been extensively investigated and is the older one.

Group 3: the specimens were smeared with Perfect Protect (VOCO GmbH) desensitizing gel, which contains 3% KNO_3 and 0.11% NaF, and left for 60 minutes on the dentin. Next, the specimens were rinsed with distilled water, brushed with a toothbrush, and stored in artificial saliva at 37°C.

Group 4: TheraSol Whitening & Sensitive (ABC Kinitron IKE, Athens, Greece) desensitizing gel, containing 8% strontium acetate, was applied evenly and left on the dentin for 60 minutes. The specimens were then rinsed with distilled water, brushed with a toothbrush, and stored in artificial saliva at 37°C. The application of the tested materials was performed according to the manufacturer's instructions. The technical information of the commercial products used in the current study is shown in Table 1.

Scanning electron microscopy observations and energy-dispersive X-ray spectroscopy analysis

To evaluate the impact of the tested treatments on dentinal tubule occlusion, SEM (JSM-840, JEOL Ltd., Tokyo, Japan) was employed. Observations were focused on the central region of the sectioned dentin surface, specifically within a defined square area measuring 4 mm by 4 mm (Figure 1). Before observations, all specimens were dried in a desiccator. The specimens were subsequently affixed to aluminum stubs and coated with a thin carbon layer approximately 200 Å thick using a low-vacuum evaporator. They were then examined under a SEM at an accelerating voltage of 20 kV.

A total of ten SEM images were captured at ×500 magnification from various regions of the dentin surface to assess alterations in surface morphology. Additionally,

Table 1. The active agents of the tested commercial products of the study, according to the manufacturers

Product	Manufacturer	Form	Application	Active agents
UltraEZ	Ultradent Products Inc., South Jordan, UT, USA	Gel	Once for 60 min after bleaching	3% KNO_3 (11,600 ppmK^+) 0.11% NaF (1,130 ppmF^-)
Perfect Protect	VOCO GmbH, Cuxhaven, Germany	Gel	Once for 60 min after bleaching	3% KNO_3 (11,600 ppmK^+) 0.11% NaF (1,130 ppmF^-)
TheraSol Whitening & Sensitive	ABC Kinitron IKE, Athens, Greece	Paste	Once for 60 min after bleaching	8% strontium acetate ($C_4H_6O_4Sr$) 0.76% MFP (1,000 ppmF^-)

KNO_3, potassium nitrate; MFP, sodium monofluorophosphate; NaF, sodium fluoride.

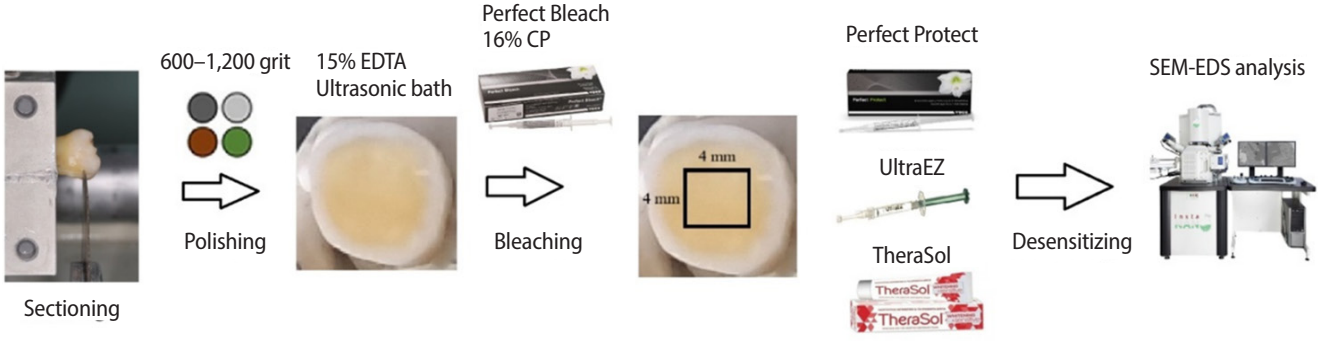

Figure 1. The workflow of the experimental part of the study. EDTA, ethylenediaminetetraacetic acid; CP, carbamide peroxide; SEM, scanning electron microscopy; EDS, energy-dispersive X-ray spectroscopy.

https://doi.org/10.5395/rde.2026.51.e8

ten more images were acquired at ×1,000 magnification to determine the percentage of dentinal tubules that were occluded, and at ×3,000 magnification to measure the degree of tubule occlusion and the posttreatment tubule diameters. For this purpose, a scale (0–2) was adopted, where "0" indicated no reduction of the diameter of the tubules (0%), "1" indicated a 50% reduction, and "2" a 100% reduction. Two experienced evaluators, blinded to the treatment groups, independently analyzed the images to assess the extent of tubule occlusion, and the average of their evaluations was recorded. Prior to SEM observations, the two examiners participated in a calibration session using a set of representative SEM images to standardize the assessment criteria for dentin tubule occlusion. Inter-examiner reliability was assessed using Cohen's kappa coefficient, which demonstrated good agreement ($\kappa = 0.82$). Additionally, EDS was employed to identify the composition of the particles responsible for occluding the dentinal tubules. The methodology of evaluating the dentin tubule occlusion was based mainly on Peyro Mousavi *et al.* [30] and Doğan *et al.* [31].

Statistical analysis

Statistical analysis was conducted using IBM SPSS ver. 25.0 (IBM Corp, Armonk, NY, USA). The sample size was determined to ensure 80% statistical power at a 0.05 significance level, with the expected effect size estimated from preliminary pilot study data, resulting in a required sample size of approximately five specimens per group. The Shapiro-Wilk test was used to assess data normality, while the Levene test evaluated homogeneity of variances. To compare the diameter of open dentinal tubules (in μm) and the number of open tubules per 0.01 mm^2, a one-way analysis of variance was performed. Tukey's *post hoc* test was then used to identify statistically significant differences among the groups at the 0.05 level. Since tubule occlusion was evaluated using a categorical scoring system, nonparametric tests were applied. The Kruskal-Wallis test was used for group comparisons, followed by the Mann-Whitney *U* test for pairwise analysis. A *p*-value below 0.05 was considered statistically significant.

RESULTS

Table 2 displays the mean values and standard deviations for the diameter of open dentinal tubules (μm), the degree of tubule occlusion (rated on a 0–2 scale), and the number of open tubules per 0.01 mm^2 of dentin surface across the experimental groups.

All desensitizing treatments significantly enhanced dentin tubule occlusion compared to the negative control ($p < 0.05$). The most effective treatment was the use of Perfect Protect gel, which achieved the highest tubule occlusion rate (79.2%), followed by the other two treatments with comparable effectiveness (56.3% UltraEZ and 58.6% TheraSol). The degree of tubule occlusion correlated with the number of occluded tubules, as shown in Table 2. Additionally, all treatments resulted in a significant decrease in the average diameter of dentin tubules compared to the untreated specimens ($p < 0.05$). Figure 2 displays representative SEM images of the treated dentin surfaces after the bleaching procedure

Table 2. Diameter of open dentinal tubules, degree of tubule occlusion, and number of open tubules in the experimental groups after treatment

Group (active agent)	Diameter of open tubules (μm)	Level of tubule occlusion (scale 0–2)	Number of open tubules per 0.01 mm^2	Percentage of occluded tubules (%)
Group 1 (control)	3.03 ± 0.53^{A}	0.00 ± 0.00^{A}	295.6 ± 45.4^{A}	3.5
Group 2 (UltraEZ)	1.73 ± 1.09^{B}	0.80 ± 0.43^{C}	133.8 ± 122.2^{C}	56.3
Group 3 (Perfect Protect)	1.14 ± 0.74^{B}	1.40 ± 0.54^{B}	63.4 ± 72.0^{B}	79.2
Group 4 (TheraSol Whitening & Sensitive)	1.49 ± 0.90^{B}	1.20 ± 0.44^{B}	126.6 ± 85.1^{C}	58.6

Values are presented as mean ± standard deviation.
The percentage of occluded tubules (%) was calculated relative to the total number of tubules visible at ×1,000 magnification.
Same uppercase superscripts in columns indicate no significant differences among the treatments ($p > 0.05$).
UltraEZ : Ultradent Products Inc., South Jordan, UT, USA; Perfect Protect: VOCO GmbH, Cuxhaven, Germany; TheraSol Whitening & Sensitive: ABC Kinitron IKE, Athens, Greece.

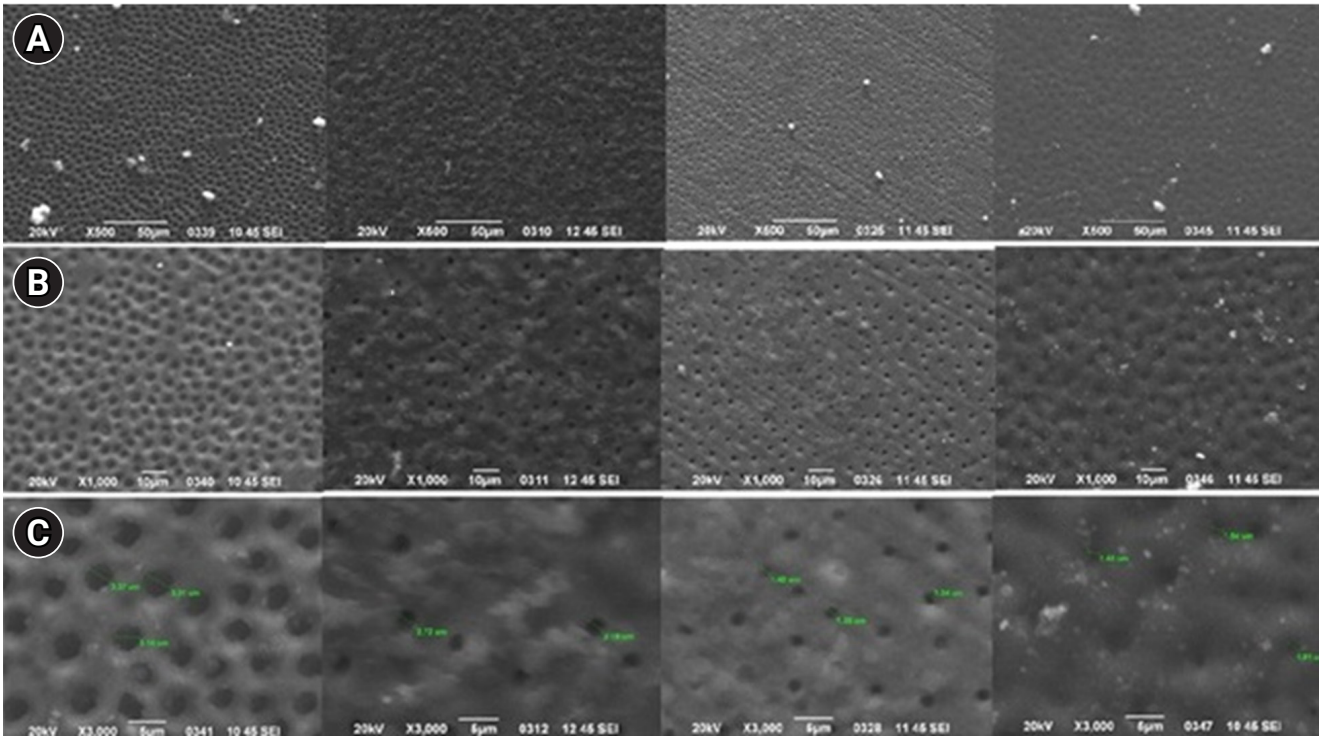

Figure 2. Representative scanning electron microscopy photomicrographs showing the dentin surface after the treatments of each experimental group at three magnifications: ×500 (A), ×1,000 (B), and ×3,000 (C). 1: control, 2: UltraEZ (Ultradent Products Inc., South Jordan, UT, USA), 3: Perfect Protect (VOCO GmbH, Cuxhaven, Germany), and 4: TheraSol Whitening & Sensitive (ABC Kinitron IKE, Athens, Greece).

for each experimental group at magnifications of ×500, ×1,000, and ×3,000, respectively.

EDS analysis identified the elemental content of the particles or precipitates responsible for tubule occlusion. In groups 2 and 3, traces of potassium and fluorine were detected, originating from the gels containing KNO_3 and NaF. In group 4, traces of strontium and fluorine were detected, originating from the paste containing strontium acetate and MFP (Figure 3). Elemental composition for each group is shown in Table 3.

DISCUSSION

According to the findings of this study, the first null hypothesis (H_{01})—which proposed that the treatments tested would not produce the same level of dentinal tubule occlusion as the untreated control group—was accepted. This means that the tested treatments were effective in occluding dentinal tubules. Moreover, the second null hypothesis (H_{02}), which proposed that the tested treatments would differ in their effectiveness at occluding dentinal tubules, was also supported. The discrepancies in effectiveness were probably attributed to different mechanisms of dentin tubule occlusion, compositions, and concentrations of the active agents, depending on the treatment applied, as reported in various previous studies [19,20,30,32,33].

The first two desensitizing gels contained KNO_3 and NaF as active agents. The effectiveness of this combination against TS has been previously documented [34]. Although the contents of these compounds were similar (3% KNO_3 and 0.11% NaF), the effectiveness on occluding dentin tubules was significantly higher for the latter product. The advantageous results for Perfect Protect (a percentage of occluded tubules of 79.2% compared to 56.3% for UltraEZ) may, however, be related to the special insertion processes used, leading to an improved microrheological profile. The optimized shear viscosity results in improved wetting of the tooth surface. Furthermore, Fick's second law indicates that increased

https://doi.org/10.5395/rde.2026.51.e8

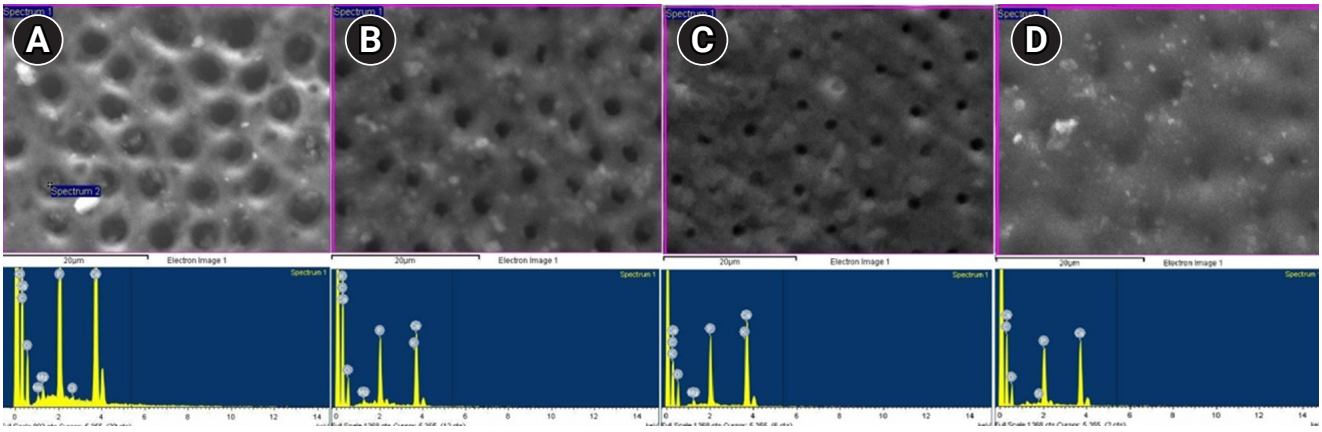

Figure 3. Representative scanning electron microscopy photomicrographs showing the dentin surface after the treatments of each experimental group at three magnifications: ×500 (A), ×1,000 (B), and ×3,000 (C).
1: control, 2: UltraEZ (Ultradent Products Inc., South Jordan, UT, USA), 3: Perfect Protect (VOCO GmbH, Cuxhaven, Germany), and 4: TheraSol Whitening & Sensitive (ABC Kinitron IKE, Athens, Greece).

Table 3. Elemental content (wt%) of the enamel surface after the desensitizing treatments for each experimental group

Element	Group 1 (control)	Group 2 (UltraEZ)	Group 3 (Perfect Protect)	Group 4 (TheraSol Whitening & Sensitive)
Ca	34.74 ± 3.59[a]	33.67 ± 3.77[a]	35.49 ± 3.91[a]	28.81 ± 3.71[a]
P	21.08 ± 2.78[a]	21.77 ± 2.42[a]	20.47 ± 2.37[a]	21.87 ± 2.58[a]
Na	0.71 ± 0.10[a]	0.00 ± 0.00[a]	0.00 ± 0.00[a]	0.00 ± 0.00[a]
Cl	0.41 ± 0.08[a]	0.00 ± 0.00[a]	0.00 ± 0.00[a]	0.00 ± 0.00[a]
Mg	1.04 ± 0.11[a]	1.59 ± 0.25[a]	1.80 ± 0.31[a]	0.00 ± 0.00[a]
Si	0.00 ± 0.00[a]	0.00 ± 0.00[b]	0.00 ± 0.00[b]	2.78 ± 0.42[b]
K	0.00 ± 0.00[a]	0.31 ± 0.09[b]	0.37 ± 0.09[c]	0.00 ± 0.19[b]
Sr	0.00 ± 0.00[a]	0.00 ± 0.00[b]	0.00 ± 0.00[a]	3.07 ± 0.53[a]
F	0.00 ± 0.00[a]	0.88 ± 0.22[a]	1.16 ± 0.31[a]	0.65 ± 0.19[a]
O	42.02 ± 4.83[a]	41.78 ± 3.40[a]	40.70 ± 3.52[a]	42.82 ± 4.10[a]

Values are presented as mean ± standard deviation.
Different lowercase superscripts in the rows denote statistically significant differences ($p < 0.05$).
UltraEZ : Ultradent Products Inc., South Jordan, UT, USA; Perfect Protect: VOCO GmbH, Cuxhaven, Germany; TheraSol Whitening & Sensitive: ABC Kinitron IKE, Athens, Greece.

gel volume leads to enhanced diffusion. Consequently, using a thinner layer of desensitizing gel limits the penetration of active ingredients into the dentin surface, potentially reducing the effectiveness of dentinal tubule occlusion [35].

Potassium salt-based products function by raising the potassium ions (K^+) concentration in nerve endings, which diminishes the nerve's capacity to send sensory signals and modifies its action potential [36]. When applied to exposed dentin, these potassium salts increase K^+ levels within the dentinal tubules and adjacent tissues, disrupting the usual processes of nerve cell depolarization and repolarization [37]. Nerve cells generate and transmit electrical signals, or action potentials, through ion movement, particularly Na^+ and K^+. Upon stimulation, Na^+ ions enter the cell, causing depolarization and triggering nerve impulse transmission. Potassium ions then exit the cell to restore its resting state. However, in high concentrations—such as those found in potassium-based desensitizing agents—the movement of K+ is disrupted. The excess potassium outside nerve cells interferes with efficient repolarization, reducing the nerve's responsiveness to stimuli. As a result, the transmission of pain signals triggered by temperature fluctuations or mechanical stimuli is reduced. This process helps alleviate TS by inhibiting nerve impulse

transmission associated with pain [1,13]. In the current study, the effectiveness of this mechanism was not investigated, as the alleviation of TS symptoms can only be evaluated clinically. Nevertheless, EDS analysis revealed traces of potassium on the dentin surface, confirming the existence of the products that included KNO_3.

The active ingredient responsible for dentin tubule occlusion in the two previously mentioned products was NaF. Fluoride aids in depositing minerals, such as calcium and phosphate, onto the dentin surface, thereby enhancing its strength and hardness, while promoting dentin remineralization [38]. Fluoride ions, upon contact with the tooth surface, aid in sealing exposed dentinal tubules [39]. The role of fluorine compounds in reducing dentin permeability has been widely studied [40,41]. These compounds contribute to an increase in the presence of CaF_2 crystals within the tubules, leading to lower dentin permeability [22]. Since these crystals are nearly insoluble in saliva, they provide a temporary protective effect. Sodium fluoride-based dental products are commonly used to reduce calcium salt content on the surface of dentin; however, these salts can be removed by saliva and tooth brushing. If fluorapatite forms posttreatment, it provides greater stability against the effects of saliva, mechanical abrasion, and dietary influences [42]. However, SEM observations in the current study did not detect such deposits on the dentin, although traces of fluorine were found by elemental analysis.

The third desensitizing product (TheraSol Whitening & Sensitive) investigated in the present study contained 8% strontium acetate and 0.76% MFP. The effectiveness of strontium acetate for TS has been affirmed in previous studies [43–45]. Strontium acetate may contribute to the occlusion of dentinal tubules by substituting calcium ions within the hydroxyapatite crystal lattice with strontium ions. In addition to this mineral interaction, it also plays a role in reducing TS by interfering with nerve depolarization processes [46]. Strontium behaves in a manner similar to calcium within the human body [47] and is capable of replacing it during the process of apatite biomineralization [48]. In the oral environment, Sr^{2+} ions—like Ca^{2+} and other divalent cations with a similar charge-to-size ratio—can readily incorporate into the hydroxyapatite matrix [20]. Studies have shown that strontium encourages dentin formation by enhancing the proliferation, differentiation, and mineralization of human dental pulp stem cells, potentially supporting the development of tertiary dentin [49].

A key characteristic of strontium salts is their ability to form complex strontium phosphate compounds, thereby chemically influencing dentin [47]. Past studies have confirmed the formation of a Ca-Sr apatite, specifically $Ca_6Sr_4(PO_4)_6(OH)_2$, which results from the substitution of intracrystalline calcium in apatite with strontium [50]. Additionally, strontium salts exhibit a strong binding affinity to dentin due to its increased permeability, which facilitates their absorption into organic connective tissues and the odontoblast process [51]. This interaction results in the precipitation of proteins and the formation of a protective film, which may contribute to reducing the transmission of external stimuli by effectively sealing the dentinal tubules [33]. In the current investigation, EDS analysis revealed traces of Sr in specimens treated with strontium acetate, indicating that Sr can be retained or integrated on the dentin surface, thereby contributing to the occlusion of dentin tubules.

TheraSol also contains MFP as an active agent. Sodium monofluorophosphate (Na_2PO_3F) alleviates TS primarily by promoting dentin tubule occlusion and dentin remineralization, reducing the transmission of pain-inducing stimuli [52]. Once applied, MFP breaks down, releasing fluoride ions (F^-). These ions integrate into the hydroxyapatite structure of the enamel and dentin, forming fluoroapatite, which is more resistant to acid attacks and wear. Additionally, fluoride reacts with calcium and phosphate in saliva and dentin, forming CaF_2 precipitates. These deposits help block opened dentinal tubules, reducing the ability of external stimuli to reach the underlying nerve endings [53]. This property of MFP was observed in SEM images, where occlusion of dentin tubules was detected. Meanwhile, EDS analysis revealed a fluorine content on the dentin surface of the TheraSol-treated specimens.

A primary limitation of this laboratory study was its inability to accurately mimic the intricate conditions of the oral environment. Factors such as saliva composition, enzymatic activity, bacterial presence, and mechanical forces from mastication and brushing, which

https://doi.org/10.5395/rde.2026.51.e8

can influence the long-term efficacy of desensitizing agents, are not accurately simulated in laboratory conditions. Additionally, the alleviation of TS symptoms could not be assessed *in vitro*. Additionally, the use of extracted teeth, which lack the dynamic interactions with pulp tissue and blood circulation, may affect the penetration and retention of the tested agents. Another limitation was that the application methods and exposure times used *in vitro* may not precisely reflect real-life clinical use, potentially leading to overestimation or underestimation of the agents' effectiveness. Furthermore, the durability of tubule occlusion over time, particularly under conditions of acidic or abrasive challenges, may not be adequately assessed in short-term laboratory studies, necessitating further *in vivo* research to validate the findings. Finally, the use of human teeth from different patients, which are inherently non-standardized, may introduce variability into the results.

CONCLUSIONS

Considering the limitations of this laboratory study, it can be deduced that the tested desensitizing agents were capable of occluding the dentin tubules to a great extent. Among the desensitizing agents, differences in their effectiveness were observed due to discrepancies in their formula composition. Particularly, Perfect Protect presented the highest degree of occlusion of dentin tubules, followed by TheraSol and UltraEZ, which did not differ from each other. From a clinical perspective, these findings suggest that Perfect Protect may offer greater potential for reducing post-bleaching sensitivity associated with tooth bleaching. However, clinicians should interpret these results cautiously, as laboratory conditions cannot fully replicate the complexity of the oral environment. Further *in vivo* studies are necessary to affirm the effectiveness of the treatments.

CONFLICT OF INTEREST

Dimitrios Dionysopoulos is an Associate Editor of *Restorative Dentistry and Endodontics* and was not involved in the review process of this article. The authors declare no other conflicts of interest.

FUNDING/SUPPORT

This research was funded by VOCO GmbH and the Research Committee of Aristotle University of Thessaloniki, Grand Number: 10468.

ACKNOWLEDGMENTS

This research was funded by VOCO GmbH and the Research Committee of Aristotle University of Thessaloniki, Project Code 10468. The authors would like to thank Dr. Stavros Oikonomidis for his technical support in SEM observations and EDS analysis of the specimens, which were conducted in the Solid State Physics Division, Department of Physics, Aristotle University of Thessaloniki, Greece. Finally, the authors acknowledge with thanks VOCO GmbH and ABC Kinitron IKE for providing the products for the purposes of the current study.

AUTHOR CONTRIBUTIONS

Conceptualization: Dionysopoulos D, Tolidis K. Methodology: Dionysopoulos D, Mourouzis P. Validation: Papageorgiou S. Formal analysis, Visualization: Mourouzis P. Investigation, Supervision, Project administration, Funding acquisition: Dionysopoulos D. Data curation: Tolidis K. Writing – original draft: Dionysopoulos D, Mourouzis P. Writing – review & editing: Tolidis K, Papageorgiou S. All authors read and approved the final manuscript.

DATA SHARING STATEMENT

The datasets are not publicly available but are available from the corresponding author upon reasonable request.

REFERENCES

1. Dionysopoulos D, Gerasimidou O, Beltes C. Dentin hypersensitivity: etiology, diagnosis and contemporary therapeutic approaches—a review in literature. Appl Sci 2023;13:11632.
2. Haywood VB. Treating sensitivity during tooth whitening. Compend Contin Educ Dent 2005;26(9 Suppl 3):11-20.
3. Närhi M, Jyväsjärvi E, Virtanen A, Huopaniemi T, Ngassapa D, Hirvonen T. Role of intradental A- and C-type nerve fibres in dental pain mechanisms. Proc Finn Dent Soc 1992;88 Suppl 1:507-516.
4. Matthews B, Andrew D, Wanachantararak S. Biology of the dental pulp with special reference to its vasculature and innervation. In: Embery G, Edgar WM, Orchardson R, Addy M, editors. Tooth wear and sensitivity. London, UK: Taylor and Francis; 2000. p. 39-51.
5. West NX, Lussi A, Seong J, Hellwig E. Dentin hypersensitivity: pain mechanisms and aetiology of exposed cervical dentin. Clin Oral Investig 2013;17 Suppl 1:S9-S19.
6. Giannakopoulou P, Neophytou C, Karakostas P, Papadimitriou K, Dionysopoulos D, Tolidis K, *et al.* Low-level laser ther-

apy for tooth sensitivity after tooth bleaching: a systematic review. Applied Sciences 2024;14:8068.
7. Joiner A. The bleaching of teeth: a review of the literature. J Dent 2006;34:412-419.
8. Patri G, Agnihotri Y, Rao SR, Lakshmi N, Das S. An in vitro spectrophotometric analysis of the penetration of bleaching agent into the pulp chamber of intact and restored teeth. J Clin Diagn Res 2013;7:3057-3059.
9. Min KS, Lee HJ, Kim SH, Lee SK, Kim HR, Pae HO, *et al*. Hydrogen peroxide induces heme oxygenase-1 and dentin sialophosphoprotein mRNA in human pulp cells. J Endod 2008;34:983-989.
10. Orchardson R, Gillam DG. The efficacy of potassium salts as agents for treating dentin hypersensitivity. J Orofac Pain 2000;14:9-19.
11. de Oliveira MB, Valadas LA, Squassi A, Mendonça JS. Evaluation of total, soluble and ionic fluoride concentration in whitening and desensitizing toothpastes. Int J Dent Hyg 2025;23:218-227.
12. Hines D, Xu S, Stranick M, Lavender S, Pilch S, Zhang YP, *et al*. Effect of a stannous fluoride toothpaste on dentinal hypersensitivity: in vitro and clinical evaluation. J Am Dent Assoc 2019;150(4S):S47-S59.
13. França IL, Sallum EA, Do Vale HF, Casati MZ, Sallum AW, Stewart B. Efficacy of a combined in-office/home-use desensitizing system containing 8% arginine and calcium carbonate in reducing dentin hypersensitivity: an 8-week randomized clinical study. Am J Dent 2015;28:45-50.
14. Vano M, Derchi G, Barone A, Covani U. Effectiveness of nano-hydroxyapatite toothpaste in reducing dentin hypersensitivity: a double-blind randomized controlled trial. Quintessence Int 2014;45:703-711.
15. Ergucu Z, Yoruk I, Erdoğan A, Boyacıoğlu H, Hill R, Baysan A. The use of toothpastes containing different formulations of fluoride and bioglass on bleached enamel. Materials (Basel) 2023;16:1368.
16. Papazisi N, Dionysopoulos D, Naka O, Strakas D, Davidopoulou S, Tolidis K. Efficiency of various tubular occlusion agents in human dentin after in-office tooth bleaching. J Funct Biomater 2023;14:430.
17. Saeki K, Marshall GW, Gansky SA, Parkinson CR, Marshall SJ. Strontium effects on root dentin tubule occlusion and nanomechanical properties. Dent Mater 2016;32:240-251.
18. Cummins D. Recent advances in dentin hypersensitivity: clinically proven treatments for instant and lasting sensitivity relief. Am J Dent 2010;23 Spec No A:3A-13A.
19. Sugawara S, Iwata K, Takamizawa T, Miyazaki M, Kobayashi M. Potassium nitrate suppresses hyperactivities of Vc neurons of the model with dentin hypersensitivity. J Oral Biosci 2024;66:41-48.
20. Barros AP, de Melo Alencar C, de Melo Pingarilho Carneiro A, da Silva Pompeu D, Barbosa GM, Araújo JL, *et al*. Combination of two desensitizing protocols to control dentin hypersensitivity in non-carious lesions: a randomized, double-blind clinical trial. Clin Oral Investig 2022;26:1299-1307.
21. Renton T, Yiangou Y, Plumpton C, Tate S, Bountra C, Anand P. Sodium channel Nav1.8 immunoreactivity in painful human dental pulp. BMC Oral Health 2005;5:5.
22. Chen CL, Parolia A, Pau A, Celerino de Moraes Porto IC. Comparative evaluation of the effectiveness of desensitizing agents in dentine tubule occlusion using scanning electron microscopy. Aust Dent J 2015;60:65-72.
23. Chan AK, Tsang YC, Jiang CM, Leung KC, Lo EC, Chu CH. Treating hypersensitivity in older adults with silver diamine fluoride: a randomised clinical trial. J Dent 2023;136:104616.
24. El-Damanhoury HM, Rahman B, Sheela S, Ngo HC. Dentinal tubule occlusion and dentin permeability efficacy of silver diamine fluoride solutions. Int J Dent Hyg 2025;23:286-293.
25. Vieira AH, Passos VF, de Assis JS, Mendonça JS, Santiago SL. Clinical evaluation of a 3% potassium oxalate gel and a GaAlAs laser for the treatment of dentinal hypersensitivity. Photomed Laser Surg 2009;27:807-812.
26. Memis I, Dionysopoulos D, Papadopoulos C, Mourouzis P, Davidopoulou S, Tolidis K. Effect of air-abrasion pretreatment with three desensitizing agents on efficacy of in-office tooth bleaching. J Esthet Restor Dent 2024;36:1426-1436.
27. Dondi dall'Orologio G, Lone A, Finger WJ. Clinical evaluation of the role of glutardialdehyde in a one-bottle adhesive. Am J Dent 2002;15:330-334.
28. Meng Y, Huang F, Wang S, Huang X, Lu Y, Li Y, *et al*. Evaluation of dentinal tubule occlusion and pulp tissue response after using 980-nm diode laser for dentin hypersensitivity treatment. Clin Oral Investig 2023;27:4843-4854.
29. Dionysopoulos D, Papageorgiou S, Papadopoulos C, Davidopoulou S, Konstantinidis A, Tolidis K. Effect of whitening toothpastes with different active agents on the abrasive wear of dentin following tooth brushing simulation. J Funct Biomater 2023;14:268.
30. Peyro Mousavi SF, Ganjovi A, Eskandarizadeh A, Saidi AR, Isaei E. Evaluating the antibacterial effect of synthesized

https://doi.org/10.5395/rde.2026.51.e8

herbal toothpastes and their efficacy for dentine tubule occlusion: scanning electron microscopy and energy-dispersive X-ray spectroscopy analysis. Microsc Res Tech 2022;85:19-27.
31. Doğan Ç, Yıldırım HS, Gürsoy H, Kuru L. Occlusion of dentinal tubules on periodontally involved teeth by dentifrice containing stannous fluoride and sodium fluoride. J Oral Sci 2023;65:149-152.
32. Aranha AC, Pimenta LA, Marchi GM. Clinical evaluation of desensitizing treatments for cervical dentin hypersensitivity. Braz Oral Res 2009;23:333-339.
33. Majji P, Murthy KR. Clinical efficacy of four interventions in the reduction of dentinal hypersensitivity: a 2-month study. Indian J Dent Res 2016;27:477-482.
34. Wang Y, Gao J, Jiang T, Liang S, Zhou Y, Matis BA. Evaluation of the efficacy of potassium nitrate and sodium fluoride as desensitizing agents during tooth bleaching treatment—a systematic review and meta-analysis. J Dent 2015;43:913-923.
35. Kwon SR, Pallavi F, Shi Y, Oyoyo U, Mohraz A, Li Y. Effect of bleaching gel viscosity on tooth whitening efficacy and pulp chamber penetration: an in vitro study. Oper Dent 2018;43:326-334.
36. Lochaiwatana Y, Poolthong S, Hirata I, Okazaki M, Swasdison S, Vongsavan N. The synthesis and characterization of a novel potassium chloride-fluoridated hydroxyapatite varnish for treating dentin hypersensitivity. Dent Mater J 2015;34:31-40.
37. Bamise CT, Esan TA. Mechanisms and treatment approaches of dentine hypersensitivity: a literature review. Oral Health Prev Dent 2011;9:353-367.
38. Dionysopoulos D, Koliniotou-Koumpia E, Tolidis K, Gerasimou P. Effect of fluoride treatments on bleached enamel microhardness and surface morphology. Oral Health Prev Dent 2017;15:169-175.
39. Sowinski JA, Battista GW, Petrone ME, Chaknis P, Zhang YP, DeVizio W, *et al*. A new desensitizing dentifrice: an 8-week clinical investigation. Compend Contin Educ Dent Suppl 2000;(27):11-16.
40. Antoniazzi RP, Machado ME, Grellmann AP, Santos RC, Zanatta FB. Effectiveness of a desensitizing agent for topical and home use for dentin hypersensitivity: a randomized clinical trial. Am J Dent 2014;27:251-257.
41. Han L, Okiji T. Dentin tubule occluding ability of dentin desensitizers. Am J Dent 2015;28:90-94.
42. Markowitz K. A new treatment alternative for sensitive teeth: a desensitizing oral rinse. J Dent 2013;41 Suppl 1:S1-S11.
43. Layer T, Hughes N. Evidence for the efficacy of an 8% strontium acetate dentifrice for instant and lasting relief of dentin hypersensitivity. J Clin Dent 2010;21:56-58.
44. Mason S, Hughes N, Sufi F, Bannon L, Maggio B, North M, *et al*. A comparative clinical study investigating the efficacy of a dentifrice containing 8% strontium acetate and 1040 ppm fluoride in a silica base and a control dentifrice containing 1450 ppm fluoride in a silica base to provide immediate relief of dentin hypersensitivity. J Clin Dent 2010;21:42-48.
45. Zang P, Shaw D. A randomized clinical study to evaluate the efficacy of an 8% (w/w) strontium acetate dentifrice in providing relief from dentinal hypersensitivity. J Clin Dent 2016;27:91-96.
46. Shiau HJ. Dentin hypersensitivity. J Evid Based Dent Pract 2012;12(3 Suppl):220-228.
47. Pompeu DD, de Paula BL, Barros AP, Nunes SC, Carneiro AM, Araújo JL, *et al*. Combination of strontium chloride and photobiomodulation in the control of tooth sensitivity post-bleaching: a split-mouth randomized clinical trial. PLoS One 2021;16:e0250501.
48. Durgalakshmi D, Ajay Rakkesh R, Kesavan M, Ganapathy S, Ajithkumar TG, Karthikeyan S, *et al*. Highly reactive crystalline-phase-embedded strontium-bioactive nanorods for multimodal bioactive applications. Biomater Sci 2018;6:1764-1776.
49. Huang M, Hill RG, Rawlinson SC. Strontium (Sr) elicits odontogenic differentiation of human dental pulp stem cells (hDPSCs): a therapeutic role for Sr in dentine repair? Acta Biomater 2016;38:201-211.
50. Dedhiya MG, Young F, Higuchi WI. Mechanism for the retardation of the acid dissolution rate of hydroxapatite by strontium. J Dent Res 1973;52:1097-1109.
51. Ross MR. Hypersensitive teeth: effect of strontium chloride in a compatible dentifrice. J Periodontol 1961;32:49-53.
52. B Low S, Allen EP, Kontogiorgos ED. Reduction in dental hypersensitivity with nano-hydroxyapatite, potassium nitrate, sodium monoflurophosphate and antioxidants. Open Dent J 2015;(9):92-97.
53. Adil HM, Jouhar R, Ahmed MA, Basha S, Ahmed N, Abbasi MS, *et al*. Comparison of casein phosphopeptide with potassium nitrate and sodium monofluorophosphate desensitizing efficacy after in-office vital bleaching—a randomized trial. Applied Sciences 2021;11:9291.

RDE Restorative Dentistry & Endodontics

Research Article

eISSN 2234-7666
Restor Dent Endod. 2026 February;51(1):e9
https://doi.org/10.5395/rde.2026.51.e9

Determination of optimal horizontal beam angulations for canal separation in mandibular molars using cone-beam computed tomography: a retrospective image-based analysis

Benedikt Schneider[1], Tamina Tepe[2], Daniel Rapp[2], Wilhelm Frank[3], Maria Lessani[4], Constantin von See[5], Sebastian Fitzek[6], Jörg Philipp Tchorz[2,*]

For further information on the authors' affiliations, see **Additional information.**

ABSTRACT

Objectives: Two-dimensional intraoral radiographs often obscure canals due to superimposition, especially in mandibular molars with complex anatomy. This cone-beam computed tomography (CBCT) study identified the horizontal beam angles at which first and second molar canals overlap and derived clinically applicable angulations for enhanced canal separation.

Methods: Eighty-five CBCT datasets from 100 patients met the inclusion criteria, yielding 318 mandibular molars (160 first, 158 second). Using ImageJ, absolute horizontal overlap angles (α) were measured to determine the corresponding theoretical separation angles defined as $\delta^* = 90° - \alpha$. Separability was modeled across horizontal beam angulation increments from −45° to +45° in five steps, and Wilson's 95% confidence intervals were computed. Group comparisons used the Mann-Whitney *U* and independent *t*-tests ($p \leq 0.05$)

Results: Minimal mesial beam angulations for effective canal separability ($\delta^* = 90° - \alpha$) ranged from approximately 7° to 15° for mesial roots and approximately 10° to 13° for distal roots. No significant mesial differences were observed between first and second molars ($p > 0.30$). Distal roots of second molars exhibited significantly higher angulations ($p = 0.003$ coronal, $p < 0.001$ apical). Mesial canals achieved ≥95% separability at approximately 25° and ≥99% at approximately 35°; distal canals required approximately 30° and approximately 40°.

Conclusions: A mesial beam angulation of 30° to 35° provides probable canal differentiation in mandibular molars, separating mesial canals in ≥99% and distal canals in ≥95% of cases. This range refines previous recommendations and supports the as low as reasonably achievable (ALARA) principle.

Keywords: Cone-beam computed tomography; Dental pulp cavity; Dental radiography; Endodontics; X-rays

Received: September 18, 2025 • **Revised:** November 23, 2025 • **Accepted:** December 15, 2025

Citation
Schneider B, Tepe T, Rapp D, Frank W, Lessani M, von See C, Fitzek S, Tchorz JP. Determination of optimal horizontal beam angulations for canal separation in mandibular molars using cone-beam computed tomography: a retrospective image-based analysis. Restor Dent Endod 2026;51(1):e9.

***Correspondence to**
Jörg Philipp Tchorz, Priv. Doz. Dr. med. Dent
Division for Endodontics, Center for Operative Dentistry and Periodontology, Department of Dentistry, Faculty of Medicine and Dentistry, Danube Private University, Steiner Landstraße 124, A-3500 Krems-Stein, Austria
Email: joerg.tchorz@dp-uni.ac.at

INTRODUCTION

The success of endodontic treatment is primarily dependent on the highest standard of chemo-mechanical preparation of the complex root canal system [1]. Untreated canals can harbor microorganisms and potentially perpetuate periapical inflammation, ultimately leading to treatment failure [2–4].

Mandibular molars exhibit highly variable and complex canal anatomy, frequently featuring multiple canals within the mesial and distal roots. Canal configurations may vary from separate canals that remain distinct to canals that merge and diverge along their course. Additionally, mandibular molars can exhibit uncommon anatomical variations, such as a third canal in the mesial root (the middle mesial canal). These complexities significantly complicate accurate endodontic diagnosis and treatment planning for both mandibular first and second molars [5,6]. Specifically, configurations involving mesiobuccal (MB), mesiolingual (ML), and possibly middle mesial canals in the mesial root, as well as distobuccal (DB) and distolingual (DL) canals in the distal root, represent considerable diagnostic challenges [2]. An important aspect influencing diagnostic accuracy is whether canals remain separate throughout the root or converge apically. Confluent canal systems may present radiographically as a single structure, whereas separate canals, particularly in buccolingual orientation, often overlap in two-dimensional (2D) projections. Thus, understanding the canal trajectory is essential to interpret radiographs accurately and avoid misdiagnosis or missed canals. The 2D intraoral radiographs remain an essential tool in the endodontic diagnosis and provision of the treatment, guiding the operator from pre-operative canal identification to intra-operative working-length verification and postoperative obturation assessment [3,7]. Despite their accessibility, low radiation dose, and cost-effectiveness, 2D images inherently suffer from geometric distortion and superimposition of anatomical structures [8–11]. Therefore, due to the limitations of orthoradial views, root canals frequently overlap, causing difficulty in distinguishing individual canals, leading to repeated exposures to obtain diagnostically acceptable results. It has been reported that retake rates among clinicians and students range from 11% to 20%, predominantly resulting from such anatomical superimpositions [12,13]. The principles of parallax aid the operator and disentangle superimposed structures. Thus, practitioners apply the SLOB (same lingual, opposite buccal) rule, which uses horizontal beam angulations to infer the spatial relationships of overlapping canals [14].

However, existing literature provides inconsistent recommendations regarding optimal mesial beam angulations, ranging from 20° to 30° [2,14–16]. Haghani *et al.* [2] specifically found a 20° mesial beam angulation to be significantly more effective than other offsets for separating all four canals in mandibular first molars. Puapichartdumrong *et al.* [15] introduced an angle-adjustable film holder to refine horizontal tube angulations but focused primarily on mechanical implementation rather than on tooth-specific angulations. Setzer and Lee [16] underscored the benefits of three-dimensional (3D) imaging for canal trajectory mapping but did not translate these trajectories into actionable 2D horizontal beam angulations.

Despite these valuable insights, to date, no comprehensive investigation has systematically defined the optimal eccentric angles for both first and second mandibular molars to visualize all roots and canals on a single periapical image.

To address this gap, the present study retrospectively analyses cone-beam computed tomography (CBCT) datasets of mandibular first and second molars to determine the horizontal beam angulations at which root canals in one single root overlap, both coronally and apically, to determine the minimal beam angulation at which differentiation between anatomical structures becomes radiographically discernible. By integrating 3D canal mapping with simulated 2D projections, we aim to establish an evidence-based approach for horizontal beam angulations to enhance diagnostic precision, minimize retakes, and ultimately reduce patient radiation exposure for endodontic procedures.

METHODS

A retrospective evaluation was conducted using CBCT datasets from 100 individuals, randomly selected from the university's imaging archives. To minimize selection

https://doi.org/10.5395/rde.2026.51.e9

bias, a random-number generator was used to select 100 datasets from a full list of pseudonymized case identifiers, which were then randomly selected for analysis. All scans were acquired with a Dentsply Sirona Orthophos SL 3D system (Dentsply Sirona, Bensheim, Germany), with unit tube voltage of 60–90 kVp and tube current of 3–16 mA. Featured fields of view were either 8 × 8 cm or 11 × 10 cm, captured in either standard or high-definition modes. These images were originally obtained for various clinical indications, including implant planning, impacted third-molar extractions, orthodontic assessments, or other diagnostic requirements, and not specifically for this investigation; therefore, no additional radiation exposure was incurred. To meet the inclusion criteria, scans had to be free from notable artifacts or recording errors and demonstrate good to excellent image quality. A cohort size of 100 CBCT volumes was chosen to align with prior research on radiographic beam angulations and canal visualization [15,17,18].

All datasets were de-identified in accordance with regional data-protection legislation to safeguard patient anonymity. Written informed consent was obtained from all participants. Ethical approval for this study protocol was granted by the Institutional Ethics Committee (DPU-EK/038).

Cone-beam computed tomography data preparation

Each CBCT's DICOM files were imported into SIDEXIS version 4.3 (Dentsply Sirona). Patient head orientation was standardized by correcting tilt and rotation: coronal, sagittal, and axial slices were realigned parallel to the transverse and horizontal reference planes by manipulating control points, following the protocol of Schneider *et al.* [19]. Next, multiplanar reconstructions were scrolled to locate axial views that displayed the entire canal anatomy of the target teeth. Coronal (c) and apical (a) reference images were acquired at standardized levels: immediately apical to the pulpal floor, and at the most apical axial level, maintaining distinguishable root contours. Coronal and apical axial slices were evaluated separately for mesial (MB–ML) and distal (DB–DL) canal pairs to maintain consistency across root levels.

Measurements

All measurements were performed by a single investigator using the open-source software ImageJ (version 1.54f, open-source; National Institutes of Health, Bethesda, MD, USA), utilizing the central axis as a standardized reference point (Figure 1). The angle at which the individual root canals located buccally would overlap with the lingual root canal was measured for each tooth, starting from the central axis of the jaw. In roots presenting a single oval-shaped canal, the angle was measured along the axis of this anatomical structure. The aim of the study was to investigate the possible superimposition in 2D intraoral radiographs, which are normally taken parallel to the jaw and not placed centrically; therefore, the angle between the jaw and the central axis was additionally measured, and the respective angles were calculated accordingly.

Statistical analysis

The continuous variables have been summarized using means and standard deviations, and the Kolmogorov–Smirnov test assessed the assumption of normality. While depending on the distribution, intergroup comparisons were made using either the independent-samples t-test or the Mann-Whitney U test, with statistical significance defined as $p \leq 0.05$. To evaluate canal overlap patterns across mandibular first and second molars, descriptive statistics of the CBCT-measured overlap angles (α) were calculated separately for mesial (MB–ML) and distal (DB–DL) canal pairs at coronal and apical levels. Subsequently, we defined the theoretical beam angulation for separation as $\delta^* = 90° - \alpha$, where α is the CBCT-measured angle at which the mesial or distal canal pair projects as a single 2D structure (overlap). For any candidate beam angulation δ, theoretical separability occurs when $\delta \geq \delta^*$. A canal pair is considered radiographically separable once the applied beam angle exceeds the tooth-specific minimal separation threshold. Accordingly, δ represents the minimal beam angulation required to obtain a separate depiction on a 2D image. We computed theoretical separability across predefined beam angulation cutoffs from −45° to +45° in 5° increments, with Wilson 95% confidence intervals, separately for coronal and apical levels and for mesial (MB–ML) and distal (DB–DL) canal pairs. Positive δ

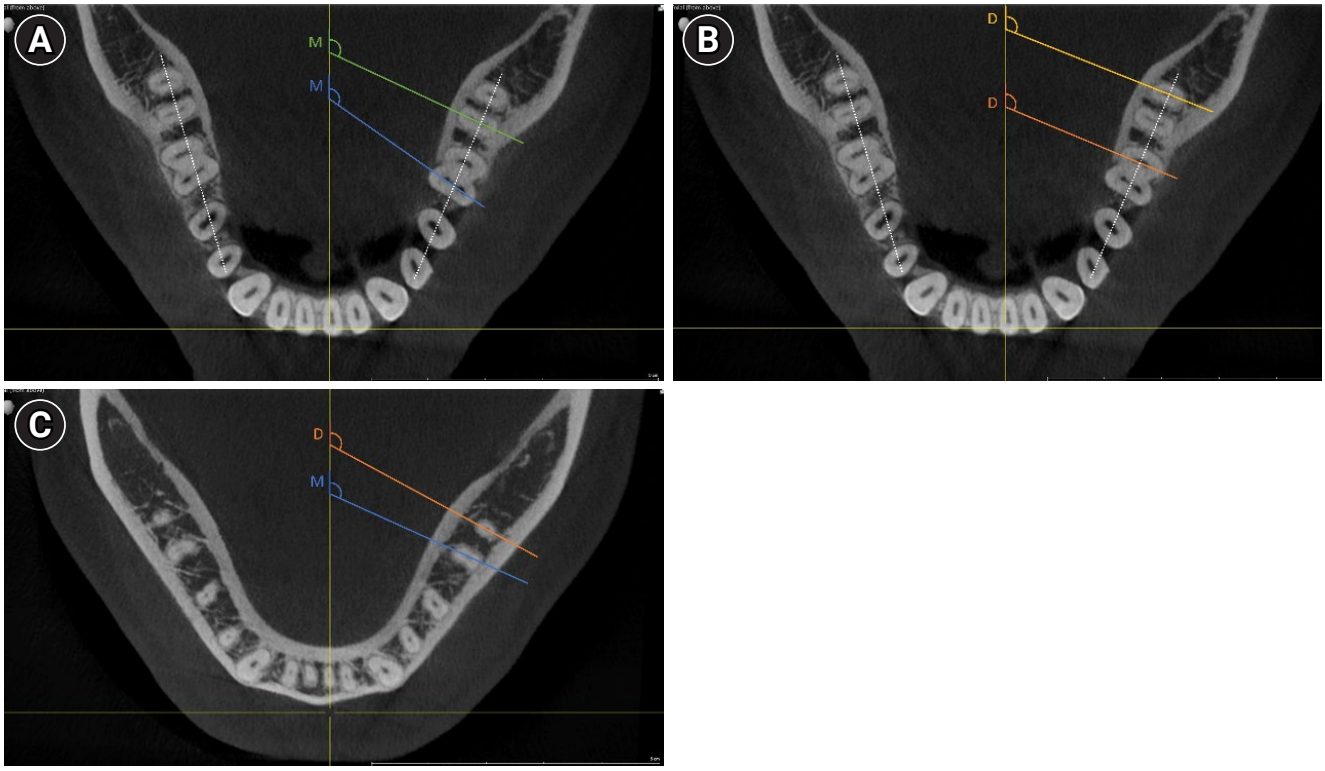

Figure 1. Examples of the cone-beam computed tomography measurements. Examples of measurements indicative of the angles at which root canals overlap. The measurement lines are colored for better visibility showing either mesial (M) or distal (D) canal pair measurements. The measurement lines are colored for better visibility showing either mesial (M) or distal (D) canal pair measurements. In roots presenting a single oval-shaped canal, the angle was measured along the axis of this anatomical structure. The dotted line represents the mandibular arch, and the angle between this reference and the X-ray central axis was also measured for final angle calculations. (A) Mesial canal pairs (mesiobuccal–mesiolingual), coronal level. (B) Distal canal pairs (distobuccal–distolingual), coronal level. (C) Mesial and distal measurements, apical level.

values represent mesial angulations and negative values represent distal angulations. Reporting focuses on the clinically relevant mesial angulations. To derive additional thresholds, we additionally identified the smallest predefined δ-cutoff at which a given separability level (≥95% or ≥99%) was first reached.

Diagnostic metrics such as sensitivity, specificity, or receiver operating characteristic (ROC)/area under the curve were not calculated, as no independent 2D radiographic gold standard was available for validation. Instead, the coverage function provides an equivalent probabilistic estimate of separability based on CBCT ground-truth geometry. All statistical analyses were performed in Python version 3.11.13 (Python Software Foundation, Wilmington, DE, USA) using the pandas and NumPy libraries.

RESULTS

Of the 100 CBCT scans initially screened, 85 datasets (59.8 % female, 39.6 % male) met the inclusion criteria. CBCTs were excluded mainly due to incomplete visualization of the mandibular molar region or because the molars did not appear in full within the volume. Final measurements were performed on 318 mandibular molars: 160 on the left side (77 first and 83 second molars) and 158 teeth from the right side (75 first and 83 second molars).

Descriptive statistics for horizontal beam angles at which root canal overlap occurred have been presented (Table 1). At the coronal level, the mean angle ± standard deviation for radiographic overlap of canals within the mesial roots was $\alpha = 83.74° \pm 10.63°$, while the corresponding angle for the distal roots was $\alpha = 79.60°$

https://doi.org/10.5395/rde.2026.51.e9

± 11.63°. At the apical level, canal overlap in the mesial roots was achieved at a mean angle of α = 82.92° ± 10.88°, and in the distal roots at α = 78.72° ± 11.92° (Figure 2). According to δ* = 90 – α, overlap values of approximately 75° to 83° translate into theoretical separation thresholds of roughly 7° to 15°. When comparing tooth types, mesial angles of canal overlap did not differ significantly between first and second mandibular molars ($p > 0.3$). In contrast, distal canal overlap angles were significantly higher in second molars, particularly at the coronal level ($p < 0.001$), reflecting increased curvature and divergence characteristics (Table 2). No significant gender-related differences were detected across any strata (all $p \geq 0.25$). To extend the overlap-based interpretation, separability was additionally evaluated across a predefined horizontal beam angulation grid from –45° to +45° in 5° increments. The proportion of separable canal pairs increased progressively with δ. At δ = 20°, approximately 90% of mesial and 85% of distal pairs were

Table 1. Mean overlap angles (α) by root level and canal pair

Position	Canal pair	N	Mean ± SD (°)
Coronal	MB–ML (mesial)	310	83.74 ± 10.63
Coronal	DB–DL (distal)	310	79.60 ± 11.63
Apical	MB–ML	305	82.92 ± 10.88
Apical	DB–DL	305	78.72 ± 11.92

Values are presented separately for mesial (MB–ML) and distal (DB–DL) canal pairs at coronal and apical levels. Angles (α, in degrees [°]) were measured from CBCT-derived canal centerlines within each root, representing the projection at which canal outlines fully overlap in two-dimensional radiographs. SD, standard deviation; MB–ML, mesiobuccal–mesiolingual; DB–DL, distobuccal–distolingual; CBCT, cone-beam computed tomography.

Table 2. Comparison of first and second mandibular molars (Welch *t*-tests for α)

Position	Canal pair	*t* (df)	*p*-value	Interpretation
Coronal	MB–ML	–0.65 (305.1)	0.518	NS (no difference)
Coronal	DB–DL	–2.96 (302.9)	0.0033*	Second molars > first molars
Apical	MB–ML	0.94 (302.7)	0.347	NS
Apical	DB–DL	–4.45 (302.7)	1.2×10^{-5}*	Second molars > first molars

Reported are test statistics, degrees of freedom (df), and two-sided *p*-values for mesial (MB–ML) and distal (DB–DL) canal pairs at coronal and apical levels.
Positive values denote higher overlap angles in second molars, consistent with increased distal root curvature.
MB–ML, mesiobuccal–mesiolingual; DB–DL, distobuccal–distolingual; NS, not significant.
*$p < 0.05$, statistically significant differences.

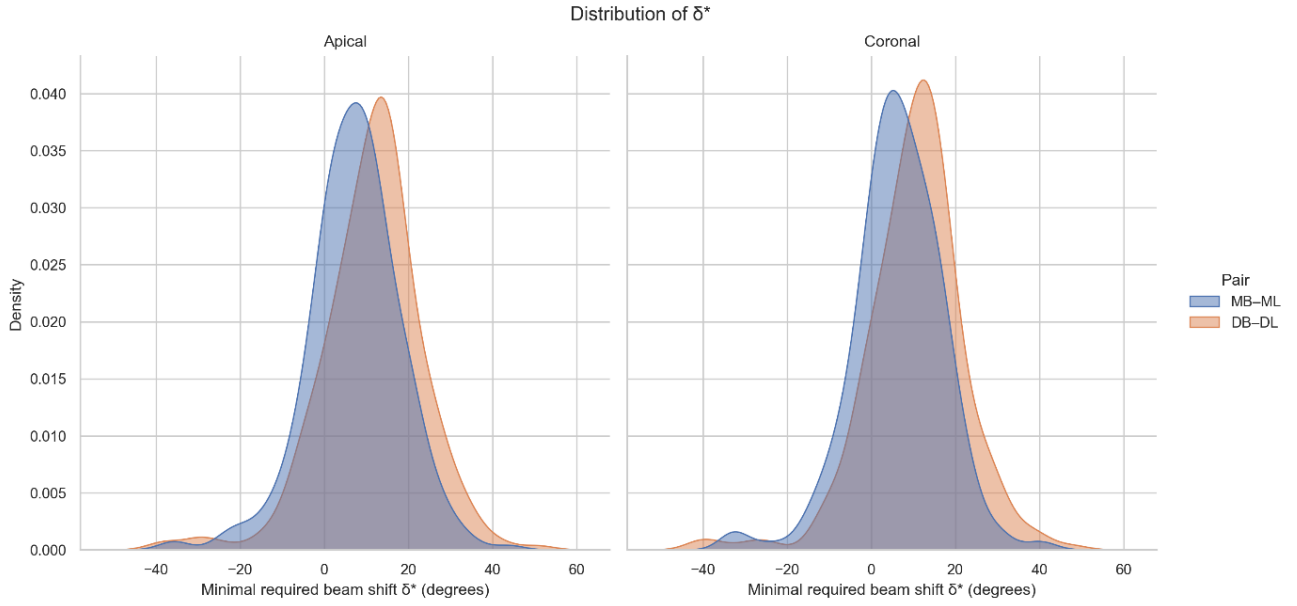

Figure 2. Distribution of δ values by canal pair and root level. Smoothed density distributions of the theoretical minimal horizontal beam angulation δ required to achieve radiographic separation of root canal pairs. Mesial (mesiobuccal–mesiolingual) and distal (distobuccal–distolingual) canal pairs are shown separately for the apical (left) and coronal (right) measurement levels. Distal canal pairs exhibit a right-shifted distribution, particularly at the coronal level, reflecting their generally higher beam angulation requirements compared with mesial canals.

separable. For mesial canals, ≥95% separability was reached at approximately 25°, and ≥99% was achieved within the 30° to 35° interval of the 5° increment grid. Distal canals required approximately 30° for ≥95% and approximately 40° for ≥99% separability. Wilson 95% confidence intervals narrowed markedly between 25° and 35°, indicating high statistical stability in this range (Tables 3 and 4). Distal roots, particularly in second molars, benefited from slightly larger mesial angulations (approximately 35°–40°), achieving near-complete separation (Figure 3).

Table 3. Theoretical beam angle thresholds (δ) for ≥95% and ≥99% canal separability

Position	Canal pair	δ for ≥95% (°)	δ for ≥99% (°)
Coronal	MB–ML	22	32
Coronal	DB–DL	30	40
Apical	MB–ML	25	32
Apical	DB–DL	30	40

Theoretical beam angulations were derived from δ* = 90° − α; thresholds represent the smallest δ at which coverage ≥95% or ≥99% was achieved. Values represent the minimal mesial horizontal angulations at which the corresponding proportion of canal pairs can be radiographically distinguished.
MB–ML, mesiobuccal–mesiolingual; DB–DL, distobuccal–distolingual.

DISCUSSION

The provision of root canal treatment relies on ra-

Table 4. Wilson 95% CIs for theoretical coverage (proportion of separable canals)

δ (°)	Mesial MB–ML coronal (%)	Distal DB–DL coronal (%)
20	92.6 (89.1–95.0)	85.5 (81.1–88.9)
25	97.7 (95.4–98.9)	91.6 (88.0–94.2)
30	98.7 (96.7–99.5)	96.8 (94.2–98.2)
35	99.3 (97.7–99.8)	98.1 (95.8–99.1)
40	99.7 (98.2–99.9)	99.0 (97.2–99.7)

Values are presented as percentage (95% confidence interval).
Coverage represents the proportion of canals achieving theoretical separability (δ* ≤ δ) at each predefined mesial beam angulation (δ). Confidence intervals narrow progressively between 25° and 35° indicating statistical stability of the separability plateau. Data were computed for coronal levels using the Wilson method for binomial proportions.
CIs, confidence intervals; MB–ML, mesiobuccal–mesiolingual; DB–DL, distobuccal–distolingual.

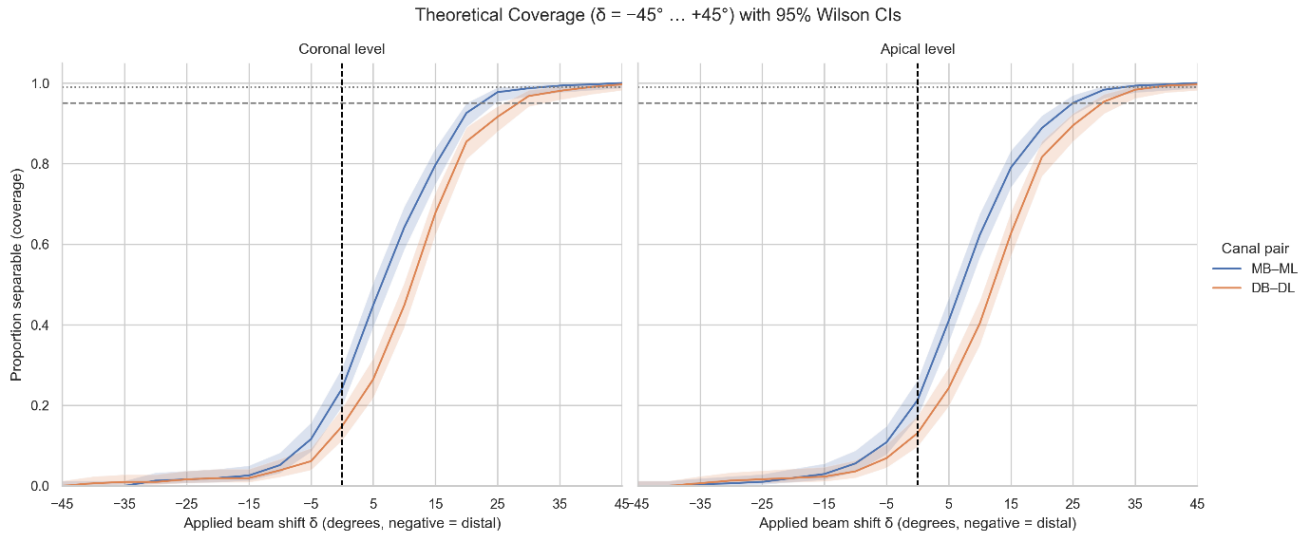

Figure 3. Theoretical coverage (δ = −45° to +45°) with 95% Wilson confidence intervals. Theoretical separability (coverage) of mesial (MB–ML) and distal (DB–DL) canal pairs plotted across the full range of applied horizontal beam angulations (δ = −45° to +45°). Curves represent the proportion of canal pairs predicted to be radiographically separable at each δ value, with shaded bands indicating 95% Wilson confidence intervals. Positive δ values correspond to mesial beam angulations; negative δ values represent distal angulations. Mesial canals (MB–ML) reach ≥95% separability between approximately 22° and 25°, and ≥99% at around 32°. Distal canals (DB–DL) require larger angulations, achieving ≥95% at approximately 30° and ≥99% at approximately 40°. The steep rise and subsequent plateau between approximately 25° and approximately 35° indicate the clinically relevant window in which most canal pairs become reliably distinguishable on a single periapical radiograph.
MB–ML, mesiobuccal–mesiolingual; DB–DL, distobuccal–distolingual.

https://doi.org/10.5395/rde.2026.51.e9

diographs (2D) and, in line with as low as reasonably achievable (ALARA) principles, operators are obliged to minimize radiation for patients while providing the highest standard of care. Many previous studies have used a trial-and-error approach with predefined horizontal beam angulations, often in *ex vivo* settings with extracted teeth, limiting clinical transferability due to artificial tooth alignment [2,17,20-22]. In contrast, *in vivo* data, such as that presented by Bardauil *et al.* [23], offer greater anatomical relevance. For this reason, the present study used a retrospective design based on existing CBCT data. This approach allowed for detailed, reproducible simulation of horizontal beam angulations and identification of precise angles at which root canal superimposition occurs, all while preserving the three-dimensional anatomical relationships of the mandibular arch. However, it must be acknowledged that CBCT imaging, while valuable for anatomical analysis, does not fully reproduce intraoral conditions such as sensor placement difficulty, variation in manufacturers' production of film holders or aiming devices, patient movement, or anatomical space limitations.

Unlike studies that focus on root outlines or apex positioning, our analysis focused on the radiographic separation of root canal spaces, which is of greater relevance in endodontics, particularly during working length determination and obturation assessment. As the apical foramen may not coincide with the anatomical apex [24,25], the ability to visualize root canals clearly at both the apical and coronal levels becomes a clinically significant objective. Accordingly, we measured superimposition at both apical and coronal levels using the center lines of the canals as radiographic targets to conclude at which beam angulations separation would be possible.

Across all mandibular molars examined, canal overlap persisted until projection angles corresponding to minimal mesial beam angulations of approximately 7° to 15°, reflecting the earliest theoretical onset of canal separability ($\delta^* = 90° - \alpha$). Distal canal systems required slightly larger minimal mesial angulations, with second molars showing the highest thresholds due to their greater root divergence. Specifically, second molars exhibited δ^* values around 9°–13°, whereas first molars showed slightly lower minimal separability thresholds of 7° to 12° ($p < 0.001$), suggesting greater root divergence or curvature in second molars. These findings reinforce previously reported anatomical differences between mandibular molars [26] and highlight the need for tailored radiographic strategies depending on molar type and root group. They also indicate that canal overlap may persist even with minor deviations from the orthoradial angle, and a slightly greater mesial beam angulation is needed to achieve total radiographic separation.

However, theoretical coverage analysis further quantified this relationship, revealing that mesial canals achieved ≥95% separability at δ approximately 25° and ≥99% at approximately 35°. Distal canal pairs required δ approximately 30° to reach 95% and approximately 40° to reach 99%, reflecting the flatter divergence trajectory of distal roots. Confidence intervals narrowed substantially between 25° and 35°, confirming statistical stability of the coverage plateau. These findings identify a narrow mesial beam angulation window in which most mesial and distal canals can be visualized simultaneously.

From a clinical perspective, this mesial beam angulation range of approximately 30° to 35° provides the highest probability of complete canal differentiation with one exposure. Notably, distal beam angulations were not considered clinically meaningful, as our coverage analysis demonstrated consistently low separability across all negative δ-increments (distal shifts), with values remaining far below diagnostic thresholds and therefore offering no practical radiographic advantage.

Anatomical variations further refine this recommendation. No significant differences were observed between first and second molars for mesial canal overlap ($p > 0.3$), whereas distal roots of second molars showed significantly higher overlap angles ($p = 0.003$ coronal, $p < 0.001$ apical), consistent with their greater curvature and divergence. Accordingly, for first molars, a mesial beam angulation of approximately 30° is sufficient to capture both canal pairs, while second molars benefit from a slightly higher angulation of approximately 35°, which compensates for their increased distal overlap.

Within this range, mesial canals are resolved in approximately 99% and distal canals in approximately 95% of cases. Thus, selecting a single exposure within this window avoids repeated imaging, in line with the ALARA principle [3,7].

If distal canal separation remains inadequate, further increase up to approximately 40° may be considered on a case-by-case basis. Coronal overlap angles were consistently higher than apical ones, confirming the increasing canal divergence toward the root apex [26]. Consequently, apical clarity should be prioritized during working length determination and obturation control. The significantly higher distal overlap in second molars supports anatomical evidence of greater root curvature and divergence in this group [26].

The coverage-based approach introduced in this study provides a continuous, quantitative analogue to conventional diagnostic performance metrics. Although sensitivity, specificity, and ROC analysis could not be computed in the absence of an independent 2D gold standard, the coverage function represents an equivalent probabilistic measure of radiographic separability derived from CBCT ground-truth geometry. Thus, it enables precise estimation of the probability of achieving canal differentiation at any given beam angle and bridges three-dimensional anatomy with 2D radiographic optimization.

It was decided to measure the distal root if there were two canals present, but through the canal cross-section if there was only one root canal. This has the advantage that the angles obtained in our study can also be used to confirm or rule out the presence of a single canal in the distal root. To do this clinically, it is important to check whether the visible canal, instrument, or gutta-percha is centrally located within the root contour when viewing a 2D X-ray. In case CBCT data is already available, the opportunity to use multiplanar reconstructions for the simulation of tube angulation should be taken. This helps to approximate individualized projection angles for intraoral radiography and improve the diagnostic yield of initial exposures. Ultimately, these findings may aid operators, both clinicians and students, by offering clinically applicable reference values for beam angulations, enhancing the quality of periapical imaging in mandibular molars. Further *in vivo* studies are warranted to validate these parameters under real-world clinical conditions and to investigate tools that could assist clinicians in achieving optimal X-ray projection geometry.

Limitations of the present study include its retrospective design and the exclusive use of CBCT data. Therefore, intraoral sensor placement or patient-specific positioning constraints could not be considered. Accordingly, no direct comparison with corresponding 2D periapical radiographs was possible. Consequently, sensitivity and specificity could not be computed in a statistically valid manner, as this would require an independent test image and dichotomous outcome classification. Deriving both the “true” and “test” conditions from the same CBCT dataset would have resulted in circular inference. Instead, the study employed a theoretical coverage approach, in which the proportion of teeth achieving canal separation at different predefined beam angles was determined. This method offers an equivalent functional interpretation of diagnostic performance across beam angulations while maintaining methodological validity. Future prospective studies combining CBCT and standardized intraoral radiographs are encouraged to validate these theoretical coverage parameters under clinical conditions.

It should also be noted that all angular measurements were performed by a single examiner, and no formal intra-observer reliability testing was undertaken. However, the measurement protocol was based on clearly defined anatomical reference points and geometric centerlines, minimizing subjective interpretation. Future studies should nonetheless include repeated measurements by multiple blinded observers to validate inter- and intra-observer consistency statistically.

Furthermore, our analysis was limited to radiographic axes where root canals appeared to overlap, independent of the actual number of canals, as multiple canals are usually situated parallel to one another within the root’s center. To distinguish between a single and multiple canals clinically, a second X-ray taken at a greater horizontal angle is required. This reveals whether the canal, an inserted file, or gutta-percha is centered within the root’s outline. A noncentral position strongly suggests an additional canal. The behavior of these axes across different root canal morphologies was not investigated and represents a potential avenue for future research.

Nonetheless, the large sample size and the narrow confidence intervals across strata support the robustness of the proposed angulation thresholds. However,

https://doi.org/10.5395/rde.2026.51.e9

the individual anatomical variation, assessed via preexisting periapical radiographs or available CBCT scans, should guide final angulation choices. Application of these parameters will respect ALARA principles, may reduce the need for retakes, lower radiation exposure, and improve radiographic diagnostic quality during endodontic treatment of mandibular molars.

CONCLUSIONS

The CBCT-based analysis provided a practical approach for selecting horizontal beam angulations in intraoral radiography of mandibular molars. Based on CBCT-derived overlap geometry, the earliest theoretical onset of canal separability occurs at small mesial beam angulations of approximately 7° to 15°. This minimal range reflects the lowest angular deviation at which the first radiographic divergence of canal systems becomes detectable.

Reliable canal separability (≥95% to 99%) was achieved only at larger mesial beam angulations. First mandibular molars reached consistent separability at approximately 30°, whereas second molars benefited from slightly higher angulations of 35°. If distal canal separation remains insufficient, increasing the beam angulation toward 40° may be considered. Together, these findings identify a practical single-exposure window of 30°–35°, which provides the highest probability of complete canal differentiation while minimizing the need for repeated radiographic exposures under ALARA principles.

ADDITIONAL INFORMATION

[1]Center for Oral and Maxillofacial Surgery, Department of Dentistry, Faculty of Medicine and Dentistry, Danube Private University, Krems, Austria
[2]Division for Endodontics, Center for Operative Dentistry and Periodontology, Department of Dentistry, Faculty of Medicine and Dentistry, Danube Private University, Krems, Austria
[3]Department of Health System Research, Faculty of Medicine and Dentistry, Danube Private University, Krems, Austria
[4]Endoclinic, Practice limited to Endodontics, North London, UK
[5]Research Center for Digital Technologies in Dentistry and CAD/CAM, Department of Dentistry, Faculty of Medicine and Dentistry, Danube Private University, Krems, Austria
[6]Medical Image Analysis & Artificial Intelligence (MIAAI) Group, Faculty of Medicine and Dentistry, Danube Private University, Krems, Austria

CONFLICT OF INTEREST

No potential conflict of interest relevant to this article was reported.

FUNDING/SUPPORT

The authors have no financial relationships relevant to this article to disclose.

AUTHOR CONTRIBUTIONS

Conceptualization, Resources, Methodology, Project administration: Schneider B, Tchorz JP. Data curation: Frank W, Fitzek S. Formal analysis: Schneider B, Tchorz JP, Frank W. Investigation, Software: Tepe T, Rapp D. Supervision: Tchorz JP, Schneider B, von See C. Validation: Lessani M, von See C, Frank W. Visualization: Frank W, Fitzek S, Lessani M. Writing - original draft: Schneider B, Tchorz JP, Tepe T, Rapp D. Writing - review & editing: Lessani M, Frank W, von See C, Schneider B, Fitzek S, Tchorz JP. All authors have read and agreed to the published version of the manuscript.

DATA SHARING STATEMENT

The datasets are not publicly available but are available from the corresponding author upon reasonable request.

REFERENCES

1. Gulabivala K, Ng YL. Factors that affect the outcomes of root canal treatment and retreatment: a reframing of the principles. Int Endod J 2023;56 Suppl 2:82-115.
2. Haghani J, Raoof M, Pourahmadi S. Ex-vivo evaluation of x-ray horizontal angle for separating the canals of four-canal first mandibular molars. Iran Endod J 2008;2:143-146.
3. Kazzi D, Horner K, Qualtrough AC, Martinez-Beneyto Y, Rushton VE. A comparative study of three periapical radiographic techniques for endodontic working length estimation. Int Endod J 2007;40:526-531.
4. Nair PN. On the causes of persistent apical periodontitis: a review. Int Endod J 2006;39:249-281.
5. Gomez F, Brea G, Gomez-Sosa JF. Root canal morphology and variations in mandibular second molars: an in vivo cone-beam computed tomography analysis. BMC Oral Health 2021;21:424.
6. Ordinola-Zapata R, Bramante CM, Versiani MA, Moldauer BI, Topham G, Gutmann JL, *et al.* Comparative accuracy of the Clearing Technique, CBCT and Micro-CT methods in studying the mesial root canal configuration of mandibular first molars. Int Endod J 2017;50:90-96.
7. Fava LR, Dummer PM. Periapical radiographic techniques during endodontic diagnosis and treatment. Int Endod J

1997;30:250-261.
8. Eliasson S, Lavstedt S, Wouters F, Ostlin L. Quality of intraoral radiographs sent by private dental practitioners for therapy evaluation by the Social Insurance Office. Swed Dent J 1990;14:81-89.
9. Patel JR. Intraoral radiographic errors. Oral Surg Oral Med Oral Pathol 1979;48:479-483.
10. Javed MQ, Kolarkodi SH, Riaz A, Nawabi S. Quality assurance audit of digital intraoral periapical radiographs at the undergraduate dental clinics. J Coll Physicians Surg Pak 2020;30:1339-1342.
11. Siddique SN, Anwar MA, Zaman H, Haider I, Ahmad A, Umair M, *et al*. Quality assessment of periapical radiographs taken by dental assistants using the recent Faculty of General Dental Practice (FGDP) guidelines. Cureus 2024;16:e68508.
12. Senior A, Winand C, Ganatra S, Lai H, Alsulfyani N, Pachêco-Pereira C. Digital intraoral imaging re-exposure rates of dental students. J Dent Educ 2018;82:61-68.
13. Almutairi N, Alharbi A. Difficulties faced by undergraduates while conducting endodontic therapy. Cureus 2024;16:e52217.
14. Abella F, Patel S, Durán-Sindreu F, Mercadé M, Roig M. Mandibular first molars with disto-lingual roots: review and clinical management. Int Endod J 2012;45:963-978.
15. Puapichartdumrong P, Eakpunyakul N, Tanpumiprathet S, Khueankaew P, Saelim P, Piyapattamin T. Efficacy of a newly designed angulation-adjustable film holder for reducing cone-cutting errors and saving time in horizontal tube-shift technique by dental students. Heliyon 2022;8:e11567.
16. Setzer FC, Lee SM. Radiology in endodontics. Dent Clin North Am 2021;65:475-486.
17. Karnasuta P, Vajrabhaya LO, Chongkonsatit W, Chavanaves C, Panrenu N. An efficacious horizontal angulation separated radiographically superimposed canals in upper premolars with different root morphologies. Heliyon 2020;6:e04294.
18. Hishikawa T, Izumi M, Naitoh M, Furukawa M, Yoshinari N, Kawase H, *et al*. The effect of horizontal X-ray beam angulation on the detection of furcation defects of mandibular first molars in intraoral radiography. Dentomaxillofac Radiol 2010;39:85-90.
19. Schneider B, Klinkhamels L, Frank W, von See C, Tchorz JP. Evaluation of the ideal horizontal X-ray beam angulation to accurately identify two separate canals in maxillary first premolars: a retrospective clinical study using cone-beam computed tomography in an Austrian subpopulation. Dent J (Basel) 2025;13:151.
20. Martínez-Lozano MA, Forner-Navarro L, Sánchez-Cortés JL. Analysis of radiologic factors in determining premolar root canal systems. Oral Surg Oral Med Oral Pathol Oral Radiol Endod 1999;88:719-722.
21. Naoum HJ, Love RM, Chandler NP, Herbison P. Effect of X-ray beam angulation and intraradicular contrast medium on radiographic interpretation of lower first molar root canal anatomy. Int Endod J 2003;36:12-19.
22. Wang Q, Yu G, Zhou XD, Peters OA, Zheng QH, Huang DM. Evaluation of X-ray projection angulation for successful radix entomolaris diagnosis in mandibular first molars in vitro. J Endod 2011;37:1063-1068.
23. Bardauil MR, Moura Netto Cd, Moura AA. Evaluation of the maxillary premolar roots dissociation using radiographic holders with conventional and digital radiography. Braz Oral Res 2010;24:284-289.
24. Martos J, Ferrer-Luque CM, González-Rodríguez MP, Castro LA. Topographical evaluation of the major apical foramen in permanent human teeth. Int Endod J 2009;42:329-334.
25. Martos J, Lubian C, Silveira LF, Suita de Castro LA, Ferrer Luque CM. Morphologic analysis of the root apex in human teeth. J Endod 2010;36:664-667.
26. Vertucci FJ. Root canal anatomy of the human permanent teeth. Oral Surg Oral Med Oral Pathol 1984;58:589-599.

https://doi.org/10.5395/rde.2026.51.e9

RDE Restorative Dentistry & Endodontics

Research Article

eISSN 2234-7666
Restor Dent Endod. 2026 February;51(1):e10
https://doi.org/10.5395/rde.2026.51.e10

Neuropeptide Y regulation of dental pulp neurogenic inflammation provoked by tooth bleaching agents: a descriptive comparative clinical study

Javier Caviedes-Bucheli[1,*], Néstor Ríos-Osorio[2,3], Mario Pérez-Villota[4], Karolina Aucú-Miño[4], Diana Escobar-Mafla[4], Hernán Darío Muñoz-Alvear[4], José Francisco Gomez-Sosa[5], Luis Diaz-Barrera[6], Edgar Güiza – Cristancho[4], Hugo Roberto Munoz[7]

For further information on the authors' affiliations, see Additional information.

ABSTRACT

Objectives: This study aimed to assess the expression of neuropeptide Y (NPY) in human dental pulp after tooth bleaching with three in-office hydrogen peroxide (H_2O_2)-based systems.

Methods: Forty pulps were collected from premolars scheduled for extraction and divided into four groups ($n = 10$): Control (no bleaching; basal NPY values); Pola Office (35% H_2O_2, 8 minutes); Opalescence Boost (40% H_2O_2, 20 minutes); and Zoom (25% H_2O_2 + cold blue light, 15 minutes). After extraction, pulps were fixed in 4% formaldehyde and processed. NPY levels were quantified using enzyme-linked immunosorbent assay. Data distribution was assessed with the Shapiro-Wilk test. One-way analysis of variance and Tukey *post-hoc* test with Bonferroni correction were applied ($p < 0.05$).

Results: NPY expression differed significantly among groups ($p = 0.0097$). The control group showed the lowest mean expression (0.026 ± 0.002 pmol/mg of pulp tissue), followed by Zoom (0.031 ± 0.005 pmol/mg), Pola Office (0.040 ± 0.004 pmol/mg), and Opalescence Boost, which exhibited the highest NPY expression (0.044 ± 0.004 pmol/mg). Post-hoc analysis revealed a statistically significant difference between the control and Opalescence Boost groups ($p = 0.0122$).

Conclusions: The increase in NPY expression—particularly with Opalescence Boost—indicates that in-office bleaching agents can elicit measurable neurobiological responses in pulp tissue after a single application. The significant difference between the control and Opalescence Boost groups suggests a possible H_2O_2 concentration- or formulation-dependent effect on pulpal neuropeptide activity, underscoring the need for further research on the biological impact of bleaching treatments.

Keywords: Dental pulp; Neurogenic inflammation; Neuropeptide Y; Tooth bleaching

Received: July 3, 2025 **Revised:** August 7, 2025 **Accepted:** November 13, 2025

Citation

Caviedes-Bucheli J, Ríos-Osorio N, Pérez-Villota M, Aucú-Miño K, Escobar-Mafla D, Muñoz-Alvear HD, Gomez-Sosa JF, Diaz-Barrera L, Güiza – Cristancho E, Munoz HR. Neuropeptide Y regulation of dental pulp neurogenic inflammation provoked by tooth bleaching agents: a descriptive comparative clinical study. Restor Dent Endod 2026;51(1):e10.

***Correspondence to**
Javier Caviedes-Bucheli, DDS, MSc
Centro de Investigaciones Odontológicas, Pontificia Universidad Javeriana, Cra 7 No. 40-62 Building 26, Bogotá 110311, Colombia
Email: javiercaviedes@gmail.com

INTRODUCTION

The human dental pulp is a highly specialized, vascularized, and innervated ectomesenchymal tissue, comprising an array of cell types, including immune cells, fibroblasts, and odontoblasts. The dental pulp can initiate a range of biological mechanisms to maintain homeostasis and pulp vitality in response to noxious stimuli, such as tooth-bleaching procedures [1,2].

Most tooth-bleaching products contain hydrogen peroxide (H_2O_2) as the active ingredient. When activated by chemicals or physical activators (i.e., enzymes, light, or heat), H_2O_2 dissociates into free radicals such as hydroxyl (OH), oxygen (O), and perhydroxyl (HO_2)—the most reactive free radical—responsible for the dentin's bleaching effect [3,4].

H_2O_2-based tooth-bleaching systems such as Pola Office (35% H_2O_2; SDI, Bayswater, VIC, Australia), Opalescence Boost (40% H_2O_2; Ultradent Products, South Jordan, UT, USA), and Zoom (25% H_2O_2 + cold blue light, Zoom! Bleaching System; Discus Dental, Culver City, CA, USA) are some of the most popular in-office bleaching products. The free radicals released by these bleaching agents can diffuse through the enamel and dentin to reach the dental pulp, thus triggering a transitory reversible neurogenic inflammatory phenomenon that may manifest as dentinal hypersensitivity, with a prevalence of 15% to 78% of cases [4–7]. The extent of the inflammatory phenomenon depends on the H_2O_2 concentration, the free radicals' interaction time with the substrates, and the activators' molecular weight in each particular bleaching system [8].

The inflammatory response that arises from the passage of free radicals into the pulp tissue is neurogenic in nature, as the nervous system governs the vascular and immune systems through the release of potent neuropeptides. Somatosensory nerve fiber stimulation causes the release of calcitonin gene-related peptide (CGRP), substance P (SP), and neurokinin A (NKA), whereas sympathetic and parasympathetic fibers release neuropeptide Y (NPY) and vasoactive intestinal peptide (VIP), respectively [9].

Neurogenic inflammation involves both myelinated Aδ and unmyelinated C fibers. Aδ and C fibers anastomose at the pulp tissue's periphery, interacting with the vascular component to form the so-called Rashkow plexus, responsible for regulating blood flow through neuropeptide influence. The release of SP, CGRP, and NKA provokes vasodilation and drives the migration of immune cells *via* chemotaxis, thus setting up an inflammatory response [4,10]. As a compensatory mechanism, NPY, a strong vasoconstrictor, and VIP, a regulatory vasodilator, are released to modulate the inflammatory process and preserve tissue homeostasis. Additionally, NPY and VIP promote pulp tissue repair by binding to specific cells, such as odontoblasts, fibroblasts, and immune cells [11].

Neuropeptides are released in response to orthodromic and/or antidromic stimuli [12,13]. An orthodromic stimulus occurs under physiological conditions, such as temperature fluctuations or masticatory function. In these situations, A-delta fibers become activated, releasing NPY or VIP neuropeptides to sustain tissue homeostasis [14,15]. In contrast, H_2O_2 free radicals that reach the dental pulp generate an antidromic signal by exciting type C nerve endings, leading to the release of SP and CGRP, which triggers an inflammatory response that increases blood flow, intrapulpal pressure, and causes pulp volume expansion, which results in fluid flow into dentinal tubules, clinically translating into dentinal hypersensitivity [4,10]. As a negative control mechanism, the sympathetic system releases NPY to counteract the neurogenic inflammatory phenomena triggered by somatosensory neuropeptides. NPY-induced vasoconstriction reduces blood flow and intrapulpal pressure [16,17]. Likewise, NPY inhibits acetylcholine- and SP-induced vasodilation and amplifies the post-synaptic effects of other vasoconstrictors such as noradrenaline [16]. NPY vasoconstriction modulates the vasodilatory impact of SP and CGRP, preventing pulp volume expansion and avoiding fluid movement in an antidromic direction into the dentinal tubules [14]. Therefore, NPY functions as a defensive mechanism by regulating the inflammatory process in the dental pulp. Similarly, it has been proposed that the presence of NPY-1 receptors in fibroblasts, undifferentiated cells, and odontoblasts may be linked to pulp mineralization processes as a defense mechanism [18,19]. However, to date, the expression of NPY in dental pulp following different bleaching protocols is unknown. This infor-

https://doi.org/10.5395/rde.2026.51.e10

mation could be valuable for evaluating NPY behavior during routine clinical procedures and, as a result, aid clinicians' decision-making to reduce pulp tissue injury.

In light of the preceding, the purpose of this study was to determine the effect of different tooth-bleaching protocols (Pola Office, Opalescence Boost, and Zoom) on NPY expression in healthy human dental pulp, aiming at identifying potential control mechanisms of neurogenic pulp inflammation and dentinal hypersensitivity following tooth-bleaching procedures.

METHODS

A descriptive comparative clinical study was conducted in accordance with the guidelines of the Colombian Ministry of Health regarding ethical considerations in research involving human tissues. The Bioethics Committee of the Universidad Cooperativa de Colombia (the members of the Medellin Sectional Bioethics Subcommittee) approved the study under resolution BIO407—Acta No.12, May 25, 2023. Written informed consent was obtained from each patient who participated in the study. The study protocol was registered in ClinicalTrials.gov (ID: NCT06606236).

The minimum sample size was calculated in advance as 10 per group using sampling software (G power ver. 3.1.9.2; Heinrich-Heine Universität Düsseldorf, Düsseldorf, Germany) based on previously published studies with a similar study population and methodological design from our group [4,17]. Forty dental pulps were collected from healthy non-smoking human donors aged 18 to 27 years who underwent premolar extractions for orthodontic purposes. All premolars were caries and restoration-free, with complete root development, confirmed both visually and radiographically, with normal response to sensitivity testing, and no evidence of periodontal disease, traumatic occlusion, or previous orthodontic force application. Teeth with similar features were selected to ensure the validity and reliability of the results, while limiting bias and any confounding factors.

Samples were randomly assigned (with the aid of a randomizer tool [random.org]) into four groups containing 10 healthy premolars each (without discriminating between maxillary and mandibular premolars): (i) control group: the teeth were not exposed to dental bleaching agents (healthy pulps with normal/basal NPY values); (ii) Pola Office group: application of Pola Office (35% H_2O_2) for 8 minutes (single application), (iii) Opalescent Boost group: application of Opalescent Boost (40% H_2O_2) for 20 minutes (single application), and (iv) Zoom group: application of Zoom! (25% H_2O_2 + cold blue light) for 15 minutes (single application). A high-intensity LED light source emitting in the visible blue spectrum (400–505 nm) was employed, delivering an average irradiance of 150–200 mW/cm^2. This corresponds to a total energy density of approximately 72–96 J/cm^2. According to the manufacturer, this energy range ensures efficient activation of the photoinitiators contained in the bleaching gel while minimizing thermal effects on dental and pulpal tissues. The manufacturer's instructions were strictly followed, but due to the nature of the research, a single application was performed in the experimental groups.

A preliminary sensitivity test was conducted to assess the normal state of the pulp. This involved using a pulp tester to evaluate the pulp's response to an electrical stimulus. Likewise, a cold test was performed using Endo Ice (1,1,1,2 tetrafluoroethane; Hygenic Corp, Akron, OH, USA) to confirm the results further. These tests collectively verified that the sensitivity of the premolars was within normal limits.

Clinical procedures and sample collection

Following tooth bleaching, teeth were anaesthetized immediately with 3% mepivacaine without vasoconstrictor infiltration injection for maxillary premolars and inferior alveolar nerve block injection for mandibular premolars. Ten minutes later, the teeth were extracted using conventional methods, employing a supraosseous luxation and extraction technique. The extraction process took no more than 5 minutes. For the control group, extraction was also performed 10 minutes after the anesthetic application. After extraction, all teeth were rinsed with 5.25% sodium hypochlorite to remove any remaining periodontal ligament that could contaminate the pulp sample. The teeth were sectioned using a Zekrya bur (Dentsply, Tulsa, OK, USA) in a high-speed handpiece, irrigated with a saline solution. Pulp tissue was collected using a sterile endodontic excavator, deposited on an Eppendorf tube with 1 mL 4% parafor-

maldehyde, and stored at –70°C until examination [17]. Tubes were identified with a code to blind the operator who would process the samples.

Enzyme-linked immunosorbent assay

Dental pulp samples were defrosted without thermal shock, dried on a filter, and weighed on an analytical balance. NPY was extracted by adding 150 mL of 0.5 mol/L of acetic acid and double boiling in a thermostat bath for 30 minutes [13]. NPY expression was determined by a specific enzyme-linked immunosorbent assay (ELISA) for NPY.

A volume of 50 μL from each standard, blank, and sample was added to the corresponding wells. All samples and standards were duplicated. The sample dilution was established by preliminary experiments. A 50 μL/well working solution with biotinylated antibody was added. The plate was covered with sealing film and incubated for 45 minutes at 37°C. After decanting the solution, each well was dispensed with 350 μL of wash buffer (soaked for 1 minute). Plates were washed three times and gently blotted before 100 μL of horseradish peroxidase-conjugated working solution was added to each well. The plate was covered with a new sealing film and incubated at 37°C for 30 minutes. After washing plates five times as previously described, the substrate was added (50 μL/well). The plate was incubated for 15 minutes at 37°C. The plate was protected from light by wrapping it in aluminum foil, which caused a color change. A volume of 50 μL/well of stop solution was added in the same order as the substrate solution was previously added. The optical density (OD) of each well was determined using a microplate reader at 450 nm [20].

A calibration curve from 31.25 to 2,000 pg/mL was prepared in duplicate according to the kit instructions (Human Neuropeptide Y ELISA Kit, E-EL-H1893; Elabscience, Houston, TX, USA) (Appendix 1). The kit's sensitivity is 18.75 pg/mL. The NPY concentration (pg/mL) was obtained by interpolating the OD results with the sample supernatants (pre-weighed tissues, macerated in phosphate-buffered saline [pH, 7.4; 100 mM] and centrifuged at 6,000 *g* at 4°C for 15 minutes). The amount of NPY/pg was then divided by the molecular weight of the neuropeptide and the amount of sample in mg to get the NPY concentration in pmol of the peptide/mg of fresh tissue.

Statistical analysis

Values were obtained in duplicate from each sample (20 per group). For each of the bleaching techniques analyzed, mean and standard error, as well as minimum and maximum values for NPY, expressed in pmol/mg of pulp tissue, were calculated. A Shapiro-Wilk test was applied to determine the distribution of the dataset. An one-way analysis of variance (ANOVA) test was performed to evaluate statistically significant differences between groups ($p < 0.05$). Since significant differences were found, the Tukey *post-hoc* test with Bonferroni correction was applied at a significance level of $p < 0.05$.

RESULTS

Table 1 outlines the NPY expression in pmol/mg of pulp tissue, revealing that the lowest expression was observed in the control group, followed by the Zoom! Pola Office and Opalescence Boost systems, respectively (one-way ANOVA: single factor $p = 0.0097$).

Table 2 displays Tukey *post-hoc* comparisons, which demonstrate that the only statistically significant difference was observed between the control and Opales-

Table 1. Expression of neuropeptide Y in dental pulps after different bleaching techniques

Group	*n*	Mean	Standard error	Median	Maximum	Minimum	95% CI	IQR	*p*-value (SW)	Single factor *p*-value (one-way ANOVA)
Control	10	0.026	0.002	0.024	0.047	0.012	0.0223–0.0302	0.012	0.169	0.0097
Pola Office	10	0.040	0.004	0.034	0.075	0.011	0.0314–0.0484	0.030	0.350	
Opalescence	10	0.044	0.004	0.037	0.086	0.019	0.0355–0.0526	0.020	0.091	
Zoom	10	0.031	0.005	0.027	0.068	0.006	0.0222–0.0406	0.033	0.200	

CI, confidence interval; IQR, interquartile range; SW, Shapiro-Wilk; ANOVA, analysis of variance.
Pola Office: SDI, Bayswater, VIC, Australia; Opalescence Boost: Ultradent Products, South Jordan, UT, USA; Zoom! Bleaching System: Discus Dental, Culver City, CA, USA.

https://doi.org/10.5395/rde.2026.51.e10

cence Boost groups ($p = 0.012$). All other pairwise comparisons showed no statistically significant differences ($p \geq 0.05$).

Figure 1 displays NPY expression levels in dental pulp tissue across the four bleaching protocols. Box plots represent NPY concentrations (pmol/mg) in control, Pola Office, Opalescence Boost, and Zoom groups. Red lines indicate medians, and black diamonds denote means. A significant increase in NPY was found in the Opalescence group compared to the control ($p < 0.05$).

DISCUSSION

Tooth bleaching has been shown to elicit a neurogenic, reversible pulpal inflammatory response, as free radicals dissociated from H_2O_2 diffuse through enamel and dentin into the pulp tissue. The magnitude of the neurogenic inflammatory response is strongly related to the bleaching system's H_2O_2 concentration, exposure time, and activation mode [1,3-6,9].

H_2O_2 free radicals activate somatosensory nerve terminals in the Rashkow plexus [11], leading to the up-regulated expression of SP, CGRP, and NKA from Aδ and C fibers, resulting in transient pulp inflammation. When the inflammatory phenomenon is not properly regulated, it can lead to the apoptosis of odontoblasts and fibroblasts, resulting in premature pulp aging, which jeopardizes the pulp tissue's protective mechanisms and homeostasis [5,9,21,22]. Furthermore, the inflammatory phenomena caused by bleaching procedures trigger antidromic stimulation due to increased blood flow and intrapulpal pressure, resulting in an increase in dental pulp volume and enhanced fluid flow into the dentinal tubules, which is clinically described as post-bleaching dentinal hypersensitivity [23].

NPY is released by exocytosis from sympathetic Aδ and C fibers as a compensatory anti-inflammatory mechanism. NPY binds to target cells *via* the NPY-1 receptor, which is expressed in fibroblasts, endothelial cells, macrophages, odontoblasts, and undifferentiated dental pulp cells. It competes and antagonizes pro-inflammatory somatosensory neuropeptides, such as SP, CGRP, and NKA [11,15,16,24]. NPY exerts a vasoconstrictor effect, aided by norepinephrine at the post-synaptic level, thus counteracting the vasodilation generated by SP and CGRP [17]. Furthermore, NPY promotes pulp tissue repair by attaching to its receptor NPY-1 in target cells, such as macrophages responsible for degrading H_2O_2 free radicals [25]. Likewise, NPY drives endothelial cells to promote angiogenesis, fibroblasts to renew and repair the extracellular matrix, and dental pulp stem cells to undergo odontoblastic differentiation, with the ultimate aim of producing tertiary dentin even up to 21 days following exposure to H_2O_2 agents [15,22,26]. All of these regulatory and reparative mechanisms lead to a decline in the inflammatory reaction a few days post-tooth bleaching, which in turn results in the control of dentinal hypersensitivity by restricting fluid flow into the dentinal tubules [23]. Additionally, when dental pulp is exposed to H_2O_2 free radicals, the up-reg-

Table 2. Tukey *post hoc* comparisons

Group 1	Group 2	Mean	Standard error	*p*-value
Control	Pola Office	0.014	0.004	0.0817
Control	Opalescence	0.018	0.004	0.0122
Control	Zoom	0.005	0.004	0.7981
Pola Office	Opalescence	0.004	0.004	0.8844
Pola Office	Zoom	0.009	0.004	0.4377
Opalescence	Zoom	0.013	0.004	0.1221

Pola Office: SDI, Bayswater, VIC, Australia; Opalescence Boost: Ultradent Products, South Jordan, UT, USA; Zoom: Discus Dental, Culver City, CA, USA.

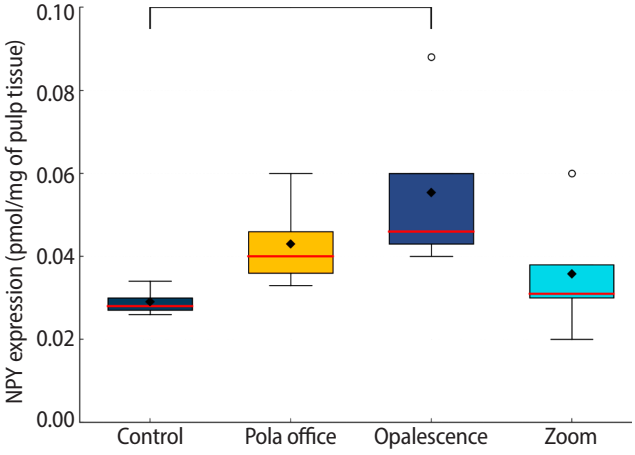

Figure 1. Boxplot of the neuropeptide Y (NPY) expression in dental pulp following different bleaching techniques. Pola Office: SDI, Bayswater, VIC, Australia; Opalescence Boost: Ultradent Products, South Jordan, UT, USA; Zoom: Discus Dental, Culver City, CA, USA.

ulated expression of dismutase and catalase, which enzymatically break down the perhydroxyl ion, provides a protective impact on the pulp cells and preserves pulp vitality over time [11,13].

Three different in-office tooth-bleaching systems—Pola Office, Opalescence Boost, and Zoom—were used in this study to quantify NPY expression in human dental pulp following tooth-bleaching procedures. We rigorously followed the manufacturer's instructions, as the detrimental impacts of H_2O_2 on pulp tissue are proportional to the concentration, application time, and activation method [27]. Depending on NPY expression, it may be feasible to infer the magnitude of the neurogenic inflammatory phenomenon following tooth-bleaching procedures and how NPY modulates the inflammatory process [23].

The ELISA test was performed to quantify NPY expression. It has been established that the ELISA test is sensitive enough to quantify neuropeptides in pmol/mg of pulp weight, the most generally used unit of measurement for neuropeptide expression in freshly extracted human dental pulp [28]. Considering the lack of previous research on NPY expression following tooth bleaching, a direct comparison was conducted between basal levels (pre-bleaching) and pulp inflammation (post-bleaching) in healthy premolars requiring extraction for orthodontic reasons [17]. Differences found between groups validate the sensitivity of the ELISA test.

All groups received 3% mepivacaine without a vasoconstrictor as a local anesthetic to prevent alpha-adrenergic agonists from minimizing neuropeptide expression. To allow NPY expression, a 10-minute interval was set aside following the removal of the bleaching agent [28]. Teeth were extracted using a supraosseous luxation and extraction technique, which should not take longer than 5 minutes to prevent endogenous endopeptidases from degrading the neuropeptide and to quantify the NPY expression linked to the bleaching procedure rather than the dental extraction [4,17].

The control group exhibited a mean NPY expression of 0.026 pmol/mg of pulp tissue, demonstrating that NPY is present in human dental pulp under physiological conditions. These values are consistent with previous studies that employed radioimmunoassay to assess NPY expression [17]. The Zoom system group (25% H_2O_2) achieved an average NPY expression of 0.031 pmol/mg of pulp tissue after 15 minutes of application and activation with a cold blue light. There was no significant difference ($p \geq 0.05$) compared to the control group's reference values. These results can be attributed to the fact that the Zoom bleaching system utilizes the lowest concentration of bleaching agents evaluated in this study, and its activation method involved a cold light lamp. Notably, the findings from this study differ from those of previous research, which assessed SP expression in human dental pulp in response to 25% Zoom bleaching with hot light activation. The Zoom system was found to elicit the highest SP expression, most likely due to the increased release of H_2O_2 free radicals by the activation source [29]. Such results confirm that the activation method of the bleaching agent impacts the expression of neuropeptides in the dental pulp and, therefore, the severity of neurogenic inflammation [4,30].

Similarly, NPY expression is directly proportional to the amount of H_2O_2 free radicals that enter the pulp tissue. The Pola Office system group (35% H_2O_2) with 8 minutes of application and the Opalescence Boost system group (40% H_2O_2) with 20 minutes of application displayed an average expression of 0.040 pmol/mg of pulp tissue and 0.044 pmol/mg of pulp tissue, respectively. No significant difference ($p \geq 0.05$) was observed between these two groups.

Opalescence Boost was the only group that showed statistically significant differences ($p < 0.05$) compared to the control group, implying that NPY expression is directly proportional to the concentration of the bleaching agent. Furthermore, it can be inferred that the Pola Office, followed by the Opalescence Boost system group, triggers a more intense inflammatory phenomenon, as evidenced by higher NPY expression, which attempts to preserve pulp tissue homeostasis [4,9].

NPY is released to modulate neurogenic inflammation mediated by somatosensory neuropeptides, thereby making pulp inflammation reversible [14,23,31]. NPY promotes protective vasoconstriction, thereby decreasing blood flow, intrapulpal pressure, and inflammatory cell chemotaxis, while also inhibiting neural activity by blocking SP and CGRP, thereby modulating the antidromic stimuli of fluid flow into dentinal tubules, which

https://doi.org/10.5395/rde.2026.51.e10

minimizes post-bleaching dentinal hypersensitivity [23,31]. However, as a long-term adverse effect, NPY release may result in premature aging of the dental pulp by eliciting pro-angiogenic defensive reactions [1,28]. It has been proposed that NPY binding to its specific receptor, NPY-1, in fibroblasts, undifferentiated mesenchymal cells, and odontoblasts may be linked to pulp mineralization processes as a defense mechanism. Apoptosis of these cells has also been observed when the effect of free radicals generated by dental bleaching surpasses the pulp tissue's tolerance [9,11,32]. When the aggression of free radicals from tooth bleaching systems exceeds the tolerance of the pulp tissue's defense mechanisms, as a result of using high concentrations of H_2O_2 and improper application times, irreversible pulpitis associated with the overexpression of NKA, SP, and CGRP may develop [4]. This leads to the destruction of immature odontoblasts and the DNA of undifferentiated cells [5,9,22], degeneration of pulp fibroblasts, and irreversible damage to immune cells, such as macrophages, which prevents pulp tissue from being repaired [26,32]. In this scenario, neither parasympathetic nor sympathetic neuropeptides, such as VIP and NPY, can regulate the inflammatory response.

This biological response suggests that bleaching protocols employing agents with higher irritative potential—particularly those containing high concentrations of peroxides or relying on unnecessary light activation—may contribute to premature pulpal aging [1,28]. Consequently, clinicians should carefully consider the selection of bleaching protocols, prioritizing the use of lower-concentration peroxide agents, minimizing the number of sessions, and avoiding light sources in products that do not require photoactivation. These findings underscore the importance of strictly adhering to the manufacturer's instructions, as deviations from the recommended protocol may increase the risk of pulpal damage without providing significant aesthetic benefits.

In light of these findings, future research should incorporate clinical sensitivity assessments alongside NPY quantification; investigate NPY responses to novel bleaching formulations, including nanoparticle-enhanced systems; examine the longitudinal effects of multiple bleaching sessions; and explore the spatial distribution patterns of NPY and NPY-1 receptors within the pulp tissue.

One of the main limitations of our study is the design of the treatment protocol. Although the single-application approach ensured methodological consistency and minimized variability, it does not fully represent routine clinical practice, where multiple bleaching sessions are commonly performed. Evidence from studies evaluating novel whitening agents suggests that cumulative exposure over successive applications may produce different biological effects on dental tissues. Therefore, a longitudinal investigation assessing NPY expression following multiple bleaching sessions would yield findings that are more representative of real-world clinical scenarios [33].

Despite the limitations of this *in vivo* study, it can be suggested that NPY expression correlates with the concentration of the bleaching agent and the intensity of the inflammatory response, thereby modulating the pulp's reactions to neurogenic pulp inflammation induced by tooth-bleaching procedures. This study found the highest NPY expression in Opalescence Boost, followed by Pola Office and Zoom. Further research on this topic should focus on correlating NPY expression with dentinal hypersensitivity levels following tooth bleaching protocols, with the goal of identifying mechanisms that contribute to dentinal hypersensitivity oversight.

CONCLUSIONS

The highest NPY expression values were found in Opalescence Boost, followed by Pola Office and Zoom. The significant increase in NPY expression, particularly in the Opalescence Boost group, demonstrates that even a single application of hydrogen peroxide-based bleaching agents can activate neurogenic signaling pathways within the dental pulp. This finding reveals a biologically active response at the molecular level, suggesting that tooth whitening procedures may induce early pulpal stress. The significant difference observed between the control and Opalescence Boost groups suggests a potential H_2O_2 concentration- or formulation-dependent effect on pulpal neuropeptide activity, highlighting the need for further longitudinal studies on the biological impact of bleaching treatments.

ADDITIONAL INFORMATION

[1]Centro de Investigaciones Odontológicas, Pontificia Universidad Javeriana, Bogotá, Colombia
[2]School of Dentistry, Fundación Universitaria Visión de Las Américas, Medellín, Colombia
[3]Postgraduate Endodontics Department, School of Dentistry, CES University, Medellin, Colombia
[4]Postgraduate Endodontics Department, School of Dentistry, Universidad Cooperativa de Colombia, Pasto, Colombia
[5]Instituto Venezolano de Investigaciones, Científicas, Caracas, Venezuela
[6]Bioprospecting Research Group, School of Engineering, Universidad de La Sabana, Chia, Colombia
[7]Endodontics Department, Universidad de San Carlos de Guatemala, Guatemala City, Guatemala

CONFLICT OF INTEREST

No potential conflict of interest relevant to this article was reported.

FUNDING/SUPPORT

The authors have no financial relationships relevant to this article to disclose.

AUTHOR CONTRIBUTIONS

Conceptualization: Caviedes-Bucheli J; Data curation: Muñoz-Alvear HD, Gomez-Sosa JF, Güiza–Cristancho E; Formal analysis: Roberto Munoz H, Ríos-Osorio N; Investigation: Pérez-Villota M, Aucú-Miño K, Escobar-Mafla D, Diaz-Barrera L; Supervision: Caviedes-Bucheli J, Muñoz-Alvear HD; Validation: Ríos-Osorio N, Roberto Munoz H; Visualization: Ríos-Osorio N; Writing - original draft: Caviedes-Bucheli J, Ríos-Osorio N; Writing - review & editing: Ríos-Osorio N. All authors read and approved the final manuscript.

DATA SHARING STATEMENT

The datasets used and/or analyzed during the current study are available from the corresponding author upon reasonable request.

REFERENCES

1. Caviedes-Bucheli J, Gomez-Sosa JF, Azuero-Holguin MM, Ormeño-Gomez M, Pinto-Pascual V, Munoz HR. Angiogenic mechanisms of human dental pulp and their relationship with substance P expression in response to occlusal trauma. Int Endod J 2017;50:339-351.
2. Pohl S, Akamp T, Smeda M, Uderhardt S, Besold D, Krastl G, *et al*. Understanding dental pulp inflammation: from signaling to structure. Front Immunol 2024;15:1474466.
3. Sun L, Liang S, Sa Y, Wang Z, Ma X, Jiang T, *et al*. Surface alteration of human tooth enamel subjected to acidic and neutral 30% hydrogen peroxide. J Dent 2011;39:686-692.
4. Caviedes-Bucheli J, Ariza-García G, Restrepo-Méndez S, Ríos-Osorio N, Lombana N, Muñoz HR. The effect of tooth bleaching on substance P expression in human dental pulp. J Endod 2008;34:1462-1465.
5. Basting RT, Amaral FL, França FM, Flório FM. Clinical comparative study of the effectiveness of and tooth sensitivity to 10% and 20% carbamide peroxide home-use and 35% and 38% hydrogen peroxide in-office bleaching materials containing desensitizing agents. Oper Dent 2012;37:464-473.
6. Minoux M, Serfaty R. Vital tooth bleaching: biologic adverse effects: a review. Quintessence Int 2008;39:645-659.
7. Meireles SS, Goettems ML, Dantas RV, Bona ÁD, Santos IS, Demarco FF. Changes in oral health related quality of life after dental bleaching in a double-blind randomized clinical trial. J Dent 2014;42:114-121.
8. Bharti R, Wadhwani K. Spectrophotometric evaluation of peroxide penetration into the pulp chamber from whitening strips and gel: an in vitro study. J Conserv Dent 2013;16:131-134.
9. Caviedes-Bucheli J, Muñoz HR, Azuero-Holguín MM, Ulate E. Neuropeptides in dental pulp: the silent protagonists. J Endod 2008;34:773-788.
10. Caviedes-Bucheli J, Lopez-Moncayo LF, Muñoz-Alvear HD, Gomez-Sosa JF, Diaz-Barrera LE, Curtidor H, *et al*. Expression of substance P, calcitonin gene-related peptide and vascular endothelial growth factor in human dental pulp under different clinical stimuli. BMC Oral Health 2021;21:152.
11. Kina JF, Huck C, Riehl H, Martinez TC, Sacono NT, Ribeiro AP, *et al*. Response of human pulps after professionally applied vital tooth bleaching. Int Endod J 2010;43:572-580.
12. Olgart L, Edwall L, Fried K. Cat dental pulp after denervation and subsequent re-innervation: changes in blood-flow regulation and distribution of neuropeptide-, GAP-43- and low-affinity neurotrophin receptor-like immunoreactivity. Brain Res 1993;625:109-119.
13. Kawashima N, Okiji T. Characteristics of inflammatory mediators in dental pulp inflammation and the potential for their control. Front Dent Med 2024;5:1426887.
14. Kim S. Neurovascular interactions in the dental pulp in health and inflammation. J Endod 1990;16:48-53.
15. El-Karim I, Lundy FT, Linden GJ, Lamey PJ. Extraction and radioimmunoassay quantitation of neuropeptide Y (NPY) and vasoactive intestinal polypeptide (VIP) from human dental pulp tissue. Arch Oral Biol 2003;48:249-254.
16. Lundy FT, Linden GJ. Neuropeptides and neurogenic mech-

https://doi.org/10.5395/rde.2026.51.e10

anisms in oral and periodontal inflammation. Crit Rev Oral Biol Med 2004;15:82-98.
17. Caviedes-Bucheli J, Lombana N, Azuero-Holguín MM, Munoz HR. Quantification of neuropeptides (calcitonin gene-related peptide, substance P, neurokinin A, neuropeptide Y and vasoactive intestinal polypeptide) expressed in healthy and inflamed human dental pulp. Int Endod J 2006;39:394-400.
18. Killough SA, Lundy FT, Irwin CR. Dental pulp fibroblasts express neuropeptide Y Y1 receptor but not neuropeptide Y. Int Endod J 2010;43:835-842.
19. Rethnam S, Raju B, Fristad I, Berggreen E, Heyeraas KJ. Differential expression of neuropeptide Y Y1 receptors during pulpal inflammation. Int Endod J 2010;43:492-498.
20. Nurhapsari A, Cilmiaty R, Prayitno A, Purwanto B, Soetrisno S. The role of Asiatic acid in preventing dental pulp inflammation: an in-vivo study. Clin Cosmet Investig Dent 2023;15:109-119.
21. Sharma H, Sharma DS. Detection of hydroxyl and perhydroxyl radical generation from bleaching agents with nuclear magnetic resonance spectroscopy. J Clin Pediatr Dent 2017;41:126-134.
22. Reis-Prado AH, Grossi IR, Chaves HG, André CB, Morgan LF, Briso AL, *et al*. Influence of hydrogen peroxide on mineralization in dental pulp cells: a systematic review. Front Dent Med 2021;2:689537.
23. Pashley DH. How can sensitive dentine become hypersensitive and can it be reversed? J Dent 2013;41 Suppl 4:S49-S55.
24. Mehboob R, Hassan S, Gilani SA, Hassan A, Tanvir I, Waseem H, *et al*. Enhanced neurokinin-1 receptor expression is associated with human dental pulp inflammation and pain severity. Biomed Res Int 2021;2021:5593520.
25. Galler KM, Weber M, Korkmaz Y, Widbiller M, Feuerer M. Inflammatory response mechanisms of the dentine-pulp complex and the periapical tissues. Int J Mol Sci 2021;22.
26. Zhan C, Huang M, Zeng J, Chen T, Lu Y, Chen J, *et al*. Irritation of dental sensory nerves promotes the occurrence of pulp calcification. J Endod 2023;49:402-409.
27. Donato MV, Dos Reis-Prado AH, Abreu LG, de Arantes LC, Goto J, Chaves HGDS, *et al*. Influence of dental bleaching on the pulp tissue: a systematic review of in vivo studies. Int Endod J 2024;57:630-654.
28. Caviedes-Bucheli J, Lopez-Moncayo LF, Muñoz-Alvear HD, Hernandez-Acosta F, Pantoja-Mora M, Rodriguez-Guerrero AS, *et al*. Expression of early angiogenesis indicators in mature versus immature teeth. BMC Oral Health 2020;20:324.
29. Gibbs JL, Hargreaves KM. Neuropeptide Y Y1 receptor effects on pulpal nociceptors. J Dent Res 2008;87:948-952.
30. Buchalla W, Attin T. External bleaching therapy with activation by heat, light or laser--a systematic review. Dent Mater 2007;23:586-596.
31. He LB, Shao MY, Tan K, Xu X, Li JY. The effects of light on bleaching and tooth sensitivity during in-office vital bleaching: a systematic review and meta-analysis. J Dent 2012;40:644-653.
32. Fernandes AM, Vilela PG, Valera MC, Bolay C, Hiller KA, Schweikl H, *et al*. Effect of bleaching agent extracts on murine macrophages. Clin Oral Investig 2018;22:1771-1781.
33. Mansoor A, Mansoor E, Hussain K, Khan S. Clinical efficacy of novel biogenically fabricated titania nanoparticles enriched mouth wash in treating the tooth dentine hypersensitivity: a randomized clinical trial. Pak J Med Sci 2025;41:1743-1748.

Concentration (pg/mL)	Absorbance (A)	Standard deviation
250	1.989	0.0095
125	2.450	0.0385
62.5	2.652	0.0265
31.25	2.839	0.0040
0	2.851	0.0140

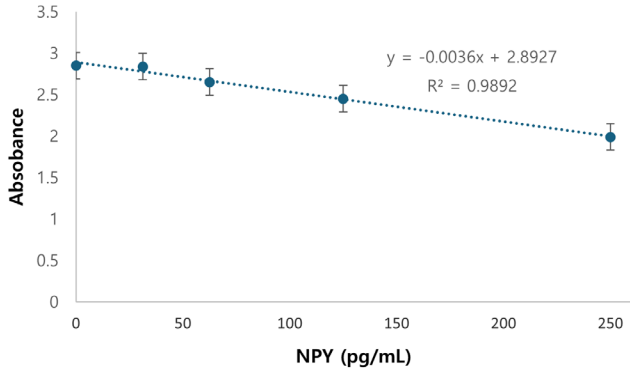

Appendix 1. Calibration curve for neuropeptide Y (NPY) quantification by competitive enzyme-linked immunosorbent assay.

https://doi.org/10.5395/rde.2026.51.e10

RDE Restorative Dentistry & Endodontics

Research Article

eISSN 2234-7666
Restor Dent Endod. 2026 February;51(1):e11
https://doi.org/10.5395/rde.2026.51.e11

Cone-beam computed tomography analysis of maxillary premolar canal anatomy: Ahmed's versus Vertucci's classifications in a Jordanian cohort

Raidan Ba-Hattab[1], **Muna M. Shaweesh**[2], **Nessrin A. Taha**[3,*], **Elham S. Abu Alhaija**[4]

[1]Department of Pre-Clinical Oral Health Sciences, College of Dental Medicine, QU Health, Qatar University, Doha, Qatar
[2]Al Thumamah Health Center, Primary Health Care Corporation, Doha, Qatar
[3]Department of Conservative Dentistry, Faculty of Dentistry, Jordan University of Science and Technology, Irbid, Jordan
[4]Department of Clinical Oral Health Sciences, College of Dental Medicine, QU Health, Qatar University, Doha, Qatar

ABSTRACT

Objectives: This study analyzed the root and canal configurations of maxillary premolars in a Jordanian subpopulation using cone-beam computed tomography (CBCT) and classified them based on Vertucci's and Ahmed's systems.

Methods: Two hundred CBCT scans of 800 maxillary premolars were retrospectively assessed for root morphology, canal configurations, and root canal divergence and merging. Data was statistically analyzed.

Results: The study included 70 males and 130 females. Most right and left maxillary first premolars (RFPM, LFPM) had two roots (59.0% and 58.5%), with a significant association between sex and root number for RFPM and LFPM ($p < 0.05$). In contrast, the right and left maxillary second premolars (RSPM, LSPM) mostly had a single root (87.5% and 88.5%), with no association with sex. Vertucci's classification showed type IV as the predominant configuration in first premolars (RFPM, 65.0% and LFPM, 67.0%) and type I in second premolars (RSPM, 44.0% and LSPM, 49.0%). A significant sex association was found only with RSPM. Ahmed's classification revealed that maxillary premolar with two separated roots and two separated canals (^{2}MP B^{1} P^{1}) was mostly found in first premolars (RFPM, 58.0% and LFPM, 56.0%), and maxillary premolar with one root and one canal (^{1}MP^{1}) in second premolars (RSPM, 44.0% and LSPM, 49.0%), with a significant sex association for RSPM and LSPM ($p < 0.05$). Age had no impact, and symmetry was observed between the right and left sides. Three-rooted premolars were identified in four cases. Almost all of Vertucci's types and numerous codes from Ahmed's classification were documented.

Conclusions: CBCT revealed diverse anatomical variations in the Jordanian subpopulation, with Ahmed's classification providing more detailed canal configurations than Vertucci's, uncovering previously overlooked variations.

Keywords: Bicuspid; Cone-beam computed tomography; Dental pulp cavity; Jordan; Tooth root

Received: July 10, 2025 **Revised:** November 26, 2025 **Accepted:** December 9, 2025

Citation
Ba-Hattab R, Shaweesh MM, Taha NA, Abu Alhaija ES. Cone-beam computed tomography analysis of maxillary premolar canal anatomy: Ahmed's versus Vertucci's classifications in a Jordanian cohort. Restor Dent Endod 2026;51(1):e11.

***Correspondence to**
Nessrin A. Taha, BDS, MFDS, GradDipClinDent, DClinDent (Endo), FRACDS, FRACDs (Endo), PhD
Department of Conservative Dentistry, Faculty of Dentistry, Jordan University of Science and Technology, Irbid 22110, Jordan
Email: n.taha@just.edu.jo

INTRODUCTION

Understanding tooth morphology is a key to successful endodontic treatment [1]. One of the main reasons for treatment failure and the need for retreatment is the presence of untreated root canals, which can occur due to the complex, varied structure of the root and its canal system. These complex systems harbor hidden microbial infections [2].

Over the years, several classification systems have been developed by Wein [3] and Vertucci [4] to describe the different root canal configurations. Vertucci [4] described eight standard canal configurations (types I–VIII) based on the ways canals branch and rejoin from the pulp chamber to the apex, a system that is still commonly applied. However, the diversity of tooth anatomy and root canal configurations reveals limitations in existing classifications. Furthermore, the increasing use of advanced imaging techniques has uncovered many previously unrecognized anatomical complexities [4]. To overcome this limitation, Ahmed *et al.* [5] proposed a coding method in which (i) the number of roots is indicated as a superscript before the tooth code, and (ii) the canal configuration for each root is noted as superscripts following the tooth code (for instance, ^{2}MP B^{1} P^{1} denotes a maxillary premolar with two roots, each containing a single independent canal). This approach enables the detailed notation of canal divergence and convergence within individual roots (e.g., $MP^{1\text{-}2\text{-}1}$, signifying a 1-2-1 canal pathway), providing greater accuracy than earlier classification systems [5].

Historically, various methods have been employed to study the internal and external anatomies of teeth. The *in vitro* clearing method involved several complex steps for preparing the teeth before injecting the ink, in preparation for examining the tooth canals [6]. Certain clinical studies employed the SLOB (Same Lingual, Opposite Buccal) technique, using two radiographs from different angulations and magnifying loupes to facilitate inspection of the pulp chamber floor and localization of root canal orifices [7].

Two previous studies have examined maxillary premolars in the Jordanian population. Awawdeh *et al.* [6] using extracted teeth and India ink, found that the first premolars were predominantly two-rooted with a Vertucci's system type IV canal configuration, though rarer configurations, such as Vertucci's system type XVI (2–3), where two canals leave the chamber; one subdivides, so the root ends with three foramina, were also observed. The prevalence of multiple canals (79.7%) in maxillary premolars was higher than in other populations, underscoring the importance of accounting for these variations in endodontic treatment [6]. Al-Ghananeem *et al.* [7] conducted a study on maxillary second premolars in a Jordanian population, examining 217 teeth to determine the number of roots and canals. The study utilized parallel and cone-shift radiographic techniques during routine endodontic procedures, and canal orifices were identified using 3.5× magnification loupes. The results revealed that 55.3% of the teeth had a single root, 44.2% had two roots, and 0.46% had three roots. In terms of root canal configurations, classified using Vertucci's system, 13.8% of the teeth had type I, 24.9% had type II, 60.8% had type IV, and 0.46% had type VIII.

Cone-beam computed tomography (CBCT) in dentistry has significantly enhanced diagnostic capabilities by providing detailed three-dimensional (3D) views of both internal structures and surrounding anatomy in coronal, sagittal, and axial planes [8]. Additionally, it has simplified the root and canal configuration procedure [9,10]. In contrast, the two-dimensional nature of periapical radiographs can lead to the missed detection of roots and canals [8]. While micro computed tomography (micro-CT) is recognized as a more accurate radiological technique for examining tooth morphology due to its higher resolution, it subjects patients to much higher radiation doses [11]. Despite this advancement, no previous study has examined the morphology of the roots and canals in Jordanian maxillary premolars using CBCT, nor has it compared the Vertucci's and Ahmed's classifications simultaneously. Therefore, the aim of this study was to assess the root morphology and canal configurations in a Jordanian subpopulation using CBCT scans, applying the Vertucci's and Ahmed's classification systems, and to compare these findings with those obtained using conventional techniques.

METHODS

This retrospective cross-sectional study was reported

https://doi.org/10.5395/rde.2026.51.e11

in accordance with the STROBE (Strengthening the Reporting of Observational Studies in Epidemiology) guidelines [12]. Ethical approval was obtained from the Institutional Research Committee of Jordan University of Science and Technology (JUST) in Irbid, Jordan, under protocol number 2023/161/36.

The CBCT images analyzed in this study were initially obtained for various diagnostic purposes as part of comprehensive treatment planning at JUST's Dental Teaching Clinics in the period from September 2016 to September 2022. As the data were anonymized and no additional interventions were involved, the ethics committee waived informed consent.

The sample size was calculated using a sample size calculator (RaoSoft, Seattle, WA, USA) with a 50% prevalence, a 5% margin of error, and a 95% confidence interval, yielding a target sample size of 384 teeth per type.

Inclusion criteria

The inclusion criteria were CBCT scans of bilateral maxillary first and second premolars with fully developed apices obtained from subjects aged 13 years or older, provided that the scans were of sufficient quality to allow visualization of individual root and canal morphology and had voxel sizes of 0.2 mm or smaller.

Exclusion criteria

Exclusion criteria included the following: missing contralateral premolar, immature teeth, teeth in which individual roots or canals were not clearly visualized, or that showed evidence of prior dental treatment or surgery altering the natural anatomy (e.g., root canal treatment, posts, metal restorations, 'apicoectomy,' root resection, resorption, etc.).

Cone-beam computed tomography imaging and analysis

CBCT scans were taken using a CS 9500 cone-beam 3D system (Carestream Health, Rochester, NY, USA) with a flat-panel detector. The CBCT machine's parameters were as follows: tube current, 10 mA; tube voltage, 90 kVp; and focal spot diameter, 0.6 mm. The possible voxel size is 0.20 or less, with an exposure time of 8.01 seconds.

The CBCT scans were analyzed independently by two specialists with 15 years of clinical experience, who were calibrated prior to the assessment using 20 CBCT scans of maxillary premolar teeth showing root canal morphology according to the Vertucci's and Ahmed's classification systems (Figure 1). Inter- and intra-examiner reliability was assessed with a 3-week interval between the first and second assessments. Disagreements were resolved through open discussion and a consensus-based approach.

The DICOM files were analyzed using Blue Sky Plan 64-bit (V4.13.64-bit; Blue Sky Bio, LLC, Libertyville, IL, USA), with adjustments to contrast, brightness, and sharpness to improve visualization. Three planes (axial, coronal, and sagittal) were assessed for tooth anatomy based on the following criteria: (1) root morphology, including i) root numbers, classified into single, double, or three-rooted [11] and ii) root bifurcation, assessed by means of a software ruler and divided into three equal sections (coronal, middle, and apical) as per Saber *et al* [11]; (2) root canal configuration: categorized based on Vertucci's scheme [4] and the updated coding system of Ahmed *et al*. [5]; and (3) levels of divergence and merging in root canals, measured using a software ruler by dividing each root canal into three equal portions (coronal, middle, and apical), as described in previous studies [11,13].

Sex and age were recorded. Age was divided into five groups in accordance with a previous report [14]: (1) 13–24 years; (2) 25–34 years; (3) 35–44 years; (4) 45–54 years; (5) ≥55 years.

Statistical analysis

Data analysis was conducted using IBM SPSS Statistics ver. 29.0 (IBM Corp., Armonk, NY, USA). The Pearson chi-square test evaluated the association of root canal morphologies based on Vertucci's and Ahmed's classifications across age and sex. Analysis of variance and independent *t*-tests were used to compare canal divergence and merging levels. The significance level was set at $p < 0.05$.

RESULTS

The kappa coefficients indicated excellent reliability, with inter-examiner values ranging from 0.803 to 1 and

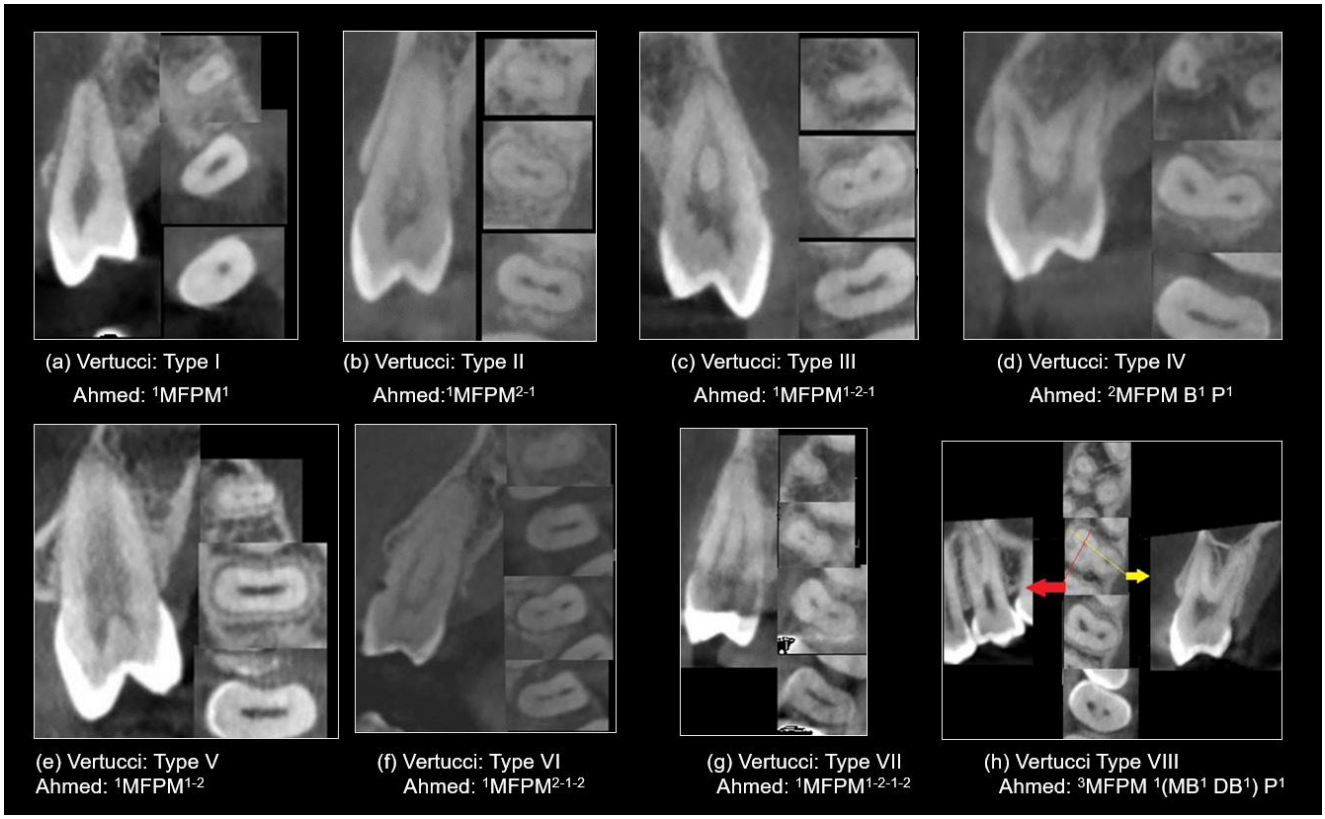

Figure 1. Representative cone-beam computed tomography images in sagittal and axial views (apical, middle, coronal), showcasing various root canal system configurations in maxillary first premolars (MFPM) based on Vertucci's and Ahmed's classifications.

intra-examiner values ranging from 0.854 to 1.

A total of 200 patients' scans have been included, meeting the inclusion criteria (400 maxillary first premolars and 400 maxillary second premolars), with 140 males (35%) and 260 females (65%). The subjects' ages ranged from 13 to 72 years (mean age, 22.8 years).

Root morphology (Table 1)

1. Maxillary first premolars

The majority of the right maxillary first premolars (RFPM) had two roots (118/200, 59%), occurring in 71.4% of males and 52.3% of females. Likewise, the majority of the left maxillary first premolars (LFPM) had two roots (117/200, 58.5%), with frequencies of 67.1% in males and 53.8% in females. Single-rooted RFPMs were less common, occurring in 81 of 200 teeth (40.5%), with a prevalence of 47.7% in females and 27.1% in males. In LFPM, single roots were also less common (82/200, 41.0%), occurring in 46.2% of females and 31.4% of males. Three-rooted configurations were rare, occurring in only 0.5% of both RFPM and LFPM, and were exclusively observed in males. The association between root number and sex was statistically significant in both RFPM and LFPM ($p = 0.004$ and $p = 0.039$, respectively).

2. Maxillary second premolars

The right maxillary second premolars (RSPM) had mostly a single root (175/200, 87.5%), with 81.4% occurring in males and 90.8% in females. Similarly, most left maxillary second premolars (LSPM) had one root (177/200, 88.5%), with a rate of 84.3% in males and 90.8% in females. Two-rooted RSPM were less frequent, found in 25 out of 200 teeth (12.5%), with 18.6% in males and 9.2% in females. In LSPM, two roots were also less common (21/200, 10.5%), with 14.3% in males and 8.5% in females. Three-rooted configurations were rare, occurring in only one case each for LSPM in both sexes. The association between root number and sex was not statistical-

https://doi.org/10.5395/rde.2026.51.e11

Table 1. Frequency distribution of number of roots and levels of root bifurcations according to sex

Sex	Number of roots					Bifurcations level[a]				
	Single root	Double roots	Three roots	Total	Pearson χ^2, *p*-value	Coronal	Middle	Apical	Total	Pearson χ^2, *p*-value
RFPM										
Male	19 (27.1)	50 (71.4)	1 (1.4)	70 (100)		19 (38.0)	25 (50.0)	6 (12.0)	50 (100)	1.957, 0.418
Female	62 (47.7)	68 (52.3)	0 (0)	130 (100)	9.421, 0.004*	18 (26.1)	42 (60.9)	9 (13.0)	69 (100)	
Total	81 (40.5)	118 (59.0)	1 (0.5)	200 (100)		37 (31.1)	67 (56.3)	15 (12.6)	119 (100)	
LFPM										
Male	22 (31.4)	47 (67.1)	1 (1.4)	70 (100)		15 (31.3)	28 (58.3)	5 (10.4)	48 (100)	0.236, 0.893
Female	60 (46.2)	70 (53.8)	0 (0)	130 (100)		20 (27.8)	43 (59.7)	9 (12.5)	72 (100)	
Total	82 (41.0)	117 (58.5)	1 (0.5)	200 (100)	5.639, 0.039*	35 (29.2)	71 (59.2)	14 (11.6)	120 (100)	
RSPM										
Male	57 (81.4)	13 (18.6)	0 (0)	70 (100)		4 (33.3)	5 (41.7)	3 (25)	12 (100)	2.873, 0.328
Female	118 (90.8)	12 (9.2)	0 (0)	130 (100)	3.630, 0.073	1 (9.1)	4 (36.4)	6 (54.5)	11 (100)	
Total	175 (87.5)	25 (12.5)	0 (0)	200 (100)		5 (21.8)	9 (39.1)	9 (39.1)	25 (100)	
LSPM										
Male	59 (84.3)	10 (14.3)	1 (1.4)	70 (100)		1 (11.1)	5 (55.6)	3 (33.3)	9 (100)	0.413, 0.850
Female	118 (90.8)	11 (8.5)	1 (0.8)	130 (100)		2 (16.6)	5 (41.7)	5 (41.7)	12 (100)	
Total	177 (88.5)	21 (10.5)	2 (1.0)	200 (100)	1.884, 0.367	3 (14.3)	10 (47.6)	8 (38.1)	23 (100)	

Values are presented as number (%).
RFPM, right maxillary first premolar; LFPM, left maxillary first premolar; RSPM, right maxillary second premolar; LSPM, left maxillary second premolar.
[a]Calculated among teeth with ≥2 roots only.
*$p < 0.05$, statistically significant.

ly significant for either RSPM or LSPM ($p \geq 0.05$).

3. Bifurcation location

In RFPM, most buccal and palatal root bifurcations were located in the middle third of the roots (56.3%), followed by the coronal and apical thirds (31.1% and 12.6%), respectively. Similarly, in LFPM, bifurcations were mainly found in the middle third of the roots (59.2%), followed by the coronal (29.2%) and apical thirds (11.6%). In RSPM, bifurcations were equally common in the middle and apical thirds (39.1%), followed by the coronal third (21.8%). In LSPM, bifurcations were most common in the middle third (47.6%), then the apical third (38.1%), and least common in the coronal third (14.3%). No association was found between root bifurcation level and sex ($p > 0.05$).

Canal configuration by sex: Vertucci's classifications (Table 2)

1. Maxillary first premolars

In both RFPM and LFPM, type IV was the most common canal configuration, seen in 65.0% and 67.0% of cases, respectively. Type V followed at 13.5% in RFPM and 12.5% in LFPM. In RFPM, types II and III were found in 7.5% and 6.0% of cases, respectively, while type I was slightly less common at 5.5%. Rare configurations included types VII and VIII, appearing in only 2.0% and 0.5% of cases, respectively, and type VI was not observed at all. In LFPM, types I and II accounted for 7.5% and 8.0%, respectively, while type III was slightly less frequent at 4.0%. The rarest configurations included types VI and VIII, each appearing in only 0.5% of cases, with type VII not observed at all. The association between canal configurations based on Vertucci and sex was not significant.

2. Maxillary second premolars

In both RSPM and LSPM, the most prevalent Vertucci's classification was type I (44.0% in RSPM, 49.0% in LSPM), followed by type V (22.5% in RSPM, 23.0% in LSPM). Less common types included type IV (16.0% in RSPM, 12.0% in LSPM) and type III (13.0% in RSPM, 9.0% in LSPM). Rare types included type II (3.0% in both RSPM and LSPM). The least frequent types in RSPM

Table 2. Maxillary premolars distribution by sex according to Vertucci's classification

Sex	Type I (1)	Type II (2-1)	Type III (1-2-1)	Type IV (2-2)	Type V (1-2)	Type VI (2-1-2)	Type VII (1-2-1-2)	Type VIII (3-3)	Total	Pearson χ^2, *p*-value
RFPM										
Male	4 (5.7)	5 (7.1)	1 (1.4)	51 (72.9)	6 (8.6)	0 (0)	2 (2.9)	1 (1.4)	70 (100)	8.992, 0.158
Female	7 (5.4)	10 (7.7)	11 (8.5)	79 (60.8)	21 (16.2)	0 (0)	2 (1.5)	0 (0)	130 (100)	
Total	11 (5.5)	15 (7.5)	12 (6.0)	130 (65.0)	27 (13.5)	0 (0)	4 (2.0)	1 (0.5)	200 (100)	
LFPM										
Male	3 (4.3)	4 (5.7)	2 (2.9)	53 (75.7)	7 (10.0)	0 (0)	0 (0)	1 (1.4)	70 (100)	6.693, 0.339
Female	12 (9.2)	12 (9.2)	6 (4.6)	81 (60.4)	18 (13.8)	1 (0.8)	0 (0)	0 (0)	130 (100)	
Total	15 (7.5)	16 (8.0)	8 (4.0)	134 (67.0)	25 (12.5)	1 (0.5)	0 (0)	1 (0.5)	200 (100)	
RSPM										
Male	26 (37.1)	4 (5.7)	6 (8.6)	15 (21.4)	16 (22.9)	1 (1.4)	2 (2.9)	0 (0)	70 (100)	12.981, 0.029*
Female	62 (47.7)	2 (1.5)	20 (15.4)	17 (13.1)	29 (22.3)	0 (0)	0 (0)	0 (0)	130 (100)	
Total	88 (44.0)	6 (3.0)	26 (13.0)	32 (16.0)	45 (22.5)	1 (0.5)	2 (1.0)	0 (0)	200 (100)	
LSPM										
Male	30 (42.9)	5 (7.1)	3 (4.3)	11 (15.7)	17 (24.3)	2 (2.9)	1 (1.4)	1 (1.4)	70 (100)	13.075, 0.053
Female	68 (52.3)	1 (0.8)	15 (11.5)	13 (10.0)	29 (22.3)	3 (2.3)	0 (0)	1 (0.8)	130 (100)	
Total	98 (49.0)	6 (3.0)	18 (9.0)	24 (12.0)	46 (23.0)	5 (2.5)	1 (0.5)	2 (1.0)	200 (100)	

Values are presented as number (%).
RFPM, right maxillary first premolar; LFPM, left maxillary first premolar; RSPM, right maxillary second premolar; LSPM, left maxillary second premolar.
*$p < 0.05$, statistically significant.

were type VII (1.0%), type VI (0.5%), and no cases of type VIII. In LSPM, type VI (2.5%), type VIII (1.0%), and type VII (0.5%) were the least common.

A significant association between sex and Vertucci's classification was found in RSPM ($p = 0.029$) but not in LSPM ($p = 0.053$).

Canal configuration by sex: Ahmed's classification (Table 3)

1. Maxillary first premolars

In both right (RFPM) and left first premolars (LFPM), the most common canal configuration was ^{2}MP B^{1} P^{1} (58.0% in RFPM, 56.0% in LFPM), followed by ^{1}MP$^{1-2}$ (12.5% in RFPM, 11.5% in LFPM). Other configurations, such as ^{1}MP$^{2-1}$, ^{1}MP^{2}, ^{1}MP^{1}, and ^{1}MP^{1-2-1}, were observed with percentages ranging from 4.5% to 9.0%. Rare types included ^{1}MP$^{1-2-1-2}$, ^{2}MP ^{1}B^{1} P^{1}, and ^{3}MP ^{1}(MB^{1} DB^{1}) P^{1}, with none of the cases exhibiting ^{1}MP^{2-1-2} in RFPM or ^{1}MP$^{1-2-1-2}$ in LFPM. There was no significant sex association with Ahmed's classification for RFPM ($p = 0.064$) or LFMP ($p = 0.446$).

2. Maxillary second premolars

In both RSPM and LSPM, the most common canal configuration was ^{1}MP^{1} (44.0% in RSPM, 49.0% in LSPM), followed by ^{1}MP$^{1-2}$ (18.0% in RSPM, 20.0% in LSPM) and ^{1}MP^{1-2-1} (13.0% in RSPM, 9.5% in LSPM). Less prevalent types included ^{2}MP B^{1} P^{1} and ^{1}MP^{2}, with rare configurations like ^{1}MP$^{2-1}$, ^{1}MP^{2-1-2}, and ^{1}MP$^{1-2-1-2}$, while ^{3}MP ^{1}(MB^{1} DB^{1}) P^{1} was either absent or very rare. The association between sex and Ahmed's classification was statistically significant for both sides, with $p = 0.0381$ for RSPM and $p = 0.023$ for LSPM.

Canal configuration by age: Vertucci's classification (Table 4)

When analyzing Vertucci's classification of maxillary first premolars across different age groups, no statistically significant association with age was found. Type IV is the most common among all age groups for both RFPM and LFPM, with the highest prevalence observed in the 13–24-year age group (66.4% for RFPM and 64.9% for LFPM). All other types of Vertucci's classification were also observed, except for type VI (Table 4).

Similarly, when examining Vertucci's classification of maxillary second premolars across different age groups, no statistically significant association was found with age. Type I is the most common among all age groups

https://doi.org/10.5395/rde.2026.51.e11

Table 3. Maxillary premolars distribution by sex according to Ahmed's classification

Sex	$^{1}MP^{1}$	$^{1}MP^{2-1}$	$^{1}MP^{1-2-1}$	$^{1}MP^{2}$	$^{1}MP^{1-2}$	$^{1}MP^{2-1-2}$	$^{1}MP^{1-2-1-2}$	$^{2}MP\ B^{1}\ P^{1}$	$^{2}MP\ ^{1}B^{1}\ P^{1}$	$^{3}MP\ ^{1}(MB^{1}\ DB^{1})\ P^{1}$	Total	Pearson χ^2, *p*-value
RFPM												
Male	4 (5.7)	5 (7.1)	1 (1.4)	2 (2.9)	5 (7.1)	0 (0)	2 (2.9)	49 (70.0)	1 (1.4)	1 (1.4)	70 (100)	14.016, 0.064
Female	7 (5.4)	10 (7.7)	11 (8.5)	12 (9.2)	20 (15.4)	0 (0)	2 (1.5)	67 (51.5)	1 (0.8)	0 (0)	130 (100)	
Total	11 (5.5)	15 (7.5)	12 (6.0)	14 (7.0)	25 (12.5)	0 (0)	4 (2.0)	116 (58.0)	2 (1.0)	1 (0.5)	200 (100)	
LFPM												
Male	3 (4.3)	4 (5.7)	2 (2.9)	5 (7.1)	8 (11.4)	0 (0)	0 (0)	46 (65.7)	1 (1.4)	1 (1.4)	70 (100)	7.951, 0.446
Female	12 (9.2)	12 (9.2)	7 (5.4)	13 (10.0)	15 (11.5)	1 (0.8)	0 (0)	66 (50.8)	4 (3.1)	0 (0)	130 (100)	
Total	15 (7.5)	16 (8.0)	9 (4.5)	18 (9.0)	23 (11.5)	1 (0.5)	0 (0)	112 (56.0)	5 (2.5)	1 (0.5)	200 (100)	
RSPM												
Male	26 (37.1)	4 (5.7)	6 (8.6)	7 (10.0)	11 (15.7)	1 (1.4)	2 (2.9)	11 (15.7)	2 (2.9)	0 (0)	70 (100)	15.341, 0.038*
Female	62 (47.7)	2 (1.5)	20 (15.4)	9 (6.9)	25 (19.2)	0 (0)	0 (0)	11 (8.5)	1 (0.8)	0 (0)	130 (100)	
Total	88 (44.0)	6 (3.0)	26 (13.0)	16 (8.0)	36 (18.0)	1 (0.5)	2 (1.0)	22 (11.0)	3 (1.5)	0 (0)	200 (100)	
LSPM												
Male	30 (42.9)	5 (7.1)	3 (4.3)	2 (2.9)	16 (22.9)	2 (2.9)	1 (1.4)	10 (14.3)	0 (0)	1 (1.4)	70 (100)	17.932, 0.023*
Female	68 (52.3)	1 (0.8)	16 (12.3)	6 (4.6)	24 (18.5)	3 (2.3)	0 (0)	8 (6.2)	3 (2.3)	1 (0.8)	130 (100)	
Total	98 (49.0)	6 (3.0)	19 (9.5)	8 (4.0)	40 (20.0)	5 (2.5)	1 (0.5)	18 (9.0)	3 (1.5)	2 (1.0)	200 (100)	

Values are presented as number (%).
RFPM, right maxillary first premolar; LFPM, left maxillary first premolar; RSPM, right maxillary second premolar; LSPM, left maxillary second premolar.
*$p < 0.05$, statistically significant.

for both RSPM and LSPM, with the highest prevalence observed in the 13–24- and 25–34-year age groups (43.3% for RSPM and 50% for LSPM). Among patients aged 55 years or older, there was an equal distribution of types I, II, and IV (33.3% each) in LSPM. All other types of Vertucci's classification were also observed.

Canal configuration by age: Ahmed's classification (Table 5)

For the maxillary first premolars, the most prevalent root and canal configuration was $^{2}MP\ B^{1}\ P^{1}$ across all age groups, with a total of $n = 228/400$ (57.0%), followed by $^{1}MP^{1-2}$ with total $n = 48/400$ (12.0%). The association between age and Ahmed's classification was not statistically significant on either the right or left side ($p > 0.05$).

For the maxillary second premolar, the most prevalent configuration across all age groups was $^{1}MP^{1}$, comprising 186/400 (46.5%), followed by $^{1}MP^{1-2}$, which accounted for 75/400 (19.0%). The association between age and Ahmed's classification was statistically insignificant for both the right and left ($p > 0.05$) sides.

Levels of merging and divergence of canals (Table 6)

The levels of merging and diverging of canals are summarized in Table 6. In the $^{1}MP^{2-1}$ configuration, canal merging occurred at the middle of the root for both RFPM and LFPM, while in the apical third in RSPM and LSPM. There was no statistical significance in the level of merging across the teeth.

For the $^{1}MP^{1-2}$ configuration, the divergence occurred at the middle of the root for RSPM and LSPM, whereas divergence occurred apically for RFPM and LFPM. Again, there was no significant difference in divergence levels across all teeth ($p > 0.05$).

In all right and left maxillary premolars, merging and diverging of the canals having the configuration $^{1}MP^{2-1-2}$ occurred at the middle and apical levels, respectively; however, this was not statistically significant ($p > 0.05$).

In canals with $^{1}MP^{1-2-1-2}$ configuration, divergence occurred at the coronal level, merging at the middle root level, and divergence again at the apical root, which was observed only in right-side teeth. The apical divergence in this configuration was statistically significant ($p < 0.001$).

DISCUSSION

Root canal treatment failure, especially in posterior

Table 4. Maxillary premolars distribution by age according to Vertucci's classification

Age (yr)	Type I (1-1)	Type II (2-1)	Type III (1-2-1)	Type IV (2-2)	Type V (1-2)	Type VI (2-1-2)	Type VII (1-2-1-2)	Type VIII (3-3)	Total	Pearson χ^2, *p*-value
RFPM										
13–24	6 (4.5)	7 (5.2)	10 (7.5)	89 (66.4)	18 (13.4)	0 (0)	4 (3.0)	0 (0)	134 (100)	19.179, 0.742
25–34	3 (6.8)	5 (11.4)	1 (2.3)	28 (63.6)	6 (13.6)	0 (0)	0 (0)	1 (2.3)	44 (100)	
35–44	1 (8.3)	2 (16.7)	0 (0)	8 (66.7)	1 (8.3)	0 (0)	0 (0)	0 (0)	12 (100)	
45–54	1 (14.3)	0 (0)	1 (14.3)	3 (42.9)	2 (28.6)	0 (0)	0 (0)	0 (0)	7 (100)	
≥55	0 (0)	1 (33.3)	0 (0)	2 (66.7)	0 (0)	0 (0)	0 (0)	0 (0)	3 (100)	
Total	11 (5.5)	15 (7.5)	12 (6.0)	130 (65.0)	27 (13.5)	0 (0)	4 (2.0)	1 (0.5)	200 (100)	
LFPM										
13–24	10 (7.5)	9 (6.7)	5 (3.7)	87 (64.9)	21 (15.7)	0 (0)	1 (0.7)	1 (0.7)	134 (100)	15.846, 0.894
25–34	2 (4.5)	4 (9.1)	3 (6.8)	33 (75.0)	2 (4.5)	0 (0)	0 (0)	0 (0)	44 (100)	
35–44	1 (8.3)	1 (8.3)	0 (0)	9 (75.0)	1 (8.3)	0 (0)	0 (0)	0 (0)	12 (100)	
45–54	2 (28.6)	1 (14.3)	0 (0)	3 (42.9)	1 (14.3)	0 (0)	0 (0)	0 (0)	7 (100)	
≥55	0 (0)	1 (33.3)	0 (0)	2 (66.7)	0 (0)	0 (0)	0 (0)	0 (0)	3 (100)	
Total	15 (7.5)	16 (8.0)	8 (4.0)	134 (67.0)	25 (12.5)	0 (0)	1 (0.5)	1 (0.5)	200 (100)	
RSPM										
13–24	58 (43.3)	0 (0)	16 (11.9)	25 (18.7)	32 (23.9)	1 (0.7)	2 (1.5)	0 (0)	134 (100)	23.953, 0.465
25–34	18 (40.9)	4 (9.1)	8 (18.2)	6 (13.6)	8 (18.2)	0 (0)	0 (0)	0 (0)	44 (100)	
35–44	6 (50.0)	1 (8.3)	1 (8.3)	0 (0)	4 (33.3)	0 (0)	0 (0)	0 (0)	12 (100)	
45–54	4 (57.1)	1 (14.3)	1 (14.3)	0 (0)	1 (14.3)	0 (0)	0 (0)	0 (0)	7 (100)	
≥55	2 (66.7)	0 (0)	0 (0)	1 (33.3)	0 (0)	0 (0)	0 (0)	0 (0)	3 (100)	
Total	88 (44.0)	6 (3.0)	26 (13.0)	32 (16.0)	45 (22.5)	1 (0.5)	2 (1)	0 (0)	200 (100)	
LSPM										
13–24	67 (50.0)	2 (1.5)	10 (7.5)	19 (14.2)	34 (25.4)	1 (0.7)	0 (0)	1 (0.7)	134 (100)	41.246, 0.051
25–34	22 (50.0)	3 (6.8)	4 (9.1)	4 (9.1)	7 (15.9)	2 (4.5)	1 (2.3)	1 (2.3)	44 (100)	
35–44	4 (33.3)	0 (0)	3 (25.0)	0 (0)	3 (25.0)	2 (16.7)	0 (0)	0 (0)	12 (100)	
45–54	4 (57.1)	0 (0)	1 (14.3)	0 (0)	2 (28.6)	0 (0)	0 (0)	0 (0)	7 (100)	
≥55	1 (33.3)	1 (33.3)	0	1 (33.3)	0 (0)	0 (0)	0 (0)	0 (0)	3 (100)	
Total	98 (49.0)	6 (3.0)	18 (9.0)	24 (12.0)	46 (23.0)	5 (2.5)	1 (0.5)	2 (1)	200 (100)	

Values are presented as number (%).
RFPM, right maxillary first premolar; LFPM, left maxillary first premolar; RSPM, right maxillary second premolar; LSPM, left maxillary second premolar

teeth such as molars and premolars, can occur due to the inability to identify and disinfect canals, resulting from a lack of knowledge of internal canal anatomy [15].

Advances in radiographic technology have made CBCT an increasingly valuable tool in dentistry, resulting in significant progress in diagnosing and evaluating oral disorders [16]. Numerous studies have demonstrated greater accuracy in identifying additional canals with CBCT than with conventional intraoral radiography [17,18].

This study investigated the root and canal morphology of maxillary premolars in a Jordanian subpopulation using CBCT, using two systems: Vertucci's and Ahmed's classifications [4,5].

Our study revealed a higher prevalence of two-rooted maxillary first premolars (Table 1), consistent with a previous study among the Jordanian population, which found that 63.2% of the studied teeth had two roots [6]. This result was consistent across both RFPM (59.0%) and LFPM (58.5%), indicating symmetry. Similarly, results from other populations have shown a high prevalence of double-rooted teeth, as in the Egyptian population (53.1%) [11] and the South African population (54.1%) [19]. The effect of sex was statistically significant (Table 1), with females having a relatively high likelihood of having a single-rooted maxillary first premolar (RFPM, 47.7% and LFPM, 46.2%), whereas this was not the case for males (RFPM, 27.1% and LFPM, 31.4%). This finding is somewhat comparable to that of Al-Zubaidi *et al.* [20], who reported that women had a high-

https://doi.org/10.5395/rde.2026.51.e11

Table 5. Maxillary premolars distribution by age according to Ahmed's classification

Age (yr)	$^{1}MP^{1}$	$^{1}MP^{2-1}$	$^{1}MP^{1-2-1}$	$^{1}MP^{2}$	$^{1}MP^{1-2}$	$^{1}MP^{2-1-2}$	$^{1}MP^{1-2-1-2}$	$^{2}MP\ B^{1}\ P^{1}$	$^{2}MP\ ^{1}B^{1}\ P^{1}$	$^{3}MP\ ^{1}$ ($MB^{1}\ DB^{1}$) P^{1}	Total	Pearson χ^2, *p*-value
RFPM												
13–24	6 (4.5)	7 (5.2)	10 (7.5)	11 (8.2)	18 (13.4)	0 (0)	4 (3.0)	77 (57.5)	1 (0.7)	0 (0)	134 (100)	31.991, 0.467
25–34	3 (6.8)	5 (11.4)	1 (2.3)	1 (2.3)	5 (11.4)	0 (0)	0 (0)	28 (63.6)	0 (0)	1 (2.3)	44 (100)	
35–44	1 (8.3)	2 (16.7)	0 (0)	2 (16.7)	0 (0)	0 (0)	0 (0)	6 (50.0)	1 (8.3)	0 (0)	12 (100)	
45–54	1 (14.3)	0 (0)	1 (14.3)	0 (0)	2 (28.6)	0 (0)	0 (0)	3 (42.9)	0 (0)	0 (0)	7 (100)	
≥55	0 (0)	1 (33.3)	0 (0)	0 (0)	0 (0)	0 (0)	0 (0)	2 (66.7)	0 (0)	0 (0)	3 (100)	
Total	11 (5.5)	15 (7.5)	12 (6.0)	14 (7.0)	25 (12.5)	0 (0)	4 (2.0)	116 (58.0)	2 (1.0)	1 (0.5)	200 (100)	
LFPM												
13–24	10 (7.5)	8 (6.0)	6 (4.5)	8 (6)	20 (14.9)	0 (0)	1 (0.7)	76 (56.7)	4 (3.0)	1 (0.7)	134 (100)	31.261, 0.504
25–34	2 (4.5)	5 (11.4)	3 (6.8)	5 (11.4)	2 (4.5)	0 (0)	0 (0)	27 (61.4)	0 (0)	0 (0)	44 (100)	
35–44	1 (8.3)	1 (8.3)	0 (0)	4 (33.3)	0 (0)	0 (0)	0 (0)	5 (41.7)	1 (8.3)	0 (0)	12 (100)	
45–54	2 (28.6)	1 (14.3)	0 (0)	1 (14.3)	1 (14.3)	0 (0)	0 (0)	2 (28.6)	0 (0)	0 (0)	7 (100)	
≥55	0 (0)	1 (33.3)	0 (0)	0 (0)	0 (0)	0 (0)	0 (0)	2 (66.7)	0 (0)	0 (0)	3 (100)	
Total	15 (7.5)	16 (8.0)	9 (4.5)	18 (9.0)	23 (11.5)	0 (0)	1 (0.5)	112 (56.0)	5 (2.5)	1 (0.5)	200 (100)	
RSPM												
13–24	58 (43.3)	0 (0)	16 (11.9)	12 (9.0)	26 (19.4)	0 (0)	1 (0.7)	2 (1.5)	17 (12.7)	2 (1.5)	134 (100)	24.609, 0.822
25–34	18 (40.9)	4 (9.1)	8 (18.2)	3 (6.8)	6 (13.6)	0 (0)	0 (0)	0 (0)	4 (9.1)	1 (2.3)	44 (100)	
35–44	6 (50.0)	1 (8.3)	1 (8.3)	1 (8.3)	3 (25.0)	0 (0)	0 (0)	0 (0)	0 (0)	0 (0)	12 (100)	
45–54	4 (57.1)	1 (14.3)	1 (14.3)	0	1 (14.3)	0 (0)	0 (0)	0 (0)	0 (0)	0 (0)	7 (100)	
≥55	2 (66.7)	0 (0)	0 (0)	0 (0)	0 (0)	0 (0)	0 (0)	0 (0)	1 (33.3)	0 (0)	3 (100)	
Total	88 (44.0)	6 (3.0)	26 (13.0)	16 (8.0)	36 (18.0)	0 (0)	1 (0.5)	2 (1.0)	22 (11.0)	3 (1.5)	200 (100)	
LSPM												
13–24	67 (50.0)	2 (1.5)	11 (8.2)	5 (3.7)	28 (20.9)	1 (0.7)	0 (0)	16 (11.9)	3 (2.2)	1 (0.7)	134 (100)	48.785, 0.076
25–34	22 (50.0)	3 (6.8)	4 (9.1)	2 (4.5)	7 (15.9)	2 (4.5)	1 (2.3)	2 (4.5)	0 (0)	1 (2.3)	44 (100)	
35–44	4 (33.3)	0 (0)	3 (25.0)	0 (0)	3 (25.0)	2 (16.7)	0 (0)	0 (0)	0 (0)	0 (0)	12 (100)	
45–54	4 (57.1)	0 (0)	1 (14.3)	0 (0)	2 (28.6)	0 (0)	0 (0)	0 (0)	0 (0)	0 (0)	7 (100)	
≥55	1 (33.3)	1 (33.3)	0 (0)	1 (33.3)	0 (0)	0 (0)	0 (0)	0 (0)	0 (0)	0 (0)	3 (100)	
Total	98 (49.0)	6 (3.0)	19 (9.5)	8 (4.0)	40 (20.0)	5 (2.5)	1 (0.5)	18 (9.0)	3 (1.5)	2 (1.0)	200 (100)	

Values are presented as number (%).
RFPM, right maxillary first premolar; LFPM, left maxillary first premolar; RSPM, right maxillary second premolar; LSPM, left maxillary second premolar.

er prevalence of single-rooted first premolars than men (56.5% vs 29.3%), whereas men exhibited a higher prevalence of double-rooted maxillary first premolars than women (67.2% vs 51.1%). In addition to this, although a three-rooted Maxillary first premolar is rare to be found (Table 1), it still needs to be considered, especially in males (0.5% for both RFPM and LFPM). The finding appears comparable to the pattern reported by Olczak *et al.* [21], who also observed a higher prevalence in males than in females (4.1% vs 1.5%), with similar frequencies on the right and left sides (2.8% and 2.3%, respectively).

It is crucial to understand the degree of root bifurcation in maxillary premolars, as it has both anatomical and clinical implications [11]. In the present study, the bifurcation level in the first premolar in more than half of the cases was in the middle third of the roots (57.8%) (Table 1), with comparable results in both RFPM (56.3%) and LFPM (59.3%), followed by the coronal third level (29.95%), with no sex difference significance. These results align with the findings of Saber *et al.* [11], who found that 78.9% of Egyptians had middle-level bifurcation. In contrast, Olczak *et al.* [21] recorded a higher incidence of bifurcation in the coronal third of the root (44.2%) in the Polish population, followed by the middle third (40.5%). Furthermore, they observed a statistically significant sex difference, with a higher incidence of the coronal bifurcation in males and a higher incidence of the middle bifurcation in females [21]. This variation might reflect racial disparities in root canal morphology, as highlighted in numerous previous studies [1]. Clini-

Table 6. ANOVA and independent t-test to compare the levels of merging and divergence of canals (mm)

Variable	$^{1}MP^{2-1}$ Level of merging	$^{1}MP^{1-2}$ Level of divergence	$^{1}MP^{2-1-2}$ Level of merging/divergence	$^{1}MP^{1-2-1}$ Level of divergence/merging	$^{1}MP^{1-2-1-2}$ Level of divergence/merging/divergence
RFPM	5.78 ± 0.922 (middle)	6.27 ± 1.35 (apical)	4.81 ± 1.44/8.81 ± 1.46 (middle/apical)	4.81 ± 1.44/8.81 ± 1.46 (middle/apical)	4.03 ± 0.577/7.49 ± 0.12/8.46 ± 0.11 (coronal/middle/apical)
LFPM	5.76 ± 1.270 (middle)	6.52 ± 1.12 (apical)	4.43 ± 1.22/7.72 ± 1.78 (middle/apical)	4.43 ± 1.22/7.72 ± 1.78 (middle/apical)	-
RSPM	8.03 ± 1.616 (apical)	5.47 ± 1.68 (middle)	5.11 ± 1.56/8.10 ± 1.42 (middle/apical)	5.11 ± 1.56/8.10 ± 1.42 (middle/apical)	5.84 ± 0.586/7.93 ± 0.04/9.36 ± 1.29 (coronal/middle/apical)
LSPM	7.95 ± 0.924 (apical)	4.98 ± 1.74 (middle)	4.09 ± 1.00/7.34 ± 1.54 (middle/apical)	4.09 ± 1.00/7.34 ± 1.54 (middle/apical)	-
p-value	0.945	0.182	0.126/0.078	0.126/0.078	0.972/0.299/<0.001[a]*

Values are presented as mean ± standard deviation (mm).
ANOVA, analysis of variance; RFPM, right maxillary first premolar; LFPM, left maxillary first premolar; RSPM, right maxillary second premolar; LSPM, left maxillary second premolar.
[a]Independent *t*-test. *$p < 0.05$, statistically significant.

cally, the bifurcation level may affect the complexity of endodontic treatment; hence, the operating microscope often enables clinicians to directly observe the site where the main canal divides into two or three branches, as well as the alignment of the canal orifices. Nevertheless, when the furcation lies deep within the tooth, or the orifices are calcified, their detection may remain difficult, even with microscopic assistance [22].

The most prevalent canal configuration in this study, according to Vertucci's classification, was type IV (2-2) (Table 2), observed in both RFPM (65.0%) and LFPM (67.0%), and a similarly high prevalence of type IV configuration has been reported across various populations [11,19,21,23]. These findings are somewhat aligned with those of Awawdeh *et al.*[6], in the Jordanian population, type IV was also identified as the most prevalent configuration in maxillary first premolars with two canals, with a reported incidence of 79.7%. However, their study, conducted on 600 extracted teeth, neither assessed the association between age and sex nor considered symmetry [6]. In contrast, the current study incorporated these variables. Furthermore, Awawdeh *et al.* [6] reported no examples of type III, VI, or VII canals in maxillary first premolars. In the present study, type III canals were observed in a few cases, while types VI, VII, and VIII were observed rarely, with seven, seven, and four occurrences, respectively (Table 2). This enhanced detection is likely due to the use of CBCT imaging, which provides more detailed insights into canal morphology than earlier techniques.

This is the first study to use Ahmed's classification among Jordanians. Type ^{2}MP B^{1} P^{1} had the highest prevalence in both RFPM and LFPM (58.0% and 56.0%, respectively), with no significant differences by sex or age (Tables 3 and 5). This is in line with research by Saber *et al.* [11] and Buchanan *et al.* [19], which also revealed that ^{2}MP B^{1} P^{1} had the highest prevalence (52.5% and 52.53%, respectively).

Using Ahmed's classification, 10 different root canal configuration types were identified among right and left side first maxillary premolars, showing a detailed canal configuration within the root, which confirms the aim of this new classification. Different configurations based on this classification were identified, highlighting the canal's divergence and merging levels. The loca-

https://doi.org/10.5395/rde.2026.51.e11

tion of canal divergence and merging is critical during root canal treatment, as detecting a divergence in the middle and apical thirds of the root is difficult, challenging, and may be missed [13]. For example, within the single-rooted premolars, a rare occurrence of canal divergence, followed by merging, and then again divergence was found, as indicated by code $^{1}MP^{1-2-1-2}$, which might have been missed in previous classifications. Similarly, in two-rooted premolars, the code $^{2}MP\ B^{1}\ P^{1}$ denotes a separate canal in each root, whereas $^{2}MP\ ^{1}B^{1}\ P^{1}$ describes a canal originating from the pulp chamber that bifurcates into two canals, one within each root. Such examples illustrate the greater descriptive capacity of Ahmed's system, which, when combined with CBCT imaging, provides precise characterization of complex canal patterns.

Regarding maxillary second premolars, the results of this study showed a high prevalence of single-rooted maxillary second premolars with a percentage of 88% (87.5 % in RSPM, 88.5% in LSPM), with no association between sex and number of roots (Table 1). This finding is comparable to a previous study of the Jordanian population, which reported that of 217 maxillary second premolars, 120 (55.3%) had one root, 96 (44.2%) had two roots, and 1 (0.5%) had three roots. The study reported an almost double likelihood of females having single-rooted premolars compared to those with double-rooted ones (64% vs 36%), whereas in males, the likelihood of having double-rooted premolars is higher than that of having single-rooted ones (51.2% vs 49.9%). Additionally, three-rooted premolars were very rare, occurring in only 0.8% of cases [7]. These results are consistent with previous studies [11,19]. A recent systematic review analyzed 16,371 maxillary premolars and reported that 84.3% had a single root, suggesting that the higher prevalence of single-rooted second premolars is likely a universal trend [1]. The study reported a prevalence of three-rooted maxillary second premolars (0.3%), comparable to our 1% prevalence, observed only in LSPM. Watanabe *et al*. [24] reported a similar rare occurrence of three-rooted maxillary second premolar among the Japanese population (0.3%).

In the less common multirooted second premolars, it is important to consider the bifurcation level. In RSPM, bifurcation occurred equally in the middle and apical thirds of the root (39.1%) and was least frequent in the coronal third level (21.8%). A comparable distribution was observed in LSPM, where bifurcation predominantly occurred in the middle third (47.6%), followed by the apical third (38.1%), and least frequently in the coronal third (14.3%) (Table 1). Saber *et al*. [11] reported that the middle third bifurcation was the most prevalent (78.5%), followed by the apical third (14%). These variations may reflect true anatomical differences between populations, as well as methodological factors, such as differences in imaging protocols, with sample size potentially contributing to the observed discrepancies.

The second maxillary premolars in this study showed a high prevalence of type I Vertucci's Classification (44% in RSPM, 49% in LSPM), followed by type V (22.5% in RSPM, 23% in LSPM) across all age groups (Table 4). This finding differs from a previous study conducted among the Jordanian population, which reported a higher prevalence of type IV at 60.8%, while type I was observed in only 13.8% [7]. Discrepancies among subpopulations may be attributed to genetic diversity, environment, and regional variations in diet and oral hygiene habits [25].

The Egyptian population also showed that type IV was the most prevalent in maxillary second premolars (44.4%), followed by type II (22.2%), with type I being less frequent (16.1%) [11]. These discrepancies across different populations may suggest that genetics plays a significant role in controlling root and canal configurations.

A significant sex effect was observed in RSPM, with females exhibiting a higher prevalence of type III than males (15.4% vs 8.6%), while males showed a higher prevalence of type IV than females (21.4% vs 13.1%). Additionally, type VII and type VI were observed in males but not in females (Table 2). These differences support the idea that maxillary second premolars exhibit considerable anatomical variation in their internal root configurations [11].

Using Ahmed's classification, the most prevalent canal configuration was $^{1}MP^{1}$ in both RSPM (44.0%) and LSPM (49.0%), among all age groups, with no significant difference between these age groups (Table 5). However, sex showed a significant difference on both sides (Table 3). While $^{2}MP\ B^{1}\ P^{1}$ and $^{1}MP^{1-2}$ are equally the

second most prevalent canal configuration in males' RSPM (15.7%), females showed a higher prevalence of $^{1}MP^{1-2}$ (19.2%) and $^{1}MP^{1-2-1}$ (15.4%) on the same side. For LSPM, the frequency of $^{1}MP^{1-2-1}$ was higher in females than in males (12.3% vs 4.3%), although the prevalence of $^{2}MP\ B^{1}\ P^{1}$ and $^{1}MP^{2-1}$ was higher in males than in females (14.3% vs 6.2% and 7.1% vs 0.8%, respectively). This aligns with findings by Algarni *et al.* [26], who also reported sex-related variation in certain Ahmed's codes on both RSPM and LSPM, with females showing higher frequencies of multi-branching patterns, such as $^{1}MP^{1-2-1}$, and males more often exhibiting $^{1}MP^{1}$ or $^{1}MP^{2-1}$ configurations. In contrast, Watanabe *et al.* [24] found no significant sex effect. These mixed results suggest that sex-related differences in canal configuration may be population-dependent rather than universal.

In this study, a significant apical level of divergence was observed in the right-side premolars of teeth with Ahmed's classification $^{1}MP^{1-2-1-2}$, with a *p*-value of <0.001 (Table 6). This is in line with a study by Martins *et al.* [13] that found that the maxillary second premolar had the highest frequency of merging root canals in the middle third and divergence in the apical third.

The findings of this investigation demonstrated consistent outcomes for the left and right sides across various parameters, highlighting possible anatomical similarities in homonymous teeth, and supporting the notion that symmetry is a universal phenomenon [1]. A previous study [27] involved 1,387 maxillary first premolars and 1,403 maxillary second premolars and found that 80.2% of the maxillary first premolars and 81.8% of the maxillary second premolars showed bilateral symmetry in the number of root canals. Furthermore, the number and shape of root canals in 72.3% of maxillary first premolars and 73.2% of maxillary second premolars displayed bilateral symmetry, underscoring the pervasive symmetry in premolar root and canal morphology. Similarly, Mashyakhy [28] found no significant differences for root number, canal number, and canal configuration between the right and left sides. Age and sex were also considered, as canal morphology can change over time due to secondary dentin deposition, apical maturation, and calcification [29], and may vary between males and females due to X-linked genetic influence [30]. Including these variables broadens the anatomical understanding and supports more informed clinical decision-making.

Utilizing CBCT in this study provided high-quality images, offering more detailed canal configurations compared to conventional radiographs. However, it is considered less accurate than micro-CT, primarily due to its lower spatial resolution and larger voxel size, which limit its ability to capture extremely fine anatomical details, such as accessory canals [31]. While this may be considered a limitation of the study, the lower radiation dose of CBCT compared to micro-CT represents a significant advantage that outweighs this limitation. Another limitation of this study is the uneven distribution of age groups, with some age categories having notably larger sample sizes than others. This imbalance may obscure potential correlations between age and specific canal configurations that are more common in older age groups.

CONCLUSIONS

Maxillary premolars in the Jordanian subpopulation showed a wide range of anatomical variations. The majority of first premolars displayed a two-rooted morphology consistent with Vertucci type IV or Ahmed $^{2}MP^{1-1}$ patterns, whereas second premolars were mainly single-rooted, corresponding to Vertucci type I or Ahmed $^{1}MP^{1}$. Applying both Vertucci's and Ahmed's classification systems in this study provided a more robust assessment of canal morphology, as Ahmed's detailed coding system captured variations that extended beyond the broader patterns defined by Vertucci. Dental practitioners need to be aware of the various possible configurations of the root and root canal to avoid missing canals, which can lead to treatment failure. Clinicians need to benefit from new radiographic advances, such as CBCT, which can improve diagnosis and treatment planning by providing a useful tool for detecting complex tooth morphology. Ahmed's classification provided a simplified, detailed canal configuration.

CONFLICT OF INTEREST

No potential conflict of interest relevant to this article was reported.

https://doi.org/10.5395/rde.2026.51.e11

FUNDING/SUPPORT

The study was supported by the Deanship of Research at Jordan University of Science and Technology, research award number 2023/161/36.

AUTHOR CONTRIBUTIONS

Conceptualization, Methodology, Formal analysis: Ba-Hattab R. Data curation: Ba-Hattab R, Taha NA, Abu Alhaija ES. Investigation: Ba-Hattab R, Shaweesh MM, Taha NA. Funding acquisition, Resources: Taha NA.
Writing - original draft: Ba-Hattab R, Shaweesh MM. Writing - review & editing: all authors. All authors have read and agreed to the published version of the manuscript.

DATA SHARING STATEMENT

The datasets used and analyzed during the current study are available from the corresponding author on reasonable request.

REFERENCES

1. Xu M, Ren H, Liu C, Zhao X, Li X. Systematic review and meta-analysis of root morphology and canal configuration of permanent premolars using cone-beam computed tomography. BMC Oral Health 2024;24:656.
2. Vertucci FJ. Root canal morphology and its relationship to endodontic procedures. Endod Topics 2005;10:3-29.
3. Weine F. Endodontic therapy. 6th ed. St. Louis: Mosby; 2003. pp. 106-110.
4. Vertucci FJ. Root canal anatomy of the human permanent teeth. Oral Surg Oral Med Oral Pathol 1984;58:589-599.
5. Ahmed HM, Versiani MA, De-Deus G, Dummer PM. A new system for classifying root and root canal morphology. Int Endod J 2017;50:761-770.
6. Awawdeh L, Abdullah H, Al-Qudah A. Root form and canal morphology of Jordanian maxillary first premolars. J Endod 2008;34:956-961.
7. Al-Ghananeem MM, Haddadin K, Al-Khreisat AS, Al-Weshah M, Al-Habahbeh N. The number of roots and canals in the maxillary second premolars in a group of Jordanian population. Int J Dent 2014;2014:797692.
8. Patel S, Dawood A, Whaites E, Pitt Ford T. New dimensions in endodontic imaging: part 1: conventional and alternative radiographic systems. Int Endod J 2009;42:447-462.
9. Almeida JC, Candemil AP, Bertolini GR, Souza-Gabriel AE, Cruz-Filho AM, Sousa-Neto MD, *et al.* Cone-beam computed tomographic evaluation of the root canal anatomy of the lower premolars and molars in a Brazilian sub-population. Imaging Sci Dent 2023;53:77-82.
10. Jung YH, Hwang JJ, Lee JS, Cho BH. Analysis of root number and canal morphology of maxillary premolars using cone-beam computed tomography. Imaging Sci Dent 2024;54:370-380.
11. Saber SE, Ahmed MH, Obeid M, Ahmed HM. Root and canal morphology of maxillary premolar teeth in an Egyptian subpopulation using two classification systems: a cone beam computed tomography study. Int Endod J 2019;52:267-278.
12. von Elm E, Altman DG, Egger M, Pocock SJ, Gøtzsche PC, Vandenbroucke JP. The Strengthening the Reporting of Observational Studies in Epidemiology (STROBE) statement: guidelines for reporting observational studies. Lancet 2007;370:1453-1457.
13. Martins JN, Marques D, Mata A, Caramês J. Root and root canal morphology of the permanent dentition in a Caucasian population: a cone-beam computed tomography study. Int Endod J 2017;50:1013-1026.
14. Yang L, Han J, Wang Q, Wang Z, Yu X, Du Y. Variations of root and canal morphology of mandibular second molars in Chinese individuals: a cone-beam computed tomography study. BMC Oral Health 2022;22:274.
15. Iqbal A. The factors responsible for endodontic treatment failure in the permanent dentitions of the patients reported to the College of Dentistry, the University of Aljouf, Kingdom of Saudi Arabia. J Clin Diagn Res 2016;10:ZC146-ZC148.
16. Shukla S, Chug A, Afrashtehfar KI. Role of cone beam computed tomography in diagnosis and treatment planning in dentistry: an update. J Int Soc Prev Community Dent 2017;7(Suppl 3):S125-S136.
17. G K, Singh N, Yadav R, Duhan J, Tewari S, Gupta A, *et al.* Comparative analysis of the accuracy of periapical radiography and cone-beam computed tomography for diagnosing complex endodontic pathoses using a gold standard reference: a prospective clinical study. Int Endod J 2021;54:1448-1461.
18. de Toubes KM, Côrtes MI, Valadares MA, Fonseca LC, Nunes E, Silveira FF. Comparative analysis of accessory mesial canal identification in mandibular first molars by using four different diagnostic methods. J Endod 2012;38:436-441.
19. Buchanan GD, Gamieldien MY, Tredoux S, Vally ZI. Root and canal configurations of maxillary premolars in a South African subpopulation using cone beam computed tomography and two classification systems. J Oral Sci 2020;62:93-97.
20. Al-Zubaidi SM, Almansour MI, Al Mansour NN, Alshammari

AS, Alshammari AF, Altamimi YS, *et al*. Assessment of root morphology and canal configuration of maxillary premolars in a Saudi subpopulation: a cone-beam computed tomographic study. BMC Oral Health 2021;21:397.
21. Olczak K, Pawlicka H, Szymański W. Root form and canal anatomy of maxillary first premolars: a cone-beam computed tomography study. Odontology 2022;110:365-375.
22. Albuquerque D, Kottoor J, Hammo M. Endodontic and clinical considerations in the management of variable anatomy in mandibular premolars: a literature review. Biomed Res Int 2014;2014:512574.
23. Aguilera J, Vallette M, Navarro P, Betancourt P. Root and root canal system morphology of maxillary first premolars in a Chilean subpopulation: a cone-beam computed tomography study. Int J Morphol 2022;40:449-454.
24. Watanabe S, Yabumoto S, Okiji T. Evaluation of root and root canal morphology in maxillary premolar teeth: a cone-beam computed tomography study using two classification systems in a Japanese population. J Dent Sci 2025;20:927-935.
25. Mustafa M, Batul R, Karobari MI, Alamri HM, Abdulwahed A, Almokhatieb AA, *et al*. Assessment of the root and canal morphology in the permanent dentition of Saudi Arabian population using cone beam computed and micro-computed tomography: a systematic review. BMC Oral Health 2024;24:343.
26. Algarni HA, Alonazi MA, Arshad H, Zahra F, Umer F, Maqbool I, *et al*. Comprehensive analysis of root canal morphology in maxillary premolars among the Pakistani subpopulation: a CBCT-based study. Eur J Med Res 2024;29:391.
27. Li YH, Bao SJ, Yang XW, Tian XM, Wei B, Zheng YL. Symmetry of root anatomy and root canal morphology in maxillary premolars analyzed using cone-beam computed tomography. Arch Oral Biol 2018;94:84-92.
28. Mashyakhy M. Anatomical evaluation of maxillary premolars in a Saudi population: an in vivo cone-beam computed tomography study. J Contemp Dent Pract 2021;22:284-289.
29. Karobari MI, Iqbal A, Batul R, Adil AH, Syed J, Algarni HA, *et al*. Exploring age and gender variations in root canal morphology of maxillary premolars in Saudi sub population: a cross-sectional CBCT study. BMC Oral Health 2024;24:543.
30. Martins JN, Marques D, Francisco H, Caramês J. Gender influence on the number of roots and root canal system configuration in human permanent teeth of a Portuguese subpopulation. Quintessence Int 2018;49:103-111.
31. Paes da Silva Ramos Fernandes LM, Rice D, Ordinola-Zapata R, Alvares Capelozza AL, Bramante CM, Jaramillo D, *et al*. Detection of various anatomic patterns of root canals in mandibular incisors using digital periapical radiography, 3 cone-beam computed tomographic scanners, and micro-computed tomographic imaging. J Endod 2014;40:42-45.

https://doi.org/10.5395/rde.2026.51.e11

RDE Restorative Dentistry & Endodontics

Research Article

eISSN 2234-7666
Restor Dent Endod. 2026 February;51(1):e12
https://doi.org/10.5395/rde.2026.51.e12

Bonding and fractographic characterization of universal adhesives applied to dentin in multimode strategies: an *in vitro* study

Samaa M. Morsy[1], Rim Bourgi[2,3,4,*], Louis Hardan[3], Carlos Enrique Cuevas-Suárez[5], Naji Kharouf[4,6], Ahmed A. Holiel[1,2]

[1]Department of Conservative Dentistry, Faculty of Dentistry, Alexandria University, Alexandria, Egypt
[2]Department of Restorative Sciences, Faculty of Dentistry, Beirut Arab University, Beirut, Lebanon
[3]Department of Restorative and Esthetic Dentistry, Faculty of Dental Medicine, Saint-Joseph University of Beirut, Beirut, Lebanon
[4]Department of Biomaterials and Bioengineering, INSERM UMR_S 1121, University of Strasbourg, Strasbourg, France
[5]Dental Materials Laboratory, Academic Area of Dentistry, Autonomous University of Hidalgo State, San Agustín Tlaxiaca, Mexico
[6]Department of Endodontics and Conservative Dentistry, Faculty of Dental Medicine, University of Strasbourg, Strasbourg, France

ABSTRACT

Objectives: Universal adhesives (UAs) are marketed as versatile systems for both self-etch (SE) and total-etch (TE) modes. While their bond strength has been widely investigated, evidence linking fracture characteristics to bonding performance remains limited. This study evaluated the micro-shear bond strength (μSBS) and failure patterns of three UAs applied in SE and TE modes, complemented by fractographic scanning electron microscopy (SEM) analysis.

Methods: Eighteen extracted human molars were sectioned to expose mid-coronal dentin and randomly allocated to SE or TE application. Three UAs were tested: Tetric N-Bond Universal, All-Bond Universal, and Single Bond Universal (SBU). Composite micro-rods (n = 72) were bonded, thermocycled for 500 cycles between 5°C and 55°C, and subjected to μSBS testing. Fracture surfaces were examined under SEM and classified as adhesive, cohesive, or mixed. Data were analyzed using two-way analysis of variance, Tukey *post hoc* test, and Spearman correlation (α = 0.05).

Results: In TE mode, SBU demonstrated the highest μSBS ($p < 0.001$), whereas no significant differences were observed among adhesives in SE mode ($p > 0.05$). SEM analysis revealed adhesive failures as interfacial fractures, cohesive failures with beach marks, and mixed failures involving crack propagation through both dentin and composite. Adhesive failures correlated negatively with μSBS ($r_s = -0.77$), while mixed failures correlated positively ($r_s = 0.81$).

Conclusions: Both the etching strategy and adhesive formulation significantly affect bond strength and fracture behavior. Fractographic SEM analysis provides critical insights into the mechanical reliability of UAs and informs their clinical application.

Keywords: Dentin; Dental adhesives; Dental bonding; Fractures, stress; Scanning electron microscopy; Shear strength

Received: September 14, 2025 **Revised:** December 17, 2025 **Accepted:** December 22, 2025

Citation
Morsy SM, Bourgi R, Hardan L, Cuevas-Suárez CE, Kharouf N, Holiel AA. Bonding and fractographic characterization of universal adhesives applied to dentin in multimode strategies: an *in vitro* study. Restor Dent Endod 2026;51(1):e12.

***Correspondence to**
Rim Bourgi, DDS, MSc, PhD
Department of Restorative and Esthetic Dentistry, Faculty of Dental Medicine, Saint-Joseph University of Beirut, Beirut 1107 2180, Lebanon
Email: rim.bourgi@hotmail.com

INTRODUCTION

The evolution of esthetic dental materials, paired with advancements in adhesive technology, has significantly reshaped restorative dentistry. Modern composites now offer not only lifelike color and translucency but also improved mechanical properties, allowing clinicians to restore both form and function with remarkable precision. Yet even the most visually seamless restoration depends on one critical factor: the strength and reliability of its bond to tooth structure [1].

Universal adhesives (UAs), classified as eighth-generation bonding agents, were developed to streamline adhesive procedures while maintaining clinical efficacy. Marketed as multimode systems, they promise the strength of traditional total-etch (TE) adhesives with the simplicity and reduced technique sensitivity of self-etch (SE) systems [2]. These dual capabilities make them a practical choice in daily practice, especially when both speed and performance are desired.

In laboratory settings, the micro-shear bond strength (μSBS) test has emerged as a reliable tool for evaluating dentin–adhesive interfaces. Compared to macro-shear tests, μSBS offers a more consistent stress distribution and fewer internal flaws, thanks to its smaller bonded area [3,4]. Moreover, it allows for multiple specimens to be bonded on a single tooth, optimizing the use of biological samples and enhancing data precision [5,6]. However, μSBS alone provides only a quantitative assessment of bonding performance and does not reveal the underlying mechanisms of failure. Fractographic analysis, examining the fracture surface post-debonding, has long been a cornerstone in material failure studies. This technique reveals how a material fractured, offering insight into the mode, speed, and origin of failure [7]. While clinical trials provide real-world performance data, they often fail to isolate the root causes of failure due to the oral environment's complexity. Controlled *in vitro* research, on the other hand, can focus on specific variables, making them ideal for analyzing the behavior of adhesives under different bonding conditions [8].

Despite its potential, the integration of fractographic scanning electron microscopy (SEM) analysis with μSBS testing remains largely unexplored in adhesive dentistry. Our study uniquely combines these complementary approaches to provide both quantitative and qualitative evaluation of UAs, including statistical correlation between bond strength and failure mode. Therefore, this study aims to evaluate the mechanical performance and failure characteristics of three UAs applied in both SE and TE modes, using μSBS testing and fractographic SEM analysis to gain deeper insight into adhesive behavior at the dentin interface. The null hypothesis tested is that there will be no significant difference in bond strength among the UAs when applied in SE or TE modes.

METHODS

Study design

In this *in vitro* study, 18 extracted human permanent molars were utilized. Each tooth's dentin surface was sectioned into four quadrants, with a composite cylinder bonded to each quadrant, yielding a total of 72 composite cylinders for μSBS evaluation. The sample size calculation was based on a power of 80% and $\alpha = 0.05$, in line with previous findings by El-Safty *et al.* [9]. This method enabled the testing of multiple composite cylinders on a single dentin surface, optimizing the use of extracted teeth [5]. Teeth were obtained from the Department of Oral Surgery, Faculty of Dentistry, Alexandria University, from patients aged 25 to 45 years and were extracted exclusively for periodontal reasons. Teeth presenting caries, cracks, restorations, attrition, abrasion, or erosion were excluded. Extracted teeth were thoroughly rinsed under running water, stored in a 0.01% (w/v) thymol solution at 4°C for disinfection [10], and polished using pumice and rubber cups. Specimens were subsequently stored in isotonic saline at room temperature, with the solution refreshed weekly to ensure hydration and minimize bacterial growth until testing [10].

Ethical approval was secured prior to the study by the Institutional Ethical Committee, Faculty of Dentistry, Alexandria University (No. 00010556-IORG 0008839). Informed consent agreement was obtained from all patients for undergoing an extraction treatment and for consent to the use of their teeth for research purposes.

https://doi.org/10.5395/rde.2026.51.e12

Preparation of dentin specimens

Each molar was vertically embedded in a rubber mold (14 mm internal diameter) containing auto-polymerizing acrylic resin, with 2 mm of the root left exposed beneath the cementoenamel junction (CEJ) [11]. The occlusal surfaces were sectioned with a fine-grit diamond disc under continuous water irrigation to obtain a standardized mid-coronal dentin surface and generate a uniform smear layer, closely simulating clinical conditions [12,13]. The cutting disc was replaced after every four teeth to maintain efficiency. All surface preparations were performed by the same operator to minimize variability. After flattening, the specimens were removed from the molds and inspected under a stereomicroscope (Olympus Optical Co. Ltd., Tokyo, Japan) to verify the complete elimination of enamel. The prepared dentin samples were then randomly divided into two experimental groups according to the adhesive approach: SE and TE.

Adhesive and composite application

Each main group was divided into three subgroups (n = 12 specimens per subgroup) according to the UA employed: Tetric N-Bond Universal (TNBU; Ivoclar Vivadent AG, Schaan, Liechtenstein), All-Bond Universal (ABU; Bisco Inc., Schaumburg, IL, USA), and Single Bond Universal (SBU; 3M ESPE, St. Paul, MN, USA). In total, 12 composite micro-rods were bonded per adhesive subgroup (four rods per tooth, using three molars). A summary of the UAs' characteristics is provided in Table 1 [14].

For the TE subgroups, an additional phosphoric acid etching step was carried out before adhesive application, strictly following the manufacturer's instructions. Composite micro-rods were fabricated with polyethylene tubes (2 mm in height, 0.9 mm inner diameter, 1 mm outer diameter) [5,6,9], which were filled with Filtek Z250 XT composite (3M ESPE). The tubes were placed perpendicularly onto the dentin surface and light-cured for 20 seconds using a light-emitting diode curing unit (Elipar S10; 3M ESPE) positioned directly against the surface to ensure optimal energy delivery, with an output intensity of 1,200 mW/cm² [15,16]. After polymerization, the polyethylene molds were gently removed with a No. 11 scalpel blade, leaving four bonded micro-rods per molar. All prepared specimens were stored in distilled water at 37°C for 24 hours before being subjected to thermocycling. Thermal cycling was performed in a custom-built apparatus for 500 cycles between 5°C and 55°C, with a 5-second dwell time at each bath, to simulate intraoral thermal stresses [17].

Micro-shear bond strength testing

All 72 specimens were subjected to μSBS testing using a universal testing machine (Instron 3345; Instron, Norwood, MA, USA) fitted with a 500 N load cell and operated at a crosshead speed of 0.5 mm/min. A stainless-steel orthodontic wire loop (0.14 mm in diameter)

Table 1. Universal adhesives tested in the study, with their respective manufacturers, batch number information, composition, pH, and application mode

Adhesive	Manufacturer (batch No.)	Composition	pH	Self-etch (SE) protocol	Total-etch protocol
TNBU	Ivoclar Vivadent, Schaan, Liechtenstein (Z031JT)	HEMA, Bis-GMA, ethanol, 10-MDP, methacrylated carboxylic acid polymer, camphorquinone, DMAEMA	2.5–3.0	Wash dentin 5 sec, blot dry (moist), apply 1 coat, rub 20 sec, gentle air 5 sec until a stable film forms; light cure 10 sec	Etch 15 sec, rinse 5 sec, blot dry, apply adhesive as per SE protocol
ABU	Bisco Inc., Schaumburg, IL, USA (2100005314)	HEMA, 10-MDP, Bis-GMA, ethanol	2.5–3.2	Wash dentin 5 sec, blot dry (moist), apply 2 coats, rub 20 sec, air dry 5 sec until a stable film forms; light cure 10 sec	Etch 15 sec, rinse 5 sec, blot dry, apply adhesive as per SE protocol
SBU	3M ESPE, St. Paul, MN, USA (2216500068)	HEMA, Bis-GMA, 10-MDP, 2-propenoic acid, ethanol, water, polyalkenoic acid polymer, DMAEMA, filler, camphorquinone, silane	2.7	Wash dentin 5 sec, blot dry (moist), apply 1 coat, rub 20 sec, air dry 5 sec until a stable film forms; light cure 10 sec	Etch 15 sec, rinse 5 sec, blot dry, apply adhesive as per SE protocol

TNBU, Tetric N-Bond Universal; ABU, All-Bond Universal; SBU, Single Bond Universal; HEMA, 2-hydroxyethyl methacrylate; Bis-GMA, bisphenol A glycidyl methacrylate; 10-MDP, 10-methacryloyloxydecyl dihydrogen phosphate; DMAEMA, N,N-dimethylaminoethyl methacrylate.

was carefully positioned at the base of each composite rod, in contact with the dentin surface, to apply a shear force parallel to the bonding interface (Figure 1). The μSBS values were expressed in megapascals (MPa) by dividing the maximum load at failure by the bonded surface area. Failure loads were recorded in newtons (N), and μSBS was determined using the formula '$\sigma = F/A$,' where σ represents μSBS in MPa, F is the failure load in N, and A is the bonded surface area in mm^2. The bonded surface area was calculated as $A = \pi r^2$, where $\pi = 3.14$ and r is the radius of each composite cylinder (0.9 mm) [9].

Fractographic analysis via scanning electron microscopy

Following μSBS testing, tooth roots were sectioned at the CEJ using a diamond disc under continuous water irrigation. The obtained dentin slices were gently air-dried to avoid dehydration and minimize the risk of extracting residual monomers or incompletely polymerized oligomers from the fractured surfaces [17]. Each slice was mounted on a metallic stub and sputter-coated with gold for 1 minute (JFC-1300; JEOL, Tokyo, Japan). The fracture interfaces were then analyzed under a SEM (JSM-IT200, JEOL) operated at 25 kV, with magnifications ranging from ×100 to ×1,000, for detailed characterization and documentation. Failure modes were categorized based on fracture location into four types: adhesive failure (at the adhesive–dentin or adhesive–composite interface), cohesive failure in dentin, cohesive failure in composite, and mixed failure (a combination of adhesive and cohesive). The frequency and percentage distribution of each failure mode were recorded for all groups [18].

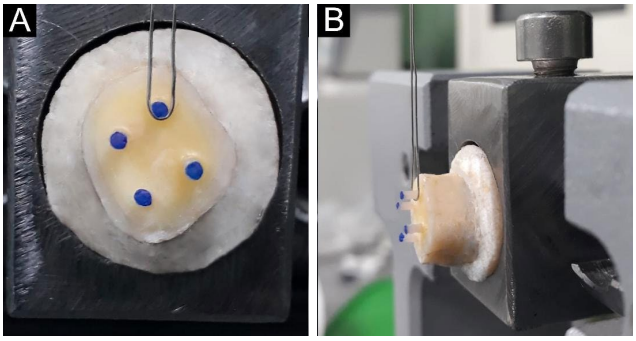

Figure 1. (A) Occlusal view of the resin cylinders. (B) Stainless-steel wire of the universal testing machine positioned perpendicular to the dentin–composite interface.

Statistical analysis

Data were analyzed using Stata/IC software ver. 13.0 (StataCorp LLC, College Station, TX, USA). Mean and standard deviation were calculated for μSBS values. Normality of the data was confirmed using the Shapiro-Wilk test. A two-way analysis of variance (ANOVA) was performed to evaluate the main effects of adhesive system (TNBU, ABU, SBU) and etching mode (SE vs TE) on μSBS, as well as their interaction. Tukey honestly significant difference test was used for pairwise comparisons. Statistical significance was set at $p < 0.05$. Bar charts were generated to illustrate group comparisons. Spearman correlation was applied to examine the association between μSBS and failure mode.

RESULTS

Micro-shear bond strength assessment

Two-way ANOVA revealed that both the adhesive system and the etching mode significantly affected μSBS (Table 2). The interaction between the adhesive system and the etching mode was significant ($p = 0.00321$). The mean μSBS values for the different adhesives under SE and TE modes are presented in Table 3. In SE mode, no significant differences were observed among TNBU, ABU, and SBU ($p > 0.05$). In TE mode, SBU exhibited significantly higher μSBS compared with TNBU and ABU ($p < 0.001$). Within-adhesive comparisons showed that SBU demonstrated a significant increase in μSBS when applied in TE versus SE mode, whereas TNBU and ABU showed no significant difference between the two etching modes.

Table 2. Two-way analysis of variance for the effects of adhesive system and etching mode on micro-shear bond strength

Source of variation	Degrees of freedom	Sum of squares	Mean squares	F	*p*-value
Etching mode (SE vs TE)	1	626.57	626.57	22.46	0.00001*
Adhesive system	2	504.35	252.17	9.04	0.00033*
Adhesive × etching interaction	2	349.84	174.92	6.27	0.00321*

F, F-statistic; SE, self-etch; TE, total-etch.
*$p < 0.05$, statistically significant.

https://doi.org/10.5395/rde.2026.51.e12

Failure analysis of debonded specimens

Fractographic evaluation of the fractured specimens showed that adhesive and mixed failures accounted for 45% of the overall failures each. Cohesive failures were observed in 10% of specimens and were limited to four subgroups. In the SE application mode, adhesive failures were more frequent, whereas in the TE mode, mixed failures were more frequent. The percentage distribution of failure modes across all subgroups is shown in Figure 2.

Correlation between the micro-shear bond strength and the failure mode

Spearman correlation analysis indicated a negative trend between adhesive failures and bond strength (r_s = –0.77), as well as a positive trend between mixed failures and bond strength (r_s = 0.81). Cohesive failures exhibited a weak positive trend with bond strength (r_s = 0.19). However, none of these associations were statistically significant ($p > 0.05$). The ABU subgroup under SE application demonstrated the lowest μSBS (12.83 ± 1.72 MPa) with a predominance of adhesive failures (80%), whereas the SBU subgroup in TE mode exhibited the highest μSBS (26.94 ± 4.22 MPa) with a higher proportion of mixed failures (80%) (Figure 3).

Table 3. Comparison of all subgroups according to micro-shear bond strength values with pairwise comparisons

Adhesive	No. of samples	SE	TE
TNBU	12	16.53 ± 6.14[a]	18.98 ± 7.84[a]
ABU	12	12.83 ± 1.72[a]	15.96 ± 3.98[a]
SBU	12	14.82 ± 5.61[a]	26.94 ± 4.22[b]

Values are presented as mean ± standard deviation.
TNBU, Tetric N-Bond Universal (Ivoclar Vivadent, Schaan, Liechtenstein); ABU, All-Bond Universal (Bisco Inc., Schaumburg, IL, USA); SBU, Single Bond Universal (3M ESPE, St. Paul, MN, USA); SE, self-etch; TE, total-etch.
Superscript letters indicate statistical differences between SE and TE modes for each adhesive (different letters mean significant difference).

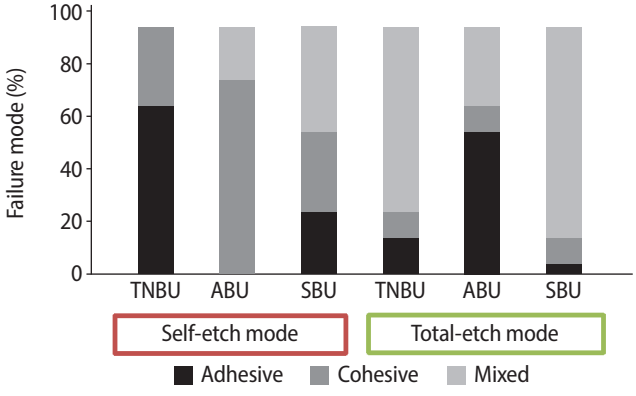

Figure 2. Percentage of failure modes in all study subgroups. TNBU, Tetric N-Bond Universal (Ivoclar Vivadent, Schaan, Liechtenstein); ABU, All-Bond Universal (Bisco Inc., Schaumburg, IL, USA); SBU, Single Bond Universal (3M ESPE, St. Paul, MN, USA).

Fractographic analysis using scanning electron microscopy

Fractured composite–dentin interfaces were first examined under SEM at low magnification (×100) to locate relevant regions, followed by imaging of selected areas at higher magnifications (up to ×1,000). The analysis identified distinct morphological patterns: adhesive failures were marked by exposed dentin partially covered with residual adhesive; cohesive failures exhibited beach mark features within either dentin or composite; and mixed failures extended across the adhesive layer into both substrates, frequently presenting wavy fracture surfaces and arrest lines, suggestive of progressive crack propagation (Figures 4–6).

DISCUSSION

The μSBS test has been advocated as a reliable method for evaluating dentin–adhesive performance, providing more uniform stress distribution and fewer internal defects than macro-shear testing due to its smaller bonded area [19,20]. In this study, the null hypothesis was partially rejected. SBU exhibited significantly higher μSBS in TE mode compared to SE mode, whereas TNBU and ABU demonstrated comparable bond strengths across both strategies. This indicates that the influence of phosphoric acid etching depends on adhesive composition. The enhanced performance of SBU under TE conditions can be attributed to its specific formulation, which includes 10-methacryloyloxydecyl dihydrogen phosphate (MDP), a functional monomer that can chemically interact with hydroxyapatite to form stable MDP–Ca salts [21]. Phosphoric acid etching increases surface energy and exposes collagen fibrils, facilitating

greater monomer infiltration [22,23]. The presence of bisphenol A-glycidyl methacrylate and 2-hydroxyethyl methacrylate further improves wettability and penetration into the demineralized dentin network [24]. In contrast, although TNBU and ABU contain functional monomers, differences in solvent type, monomer concentration, and pH appear to reduce their sensitivity to prior acid etching. These findings align with studies reporting that the use of UAs in TE mode does not negatively impact dentin bonding and may even enhance performance in some formulations [25–27]. Overall, these results support the versatile application of UAs in both SE and TE modes, while recognizing that certain systems, such as SBU, may benefit more distinctly from phosphoric acid etching.

Failure pattern analysis further supported the μSBS findings. Non-etched dentin predominantly demonstrated adhesive failures, whereas etched specimens exhibited higher proportions of mixed failures, suggesting improved micromechanical interlocking and chemical adhesion after etching. Cohesive failures were uncommon, appearing in only six specimens. SEM confirmed a direct relationship between μSBS and failure mode: mixed failures were associated with higher bond

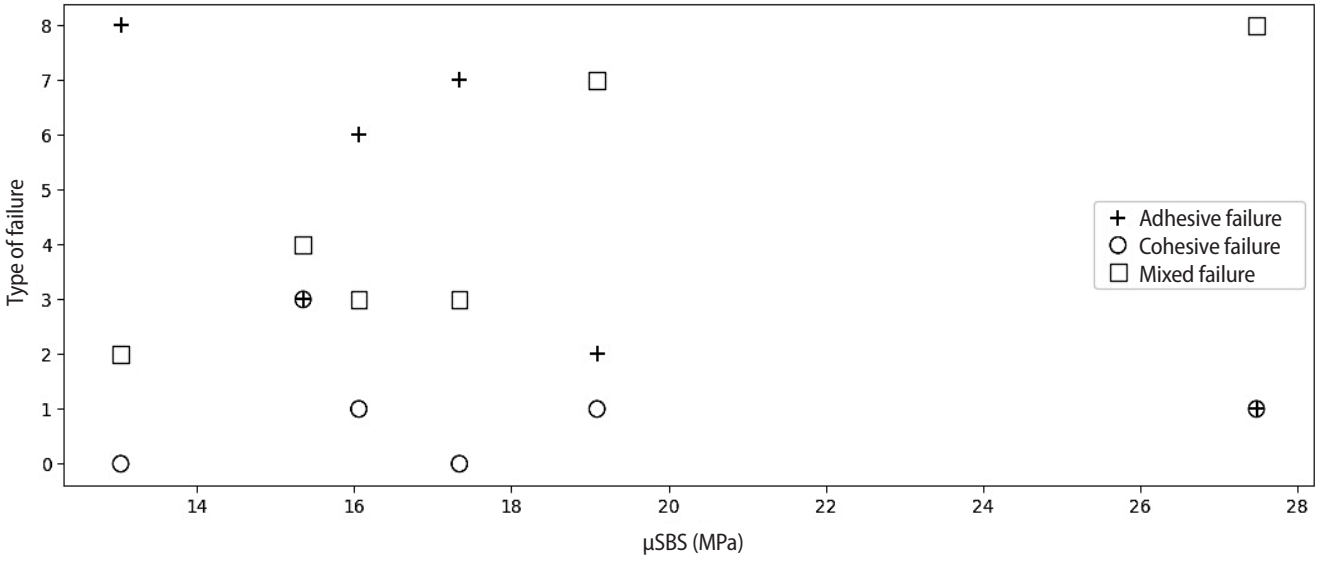

Figure 3. Correlation between micro-shear bond strength (μSBS) values and adhesive, cohesive, and mixed modes of failure.

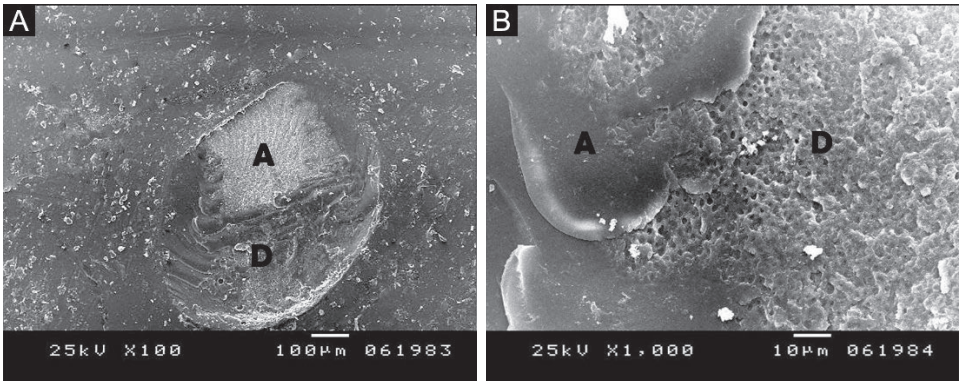

Figure 4. (A) Scanning electron microscopy image showing fracture of the adhesive layer, exposing underlying dentin; failure likely initiated at the dentin–adhesive interface and propagated through the adhesive, indicating adhesive failure. (B) Higher magnification of panel A highlighting adhesive remnants on dentin with no composite traces. (A) ×100; (B) ×1,000. A, adhesive; D, dentin.

https://doi.org/10.5395/rde.2026.51.e12

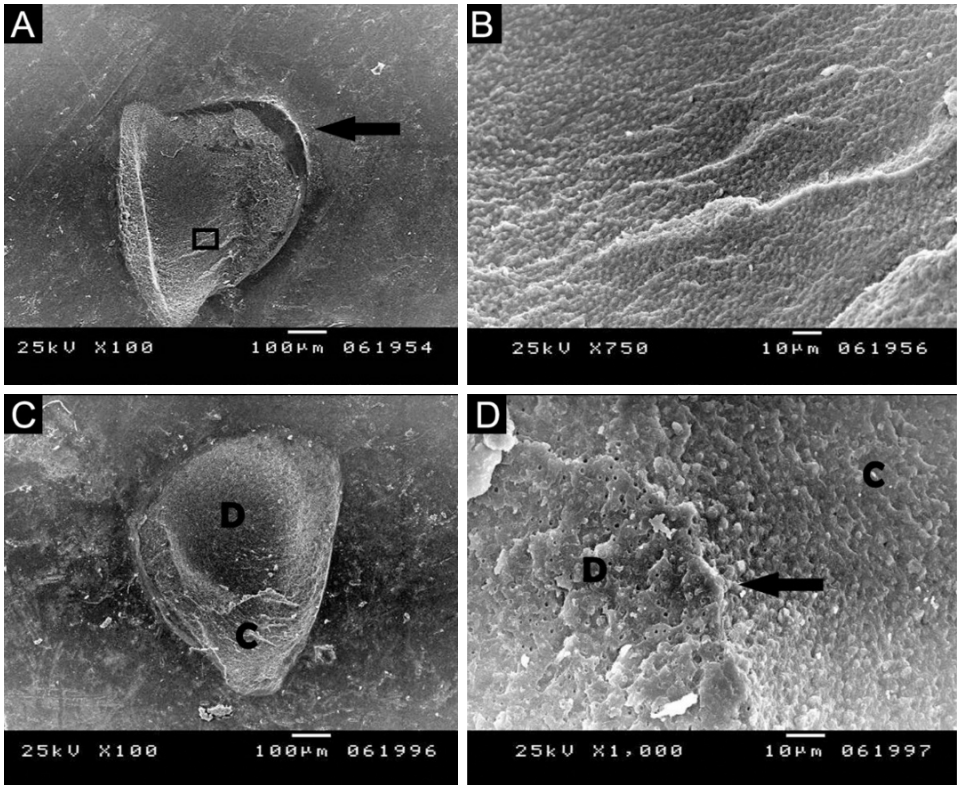

Figure 5. (A) Scanning electron microscopy (SEM) image showing a semicircular flaw (arrow), indicating cohesive failure within dentin. (B) Higher magnification of panel A revealing typical beach marks at the fractured dentin plane, with no composite observed. (C, D) SEM images of the marked area illustrating cohesive failure in both dentin and composite, with the fracture line propagating as a separating slope (arrow). (A, C) ×100; (B, D) ×1,000. D, dentin; C, composite resin.

strength, while adhesive failures dominated when μSBS values were lower, consistent with mechanistic observations reported by El-Safty *et al.* [9] and Sabatini [28]. Overall, the predominance of adhesive and mixed failures over cohesive failures aligns with prior studies by Luque-Martinez *et al.* [29] and Muñoz *et al.* [30] indicating effective resistance to interfacial crack propagation by the tested adhesives. Pre-etching increased mixed failures in SBU, confirming enhanced resin infiltration and stable MDP–Ca bond formation. TNBU and ABU showed less variation with etching, consistent with their comparable μSBS values. Differences from Firat *et al.* [31], who reported more cohesive failures in etched groups, likely reflect variations in adhesive chemistry and methodology. The occurrence of dentin pull-out in some specimens may lead to underestimation of true bond strength in μSBS testing, highlighting the importance of interpreting numerical results alongside fractographic and mechanistic observations [6].

Fractography serves as an essential tool for relating the stress at failure, the nature of the applied stress, and the dimensions of initial cracks and surrounding microtopography. Characteristic fractographic markings provide insight into failure mechanisms and support more accurate interpretation of adhesive behavior. As a well-established method for failure analysis, fractography is based on the principle that the entire fracture history is recorded on the fractured surface of the tested material [32]. SEM was employed in this study for fractographic evaluation, revealing the morphological features of dentin and providing insight into failure modes and crack propagation. In cohesive failure micrographs, beach marks (or tide marks) were observed, which represent the incremental positions of a slowly advancing crack, reflecting intermittent or low-level stress within the dentin, as described by Van Meerbeek *et al.* [8]. Oth-

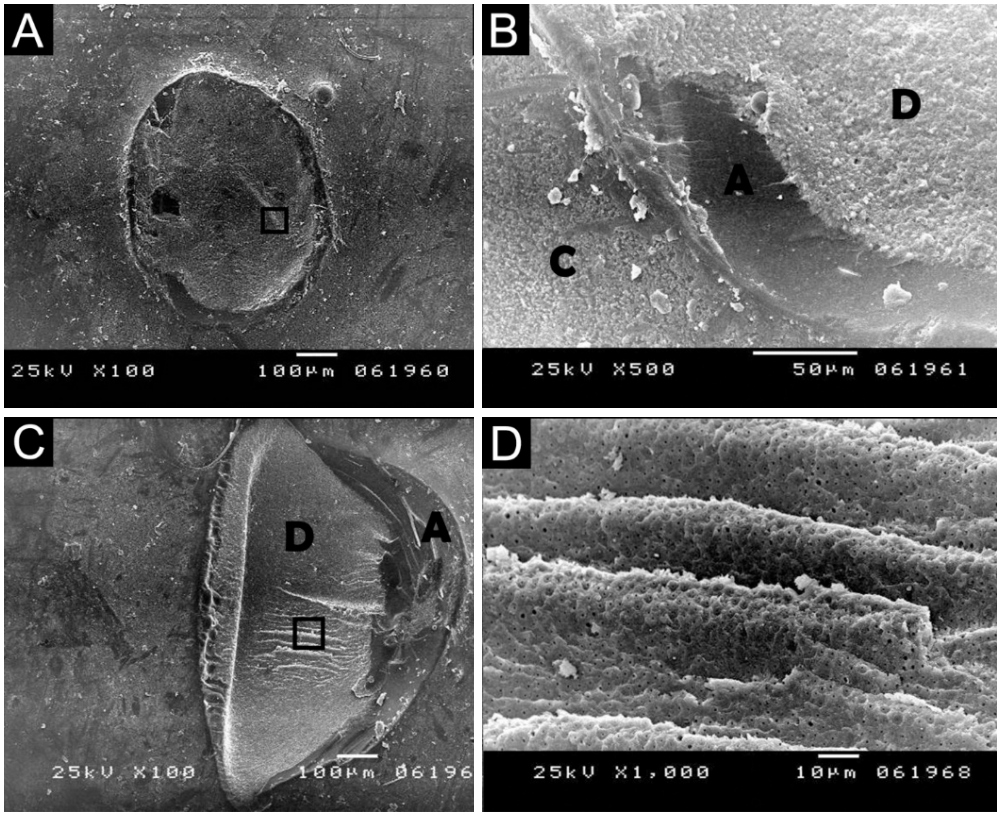

Figure 6. (A, B) Scanning electron microscopy (SEM) images of the marked area showing mixed failure mode extending from the adhesive into dentin and composite, suggesting the adhesive as the crack origin. (C) SEM image also showing mixed failure beginning with the adhesive and propagating into the dentin. (D) SEM of the square-marked area showing a wavy appearance of dentin with arrest lines indicating crack propagation. (A, C) ×100; (B) ×500; (D) ×1,000. A, adhesive layer; D, dentin; C, composite resin.

er micrographs indicated that when applied stress exceeds the material's strength, cracks tend to propagate along paths of least resistance, often following dentinal tubules [33]. In such cases, cracks likely initiated at weak points along the composite–dentin interface and propagated into both dentin and composite, resulting in cohesive failure in both substrates. Analysis of the present findings further suggests that specimens with higher bond strengths exhibited larger fractions of the fractured surface composed of mechanically stronger materials, such as composite resin or dentin. This indicates that cohesive failure occupied a greater area in these specimens, consistent with observations by Hashimoto *et al.* [34].

In this study, the presence of separating slopes was classified as an indicator of mixed failure, reflecting cracks that propagated from the center of the composite microrod toward its periphery at varying depths, shallower on one side, exposing the resin composite, and deeper on the other, exposing dentin. These patterns demonstrate the involvement of both adhesive and cohesive components. In multiple mixed-failure specimens, the adhesive layer acted as the weakest link, with cracks propagating into both the composite and dentin. In some cases, shear forces produced layered separations within the adhesive region, indicating that bond failure was readily initiated in the adhesive zone. In contrast, adhesive-failure micrographs typically exhibited corner-initiated fractures, where failure likely began at the dentin–adhesive interface and progressed through the adhesive layer. Crack nucleation generally occurs at preexisting flaws within materials or at interfaces, such as scratches, voids, or inclusions, which act as stress concentrators under applied loads. The presence of wavy arrest lines in several specimens further reflected localized changes in crack trajectory and transient stress

https://doi.org/10.5395/rde.2026.51.e12

redistribution at the adhesive–dentin interface during rapid μSBS-induced fracture, rather than gradual crack propagation. These observations align with interfacial fracture-mechanics principles and recent reports by Călinoiu *et al.* [7] and Pfeifer *et al.* [35], demonstrating that crack initiation and propagation in bonded interfaces under shear loading are governed by interfacial heterogeneity, local stress intensity, and energy-release patterns. Overall, the observed differences in failure patterns between SE and TE modes suggest that the etching strategy influences local stress distribution and interfacial interactions, consistent with the μSBS outcomes.

Evaluation of bond strength should be complemented by failure mode and fractographic analyses to provide a comprehensive understanding of adhesive resin behavior. Higher μSBS values are generally associated with slower and more stable crack propagation, producing characteristic peaks and valleys indicative of cohesive features. Conversely, lower bond strengths typically correspond to rapid, unstable fractures and a predominance of adhesive failure. These distinctions are consistent with the observations of Hiraishi *et al.* [36], who reported clear morphological differences between specimens exhibiting high and low bond strengths. Moreover, non-uniform stress distribution within the shear zone plays a significant role in shaping failure patterns; complex interfacial stresses can destabilize crack growth and contribute to the occurrence of mixed failures, as documented in earlier investigations [37–39].

A key strength of the present study is the combined use of conventional failure mode evaluation and high-resolution fractographic analysis, enabling detailed visualization of crack initiation and propagation paths, providing mechanistic insights into adhesive performance beyond simple bond strength metrics. However, some limitations must be considered. This *in vitro* study does not fully replicate the dynamic oral environment, where saliva, occlusal loading, biofilm, and pH fluctuations influence adhesive longevity. Only short-term performance after thermocycling was evaluated; no assessment of long-term hydrolytic degradation was performed. Although the μSBS method offers consistent stress distribution, it does not simulate the complex multidirectional forces encountered clinically. The sample size was appropriate for statistical analysis, but it may limit broad generalizability. Finally, only three UAs were examined, and findings cannot be extrapolated to all commercially available formulations. Future studies incorporating long-term durability testing and expanded fractographic evaluation are needed to further elucidate how UAs respond to etching strategies and interfacial stresses.

CONCLUSIONS

Acid etching enhances the bonding performance of UAs, particularly SBU, resulting in predominantly mixed-failure patterns, whereas TNBU and ABU are less affected by etching. The integration of fractographic analysis with conventional failure mode evaluation and bond strength testing provides critical insights into crack propagation and interfacial integrity, offering a comprehensive assessment of adhesive behavior and guiding clinical application strategies.

CONFLICT OF INTEREST

No potential conflict of interest relevant to this article was reported.

FUNDING/SUPPORT

The authors have no financial relationships relevant to this article to disclose.

AUTHOR CONTRIBUTIONS

Conceptualization, Formal analysis, Methodology: Morsy SM, Holiel AA. Data curation: Morsy SM, Bourgi R, Hardan L, Cuevas-Suárez CE, Holiel AA. Investigation: All authors. Project administration, Supervision, Visualization: Holiel AA. Resources: Morsy SM, Bourgi R, Hardan L, Cuevas-Suárez CE. Software: Morsy SM, Kharouf N, Hardan L, Holiel AA. Validation: Holiel AA, Kharouf N, Bourgi R, Hardan L. Writing - original draft: All authors. Writing - review & editing: Morsy SM, Bourgi R, Holiel AA. All authors read and approved the final manuscript.

DATA SHARING STATEMENT

The datasets are not publicly available but are available from the corresponding author upon reasonable request.

REFERENCES

1. El-Salamouny NA, Elmahy WA, Holiel AA. Comparative evaluation of bioactive alkasite-based material in different application modes: a 1-year randomized controlled clinical

trial. Odontology 2025;113:1689-1700.
2. Polesso Patias M, Fernandes-E-Silva P, Carreño NL, Lund RG, Piva E, da Silva AF, *et al*. Comparative clinical performance of universal adhesives versus etch-and-rinse and self-etch adhesives: a meta-analysis. Clin Oral Investig 2025;29:352.
3. Hosseini M, Raji Z, Kazemian M. Microshear bond strength of composite to superficial dentin by use of universal adhesives with different pH values in self-etch and etch & rinse modes. Dent Res J (Isfahan) 2023;20:5.
4. Ahmed B, Hamama HH, Mahmoud SH. Microshear bond strength of bioactive materials to dentin and resin composite. Eur J Dent 2023;17:917-923.
5. Ismail AM, Bourauel C, ElBanna A, Salah Eldin T. Micro versus macro shear bond strength testing of dentin-composite interface using chisel and wireloop loading techniques. Dent J (Basel) 2021;9:140.
6. Bahadır HS, Tuğutlu EC. Micro-shear bond strength of an alternative self-etch application of "no wait" universal adhesive to caries-affected and sound dentin in permanent and primary teeth. Oper Dent 2024;49:273-281.
7. Călinoiu ȘG, Bîcleșanu C, Florescu A, Stoia DI, Dumitru C, Miculescu M. Comparative study on interface fracture of 4th generation 3-steps adhesive and 7th generation universal adhesive. Materials (Basel) 2023;16:5834.
8. Van Meerbeek B, De Munck J, Yoshida Y, Inoue S, Vargas M, Vijay P, *et al*. Buonocore memorial lecture: adhesion to enamel and dentin: current status and future challenges. Oper Dent 2003;28:215-235.
9. El-Safty MM, Nour KA, Mustafa DS. Effect of saliva contamination and different decontamination protocols on microshear bond strength of a universal adhesive to dentin. Braz Dent Sci 2024;27:e4159.
10. Salem-Milani A, Zand V, Asghari-Jafarabadi M, Zakeri-Milani P, Banifatemeh A. The effect of protocol for disinfection of extracted teeth recommended by Center for Disease Control (CDC) on microhardness of enamel and dentin. J Clin Exp Dent 2015;7:e552-e556.
11. Jayasheel A, Niranjan N, Pamidi H, Suryakanth MB. Comparative evaluation of shear bond strength of universal dental adhesives: an in vitro study. J Clin Exp Dent 2017;9:e892-e896.
12. Gökce D, Usumez A, Polat ZS, Ayna E. Evaluation of four different adhesive systems' bonding strength between superficial and deep dentin. Materials (Basel) 2025;18:3107.
13. Gonzaga JA, Ávila AJ, Hardan L, Alonso NV, Suárez CE, Nassar N, *et al*. Calcium and microhardness quantification in healthy and fluorotic dentin conditioned with a self-etching system: an in vitro study. Dent J (Basel) 2025;13:168.
14. Arandi NZ. The classification and selection of adhesive agents; an overview for the general dentist. Clin Cosmet Investig Dent 2023;15:165-180.
15. SG Shirsath, K Bhargava, S Mulay, A Gambhir, R Kakodkar. Comparative evaluation of shear bond strength of TheraBase and composite resins to dentin: an in vitro study. J Stomatol 2025;78:1-5.
16. Öztürk E, Meric OT, Helvacioglu-Yigit D. Does reducing the acid-etching time increase the micro-tensile bond strength of a bulk fill composite to dentin using different universal adhesives? BMC Oral Health 2025;25:412.
17. McDonough WG, Antonucci JM, He J, Shimada Y, Chiang MY, Schumacher GE, *et al*. A microshear test to measure bond strengths of dentin-polymer interfaces. Biomaterials 2002;23:3603-3608.
18. Elraggal A, Raheem IA, Holiel A, Alhotan A, Alshabib A, Silikas N, *et al*. Bond strength, microleakage, microgaps, and marginal adaptation of self-adhesive resin composites to tooth substrates with and without preconditioning with universal adhesives. J Adhes Dent 2024;26:53-64.
19. Eren D, Bektaş ÖÖ, Siso SH. Three different adhesive systems; three different bond strength test methods. Acta Odontol Scand 2013;71:978-983.
20. Braga RR, Meira JB, Boaro LC, Xavier TA. Adhesion to tooth structure: a critical review of "macro" test methods. Dent Mater 2010;26:e38-e49.
21. Delgado AH, Ahmed MH, Nunes Ferreira M, Mano Azul A, Polido M, Yoshihara K, *et al*. Physico-chemical properties and performance of functional monomers used in contemporary dental adhesive technology. J Adhes Dent 2025;27:175-193.
22. Holiel A, Abdel-Fattah W, El Mallakh B. Bond strength and interfacial morphology of a multimode adhesive resin cement to enamel and dentin. Alex Dent J 2015;40:133-139.
23. Han F, Sun Z, Xie H, Chen C. Improved bond performances of self-etch adhesives to enamel through increased MDP-Ca salt formation via phosphoric acid pre-etching. Dent Mater 2022;38:133-146.
24. Alomran WK, Nizami MZ, Xu HH, Sun J. Evolution of dental resin adhesives: a comprehensive review. J Funct Biomater 2025;16:104.

https://doi.org/10.5395/rde.2026.51.e12

25. Takamizawa T, Barkmeier WW, Tsujimoto A, Berry TP, Watanabe H, Erickson RL, *et al*. Influence of different etching modes on bond strength and fatigue strength to dentin using universal adhesive systems. Dent Mater 2016;32:e9-e21.
26. Wagner A, Wendler M, Petschelt A, Belli R, Lohbauer U. Bonding performance of universal adhesives in different etching modes. J Dent 2014;42:800-807.
27. Bourgi R, Kharouf N, Cuevas-Suárez N, Lukomska-Szymanska M, Haikel Y, Hardan L. Adhesive systems in dentistry: key components and clinical applications. Appl Sci 2024;14:8111.
28. Sabatini C. Effect of phosphoric acid etching on the shear bond strength of two self-etch adhesives. J Appl Oral Sci 2013;21:56-62.
29. Luque-Martinez IV, Perdigão J, Muñoz MA, Sezinando A, Reis A, Loguercio AD. Effects of solvent evaporation time on immediate adhesive properties of universal adhesives to dentin. Dent Mater 2014;30:1126-1135.
30. Muñoz MA, Luque I, Hass V, Reis A, Loguercio AD, Bombarda NH. Immediate bonding properties of universal adhesives to dentine. J Dent 2013;41:404-411.
31. Firat E, Gurgan S, Gutknecht N. Microtensile bond strength of an etch-and-rinse adhesive to enamel and dentin after Er:YAG laser pretreatment with different pulse durations. Lasers Med Sci 2012;27:15-21.
32. Abdelaal AM, Kehela HA, Holiel AA. Fracture resistance and fractographic analysis of pressable glass-ceramics with different partial coverage designs for maxillary premolars. BMC Oral Health 2024;24:1078.
33. Levrini L, Di Benedetto G, Raspanti M. Dental wear: a scanning electron microscope study. Biomed Res Int 2014;2014:340425.
34. Hashimoto M, Ohno H, Kaga M, Endo K, Sano H, Oguchi H. In vivo degradation of resin-dentin bonds in humans over 1 to 3 years. J Dent Res 2000;79:1385-1391.
35. Pfeifer CS, Lucena FS, Tsuzuki FM. Preservation strategies for interfacial integrity in restorative dentistry: a non-comprehensive literature review. J Funct Biomater 2025;16:42.
36. Hiraishi N, Nishiyama N, Ikemura K, Yau JY, King NM, Tagami J, *et al*. Water concentration in self-etching primers affects their aggressiveness and bonding efficacy to dentin. J Dent Res 2005;84:653-658.
37. Abouelleil H, Villat C, Attik N, Grosgogeat B, Farge P. Evaluation of interfacial fracture type using two adhesive systems. Dentistry 2014;4:1000212.
38. Gönder HY, Mohammadi R, Harmankaya A, Yüksel İB, Fidancıoğlu YD, Karabekiroğlu S. Teeth restored with bulk-fill composites and conventional resin composites; investigation of stress distribution and fracture lifespan on enamel, dentin, and restorative materials via three-dimensional finite element analysis. Polymers (Basel) 2023;15:1637.
39. Walshaw PR, Tam LE, McComb D. Bond failure at dentin-composite interfaces with 'single-bottle' adhesives. J Dent 2003;31:117-125.

RDE Restorative Dentistry & Endodontics

Case Report

eISSN 2234-7666
Restor Dent Endod. 2026 February;51(1):e1
https://doi.org/10.5395/rde.2026.51.e1

Fifty-year follow-up of dens invaginatus treated by nonsurgical and surgical endodontic treatments: a case report

Qais Arow[1,*], Eyal Rosen[1], Galit Sela[2], Shlomo Elbahary[3], Igor Tsesis[1]

[1]Department of Endodontics, Maurice and Gabriela Goldschleger School of Dental Medicine, Tel Aviv University, Tel Aviv, Israel
[2]Private Practice, Tel-Aviv, Israel
[3]Department of Endodontics, College of Dentistry, University of Illinois Chicago, Chicago, IL, USA

ABSTRACT

This case report presents a lateral maxillary incisor with dens invaginatus (DI) type IIIb that was treated both nonsurgically and surgically over 50 years. Treatment of teeth with DI can be challenging. Suggested options may include nonsurgical root canal treatment, endodontic surgery, or extraction. In this case report, a 13-year-old patient with a lateral maxillary incisor with DI type IIIb was treated by nonsurgical root canal treatment, modern endodontic surgery, and reoperation over the course of 50 years. There was complete healing at the last follow-up, 11 years after the reoperation. Correct diagnosis and proper treatment using modern endodontic techniques can enable teeth with DI to survive throughout the life span of the patient.

Keywords: Apicoectomy; Dens in dente; Endodontics; Treatment outcome

INTRODUCTION

Dens invaginatus (DI) is a malformation of the teeth characterized by an early invagination of the enamel and dentine that can extend deep into the pulp cavity and the roots and may sometimes reach the apex [1]. The condition results from the invagination of the enamel during the soft tissue stage of development before the hard tissue mineralizes [2].

The etiology of DI malformation is controversial and remains unclear: Kronfeld [3] proposed that the condition is caused by a focal failure of growth of the internal enamel epithelium, which leads to proliferation of the surrounding normal epithelium with eventual engulfment of the static area. In contrast, Rushton [4] suggested that the invagination is a result of rapid and aggressive proliferation of a part of the internal enamel epithelium that then invades the dental papilla. He regarded this as a 'benign neoplasm of limited growth.' An alternative option was suggested by Oehlers [5], who considered that distortion of the enamel organ occurs during tooth development and results in protrusion of a

Received: April 9, 2025 **Revised:** July 25, 2025 **Accepted:** August 26, 2025

Citation
Arow Q, Rosen E, Sela G, Elbahary S, Tsesis I. Fifty-year follow-up of dens invaginatus treated by nonsurgical and surgical endodontic treatments: a case report. Restor Dent Endod 2026;51(1):e1.

***Correspondence to**
Qais Arow, DMD, BSc (Pharm)
Department of Endodontics, Maurice and Gabriela Goldschleger School of Dental Medicine, Tel Aviv University, P.O. Box 39040, Tel Aviv 69978, Israel
Email: qais.arow@gmail.com

part of the enamel organ. Additional theories implicate fusion of tooth germs, infection, trauma, and genetics as possible contributing factors [1].

As a result of the changes, the arrangement of the mineralized tissue in DI appears opposite to normal, with the enamel located in the center and the dentine on the edges [6]. The prevalence of permanent teeth affected by DI is variable, ranging from 0.04% to 10% [7,8]. The most commonly affected permanent tooth is the maxillary lateral incisor (approximately 42% of all cases) [8].

Oehlers [5] classified DI into three categories: Type I, the invagination is confined within the crown, up to the cementoenamel junction; Type II, the invagination extends apically beyond the cementoenamel junction, where a connection between the invagination and the pulp is possible; Type III, the invagination extends beyond the cementoenamel junction and may involve a second foramen into the lateral periodontal ligament (IIIa) or periradicular tissue (IIIb).

The abnormal morphology of DI can be plaque retentive, thereby increasing the risk of caries, periodontal inflammation, and pulp necrosis [9]. In most cases, the thin or incomplete enamel lining of the invagination cannot prevent entry of bacteria into the pulp, which leads to pulp necrosis with an eventual periapical inflammatory response. The complex and atypical anatomy can hinder effective root canal instrumentation, thorough disinfection, and proper obturation of the canal system [1,10]. These anatomical irregularities increase the risk of residual infection and may compromise the overall success of endodontic treatment [11].

The difficulty in endodontic management is to gain adequate access to the canal space without severely compromising the strength of the tooth if the entire invagination is removed [12]. Advancements in endodontic diagnosis and treatment using cone-beam computed tomography (CBCT), magnification devices, modern endodontic surgery, and new bioceramic materials have significantly contributed to the effective management of complex cases such as DI [13,14]. In addition, guided endodontics offers a precise and minimally invasive approach to treating teeth with complex root canal systems [15]. The current case report presents a DI that was treated both nonsurgically and surgically over 50 years.

CASE REPORT

A 13-year-old girl was referred to the endodontic department in 1972, with a diagnosis of DI, pulp necrosis, and a chronic apical abscess in the left lateral maxillary incisor. Nonsurgical root canal treatment (NSRCT) was performed over three visits as described in a previous case report [16]. At the third visit, the tooth was asymptomatic and was obturated with gutta-percha and AH26 cement (DeTrey, Zurich, Switzerland) using the lateral condensation technique. A radiograph taken two years later showed evidence of healing of the periapical radiolucency (Figure 1), and complete healing was observed at the 3-year follow-up, as documented in the case report by Tagger [16].

Thirty years later (2002), the patient came back to the department with a complaint of pain and swelling and was diagnosed with an acute apical abscess in tooth #22. Informed consent was obtained and endodontic surgery was performed in the department (Figure 2). The tooth was treated with a modern surgical endodontic protocol, involving a dental operating microscope: local anesthesia with lidocaine 2% with epinephrine 1:100,000, triangular full mucoperiosteal flap, osteotomy, root-end resection with no bevel using a high-speed bur, curettage, retrograde preparation using ultrasonic tips, and root-end filling with intermediate restorative material (IRM; L.D. Caulk Company, Milford, DE, USA).

Clinical and radiographic follow-up was scheduled annually. Radiographic outcomes were assessed based on the criteria established by Rud *et al.* [17]. At a 2-year follow-up, the tooth was clinically asymptomatic, with good adaptation of the crown to the tooth and with radiographically normal periapical tissue (Figure 2C). The tooth remained asymptomatic with radiographically complete healing at an additional follow-up visit in 2006 (Figure 2D).

In 2011, 9 years later, the patient came back with a complaint of sensitivity in the area and purulent exudate. Clinically, the tooth was sensitive to percussion and palpation in the periapical area with signs of a sinus tract in the buccal apical area. A diagnosis of chronic apical abscess was made. A second endodontic surgery used the same technique as the previous treatment, taking care to minimize the apical resection in order not to

https://doi.org/10.5395/rde.2026.51.e1

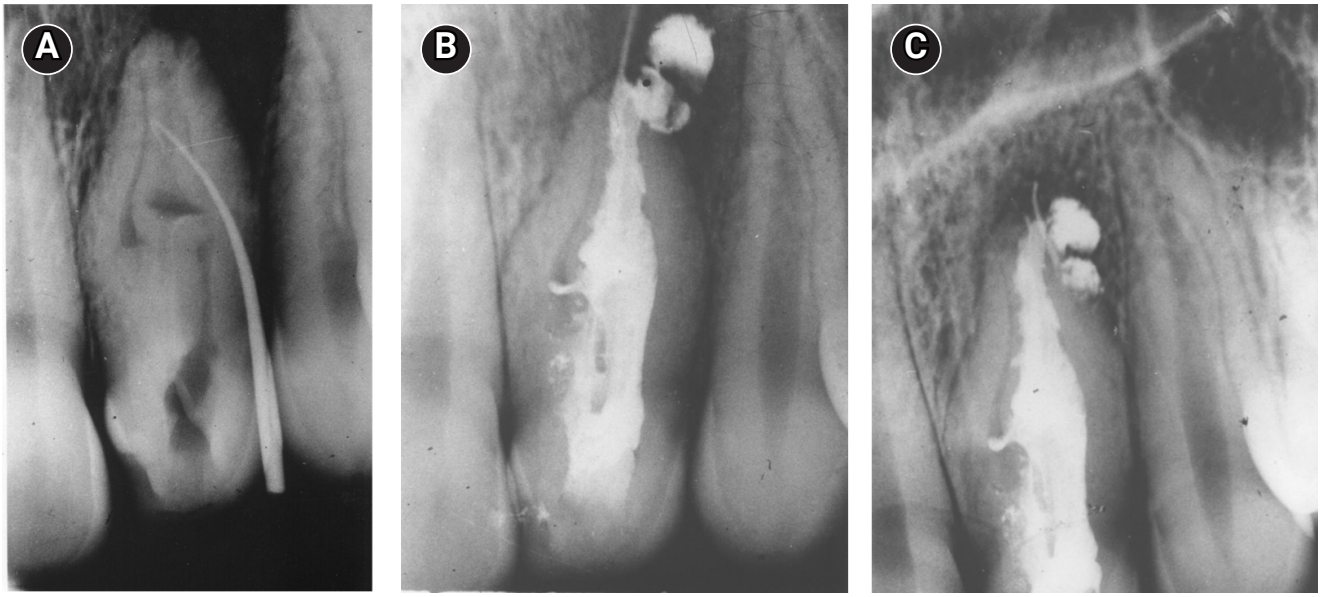

Figure 1. Nonsurgical root canal treatment on tooth #22. (A) Preoperative radiograph in 1972 showing a periapical radiolucent area that extends mostly on the distal surface of the root. Note: an access cavity was present. Gutta-percha cone inserted in the sinus tract leading to the sulcus of the tooth. Three pulp cavities are visible: the distal one exposed by the access cavity, the middle one partly lined with enamel, and the mesial one is closed and present only in the apical half of the root. (B) Postoperative radiograph in 1972. Note the extruded cement and gutta-percha point beyond the apex. Mesial cavity unfilled. (C) Two-year follow-up radiograph in 1974 showing a decrease in the size of periapical radiolucency. Excess filling material settled on the distal aspect of the root. Reprinted from the article of Tagger *et al.* [16] with the permission of Elsevier.

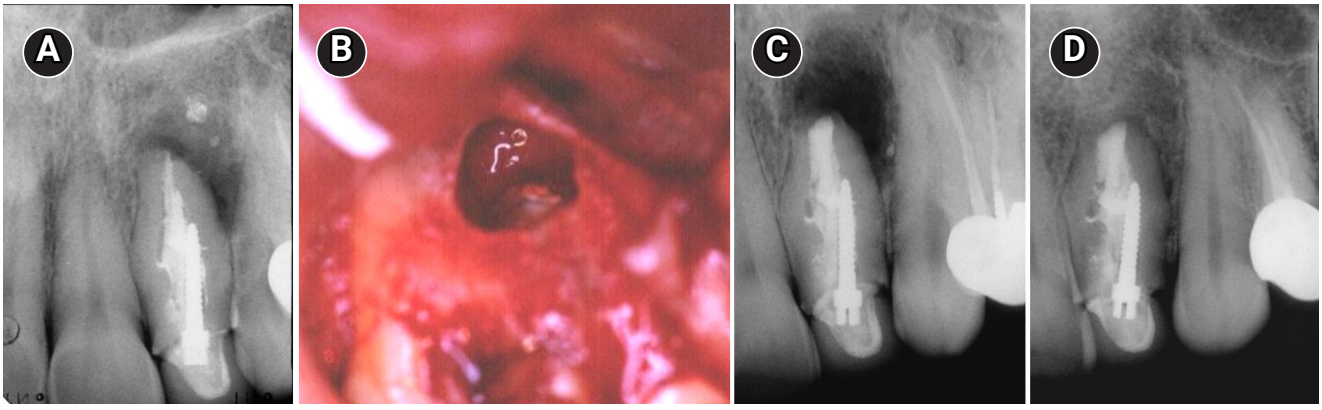

Figure 2. Endodontic surgery on tooth #22. (A) Preoperative radiograph in 2002 showing periapical radiolucent area around the apex and distal aspect of the root. Note the excess filling material outside the root. At the time of referral, the tooth had been restored with a post and crown. Marginal defects can be seen in the final restoration. (B) Intraoperative photograph in 2002. (C) Postoperative radiograph in 2002. The apical part of the mesial cavity was prepared and filled. Excess filling material that was outside the root was removed. (D) Four-year follow-up radiograph in 2006 showing complete healing with no periapical radiolucency present.

compromise the crown-root ratio. Two years following the second surgery, the tooth was asymptomatic and completely healed radiographically (Figure 3).

In 2021, when the patient (now aged 63 years) was referred by the treating dentist for evaluation, the tooth was still clinically asymptomatic with normal periapical tissues (Figure 4). The patient did not attend any follow-up appointments after 2021, despite multiple attempts to contact and recall her. A summary of events and outcomes is presented in Table 1.

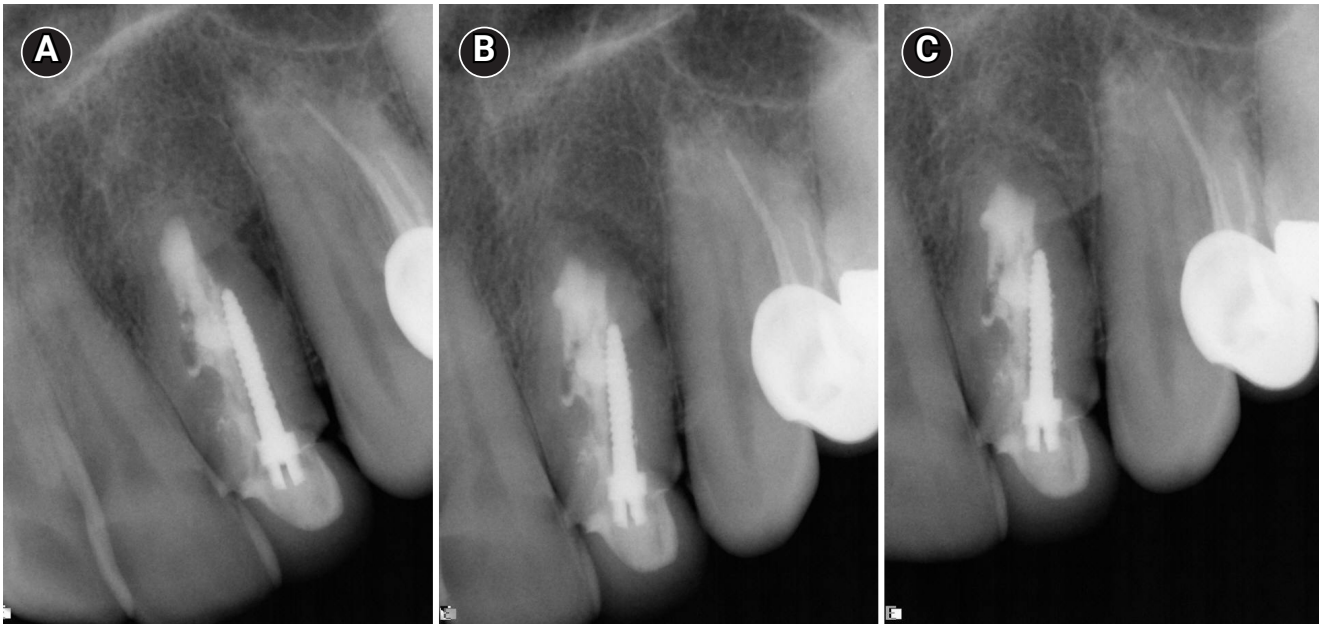

Figure 3. Endodontic reoperation on tooth #22. (A) Preoperative radiograph in 2011. (B) Postoperative radiograph in 2011 showing minimal apical resection. (C) Two-year follow-up radiograph in 2012 showing complete healing with normal periodontal ligament space.

Figure 4. Radiograph taken in 2021 of tooth #22 showing normal periapical tissues, 10 years after endodontic reoperation.

DISCUSSION

Treatment of teeth with DI can be challenging due to the complex morphology. Identifying the invagination type is important for choosing the proper treatment. Following the first classification of DI published by Hallett [18], Schulze and Brand [19] proposed a more detailed classification, including invaginations starting at the incisal edge or the top of the crown, and also described dysmorphic root configuration. The classification scheme of Oehlers [5] is probably the most useful version and simplifies evaluation and treatment planning.

Various treatment methods may be suggested for the management of DI. These include NSRCT, endodontic apical surgery, intentional replantation, and extraction. Nonsurgical treatment sometimes fails because it is difficult to gain access to all parts of the root canal system [8], and additional treatment should be considered for a successful outcome.

Over the past five decades, there has been a significant advancement in root canal diagnosis and treatments with the integration of new technologies and materials such as CBCT, operating microscope, and bioceramics [13,20,21]. As a result, nowadays, the management of challenging cases with DI would follow a more advanced and evidence-based approach.

CBCT has transformed endodontic diagnostics by providing three-dimensional imaging of the tooth and surrounding structures and has led to more accurate

https://doi.org/10.5395/rde.2026.51.e1

Table 1. Summary of events and outcomes

Date	Clinical findings	Radiographic findings	Diagnosis	Treatment	Outcome
1972	Sinus tract	Periapical radiolucency	Chronic apical abscess	Nonsurgical root canal treatment	1975: Complete healing 2002: Failure
2002	Swelling	Periapical radiolucency	Acute apical abscess	Endodontic surgery	2006: Complete healing 2011: Failure
2011	Sinus tract	Normal apical tissues	Chronic apical abscess	Reoperation	2013: Complete healing
2021	No signs/ symptoms	Normal apical tissues	Normal apical tissues	Evaluation	Complete healing

treatment planning [22]. It is particularly useful for assessing teeth with known complex anatomy, such as DI [23]. The increased diagnostic data (e.g., canal morphology, the extent of invagination, and periapical pathology) should result in more accurate diagnosis and, therefore, improved decision-making for the management of these cases [13]. While CBCT was not used in this case report, it should be considered for the management of complex endodontic cases [24].

Surgical operating microscope offers magnification and enhanced lighting, enabling endodontists to visualize the root canal system with greater clarity. This advancement has improved the success rates of nonsurgical and surgical procedures by allowing more precise interventions [25].

In the early 1990s, mineral trioxide aggregate (MTA) was introduced, and since then, there has been a great development of more bioceramic materials [26]. Bioactivity, biocompatibility, physical properties, and good sealing ability of these materials have highly advanced the clinical practice of endodontics [21,26,27].

This case presents a unique opportunity to observe the outcome of nonsurgical and surgical endodontic treatment of teeth with DI across a span of 50 years. Schmitz *et al.* [28] reported a case of NSRCT and endodontic surgery of a lateral maxillary incisor with DI, with a long-term follow-up showing complete healing after 11 years. In their case, the tooth had an open apex and DI type I. Surgical intervention was required due to the persistence of exudates and incomplete root canal development after conservative endodontic treatment. Retrograde preparation was deemed unnecessary.

We are not aware of any publications on DI that reported outcomes of endodontic reoperation on our cases with follow-up periods longer than 11 years following surgical treatment.

In our case, the intention was to conduct annual clinical and radiographic follow-up of the treatment. However, the patient did not attend all scheduled follow-up appointments despite multiple attempts to contact her. The tooth was treated for the first time in 1977 by Tagger [16]. At the 3-year follow-up, the periapical radiograph showed complete healing [16]. That case was managed before the introduction of diagnostic tools such as CBCT, the development of the modern apex locators, the introduction of the dental operating microscope, ultrasonic instrumentation, and advanced obturating materials. Thus, access cavity design, canal shaping, and obturation were limited to manual methods and relatively rudimentary instruments and obturation using gutta-percha with AH26 sealer.

Today, a different approach would be recommended, including CBCT before the treatment, the use of a dental operating microscope during the treatment, and obturation using a bioceramic material [14,29]. In recent years, guided endodontics has also emerged as a valuable tool for the treatment of such cases, enhancing the clinician's ability to navigate challenging anatomy with greater accuracy and confidence [15].

The tooth was referred to our department thirty years after the initial treatment and was diagnosed with an acute apical abscess. The complex anatomy of DI limits the effectiveness of optimal instrumentation and irrigation, compromising thorough disinfection and sealing of the root canal system [1,10]. This limitation may increase the risk of treatment failure and subsequent reinfection [11]. At the time of referral, the tooth had been restored with a post and crown. Currently, the placement of a post in such teeth is not recommended due to the risk of compromising the remaining tooth structure. Marginal defects were noted in the final restoration, a factor known to affect the long-term prognosis of the tooth. Nevertheless, clinical examination revealed good adaptation of the crown to the tooth.

The surgical endodontic treatment performed decades later reflects a dramatic shift in both philosophy and technology. The introduction of the dental operating microscope allowed precise root-end resection with a minimal bevel and retrograde preparation using ultrasonic tips [14]. The meta-analysis by Tsesis *et al.* [14] showed a 89% success rate for endodontic surgery using the modern technique. Setzer *et al.*'s meta-analysis [29] reported a significantly lower success rate of 59% with the traditional technique without magnification and using surgical burs and amalgam for root-end filling.

Although IRM was used as the retro-filling material, the technique employed in the 2011 reoperation already incorporated principles of modern endodontic microsurgery. IRM has been considered an available, easy-to-manipulate, dimensionally stable, and non-expensive material for many years [30–32]. While studies found no conclusive significant difference in outcomes between MTA and IRM [33], MTA and newer-generation fast-setting bioceramics with improved handling properties are now preferred over traditional materials like IRM for root-end fillings [33,34]. These materials offer superior sealing ability and biocompatibility, enhancing surgical outcomes [14,21].

Endodontic surgery may be considered to manage permanent teeth with apical periodontitis when nonsurgical root canal retreatment is impractical [14,35]. Endodontic reoperation is a valid alternative to extraction with reported success rates of >90% [36].

Root canal treatment and endodontic surgery are predictable procedures with an excellent long-term prognosis. A success rate of 95% was reported for NSRCT with a follow-up period of more than 20 years [37] and survival rates of 97% after eight years of follow-up [38]. Long-term success rates of >90% were reported for surgical endodontic treatment using modern techniques [14,36], when outcome was assessed as healed based on the criteria established by Rud *et al.* [17].

Long-term failures following endodontic surgery have been reported, where 5% to 25% of teeth recorded as healed at the short-term have been reported to regress when observed 3 years or longer after surgery [39,40]. While this regression may occur due to a variety of causative factors, including missed anatomy, insufficient root resection or root-end filling, and residual biofilm in isthmuses [41,42], in the present case, the failure of the apical seal was suspected as the reason for the recurrent lesion. Therefore, after a late failure in this case report, reoperation was performed using a modern technique, resulting in a successful outcome. A comparison of endodontically treated teeth and dental implants is challenging [43–45]. For example, while strict success criteria are very often used in endodontic outcome studies, the majority of implant studies rely solely on survival for outcome evaluation [43–45].

Advantages of endodontically treated teeth over implants include better function in that the former can return to a level of masticatory function that is similar to that of natural teeth, while an implant-supported crown tends to have reduced levels of masticatory function [46]. In addition, endodontically treated teeth tend to have better esthetics, especially in the anterior maxilla, and are less susceptible to biological and technical complications [44].

Although both treatment options are predictable with reported survival rates of ≥95% [44], there are no lifetime guarantees for either a natural tooth or a dental implant. For this reason, it is conceivable to assume that the two options should complement each other, and priority should be given to preserving the natural dentition rather than extraction when nonsurgical or surgical endodontic treatment can provide a good prognosis.

In this case report, a lateral maxillary incisor with DI type IIIb, was treated by NSRCT, followed by endodontic surgery and reoperation. Fifty years after the initial treatment, 11 years after the reoperation, the tooth appeared completely healed.

We therefore conclude that correct diagnosis and proper treatment using modern endodontic techniques and tools can result in survival of the natural tooth throughout the life span of a patient.

CONFLICT OF INTEREST

No potential conflict of interest relevant to this article was reported.

FUNDING/SUPPORT

The authors have no financial relationships relevant to this article to disclose.

https://doi.org/10.5395/rde.2026.51.e1

AUTHOR CONTRIBUTIONS

Conceptualization: Tsesis I, Rosen E. Data curation, Methodology: Arow Q, Tsesis I. Investigation: Tsesis I. Project administration, Visualization: Arow Q. Supervision: Rosen E, Sela G, Elbahary S. Writing - original draft: Arow Q, Tsesis I. Writing - review & editing: Arow Q, Rosen E, Sela G, Elbahary S, Tsesis I. All authors read and approved the final manuscript.

DATA SHARING STATEMENT

The datasets are not publicly available but are available from the corresponding author upon reasonable request.

REFERENCES

1. Hülsmann M. Dens invaginatus: aetiology, classification, prevalence, diagnosis, and treatment considerations. Int Endod J 1997;30:79-90.
2. de Sousa SM, Bramante CM. Dens invaginatus: treatment choices. Endod Dent Traumatol 1998;14:152-158.
3. Kronfeld R. Dens in dente. J Dent Res 1934;14:49-66.
4. Rushton MA. A collection of dilated composite odontomas. Br Dent J 1937;63:65-86.
5. Oehlers FA. Dens invaginatus (dilated composite odontome). I. Variations of the invagination process and associated anterior crown forms. Oral Surg Oral Med Oral Pathol 1957;10:1204-1218 contd.
6. Della Corte M, Malzone A, Palomba M, Attanasio G. [Clinical case of "dens invaginatus"]. Arch Stomatol (Napoli) 1990;31:649-652. Italian.
7. Gonçalves A, Gonçalves M, Oliveira DP, Gonçalves N. Dens invaginatus type III: report of a case and 10-year radiographic follow-up. Int Endod J 2002;35:873-879.
8. Rotstein I, Stabholz A, Heling I, Friedman S. Clinical considerations in the treatment of dens invaginatus. Endod Dent Traumatol 1987;3:249-254.
9. Clarke P, Longridge N, Gartshore L. A multidisciplinary management of a type III dens invaginatus in a maxillary permanent canine. Eur Arch Paediatr Dent 2016;17:131-136.
10. Sübay RK, Kayataş M. Dens invaginatus in an immature maxillary lateral incisor: a case report of complex endodontic treatment. Oral Surg Oral Med Oral Pathol Oral Radiol Endod 2006;102:e37-e41.
11. Versiani MA, Martins J, Ordinola-Zapata R. Anatomical complexities affecting root canal preparation: a narrative review. Aust Dent J 2023;68 Suppl 1:S5-S23.
12. Lindner C, Messer HH, Tyas MJ. A complex treatment of dens invaginatus. Endod Dent Traumatol 1995;11:153-155.
13. Patel S, Durack C, Abella F, Shemesh H, Roig M, Lemberg K. Cone beam computed tomography in Endodontics: a review. Int Endod J 2015;48:3-15.
14. Tsesis I, Rosen E, Taschieri S, Telishevsky Strauss Y, Ceresoli V, Del Fabbro M. Outcomes of surgical endodontic treatment performed by a modern technique: an updated meta-analysis of the literature. J Endod 2013;39:332-339.
15. Wei X, Du Y, Zhou X, Yue L, Yu Q, Hou B, *et al*. Expert consensus on digital guided therapy for endodontic diseases. Int J Oral Sci 2023;15:54.
16. Tagger M. Nonsurgical endodontic therapy of tooth invagination: report of a case. Oral Surg Oral Med Oral Pathol 1977;43:124-129.
17. Rud J, Andreasen JO, Jensen JE. Radiographic criteria for the assessment of healing after endodontic surgery. Int J Oral Surg 1972;1:195-214.
18. Hallett GE. Incidence, nature, and clinical significance of palatal invaginations in the maxillary incisor teeth. Proc R Soc Med 1953;46:491-499.
19. Schulze C, Brand E. [Dens invaginatus (dens in dente)]. ZWR 1972;81:653-660 contd. German.
20. Kishen A, Peters OA, Zehnder M, Diogenes AR, Nair MK. Advances in endodontics: potential applications in clinical practice. J Conserv Dent 2016;19:199-206.
21. Torabinejad M, Parirokh M, Dummer PM. Mineral trioxide aggregate and other bioactive endodontic cements: an updated overview: part II: other clinical applications and complications. Int Endod J 2018;51:284-317.
22. Rosen E, Taschieri S, Del Fabbro M, Beitlitum I, Tsesis I. The diagnostic efficacy of cone-beam computed tomography in endodontics: a systematic review and analysis by a hierarchical model of efficacy. J Endod 2015;41:1008-1014.
23. Alkadi M, Almohareb R, Mansour S, Mehanny M, Alsadhan R. Assessment of dens invaginatus and its characteristics in maxillary anterior teeth using cone-beam computed tomography. Sci Rep 2021;11:19727.
24. American Association of Endodontists; American Academy of Oral and Maxillofacial Radiology. AAE and AAOMR joint position statement: use of cone beam computed tomography in endodontics 2015 update. J Endod 2015;41:1393-1396.
25. Setzer FC, Kohli MR, Shah SB, Karabucak B, Kim S. Outcome of endodontic surgery: a meta-analysis of the literature: part 2: comparison of endodontic microsurgical techniques with and without the use of higher magnification. J Endod 2012;38:1-10.

26. Parirokh M, Torabinejad M, Dummer PM. Mineral trioxide aggregate and other bioactive endodontic cements: an updated overview: part I: vital pulp therapy. Int Endod J 2018;51:177-205.
27. Dong X, Xu X. Bioceramics in endodontics: updates and future perspectives. Bioengineering (Basel) 2023;10:354.
28. Schmitz MS, Montagner F, Flores CB, Morari VH, Quesada GA, Gomes BP. Management of dens invaginatus type I and open apex: report of three cases. J Endod 2010;36:1079-1085.
29. Setzer FC, Shah SB, Kohli MR, Karabucak B, Kim S. Outcome of endodontic surgery: a meta-analysis of the literature: part 1: comparison of traditional root-end surgery and endodontic microsurgery. J Endod 2010;36:1757-1765.
30. Johnson BR, Fayad MI, Berman LH, Hargreaves KM, Rotstein I. Periradicular surgery. In: Hargreaves KM, Berman LH, Rotstein I, eds. Cohen's pathways of the pulp. 12th ed. St. Louis, MO: Elsevier; 2021. p774-815.
31. Torabinejad M, Sabeti M, Glickman GN. Surgical endodontics. In: Ingle JI, Bakland LK, Baumgartner JC, eds. Ingle's endodontics. 7th ed. Shelton, CT: People's Medical Publishing House; 2019. p1100–1152.
32. Crooks WG, Anderson RW, Powell BJ, Kimbrough WF. Longitudinal evaluation of the seal of IRM root end fillings. J Endod 1994;20:250-252.
33. Ma X, Li C, Jia L, Wang Y, Liu W, Zhou X, *et al*. Materials for retrograde filling in root canal therapy. Cochrane Database Syst Rev 2016;12:CD005517.
34. Camilleri J, Atmeh A, Li X, Meschi N. Present status and future directions: hydraulic materials for endodontic use. Int Endod J 2022;55 Suppl 3(Suppl 3):710-777.
35. Duncan HF, Kirkevang LL, Peters OA, El-Karim I, Krastl G, Del Fabbro M, *et al*. Treatment of pulpal and apical disease: the European Society of Endodontology (ESE) S3-level clinical practice guideline. Int Endod J 2023;56 Suppl 3:238-295.
36. Song M, Shin SJ, Kim E. Outcomes of endodontic micro-resurgery: a prospective clinical study. J Endod 2011;37:316-320.
37. Molven O, Halse A, Fristad I; MacDonald-Jankowski D. Periapical changes following root-canal treatment observed 20-27 years postoperatively. Int Endod J 2002;35:784-790.
38. Salehrabi R, Rotstein I. Endodontic treatment outcomes in a large patient population in the USA: an epidemiological study. J Endod 2004;30:846-850.
39. Rubinstein RA, Kim S. Long-term follow-up of cases considered healed one year after apical microsurgery. J Endod 2002;28:378-383.
40. von Arx T, Jensen SS, Hänni S, Friedman S. Five-year longitudinal assessment of the prognosis of apical microsurgery. J Endod 2012;38:570-579.
41. Setzer F, Harley M, Cheung J, Karabucak B. Possible causes for failure of endodontic surgery: a retrospective series of 20 resurgery cases. Eur Endod J 2021;6:235-241.
42. Wang X, Peng L. Removing biofilms in the isthmus by endodontic surgery. Arch Oral Maxillofac Surg 2022;5:180-185.
43. Setzer FC, Kim S. Preserving the natural tooth versus extraction and implant placement: an evidence-based approach. In: Fonseca RJ, ed. Evidence-Based Decision Making in Dentistry. Shelton, CT: People's Medical Publishing House; 2017. p73-95.
44. Setzer FC, Kim S. Comparison of long-term survival of implants and endodontically treated teeth. J Dent Res 2014;93:19-26.
45. Doyle SL, Hodges JS, Pesun IJ, Law AS, Bowles WR. Retrospective cross sectional comparison of initial nonsurgical endodontic treatment and single-tooth implants. Compend Contin Educ Dent 2007;28:296-301.
46. Woodmansey KF, Ayik M, Buschang PH, White CA, He J. Differences in masticatory function in patients with endodontically treated teeth and single-implant-supported prostheses: a pilot study. J Endod 2009;35:10-14.

https://doi.org/10.5395/rde.2026.51.e1

Restorative Dentistry and Endodontics (*Restor Dent Endod, RDE*) is a peer-reviewed and open-access electronic journal providing up-to-date information regarding the research and developments on new knowledge and innovations pertinent to the field of contemporary clinical operative dentistry, restorative dentistry, and endodontics. In the field of operative and restorative dentistry, the journal deals with diagnosis, treatment planning, treatment concepts and techniques, adhesive dentistry, esthetic dentistry, tooth whitening, dental materials, and implant restoration. In the field of endodontics, the journal deals with a variety of topics such as etiology of periapical lesions, outcome of endodontic treatment, surgical endodontics including replantation, transplantation and implantation, dental trauma, intracanal microbiology, endodontic materials (MTA, nickel-titanium instruments, etc), molecular biology techniques, and stem cell biology. *RDE* publishes research articles, review articles and case reports dealing with aforementioned topics from all over the world.

Manuscripts submitted to *RDE* should be prepared according to the instructions below. For issues not addressed in these instructions, the author should refer to the Recommendations for the Conduct, Reporting, Editing, and Publication of Scholarly Work in Medical Journals (http://www.icmje.org/recommendations/) from the International Committee of Medical Journal Editors (ICMJE).

Research and Publication Ethics

All of the manuscripts should be prepared based on strict observation of research and publication ethics guidelines recommended by the Council of Science Editors (https://www.councilscienceeditors.org), International Committee of Medical Journal Editors (ICMJE, https://www.icmje.org), World Association of Medical Editors (WAME, https://www.wame.org), and the Korean Association of Medical Journal Editors (KAMJE, https://www.kamje.or.kr/en/main_en).

All studies involving human subjects or human data must be reviewed and approved by a responsible Institutional Review Board (IRB). Please refer to the principles embodied in the Declaration of Helsinki (https://www.wma.net/policies-post/wma-declaration-of-helsinki-ethical-principles-for-medical-research-involving-human-subjects) for all investigations involving human materials. Animal experiments also should be reviewed by an appropriate committee (IACUC) for the care and use of animals. Also, studies with pathogens requiring a high degree of biosafety should pass review of a relevant committee (Institutional Biosafety Committee). The approval should be described in the Methods section. For studies of humans including case reports, state whether informed consents were obtained from the study participants (or from a parent or legal guardian if the participant is unable to provide consent). The editor of *RDE* may request submission of copies of the documents regarding ethical issues.

The *RDE* will follow the guidelines of the Committee on Publication Ethics (COPE, https://publicationethics.org) for the settlement of any misconduct.

Authorship

Authorship credit should be based on (1) substantial contributions to conception and design, acquisition of data, and analysis and interpretation of data; (2) drafting the article or revising it critically for important intellectual content; (3) final approval of the version to be published; and (4) agreement to be accountable for all aspects of the work in ensuring that questions related to the accuracy or integrity of any part of the work are appropriately investigated and resolved. Authors should meet these four conditions.

Role of Corresponding Author: The corresponding author takes primary responsibility for communication with the journal during the manuscript submission, peer review, and publication process. The corresponding author typically ensures that all of the journal's administrative requirements, such as providing the details of authorship, ethics committee approval, clinical trial registration documentation, and conflict of interest forms and statements, are properly completed, although these duties may be delegated to one or more

co-authors. The corresponding author should be available throughout the submission and peer review process to respond to editorial queries in a timely manner, and after publication, should be available to respond to critiques of the work and cooperate with any requests from the journal for data or additional information or questions about the article.

Contributors: Any researcher who does not meet all four ICMJE criteria for authorship discussed above but contribute substantively to the study in terms of idea development, manuscript writing, conducting research, data analysis, and financial support should have their contributions listed in the Acknowledgments section of the article.

Changes to Authorship: Any changes to authorship (the addition, deletion or rearrangement of author names in the authorship of accepted manuscript) needs to be approved by the Editor-in-Chief after a written confirmation by a corresponding author including the reason the name should be rearranged and all the signature of co-authors.

For more information, please refer to the Research and Publication Ethics page on the journal website.

Copyrights, Open Access, Data Sharing, and Archiving

Copyright: Copyright in all published material is owned by the Korean Academy of Conservative Dentistry. Authors must agree to transfer copyright (https://rde.ac/src/author_form.pdf) during the submission process. The corresponding author is responsible for submitting the copyright transfer agreement to the publisher.

Open Access Policy: *RDE* is an open-access journal. Articles are distributed under the terms of the Creative Commons Attribution License (https://creativecommons.org/licenses/by-nc/4.0/), which permits unrestricted non-commercial use, distribution, and reproduction in any medium, provided the original work is properly cited. Author(s) do not need permission to use tables or figures published in *RDE* in other journals, books, or media for scholarly and educational purposes.

Data Sharing: *RDE* encourages data sharing wherever possible unless this is prevented by ethical, privacy, or confidentiality matters. Authors may deposit their data in a publicly accessible repository and include a link to the DOI within the text of the manuscript.

Clinical Trials: *RDE* accepts the ICMJE Recommendations for data sharing statement policy. Authors may refer to the editorial, "Data Sharing Statements for Clinical Trials: A Requirement of the International Committee of Medical Journal Editors," in the Journal of Korean Medical Science (https://doi.org/10.3346/jkms.2017.32.7.1051).

Archiving Policy: It is accessible without barrier from PubMed Central (https://www.ncbi.nlm.nih.gov/pmc/journals/2010/), Korea Citation Index (https://kci.go.kr), or National Library of Korea (https://nl.go.kr) in the event a journal is no longer published.

For more information, please refer to the Editorial Policy page on the journal website.

Article Processing Charge

There are no author submission fees or other publication-related charges. All cost for the publication process is supported by the Publisher.

Submission of Manuscripts

Copyright Assignment: Authors submitting a paper do so on the understanding that the work and its essential substance have not been published before and are not being considered for publication elsewhere. The submission of the manuscript by the authors means that the authors automatically agree to assign exclusive copyright to *RDE* if and when the manuscript is accepted for publication.

Submission: *RDE* requires electronic submission of all manuscripts. All manuscripts must be submitted to *RDE* through the website (https://www.editorialmanager.

com/rde/) with a cover letter to the editor. Manuscripts may be submitted at any time. Authors may send queries concerning the submission process, manuscript status, or journal procedures to the Editor. Please contact the Editor by E-mail at editor@rde.ac.

Blinded Peer Review Process: Manuscripts that do not conform to the general aims and scope of the journal will be returned immediately without review. All other manuscripts will be reviewed by experts in the corresponding field (at least two referees). The Editorial Board may request authors to revise the manuscripts according to the reviewer's opinion. The revised manuscript may go through a second review by referees. A final decision on approval of publication of the submitted manuscripts is made by the Editorial Board.

Manuscript Preparation

General Requirements

- **Publication types:** Articles falling into the following categories are invited for submission: Research Articles, Case Reports, Review Articles, Editorials, Open Lectures, and Comments for the Reader's Forum.
- **Language:** The language of publication is English. It is recommended that international authors who are not native speakers of English seek help during manuscript preparation. The authors must have the article reviewed by a professional English editorial service before submission and submit the certificate of English proofreading as a supplement. The terminology used should follow the most recent edition of Dorland's Illustrated Medical Dictionary.
- **General text style:** Use Times New Roman 10-point font. Scientific units should be followed by the International System of Units. When non-standard terms appearing 3 or more times in the manuscript are to be abbreviated, they should be written out completely in the text when first used with the abbreviation in parenthesis. For medicine, use generic names. If a brand name should be used, insert it in parentheses after the generic name.
- **Statistical analysis:** Authors are strongly encouraged to consult a statistician for statistical analysis. Manuscripts with inappropriate statistical analysis methods will be returned to the authors without being reviewed.
- **Ethical approval:** All studies using human and animal subjects or specimens obtained from such subjects (such as extracted teeth) should include an explicit statement in the Methods section identifying the review and approval by the ethics committee for each study and provide an approval number. Manuscripts must be accompanied by a statement in the cover letter that the experiments were undertaken with the understanding and written consent of each subject and according to the above-mentioned principles.
- **Permissions:** If all or parts of previously published quotations, tables, or illustrations are used, permission must be obtained from the copyright holder concerned. The authors will be held responsible for failing to acquire proper permission before submission.
- **Reporting guideline:** For specific study designs, such as randomized controlled trials, studies of diagnostic accuracy, meta-analyses, observational studies, and non-randomized studies, we strongly recommend that authors follow and adhere to the reporting guidelines relevant to their specific research design. Randomized controlled trials should be presented according to the CONSORT guidelines (http://www.consort-statement.org). For case reports, authors should follow the CARE guidelines (https://www.care-statement.org). Authors should upload a completed checklist for the appropriate reporting guidelines during initial submission. Some reliable sources of reporting guidelines are EQUATOR Network (https://www.equator-network.org/) and NLM (https://www.nlm.nih.gov/services/research_report_guide.html).
- **Data statement:** Authors should state the availability of data in submission. If you have made your research data available in a data repository, you can link your article directly to the dataset. If the data is unavailable to access or unsuitable to post, authors must indicate why during the submission process, for example by stating that the research data is confidential. The statement will appear with your published article.

Manuscript Structure and Format

Key features and limits of articles are summarized below. However, the limits are negotiable with the editor.

Type	Abstract	Reference (max)	Table/Fig (max)
Review Article	· Unstructured · Max 200 words	70	NL
Research Article	· Structured : Objectives / Methods / Results / Conclusions · Max 250 words	40	Total 8
Case Report	· Unstructured · Max 200 words	30	Total 6
Editorial	No abstract	10	Total 2
Open Lectures	No abstract	NL	NL
Comments for the Reader's Forum	No abstract	NL	NL

NL, no limit.

Units, symbols, figures, tables, and references used must conform to the current issue or the linked article on our website.

- **Title page:** The title page of the manuscript should include the title of the article, the full name of the author(s), academic degrees, institutional affiliations, a running title (of seven or fewer words), correspondence, and declarations.
  - Title: The title should be concise and precise. It should be of 20 or less words, or it should fit within two lines. Only the first letter of the first word of the title should be capitalized.
  - Authors: Listed authors should include only those individuals who have made a significant creative contribution. *RDE* allows multiple authors to be specified as having equally contributed to the article as co-first authors or co-corresponding authors. While the contact information of all the corresponding authors is published in the article, only one corresponding author (the submitting author) is solely responsible for communicating with the journal.
  - Correspondence: The affiliation, address, telephone number, and e-mail address should be given.
  - Declarations: The declarations include conflicts of interest, funding, authors' contributions, ORCID, data availability statement, and acknowledgments.

Conflicts of interest	If there are any conflicts of interest, authors should disclose them in the manuscript. Disclosures allow editors, reviewers, and readers to approach the manuscript with an understanding of the situation and background of the completed research. If there are no conflicts of interest, authors should include the following sentence: "No potential conflict of interest relevant to this article was reported."
Funding	All sources of funding applicable to the study should be stated here explicitly.
Authors' contributions	The contributions of all authors must be described using the CRediT (https://casrai.org/credit/) taxonomy of author roles.
	Author Contributions Conceptualization: name; Data curation: name; Formal analysis: name; Funding acquisition: name; Investigation: name; Methodology: name; Project administration: name; Resources: name; Software: name; Supervision: name; Validation: name; Visualization: name; Writing - original draft: name; Writing - review & editing: name. (name: the last name and initials; eg, Cho BH)
ORCID	All authors are required to provide ORCID identification numbers. Please list the names of all authors and include the corresponding ORCID iD next to each name.
	ORCID Byeong-Hoon Cho https://orcid.org/0000-0001-9641-5507 Kyung-San Min https://orcid.org/0000-0002-1928-3384
Data availability statement	**Data are available in a public, open-access repository:** Please state the repository name, the persistent URL, and any conditions of reuse. All data that are publicly available and used in the writing of an article should be cited in the text and the reference list, whether they are data generated by the author(s) or by other researchers. **Data are available upon reasonable request:** Please describe the data (eg, de-identified participant data), who has access to the data, their publishable contact information, and the conditions under which reuse is permitted. **All study-related data is included in the publication or provided as supplementary information:** Please ensure this does not include patient identifiable data. **Data sharing is not relevant because no datasets were created and/or analyzed for this study:** Please state 'Not applicable' in this section. **No data are available:** Please state 'Not applicable' in this section.

Acknowledgments	All persons who have made substantial contributions, but who have not met the criteria for authorship, are acknowledged here.

- **Abstract:** The abstract should consist of a single paragraph with no more than 250 words for research articles and 200 words for case reports or review articles and should give details of what was done. The structured abstracts of research articles are to contain the following major headings: **Objective, Methods, Results, Conclusion**; and Keywords of no more than six words in alphabetical order. The abstracts of review articles or case reports don't need a structured format, but keywords should be listed. The keywords should be from Medical Subject Headings (MeSH) when possible (https://meshb.nlm.nih.gov/search) but non-MeSH subject headings may be used if deemed appropriate by the authors. Keywords should be written in small alphabetic letters with the first letter in capital. Separate each word by a semicolon.
- **Main text**
  - Introduction: The introduction should briefly review the pertinent literature in order to identify the gap in knowledge that the study is intended to address. The purpose of the study, the tested hypothesis, and its scope should be described.
  - Methods: The explanation of the experimental methods should be concise and sufficient for repetition by other qualified investigators. Procedures that have been published previously should not be described in detail. However, new or significant modifications of previously published procedures need full descriptions. Clinical studies or experiments using laboratory animals or pathogens should mention approval of the studies by relevant committees in this section. The sources of special chemicals or preparations should be given along with their location (name of company, city and state, and country). If the study utilized a commercial product, the generic term should be used and the product name, manufacturer, city, and country should be stated in parentheses. The methods of statistical analysis and the criteria for determining significance levels should be described.

An **ethics statement** should be placed here when the studies are performed using clinical samples or data, and animals. An exemplary is shown below.

Human	The study protocol was approved by the Institutional Review Board of OOO (IRB No: OO-OO-OO). Informed consent was obtained by all participants (or the participant's legal guardian) / Informed consent was waived by the IRB.
Animal	The procedures used and the care of animals were approved by the Institutional Animal Care and Use Committee at OOO University (approval No. ******).
Clinical trial	This is a randomized clinical trial on the second phase, registered at the Clinical Research Information Service (CRIS, https://cris.nih.go.kr), No. *******. * Other international registration is also acceptable.

Description of participants: Ensure correct use of the terms sex (when reporting biological factors) and gender (identity, psychosocial or cultural factors), and, unless inappropriate, report the sex or gender of study participants, the sex of animals or cells, and describe the methods used to determine sex or gender. If the study was done involving an exclusive population, for example in only one sex, authors should justify why, except in obvious cases (eg, prostate cancer). Authors should define how they determined race or ethnicity and justify their relevance.

  - Results: This section should present only the observations with minimal reference to earlier literature or possible interpretations by the authors. Data must not be duplicated in Tables and Figures. In tables and figures, magnification rates and units should be stated. SI (Le système International d'Unités) units should be used. Tables, figures, and legends of tables and figures may be included in the text or attached as separate pages at the end of the manuscript. Files containing figures and tables must also be submitted as separate files.
  - Discussion: The discussion section should describe the major findings of the study. Both the strengths and the weaknesses of the observations should be discussed. In addition, suggestions for further research topics may be included if needed.
  - Conclusions: A brief conclusion based on the findings of the study and a comment on the potential clinical relevance of the findings should be summarized. The conclusion section should be described in a narrative manner, without numbering.
- **References:** References should be obviously related

to the document. In the text, references should be cited with Arabic numerals in brackets, numbered in the order cited. The reference list should be typed double-spaced on a separate page and numbered in the order the reference citations appear in the text. For journal citations, include surnames and initials of authors, complete title of article, name of journal (abbreviated according to the NLM Catalog; https://www.ncbi.nlm.nih.gov/nlmcatalog/journals/), volume, inclusive page numbers, and year of publication. When books are cited, either inclusive page numbers or chapter numbers should be included. Please note that theses or doctoral dissertations, which have not been published in peer-reviewed journals, should not be cited as references.

If needed, single or double authors should be acknowledged in the text, eg, Ford and Roberts. If there are more than two authors, the first author followed by *et al*. is sufficient, eg, Tobias *et al*.

We recommend the use of EndNote for reference management and formatting. For reference style and format, please refer to the following examples.

Journal article	1. Oh HK, Shin DH. Effect of adhesive application method on repair bond strength of composite. Restor Dent Endod 2021;46:e32. List all authors when six or fewer (ex. reference 1); when seven or more, list six and add *et al*. (ex. reference 2 and 4). 2. Bergamo ET, Yamaguchi S, Lopes AC, Coelho PG, de Araújo-Júnior EN, Benalcázar Jalkh EB, *et al*. Performance of crowns cemented on a fiber-reinforced composite framework 5-unit implant-supported prostheses: in silico and fatigue analyses. Dent Mater 2021;37:1783-1793. 3. Shah RA, Hsu JI, Patel RR, Mui UN, Tyring SK. Antibiotic resistance in dermatology: the scope of the problem and strategies to address it. J Am Acad Dermatol 2021 Sep 20 [Epub]. https://doi.org/10.1016/j.jaad.2021.09.024. 4. Van Meerbeek B, Vargas M, Inoue S, Yoshida Y, Peumans M, Lambrechts P, *et al*. Adhesives and cements to promote preservation dentistry. Oper Dent 2001;(Supplement 6):119-144. 5. Yoshida Y, Van Meerbeek B, Okazaki M, Shintani H, Suzuki K. Comparative study on adhesive performance of functional monomers. J Dent Res 2003;82(Special Issue B):Abstract 0051, pB-19.
Book & Book chapter	6. Seltzer S, Bender IB. The dental pulp: biologic considerations in dental procedures. 3rd ed. Lippincott; 1984. p400. 7. Fouad AF, Levin L. Pulpal reactions to caries and dental procedures. In: Hargreaves KM, Cohen S, Berman LH, eds. Cohen's pathways of the pulp. 10th ed. Mosby Elsevier; 2010. p504-528.
Website	8. International Association of Dental Traumatology (IADT). The dental trauma guide [Internet]. IADT; 2014 [cited 2021 Jun 10]. Available from: https://dentaltraumaguide.org
Corporate publication	9. ISO-Standards ISO 4287 Geometrical Product Specifications Surface texture. Profile method: terms, definitions and surface texture parameters. 1st ed. Geneve: International Organization for Standardization; 1997. p1-25.

- **Tables:** Tables should be included in the text so that they may be edited if necessary. The title of each table should be placed on the top. The first letter of the first word should be capitalized. All abbreviations should be explained in each table. Footnotes should be indicated in superscript as [a), b), c)], and so on.
- **Figures:** Illustrations must be submitted in electronic format with file sizes appropriate for publication. Figures should be submitted as .tif or .jpg files. PowerPoint files are not accepted. All images should be at least 300 dpi and 5 × 5 cm in size, with 500 dpi recommended. If the figures represent a series of related content, it is recommended to present them as panels (A, B, C...) within a single figure. Figure legends should be included as text so that they be edited if necessary. All abbreviations should be explained in each figure. Microscopic images should include the staining method and magnification (eg, hematoxylin and eosin stain, ×400). Figures may use arrows, arrowheads, asterisks, circles, or other indicators as needed for clarity, with each indicated element described in the figure legends.
- **Other types of articles**
  - Review articles: Review articles should be divided into Introduction, Review, and Conclusions. The Introduction section should focus on placing the subject matter in context and justifying the need for the review. The Review section should be divided into logical sub-sections in order to improve readability and enhance understanding. Search strategies must be described and the use of state-of-the-art evi-

dence-based systematic approaches is expected. The use of tabulated and illustrative material is encouraged. The Conclusion section should reach clear conclusions and/or recommendations on the basis of the evidence presented. If a review includes a meta-analysis as part of a systematic review, it should be submitted as a research article.

- Case reports: Case reports should be divided into Introduction, Case Report(s), Discussion, and Conclusions. They should be well illustrated with clinical images, radiographs, diagrams, and where appropriate, supporting tables and graphs. However, all illustrations must be of the highest quality.
- Comments for the Reader's forum: Reader's forum will present various questions, suggestions, and critiques on the subjects of operative dentistry, restorative dentistry, and endodontics from the readers.

Manuscript Files Accepted

- **Final version:** After a paper has been accepted for publication, the author(s) should submit the final version of the manuscript. The names and affiliations of authors should be double-checked, and if the originally submitted image files were of poor resolution, higher-resolution image files should be submitted at this time. Illustrations must be submitted in electronic format with file sizes appropriate for publication. All images should be at least 300 dpi and 5 × 5 cm in size, with 500 dpi recommended. Symbols (eg, circles, triangles, squares), letters (eg, words, abbreviations), and numbers should be large enough to be legible on reduction to the journal's column widths. All symbols must be defined in the figure caption. When submitted as separate files, name of the author, and illustration number should be stated in the file name. If references, tables, or figures are moved, added, or deleted during the revision process, renumber them to reflect such changes so that all tables, references, and figures are cited in numeric order.
- **Errata and Corrigenda:** To correct errors in published articles, the corresponding author should contact the journal's Editorial Office with a detailed description of the proposed correction. Corrections that profoundly affect the interpretation or conclusions of the article will be reviewed by the editors. Corrections will be published as corrigenda (corrections of author's errors) or errata (corrections of publisher's errors) in a later issue of the journal.

Contacting the Journal

Editorial assistant: Hye-Young Lee
RDE editorial office
The Korean Academy of Conservative Dentistry
B163, Seoul National University Dental Hospital, 101 Daehak-ro, Jongno-gu, Seoul 03080, Korea
Tel: +82-2-763-3818, Fax: +82-2-763-3819, E-mail: editor@rde.ac

History of the Recommendations

Enacted in March 2, 2012
Modified: August 4, 2023
Last modified: November 4, 2024

RDE Restorative Dentistry & Endodontics

Author's checklist

Authors have written the manuscript in compliance with Instructions to Authors and Recommendations for the Conduct, Reporting, Editing, and Publication of Scholarly Work in Medical Journals (https://www.icmje.org/icmje-recommendations.pdf) from the International Committee of Medical Journal Editors, and the Guideline of Committee on Publication Ethics (https://publicationethics.org).

Cover letter

☐ Manuscript's title
☐ Statement that your paper has not been previously published and is not currently under consideration by another journal.
☐ Brief description of the research you are reporting in your paper, why it is important, and why you think the readers of the journal would be interested in it.
☐ Contact information for you and any co-authors.
☐ Confirmation that you have no competing interests to disclose.

Title page

☐ Title page including the title of the article, the full name of the author(s), academic degrees, positions, institutional affiliations, a running title (of 7 or less words), correspondence, and declarations.

Declaration

☐ Conflicts of interest, funding, authors' contributions, ORCID, data availability statement, and acknowledgments

Abstract

☐ Original article: <250 words; structured abstract— Objective, Methods, Results, Conclusion
☐ Review article: <200 words; unstructured abstract
☐ Case report: <200 words; unstructured abstract

Keyword

☐ Keywords should be from MeSH subject headings when possible.

Main text

☐ Information regarding approval of an institutional review board and obtaining informed consent should be mentioned.
☐ Original article: Introduction/Methods/Results/Discussion/Conclusions
☐ Review article: Introduction/Review/Conclusions
☐ Case report: Introduction/Case Report(s)/Discussion/Conclusions

Reference

☐ Refer to the reference format in the author's guideline.

Table

☐ If tables are included, they should be included as text and not as illustrations so that they may be edited if necessary.

Figure

☐ Figure legends should be included as text and not as illustrations so that they may be edited if necessary.

Author's form

☐ All authors have completed the Copyright Transfer Agreement and Ethics Concerning Human Subjects.

Conflict of interest form

☐ All authors have completed the COI Statement.

Permission

☐ The authors are responsible for obtaining permission from the copyright holder to reprint any previously published material in RDE.

RDE Restorative Dentistry & Endodontics

Copyright transfer agreement

Manuscript title _____

_____

Corresponding author name _____

Fax _____ E-mail _____

The authors of the article hereby agree that the Korean Academy of Conservative Dentistry holds the copyright on all submitted materials and the right to publish, transmit, sell, and distribute them in the journal or othermedia.

Corresponding author

Print name _____

Signed _____ **Date** _____

Co-authors

Print name _____ **Print name** _____

Signature/Date _____ **Signature/Date** _____

Print name _____ **Print name** _____

Signature/Date _____ **Signature/Date** _____

Print name _____ **Print name** _____

Signature/Date _____ **Signature/Date** _____

Print name _____ **Print name** _____

Signature/Date _____ **Signature/Date** _____

RDE Restorative Dentistry & Endodontics

Conflict of interest form

Manuscript title _____

_____

As the corresponding author, I declare the following information regarding the specific conflicts of interest of authors of our aforementioned manuscript.

Examples of conflicts of interest include the following: source of funding, paid consultant to sponsor, study investigator funded by sponsor, employee of sponsor, board membership with sponsor, stockholder for mentioned product, any financial relationship to competitors of mentioned product, and others (please specify).

Author	No conflict involved	Conflict (specify)

I accept the responsibility for the completion of this document and attest to its validity on behalf of all co-authors.

Corresponding author (name/signature) _____ _____

Date _____